

SPECTROSCOPIC AND MAGNETIC PROPERTIES OF PYRIDINE AND PYRAZINE  
COMPLEXES OF DIVALENT IRON AND COPPER

by

JOHN STEPHEN HAYNES

M.Sc., University Of British Columbia, 1980

A THESIS SUBMITTED IN PARTIAL FULFILMENT OF  
THE REQUIREMENTS FOR THE DEGREE OF  
DOCTOR OF PHILOSOPHY

in

THE FACULTY OF GRADUATE STUDIES  
Department Of Chemistry

We accept this thesis as conforming  
to the required standard

THE UNIVERSITY OF BRITISH COLUMBIA

July 1985

© John Stephen Haynes, 1985

22

In presenting this thesis in partial fulfilment of the requirements for an advanced degree at the University of British Columbia, I agree that the Library shall make it freely available for reference and study. I further agree that permission for extensive copying of this thesis for scholarly purposes may be granted by the head of my department or by his or her representatives. It is understood that copying or publication of this thesis for financial gain shall not be allowed without my written permission.

Department of

Chronology

The University of British Columbia  
1956 Main Mall  
Vancouver, Canada  
V6T 1Y3

Date

August 28 1981

### Abstract

Magneto-structural correlations have been made for a number of pyridine and pyrazine complexes of iron(II) and copper(II), involving anions of a range of coordinating abilities, for example, sulfonate,  $\text{RSO}_3^-$  (where R is  $\text{CF}_3$ ,  $\text{CH}_3$ , or  $p\text{-CH}_3\text{C}_6\text{H}_4$ ); halide,  $\text{Cl}^-$ ,  $\text{Br}^-$  or  $\text{I}^-$ ; pseudohalide,  $\text{NCO}^-$  or  $\text{NCS}^-$ ; perchlorate and hexafluoroarsenate. Structure was determined by infrared, electronic and Mössbauer spectroscopy and differential scanning calorimetry, and, in some instances, by single-crystal X-ray diffraction. Spectroscopic results were used to investigate the nature of both anion and neutral ligand coordination.

In complexes of stoichiometry  $\text{ML}_4(\text{RSO}_3)_2$  (where M is Fe or Cu, L is pyridine, pyrazine or 2-methylpyrazine and R is  $\text{CF}_3$ ,  $\text{CH}_3$  or  $p\text{-CH}_3\text{C}_6\text{H}_4$ ), the neutral ligands were found to adopt a unidentate mode of coordination. For several of these complexes, X-ray crystallography revealed a square-planar array of pyridine ligands around the central metal, with anions coordinated in a unidentate mode above and below this plane. A monomeric molecular structure results in which the paramagnetic centres are well isolated from each other giving rise to magnetically-dilute species.

In complexes of stoichiometry  $\text{M}(\text{pyz})_2\text{X}_2$  (where M is Fe or Cu and  $\text{X}^-$  is  $\text{CF}_3\text{SO}_3^-$ ,  $\text{CH}_3\text{SO}_3^-$ ,  $\text{Cl}^-$ ,  $\text{Br}^-$ ,  $\text{I}^-$ ,  $\text{ClO}_4^-$  or  $\text{NCS}^-$ ), pyrazine was found to coordinate through both nitrogen donor atoms and inorganic coordination polymers were produced. X-ray crystallography revealed a two-dimensional lattice in  $\text{Cu}(\text{pyz})_2(\text{CH}_3\text{SO}_3)_2$  with two distinct kinds of bridging pyrazine

groups and monodentate sulfonate anions. For the remaining bis(pyrazine) complexes, spectroscopic evidence supports similar structures with unidentate anion coordination and bidentate bridging pyrazine ligands leading to sheet-like polymers.  $\text{Cu}(\text{pyz})_2(\text{CH}_3\text{SO}_3)_2$  and  $\text{Fe}(\text{pyz})_2(\text{NCS})_2$  exhibit magnetic susceptibilities which reveal the antiferromagnetic nature of these materials ( $\chi_{\text{max}}$  at temperatures of 7.0 and 8.0 K respectively); the data were analysed in terms of a two-dimensional Heisenberg model. For the copper complex, in which the structure shows stronger pyrazine coordination along one dimension, the data were also analysed in terms of a linear chain model. Mössbauer spectroscopy showed  $\text{Fe}(\text{pyz})_2(\text{NCS})_2$  to undergo a transition to a magnetically-ordered state at 9.2 K. The magnitude of the exchange coupling through bridging pyrazine in  $\text{Fe}(\text{pyz})_2\text{X}_2$  complexes (where  $\text{X}^-$  is  $\text{CF}_3\text{SO}_3^-$ ,  $\text{CH}_3\text{SO}_3^-$ ,  $\text{Cl}^-$ ,  $\text{Br}^-$ ,  $\text{I}^-$  or  $\text{ClO}_4^-$ ) is considerably less than that present in either  $\text{Cu}(\text{pyz})_2(\text{CH}_3\text{SO}_3)_2$  or  $\text{Fe}(\text{pyz})_2(\text{NCS})_2$ .

Spectroscopic evidence indicates that for  $\text{Fe}(\text{pyz})_2(\text{CF}_3\text{SO}_3)_2$  and complexes of stoichiometry  $\text{M}(\text{pyz})\text{X}_2$  (where M is Fe or Cu and  $\text{X}^-$  is  $\text{CF}_3\text{SO}_3^-$ ,  $\text{p-CH}_3\text{C}_6\text{H}_4\text{SO}_3^-$ ,  $\text{Cl}^-$  or  $\text{NCO}^-$ ) bridging anionic ligands are present and for the mono(pyrazine) complexes the neutral ligand also coordinates in a bridging mode.  $\text{Fe}(\text{pyz})(\text{CF}_3\text{SO}_3)_2$ ,  $\text{Fe}(\text{pyz})(\text{NCO})_2$  and  $\text{Cu}(\text{pyz})(\text{CF}_3\text{SO}_3)_2$  all exhibit magnetic susceptibility data characteristic of antiferromagnetic materials ( $\chi_{\text{max}}$  at temperatures of 4.4, 38 and 7.0 K respectively). The magnetic susceptibilities for these materials were analysed in terms of the two-dimensional



Heisenberg model and a linear chain model. Mössbauer spectroscopy shows both  $\text{Fe}(\text{pyz})(\text{CF}_3\text{SO}_3)_2$  and  $\text{Fe}(\text{pyz})(\text{NCO})_2$  to undergo a transition to long-range magnetic ordering at temperatures of 3.9 and 27.0 K respectively.

Low-temperature (4.2-130 K) magnetic susceptibility measurements for the iron(II) sulfonate compounds,  $\text{Fe}(\text{RSO}_3)_2$  (where R is F,  $\text{CF}_3$ ,  $\text{CH}_3$  or  $\text{p-CH}_3\text{C}_6\text{H}_4$ ) are reported. For the compounds where R is F,  $\text{CF}_3$  or  $\text{p-CH}_3\text{C}_6\text{H}_4$  the magnetic moment data were assessed in terms of crystal-field splitting effects. The magnetic moment data for  $\alpha$  and  $\beta$  forms of  $\text{Fe}(\text{CH}_3\text{SO}_3)_2$  are indicative of antiferromagnetic exchange interactions and the characteristics of the susceptibility curve for the  $\beta$  isomer are explained on the basis of a transition from short-range to long range three-dimensional magnetic ordering at 22 K.

<u>Table of Contents</u>	<u>Page</u>
Abstract .....	ii
Table of Contents .....	v
List of Tables .....	xi
List of Figures .....	xii
List of Abbreviations and Symbols .....	xv
Acknowledgements .....	xvi
CHAPTER 1	
INTRODUCTION .....	1
1.1 GENERAL INTRODUCTION .....	1
1.2 OBJECTIVES, PREVIOUS WORK AND SCOPE OF THE THESIS .....	6
1.3 METHODS OF COMPOUND CHARACTERISATION .....	16
1.4 ORGANISATION OF THE THESIS .....	21
CHAPTER 2	
EXPERIMENTAL PROCEDURES .....	23
2.1 GENERAL SYNTHETIC METHODS .....	23
2.2 PHYSICAL EXPERIMENTAL TECHNIQUES .....	24
2.2.1 Infrared Spectroscopy .....	24
2.2.2 Electronic Spectroscopy .....	24
2.2.3 Magnetic Susceptibility Measurements .....	24
2.2.4 Mössbauer Spectroscopy .....	26
2.2.5 X-Ray Crystallography .....	27
2.2.6 Differential Scanning Calorimetry .....	27
2.2.7 Elemental Analysis .....	29
CHAPTER 3	
COMPLEXES CONTAINING AN $Mn_4X_2$ CHROMOPHORE .....	30
3.1 INTRODUCTION .....	30
3.2 SYNTHETIC METHODS .....	33
3.2.1 Tetrakis(pyridine) Complexes .....	33

3.2.1.1	<u>Trans</u> -bis(trifluoromethanesulfonato-O)tetrakis-(pyridine)iron(II), $\text{Fe}(\text{py})_4(\text{CF}_3\text{SO}_3)_2$ .....	34
3.2.1.2	<u>Trans</u> -bis(methanesulfonato-O)tetrakis(pyridine)-iron(II), $\text{Fe}(\text{py})_4(\text{CH}_3\text{SO}_3)_2$ .....	34
3.2.1.3	<u>Trans</u> -bis(p-toluenesulfonato-O)tetrakis(pyridine)-iron(II), $\text{Fe}(\text{py})_4(\text{p-CH}_3\text{C}_6\text{H}_4\text{SO}_3)_2$ .....	35
3.2.1.4	Tetrakis(pyridine)iron(II) fluorosulfonate, $\text{Fe}(\text{py})_4(\text{FSO}_3)_2$ .....	35
3.2.1.5	<u>Trans</u> -bis(trifluoromethanesulfonato-O)tetrakis-(pyridine)copper(II), $\text{Cu}(\text{py})_4(\text{CF}_3\text{SO}_3)_2$ .....	37
3.2.1.6	Tetrakis(pyridine)copper(II) methanesulfonate, $\text{Cu}(\text{py})_4(\text{CH}_3\text{SO}_3)_2$ .....	38
3.2.2	Tetrakis(pyrazine) and Tetrakis(2-methylpyrazine) Complexes .....	38
3.2.2.1	Tetrakis(2-methylpyrazine)iron(II) methanesulfonate, $\text{Fe}(\text{2-mepyz})_4(\text{CH}_3\text{SO}_3)_2$ .....	39
3.2.2.2	Tetrakis(pyrazine)iron(II) hexafluoroarsenate dihydrate, $\text{Fe}(\text{pyz})_4(\text{AsF}_6)_2 \cdot 2\text{H}_2\text{O}$ .....	39
3.2.2.3	Tetrakis(pyrazine)copper(II) trifluoromethanesulfonate monohydrate, $\text{Cu}(\text{pyz})_4(\text{CF}_3\text{SO}_3)_2 \cdot \text{H}_2\text{O}$ .....	41
3.2.3	Bis(pyrazine) Complexes .....	41
3.2.3.1	Bis(pyrazine)iron(II) trifluoromethanesulfonate methanol solvate, $\text{Fe}(\text{pyz})_2(\text{CF}_3\text{SO}_3)_2 \cdot \text{CH}_3\text{OH}$ .....	41
3.2.3.2	Bis(pyrazine)iron(II) methanesulfonate, $\text{Fe}(\text{pyz})_2(\text{CH}_3\text{SO}_3)_2$ .....	42
3.2.3.3	<u>Trans</u> -bis(methanesulfonato-O)bis( $\mu$ -pyrazine)-copper(II), $\text{Cu}(\text{pyz})_2(\text{CH}_3\text{SO}_3)_2$ .....	43
3.2.3.4	Bis(pyrazine)iron(II) chloride, $\text{Fe}(\text{pyz})_2\text{Cl}_2$ ...	43
3.2.3.5	Bis(pyrazine)iron(II) bromide, $\text{Fe}(\text{pyz})_2\text{Br}_2$ ....	44
3.2.3.6	Bis(pyrazine)iron(II) iodide, $\text{Fe}(\text{pyz})_2\text{I}_2$ .....	45
3.2.3.7	Bis(pyrazine)iron(II) thiocyanate, $\text{Fe}(\text{pyz})_2(\text{NCS})_2$ .....	45
3.2.3.8	Bis(pyrazine)iron(II) perchlorate, $\text{Fe}(\text{pyz})_2(\text{ClO}_4)_2$ .....	46

3.2.4 Attempted Preparations .....	47
3.3 RESULTS AND DISCUSSIONS .....	48
3.3.1 X-Ray Structure Determinations .....	48
3.3.1.1 X-Ray structure determination of $\text{Fe}(\text{py})_4(\text{RSO}_3)_2$ complexes .....	48
3.3.1.2 X-ray structure determination of $\text{Cu}(\text{py})_4(\text{CF}_3\text{SO}_3)_2$ .....	58
3.3.1.3 X-ray structure determination of $\text{Cu}(\text{pyz})_2(\text{CH}_3\text{SO}_3)_2$ .....	62
3.3.2 Infrared Spectroscopy .....	73
3.3.2.1 Infrared spectral results for tetrakis- (pyridine) complexes .....	74
3.3.2.2 Infrared spectral results for bis- (pyrazine)iron(II) halide and thiocyanate complexes .....	81
3.3.2.3 Infrared spectral results for bis-(pyrazine) complexes containing sulfonate or perchlorate anions .....	87
3.3.2.4 Infrared spectral results for tetrakis- (pyrazine) complexes .....	93
3.3.3 Electronic Spectroscopy .....	99
3.3.3.1 Electronic spectral results for complexes containing an $\text{FeN}_4\text{O}_2$ chromophore .....	99
3.3.3.2 Electronic spectral results for complexes containing a $\text{CuN}_4\text{O}_2$ chromophore .....	103
3.3.3.3 Electronic spectral results for complexes containing an $\text{FeN}_4\text{X}_2$ chromophore .....	107
3.3.4 Magnetic Properties .....	111
3.3.4.1 Magnetic susceptibility results for complexes containing a $\text{CuN}_4\text{O}_2$ chromophore .....	111
3.3.4.2 Magnetic susceptibility results for complexes containing an $\text{FeN}_4\text{O}_2$ chromophore .....	121
3.3.4.3 Magnetic susceptibility results for complexes containing an $\text{FeN}_4\text{X}_2$ chromophore .....	137
3.3.5 Mössbauer Spectroscopy .....	147

3.3.5.1	Mössbauer spectral parameters for complexes containing an $\text{FeN}_4\text{O}_2$ chromophore .....	151
3.3.5.2	Mössbauer spectral parameters for bis-(pyrazine)iron(II) halide and thiocyanate complexes and $\text{Fe}(\text{pyz})_4(\text{AsF}_6)_2 \cdot 2\text{H}_2\text{O}$ .....	155
3.3.5.3	Low-Temperature Mössbauer Spectra of $\text{Fe}(\text{pyz})_2(\text{NCS})_2$ .....	156
3.3.6	Thermal Studies .....	166
CHAPTER 4		
	COMPLEXES CONTAINING AN $\text{MN}_2\text{X}_4$ CHROMOPHORE .....	184
4.1	INTRODUCTION .....	184
4.2	SYNTHETIC METHODS .....	188
4.2.1	Bis(pyridine) Complexes .....	189
4.2.1.1	Bis(pyridine)iron(II) trifluoromethanesulfonate, $\text{Fe}(\text{py})_2(\text{CF}_3\text{SO}_3)_2$ .....	190
4.2.2	Mono(pyrazine) Complexes .....	190
4.2.2.1	Mono(pyrazine)iron(II) trifluoromethanesulfonate, $\text{Fe}(\text{pyz})(\text{CF}_3\text{SO}_3)_2$ .....	190
4.2.2.2	Mono(pyrazine)iron(II) p-toluenesulfonate bis(methanol) solvate, $\text{Fe}(\text{pyz})(\text{p-CH}_3\text{C}_6\text{H}_4\text{SO}_3)_2 \cdot 2\text{CH}_3\text{OH}$ .....	191
4.2.2.3	Mono(pyrazine)iron(II) p-toluenesulfonate, $\text{Fe}(\text{pyz})(\text{p-CH}_3\text{C}_6\text{H}_4\text{SO}_3)_2$ .....	192
4.2.2.4	Mono(pyrazine)copper(II) trifluoromethanesulfonate, $\text{Cu}(\text{pyz})(\text{CF}_3\text{SO}_3)_2$ .....	192
4.2.2.5	Mono(pyrazine)iron(II) chloride, $\text{Fe}(\text{pyz})\text{Cl}_2$ ...	192
4.2.2.6	Mono(pyrazine)iron(II) cyanate, $\text{Fe}(\text{pyz})(\text{NCO})_2$ .	193
4.3	RESULTS AND DISCUSSION .....	194
4.3.1	Infrared Spectroscopy .....	194
4.3.1.1	$\text{Fe}(\text{py})_2(\text{CF}_3\text{SO}_3)_2$ .....	194
4.3.1.2	$\text{Fe}(\text{pyz})\text{Cl}_2$ and $\text{Fe}(\text{pyz})(\text{NCO})_2$ .....	196
4.3.1.3	Mono(pyrazine) sulfonate complexes .....	199
4.3.2	Electronic Spectroscopy .....	204

4.3.2.1	Fe(pyz)(CF <sub>3</sub> SO <sub>3</sub> ) <sub>2</sub> , Fe(pyz)(p-CH <sub>3</sub> C <sub>6</sub> H <sub>4</sub> SO <sub>3</sub> ) <sub>2</sub> and its bis(methanol) solvate, Fe(pyz)(CF <sub>3</sub> SO <sub>3</sub> ) and Cu(pyz)(CF <sub>3</sub> SO <sub>3</sub> ) <sub>2</sub> .....	204
4.3.2.2	Fe(pyz)Cl <sub>2</sub> and Fe(pyz)(NCO) <sub>2</sub> .....	205
4.3.3	Magnetic Properties .....	207
4.3.3.1	Cu(pyz)(CF <sub>3</sub> SO <sub>3</sub> ) <sub>2</sub> .....	207
4.3.3.2	Mono(pyrazine) and bis(pyridine)iron(II) complexes .....	211
4.3.4	Mössbauer Spectroscopy .....	224
4.3.4.1	Low-temperature Mössbauer studies on Fe(pyz)(NCO) <sub>2</sub> and Fe(pyz)(CF <sub>3</sub> SO <sub>3</sub> ) <sub>2</sub> .....	225
4.3.5	Thermal Studies .....	240
CHAPTER 5		
MAGNETIC PROPERTIES OF IRON(II) SULFONATE COMPLEXES .....		243
5.1	INTRODUCTION .....	243
5.2	SYNTHETIC METHODS .....	245
5.3	RESULTS AND DISCUSSION .....	245
5.3.1	Fe(FSO <sub>3</sub> ) <sub>2</sub> , Fe(CF <sub>3</sub> SO <sub>3</sub> ) <sub>2</sub> and Fe(p-CH <sub>3</sub> C <sub>6</sub> H <sub>4</sub> SO <sub>3</sub> ) <sub>2</sub> .....	245
5.3.2	$\alpha$ - and $\beta$ -Fe(CH <sub>3</sub> SO <sub>3</sub> ) <sub>2</sub> .....	249
CHAPTER 6		
SUMMARY AND CONCLUSIONS .....		254
REFERENCES .....		262
APPENDICES		
I.	Complete X-Ray Structural Parameters .....	273
II.	Vibrational Assignments for Pyridine and some of its Complexes .....	288
III.	Vibrational Assignments for Sulfonate Anions and Unassigned Bands .....	289
IV.	Vibrational Assignments for Pyrazine and Bis(pyrazine) Complexes .....	291

V.	Vibrational Assignments for the Neutral Ligands in $\text{Fe}(2\text{-mepyz})_4(\text{CH}_3\text{SO}_3)_2$ , $\text{Cu}(\text{pyz})_4(\text{CF}_3\text{SO}_3)_2 \cdot \text{H}_2\text{O}$ and $\text{Fe}(\text{pyz})_4(\text{AsF}_6)_2 \cdot 2\text{H}_2\text{O}$ .....	292
VI.	Vibrational Assignments for Pyrazine and Mono(pyrazine) Complexes .....	293
VII.	Electronic Spectral Results .....	294
VIII.	Magnetic Susceptibility Results for Copper(II) Complexes .....	296
IX.	Magnetic Susceptibility Results for Iron(II) Complexes .....	298
X.	Mössbauer Spectral Results .....	306

<u>List of Tables</u>	<u>Page</u>
3.1 Selected Mean Bond Distances (Å) and Angles (°) for some $\text{Fe}(\text{py})_4(\text{RSO}_3)_2$ Complexes .....	50
3.2 Selected Bond Distances (Å) and Angles (°) for $\text{Cu}(\text{py})_4(\text{CF}_3\text{SO}_3)_2$ .....	59
3.3 Selected Bond Distances (Å) and Angles (°) for $\text{Cu}(\text{pyz})_2(\text{CH}_3\text{SO}_3)_2$ .....	64
3.4 Vibrations of the Perchlorate Anion as a Function of Symmetry .....	90
3.5 Crystal Field Parameters for $\text{Fe}(\text{py})_4(\text{RSO}_3)_2$ Complexes .....	126
3.6 Zero-Field Splitting Parameters .....	129
3.7 Low-temperature Mössbauer Spectral Parameters for $\text{Fe}(\text{pyz})_2(\text{NCS})_2$ .....	157
3.8 Thermal Parameters for Tetrakis(pyridine) and Bis(pyrazine) Complexes .....	167
3.9 Thermal Parameters for Bis(pyrazine)iron(II) Halide and Thiocyanate Complexes .....	177
3.10 Thermal Parameters for $\text{Fe}(\text{2-mepyz})_4(\text{CH}_3\text{SO}_3)_2$ , $\text{Cu}(\text{pyz})_4(\text{CF}_3\text{SO}_3)_2 \cdot \text{H}_2\text{O}$ and $\text{Fe}(\text{pyz})_4(\text{AsF}_6)_2 \cdot 2\text{H}_2\text{O}$ ....	179
4.1 Selected Magnetic Moment Data for Iron(II) Triflate Complexes .....	222
4.2 Linewidths and Intensities (27.0-31.4 K) for $\text{Fe}(\text{pyz})(\text{NCO})_2$ .....	229
4.3 Internal Hyperfine Field and Line Intensity Ratios for $\text{Fe}(\text{pyz})(\text{NCO})_2$ .....	231
4.4 Thermal Parameters for Bis(pyridine) and Mono(pyrazine) Complexes .....	241
5.1 Crystal-Field Splitting Parameters for $\text{Fe}(\text{RSO}_3)_2$ Compounds .....	247
6.1 Classification of Complexes .....	255



<u>List of Figures</u>	<u>Page</u>
1.1 Pyrazine and Pyridine .....	6
1.2 Two Possible Structures for M(pyz) <sub>2</sub> X <sub>2</sub> Complexes .....	8
3.1 ORTEP Plot of the Structure of Fe(py) <sub>4</sub> (CF <sub>3</sub> SO <sub>3</sub> ) <sub>2</sub> ...	51
3.2 ORTEP Plots of the Structure of Fe(py) <sub>4</sub> (CH <sub>3</sub> SO <sub>3</sub> ) <sub>2</sub> ..	52
3.3 ORTEP Plot of the Structure of Fe(py) <sub>4</sub> (p-CH <sub>3</sub> C <sub>6</sub> H <sub>4</sub> SO <sub>3</sub> ) <sub>2</sub> .....	53
3.4 ORTEP Plot of the Structure of Cu(py) <sub>4</sub> (CF <sub>3</sub> SO <sub>3</sub> ) <sub>2</sub> ...	60
3.5 View of a Single Layer in Cu(pyz) <sub>2</sub> (CH <sub>3</sub> SO <sub>3</sub> ) <sub>2</sub> .....	65
3.6 ORTEP Plot of the Inner Coordination Sphere About Copper in Cu(pyz) <sub>2</sub> (CH <sub>3</sub> SO <sub>3</sub> ) <sub>2</sub> .....	66
3.7 Two Adjacent Layers in Cu(pyz) <sub>2</sub> (CH <sub>3</sub> SO <sub>3</sub> ) <sub>2</sub> Viewed Along the c-Axis .....	69
3.8 Two Adjacent Layers in Cu(pyz) <sub>2</sub> (CH <sub>3</sub> SO <sub>3</sub> ) <sub>2</sub> Viewed Along the b-Axis .....	70
3.9 Infrared Spectra of Fe(py) <sub>4</sub> (CH <sub>3</sub> SO <sub>3</sub> ) <sub>2</sub> , Fe(pyz) <sub>2</sub> (CH <sub>3</sub> SO <sub>3</sub> ) <sub>2</sub> and Fe(2-mepyz) <sub>4</sub> (CH <sub>3</sub> SO <sub>3</sub> ) <sub>2</sub> .....	75
3.10 Infrared Spectra of Cu(py) <sub>4</sub> (CH <sub>3</sub> SO <sub>3</sub> ) <sub>2</sub> and Cu(pyz) <sub>2</sub> (CH <sub>3</sub> SO <sub>3</sub> ) <sub>2</sub> .....	77
3.11 Infrared Spectra of Fe(pyz) <sub>2</sub> I <sub>2</sub> and Fe(pyz) <sub>2</sub> (NCS) <sub>2</sub> .....	83
3.12 Infrared Spectrum of Fe(pyz) <sub>4</sub> (AsF <sub>6</sub> ) <sub>2</sub> ·2H <sub>2</sub> O .....	96
3.13 Electronic Energy Levels for High-Spin Iron(II) ...	101
3.14 Electronic Spectra of Fe(py) <sub>4</sub> (RSO <sub>3</sub> ) <sub>2</sub> Complexes .....	101
3.15 2-methylpyrazine .....	101
3.16 Electronic Energy Levels for Copper(II) .....	104
3.17 Magnetic Moments vs Temperature for Cu(py) <sub>4</sub> (CH <sub>3</sub> SO <sub>3</sub> ) <sub>2</sub> and Cu(pyz) <sub>2</sub> (CH <sub>3</sub> SO <sub>3</sub> ) <sub>2</sub> .....	113

3.18	Magnetic Susceptibility vs Temperature for $\text{Cu}(\text{pyz})_2(\text{CH}_3\text{SO}_3)_2$ .....	114
3.19	Magnetic Moments vs Temperature for $\text{Fe}(\text{py})_4(\text{RSO}_3)_2$ Complexes .....	122
3.20	Zero-Field Splitting for High-Spin Iron(II) .....	127
3.21	Magnetic Susceptibility vs Temperature for $\text{Fe}(\text{py})_4(\text{CH}_3\text{SO}_3)_2$ .....	129
3.22	Magnetic Moments vs Temperature for $\text{Fe}(\text{py})_4(\text{CH}_3\text{SO}_3)_2$ and $\text{Fe}(\text{pyz})_2(\text{CH}_3\text{SO}_3)_2$ .....	132
3.23	Magnetic Susceptibility vs Temperature for $\text{Fe}(\text{pyz})_2(\text{CF}_3\text{SO}_3)_2 \cdot \text{CH}_3\text{OH}$ .....	133
3.24	Magnetic Susceptibility vs Temperature for $\text{Fe}(\text{pyz})_2(\text{CH}_3\text{SO}_3)_2$ .....	135
3.25	Magnetic Moments vs Temperature for $\text{Fe}(\text{pyz})_2\text{X}_2$ Complexes .....	137
3.26	Magnetic Moment vs Temperature for $\text{Fe}(\text{pyz})_2(\text{NCS})_2$ .....	141
3.27	Magnetic Susceptibility vs Temperature for $\text{Fe}(\text{pyz})_2(\text{NCS})_2$ .....	141
3.28	1,2,4-Triazole .....	144
3.29	Isomer Shift and Quadrupole Splitting .....	148
3.30	Mössbauer Spectrum of $\text{Fe}(\text{py})_4(\text{CH}_3\text{SO}_3)_2$ at 78 K ....	152
3.31	Low-temperature Mössbauer Spectra of $\text{Fe}(\text{pyz})_2(\text{NCS})_2$ .....	158
3.32	Combined Effects of Magnetic and Quadrupole Interactions .....	161
3.33	Relation Between $H_{\text{int}}$ and the E.F.G. Axis System .....	163
3.34	D.S.C. Curves for $\text{Fe}(\text{py})_4(\text{CF}_3\text{SO}_3)_2$ and $\text{Fe}(\text{py})_4(\text{CH}_3\text{SO}_3)_2$ .....	168
3.35	D.S.C. Curves for $\text{Cu}(\text{py})_4(\text{CF}_3\text{SO}_3)_2$ and $\text{Cu}(\text{py})_4(\text{CH}_3\text{SO}_3)_2$ .....	173
3.36	D.S.C. Curve for $\text{Fe}(2\text{-mepyz})_4(\text{CH}_3\text{SO}_3)_2$ .....	180
3.37	D.S.C. Curve for $\text{Cu}(\text{pyz})_4(\text{CF}_3\text{SO}_3)_2 \cdot \text{H}_2\text{O}$ .....	181

3.38	D.S.C. Curve for $\text{Fe}(\text{pyz})_4(\text{AsF}_6)_2 \cdot 2\text{H}_2\text{O}$ .....	183
4.1	Some Possible Structures of Mono(pyrazine) and Bis(pyridine) Complexes .....	186
4.2	Infrared Spectra of $\text{Fe}(\text{pyz})\text{Cl}_2$ and $\text{Fe}(\text{pyz})(\text{NCO})_2$ .....	197
4.3	Infrared Spectrum of $\text{Fe}(\text{pyz})(\text{CF}_3\text{SO}_3)_2$ .....	200
4.4	Magnetic Moments vs Temperature for $\text{Cu}(\text{pyz})(\text{CF}_3\text{SO}_3)_2$ and $\text{Cu}(\text{pyz})_4(\text{CF}_3\text{SO}_3)_2 \cdot \text{H}_2\text{O}$ .....	208
4.5	Magnetic Susceptibility vs Temperature for $\text{Cu}(\text{pyz})(\text{CF}_3\text{SO}_3)_2$ .....	209
4.6	Magnetic Moments vs Temperature for $\text{Fe}(\text{pyz})(\text{NCO})_2$ and $\text{Fe}(\text{pyz})(\text{CF}_3\text{SO}_3)_2$ .....	213
4.7	Magnetic Susceptibility vs Temperature for $\text{Fe}(\text{pyz})(\text{NCO})_2$ .....	214
4.8	Magnetic Susceptibility vs Temperature for $\text{Fe}(\text{pyz})(\text{CF}_3\text{SO}_3)_2$ .....	215
4.9	Low-temperature Mössbauer Spectra of $\text{Fe}(\text{pyz})(\text{NCO})_2$ .....	226
4.10	Possible E.F.G. Axis System for $\text{Fe}(\text{pyz})(\text{NCO})_2$ .....	232
4.11	Hyperfine Field vs Temperature for $\text{Fe}(\text{pyz})(\text{NCO})_2$ .....	233
4.12	Low-temperature Mössbauer Spectra of $\text{Fe}(\text{pyz})(\text{CF}_3\text{SO}_3)_2$ .....	237
4.13	Mössbauer Spectrum of $\text{Fe}(\text{pyz})(\text{CF}_3\text{SO}_3)_2$ at 1.60 K .....	239
4.14	D.S.C. Curve for $\text{Fe}(\text{pyz})(\text{NCO})_2$ .....	242
4.15	D.S.C. Curves for $\text{Fe}(\text{pyz})(\text{p-CH}_3\text{C}_6\text{H}_4\text{SO}_3)_2 \cdot 2\text{CH}_3\text{OH}$ and $\text{Fe}(\text{pyz})(\text{p-CH}_3\text{C}_6\text{H}_4\text{SO}_3)_2$ .....	242
5.1	Proposed Structure of $\text{Fe}(\text{RSO}_3)_2$ Compounds .....	244
5.2	Magnetic Moments vs Temperature for $\text{Fe}(\text{RSO}_3)_2$ Compounds .....	246
5.3	Magnetic Moment vs Temperature for $\text{Fe}(\text{CF}_3\text{SO}_3)_2$ .....	248
5.4	Magnetic Susceptibility vs Temperature for $\beta\text{-Fe}(\text{CH}_3\text{SO}_3)_2$ .....	250

List of Abbreviations and Symbols

triflate	:	Trifluoromethanesulfonate, $\text{CF}_3\text{SO}_3^-$
p-tosylate	:	p-Toluenesulfonate, $\text{p-CH}_3\text{C}_6\text{H}_4\text{SO}_3^-$
py	:	Pyridine
pyz	:	Pyrazine
s	:	Strong
m	:	Medium
w	:	Weak
br	:	Broad
sh	:	Shoulder
B.M.	:	Bohr Magneton
g	:	Lande splitting factor
N	:	Avagadro's number
k	:	Boltzmann's constant
$\chi_m$	:	Molar magnetic susceptibility
$\mu_{\text{eff.}}$	:	Effective magnetic moment
J	:	Exchange coupling constant
E.F.G.	:	Electric field gradient
D.S.C.	:	Differential scanning calorimetry
$T_N$	:	Néel temperature
$\delta$	:	Isomer shift
$\Delta E_q$	:	Quadrupole splitting
$\Gamma$	:	Mössbauer linewidth
Anal. Calcd	:	Analysis calculated

Acknowledgements

I would like to express sincerest thanks to my research directors Dr. R.C. Thompson and Dr. J.R. Sams for the enlightening discussions throughout the last four years. Thanks go to Dr. F. Aubke for his constructive remarks during the final preparation of this thesis.

The research described in this thesis would have been rendered painstakingly slow if it were not for the technical expertise of the mechanical, electronic and glassblowing shops. In particular, many thanks go to M. Vagg whose ingenuity was tested many times by the vibrating sample magnetometer.

Many thanks go to Dr. S.J. Rettig for the crystal structure determinations, A. Sallos for processing Mössbauer data, P. Borda for his microanalytical services and to Dr. I. Thorburn and L. Gradnitzer for their proof-reading abilities.

Financial aid from the U.B.C. Graduate Scholarship Committee is gratefully acknowledged.

I would like to express a special thank you to Louisa Gradnitzer whose many words of encouragement during the last four years extended well beyond the call of duty.

## CHAPTER 1

### INTRODUCTION

#### 1.1 GENERAL INTRODUCTION

In recent years, there has been an increasing interest shown by both physicists and chemists in the solid-state properties of low-dimensional materials.<sup>1</sup> Low dimensionality is ascribed to substances that exhibit large, anisotropic ratios in some of their physical properties. Chemists have been involved in the synthesis of a diverse range of such compounds whose electrical, magnetic, optical, as well as structural and chemical properties have been evaluated. The use of a wide array of techniques to classify these compounds has permitted structure-property relationships to be examined in an attempt to provide a rational approach to the design of new materials having specific properties. To a large degree, however, the ability to perform such custom design of materials with predictable magnetic and electrical properties still lies in the future.

The types of compounds which have been studied are varied, and range from compounds of an organic nature to inorganic coordination polymers. Examples of polymeric organic compounds include donor-acceptor complexes, the so-called organic metals,<sup>2</sup> such as tetrathiafulvalene-tetracyanoquinodimethane (TTF-TCNQ), where both the donors and acceptors are arranged in stacks to form pseudo-one-dimensional conductors; polyacetylenes<sup>3</sup> comprise

another class of organic polymers and the linear chain polysulfurnitride complexes<sup>4</sup> provide an inorganic example. Intercalation compounds of linear chain compounds, for example, polymeric (SN)<sub>x</sub><sup>5</sup> as well as two-dimensional layer materials such as graphite,<sup>6</sup> FeOCl,<sup>7</sup> and the group 4 and 5 metal chalcogenides, for example, TiS<sub>2</sub>,<sup>8</sup> and TaS<sub>2</sub>,<sup>9</sup> are currently being investigated in an attempt to modify the host lattice by the presence of a suitable intercalant. The intercalation of lithium into layered dichalcogenides has led to the recent development of a new, high-energy density, rechargeable battery.<sup>10</sup>

Inorganic polymers have been studied for over a century. In 1842, K<sub>2</sub>Pt(CN)<sub>4</sub>Cl<sub>0.3</sub>.xH<sub>2</sub>O was first synthesised,<sup>11</sup> and was later found to possess a high conductivity, and in 1968 an X-ray structure determination revealed it to be a linear chain polymer.<sup>12</sup> More recently, inorganic polymers have been prepared from a wide range of transition metals and ligands; for example, transition-metal complexes of porphyrins, phthalocyanines and glyoximes have been found to exhibit interesting conduction, electrical and optical properties.<sup>13</sup> Inorganic coordination polymers may also be formed by utilising anions with the ability to bridge metal centres. Examples of this type include phosphinates, R<sub>2</sub>PO<sub>2</sub><sup>-</sup>,<sup>14</sup> where the anions bridge metal atoms to form linear chains, and phosphate<sup>15</sup> and sulfonate complexes,<sup>16</sup> in which RPO<sub>3</sub><sup>2-</sup> and RSO<sub>3</sub><sup>-</sup> anions have the potential to bridge three metal centres to form two-dimensional layered structures.

A common feature of these inorganic coordination polymers is that metal ions are much more closely spaced in some

directions than others. In the case of transition-metal coordination polymers, the metal ions are separated from each other by either  $\sigma$ - or  $\sigma$ - and  $\pi$ -bonded fragments. These intervening groups are found to influence the magnetic properties of the complex, and give rise to the so-called superexchange effects. At the present time, there is a wide interest in compounds which exhibit these magnetic exchange phenomena. Initially, coordination chemists investigated simple magnetic exchange interactions and the dimeric copper(II) carboxylates<sup>17, 18</sup> were among the first to be extensively studied. In recent years, researchers have studied empirically the variation of the exchange constant,  $J$ , with bond lengths and angles in a variety of dimers, trimers, and small clusters, as well as in polymeric materials. For example, in a series of planar bis- $\mu$ -hydroxo copper(II) dimers Crawford et al.<sup>19</sup> demonstrated that the exchange coupling varies linearly with the Cu-O-Cu angle and that the exchange changes from ferromagnetic to antiferromagnetic as the bridging angle is increased. Other factors, such as the stereochemistry around the metal and the nature of non-bridging ligands, are also important in determining magnetic exchange interactions.

The coordination chemist can interpret magnetic susceptibility data by using models for magnetic exchange developed primarily by physicists. In this way, progress in understanding the chemistry and physics associated with low-dimensional materials has involved the collaboration of chemists, physicists and material scientist alike.



Extensive research has been carried out in this laboratory on transition-metal phosphinate and sulfonate compounds in an attempt to correlate their structural and magnetic properties. It was found in the case of the linear chain copper(II) dialkylphosphinates<sup>14, 20-21</sup> that two types of distortion of the  $\text{CuO}_4$  chromophore are possible and it is this distortion which plays an important role in determining the nature of the magnetic exchange interaction. For the complexes  $\text{Cu}(\text{R}_2\text{PO}_2)_2$ , where R is n-octyl, n-decyl or n-dodecyl,<sup>21</sup> two structural modifications have been isolated and magnetic susceptibility measurements at low temperatures have distinguished these two forms. The  $\alpha$  modifications are antiferromagnetic, whereas, the  $\beta$  isomers are ferromagnetic; the superexchange interaction is propagated through the O-P-O bridges. Studies on the anhydrous and hydrated dimethylphosphinates of manganese(II)<sup>22</sup> indicate that strong antiferromagnetic exchange interactions are also present in the anhydrous species. Conversely, in the dihydrate,  $\text{Mn}((\text{CH}_3)_2\text{PO}_2)_2 \cdot 2\text{H}_2\text{O}$ , a temperature-independent magnetic moment has been observed. An X-ray structure determination of the dihydrate revealed the existence of a strong hydrogen-bonding network linking the chains together, and it is thought that this effectively dampens magnetic exchange in this material.

The transition-metal sulfonate compounds,  $\text{M}(\text{RSO}_3)_2$  are thought to adopt a polymeric two-dimensional layered structure, as has been found for  $\text{Ca}(\text{CH}_3\text{SO}_3)_2$ .<sup>16</sup> No X-ray structural data exist for the anhydrous iron(II) sulfonates,  $\text{Fe}(\text{RSO}_3)_2$ , where R is F,  $\text{CF}_3$ ,  $\text{CH}_3$  or  $p\text{-CH}_3\text{C}_6\text{H}_4$ ; however, application of a

combination of techniques, the so-called "sporting methods", has enabled the structures of the complexes to be proposed.<sup>23-25</sup> The techniques of infrared, Mössbauer and electronic spectroscopy indicate a distorted  $\text{FeO}_6$  chromophore with each sulfonate anion bridging to three different metal centres resulting in a two-dimensional lattice.  $\text{Fe}(\text{CH}_3\text{SO}_3)_2$  exists in two forms and the  $\beta$  isomer has been shown by Mössbauer spectroscopy to undergo a transition to an antiferromagnetically-ordered state;<sup>26</sup> presumably the superexchange in this material is via the O-S-O bridging units. The other iron(II) sulfonate compounds are magnetically dilute.

Several conclusions may be drawn from these earlier studies on phosphinates and sulfonates which are applicable to this study. The combination of X-ray structure determinations and magnetic susceptibility measurements is important if meaningful conclusions are to be drawn concerning the nature of the bridging ligand, the metal chromophore and the effects of these on superexchange. In the absence of X-ray diffraction studies, it is important to examine a large number of closely related complexes by a variety of physical techniques in order to correlate magnetic and structural properties. Finally, magnetic susceptibility measurements have to be made at low temperatures in order to probe weak exchange interactions often observed in multi-atom bridges.

## 1.2 OBJECTIVES, PREVIOUS WORK AND SCOPE OF THE THESIS

This section provides the main objectives of the present study and outlines previous research in the field of transition-metal pyrazine chemistry. An overview of the research carried out in the current study is also given.

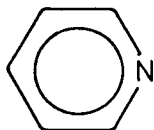
One objective was to synthesise inorganic coordination polymers of divalent iron and copper. The strategy adopted to induce polymer formation was to use both nitrogen donor atoms of pyrazine (1,4-diazine, Fig. 1.1) to bridge metal centres.

Fig. 1.1 Pyrazine and Pyridine

1,4-Diazine  
Pyrazine, pyz



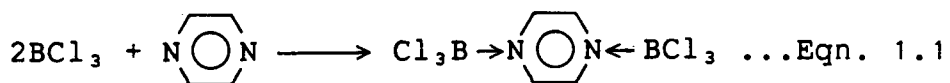
Azine  
Pyridine, py



Several of the anionic ligands used in the present study also have the ability to act as multidentate groups and to bridge metal centres. For example, the sulfonate ligands,  $\text{RSO}_3^-$ , can coordinate through more than one of the oxygen donor atoms. The complexes were characterised by a variety of spectroscopic techniques and in some instances structure was determined by X-ray crystallography. The objective of these spectroscopic and X-ray studies was to identify the metal chromophore and the nature of the bridging ligand system. Once these factors were

elucidated, a primary aim of the research was to investigate the magnetic properties of the materials and to probe magneto-structural correlations.

When the basicities of the two nitrogen atoms of pyrazine (pK<sub>a</sub> values of 0.6 and -6.0 respectively<sup>27, 28</sup>) were taken into account, it was initially thought that the ability of pyrazine to use both nitrogen atoms in a bridging fashion would be rather poor. For comparison, the basicity of the single nitrogen atom of pyridine (azine, Fig. 1.1) is considerably higher as measured by its pK<sub>a</sub> value of 5.2.<sup>29</sup> These observations, combined with the fact that experimentally it is found that pyrazine only quaternises at one nitrogen atom,<sup>30</sup> suggested that the second nitrogen of pyrazine is deactivated after the first is protonated. Experimental evidence, however, indicates that pyrazine often uses both nitrogen atoms when it reacts with Lewis acids. For example, the bis(pyrazine) adduct is formed upon reaction of pyrazine with two moles of boron trichloride (Eqn. 1.1).<sup>31</sup>

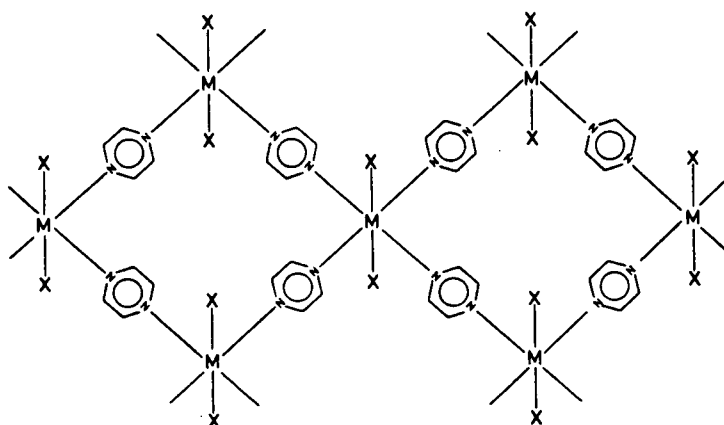


In the early 1960's, Lever, Lewis and Nyholm were the first to investigate a series of pyrazine and methyl-substituted pyrazine complexes of cobalt-, nickel- and copper halides.<sup>31-34</sup> They were particularly interested in a comparison with the well characterised pyridine analogues,<sup>35, 36</sup> and used room-temperature magnetic susceptibility measurements and ultraviolet-visible and infrared spectroscopy as a means of probing the nature of the

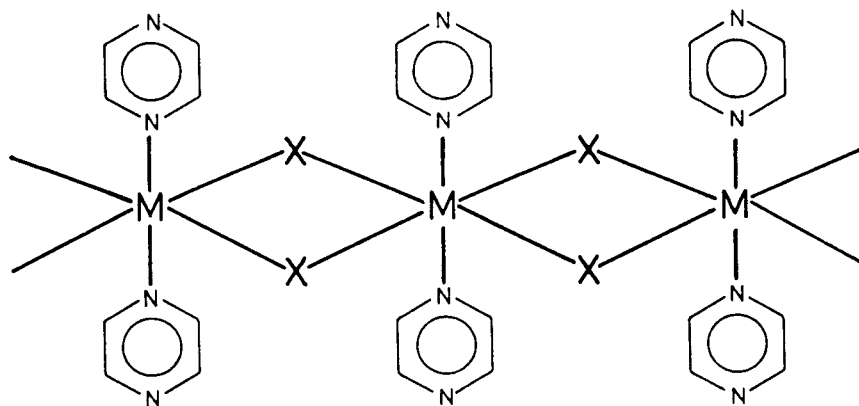
metal chromophore. Their initial studies on metal-pyrazine halide complexes concluded that polymeric systems were indeed formed, however, there was debate as to whether the polymers contained bridging pyrazine and terminal halide anions or terminal pyrazine ligands and bridging halide anions (Fig. 1.2).

Fig. 1.2 Two Possible Structures for  $M(\text{pyz})_2\text{X}_2$  Complexes

a). Two-Dimensional Layer



b). Linear Chain



Infrared spectral results for these complexes caused confusion regarding the mode of pyrazine coordination and both bidentate bridging and terminal modes were proposed.<sup>31-34, 37-39</sup> An X-ray structure determination of  $\text{Co}(\text{pyz})_2\text{Cl}_2$ <sup>40</sup> proved definitive and shows pyrazine to be bridging to form a polymeric two-dimensional lattice with trans-oriented terminal chloride anions. Other studies have demonstrated the ability of pyrazine to link metals to form chains (as in  $\text{Ag}(\text{pyz})\text{NO}_3$ <sup>41</sup> and  $\text{Cu}(\text{pyz})(\text{NO}_3)_2$ <sup>42</sup>) and to form layer compounds (as in  $\text{Cu}(\text{pyz})_2(\text{ClO}_4)_2$ <sup>43</sup>). After the initial debate, it was concluded that a combination of infrared and Raman spectroscopy provides definite criteria for the mode of pyrazine coordination in such complexes.<sup>44</sup>

A bridging pyrazine molecule is also present in the extensively studied Creutz-Taube complex,<sup>45, 46</sup>  $[(\text{NH}_3)_5\text{Ru}(\text{pyz})\text{Ru}(\text{NH}_3)_5]^{5+}$ ; there is still, however, conflicting evidence concerning the electronic structure of this mixed-valence ion.<sup>47</sup>

Pyrazine-bridged complexes are of interest to magnetochemists as they represent examples of materials which may exist as one-dimensional linear chains or two-dimensional lattices with the possibility of magnetic exchange interactions propagating through the bridging pyrazine system. The most extensive series of pyrazine complexes investigated have been derivatives of copper(II). Copper(II) chloride and bromide complexes have been synthesised with a series of mono- and dimethyl-substituted pyrazine ligands;<sup>48</sup> all exhibit a maximum

in the magnetic susceptibility versus temperature curve, indicative of antiferromagnetic interactions. In these initial studies, however, the infrared data were interpreted as indicating the presence of terminal pyrazine ligands and it was suggested that the exchange occurred through bridging halide anions rather than through bridging pyrazine ligands. In 1971, Villa and Hatfield<sup>49</sup> established pyrazine as a ligand capable of transmitting magnetic information in the nitrate complex,  $\text{Cu}(\text{pyz})(\text{NO}_3)_2$ . Previous researchers<sup>42</sup> found that bridging pyrazine leads to a linear chain structure in this complex and although the copper ions are separated by nearly 7 Å, a maximum is observed in the magnetic susceptibility data as a result of superexchange via the bridging pyrazine groups. The single-crystal magnetic susceptibility data have been fit to the Heisenberg linear chain model.<sup>50</sup>

The superexchange mechanism in polymeric, pyrazine-bridged copper(II) complexes of the type  $\text{CuL}(\text{NO}_3)_2$ , was investigated by using a variety of substituted pyrazine ligands, L.<sup>51</sup> Richardson and Hatfield elegantly demonstrated that the variation in antiferromagnetic coupling correlates neither with the  $\sigma$ -basicity nor with steric factors associated with the ligand but with the energy of the  $\pi-\pi^*$  transition of the pyrazine ligand, L in the complex. These results indicate the presence of an exchange mechanism involving the pyrazine  $\pi$ -system.

The importance of the pyrazine  $\pi$ -system in propagating magnetic exchange interactions has been further demonstrated through the use of magnetic measurements on two copper(II)

dimers of the type  $[\text{Cu}_2(\text{tren})_2\text{L}](\text{ClO}_4)_4$ ,<sup>52</sup> (where tren is 2,2',2''-triaminotriethylamine). One complex, containing pyrazine as the bridging ligand, L, shows magnetic exchange interactions; whereas, in the second dimer, where L is DABCO (DABCO is 1,4-diazobicyclo[2.2.2]octane), no magnetic exchange interactions are observed. The lack of a  $\pi$ -system in DABCO has been proposed to account for the magnetic properties of this compound.

Another important factor in determining the nature of the magnetic exchange interactions in copper(II) pyrazine complexes has been found to be the overlap between the copper d-orbitals and the pyrazine  $\pi$ -system. This interaction is influenced by the degree of tilting of the pyrazine ring with respect to the xy coordination plane. For example, in  $\text{Cu}(\text{pyz})(\text{NO}_3)_2$ ,<sup>42</sup> this angle is  $48^\circ$  and orbital overlap between the pyrazine  $\pi$ -system and the  $d_{x^2-y^2}$  ground state of copper is possible, resulting in an effective route for magnetic exchange interactions. However, in  $\text{Cu}(\text{pyz})(\text{hfac})_2$ ,<sup>53</sup> (where hfac is hexafluoropentane-1,4-dionate) a linear chain structure results from pyrazine bridging between the square-planar  $\text{Cu}(\text{hfac})_2$  units, with pyrazine coordinating along the direction of the z-axis. There is no effective  $\pi$ -orbital overlap between pyrazine and the copper  $d_{x^2-y^2}$  ground state, and no magnetic exchange interactions are observed.<sup>54</sup>  $\text{Cu}_2(\text{OAc})_4(\text{pyz})$ , (where OAc is acetate) is another copper-pyrazine system which has been investigated. The structure consists of copper acetate dimers linked in a linear chain through bridging pyrazine groups.<sup>55</sup> An



alternating-dimer model has been proposed with strong intradimer exchange through bridging acetate ligands,  $J = -325 \text{ cm}^{-1}$ , and weak interdimer exchange through bridging pyrazine,  $J = -0.1 \text{ cm}^{-1}$ .<sup>56</sup>  $\text{Cu}(\text{pyz})_2(\text{ClO}_4)_2$  has been shown to exist as a two-dimensional sheet-like polymer<sup>43</sup> in which the bridging pyrazine groups are canted at an angle of  $66.1^\circ$  to the  $\text{CuN}_4$  plane; in this orientation pyrazine provides an effective route for antiferromagnetic exchange interactions.

Pyrazine complexes of other transition metals have also been investigated; for example, the lanthanide ytterbium forms the dimer,  $(\eta^5\text{-Cp}_3\text{Yb})_2(\text{pyz})$ .<sup>57</sup> In this complex there is no evidence of magnetic interactions even at temperatures as low as 3 K and formulation of the bonding as largely ionic is proposed to account for this situation. Investigations on cobalt(II) pyrazine halides,  $\text{Co}(\text{pyz})_2\text{X}_2$ ,<sup>58</sup> (where  $\text{X}^-$  is  $\text{Cl}^-$  or  $\text{Br}^-$ ), over the temperature range 1.8–300 K, show no evidence for magnetic interactions. Similarly, for the nickel(II) derivatives,  $\text{Ni}(\text{pyz})_2\text{X}_2$ ,<sup>37</sup> (where  $\text{X}^-$  is  $\text{Cl}^-$ ,  $\text{Br}^-$  or  $\text{I}^-$ ), a temperature-independent magnetic moment is observed between 90 and 300 K. Evidence for magnetic exchange, however, has been found in the silver(II) complex,  $\text{Ag}(\text{pyz})_2\text{S}_2\text{O}_8$ ; in this case the magnetic moment is observed to decrease from 1.61 B.M. at room temperature to 1.27 B.M. at 80 K.<sup>59</sup>

The studies described above clearly demonstrate the ability of pyrazine to form inorganic coordination polymers with a variety of anions and transition metals. For these complexes low-temperature magnetic susceptibility measurements yield

valuable information regarding the nature of the spin system and the magnitude of the magnetic exchange. Relatively little research has been undertaken on iron(II) complexes of pyrazine, a fact which may be due to the problems associated with the relative ease of oxidation of iron(II) to iron(III), and to the difficulties in analysing magnetic susceptibility data in iron(II) systems. The present study includes the synthesis and characterisation of some iron(II) pyrazine complexes.

Previous work on the iron(II) pyrazine halides involved the preparation of  $\text{Fe}(\text{pyz})\text{Cl}_2$ ,<sup>60</sup>  $\text{Fe}(\text{pyz})_2\text{Cl}_2$ ,<sup>61</sup> and  $\text{Fe}(\text{pyz})_2\text{Br}_2$ ,<sup>62</sup> and a hydrate,  $\text{Fe}(\text{pyz})_2\text{Cl}_2 \cdot \text{H}_2\text{O}$ .<sup>62</sup> Characterisation of these complexes has included thermal studies,<sup>61</sup> infrared spectroscopy,<sup>60, 62, 63</sup> and room-temperature magnetic susceptibility measurements.<sup>62</sup> The pseudohalide complex,  $\text{Fe}(\text{pyz})_2(\text{NCS})_2$ ,<sup>64</sup> has been reported, but no synthetic procedure was given and the sole method of characterisation involved magnetic susceptibility measurements in the 80-300 K temperature region. In the case of pyrazine complexes, the magnitude of  $J$ , the exchange coupling parameter, is likely to be small, and hence, it is important that low-temperature magnetic studies are carried out. The synthesis of the complex  $\text{Fe}(\text{pyz})_2(\text{ClO}_4)_2 \cdot 2\text{H}_2\text{O}$ <sup>60</sup> has also been reported, however, characterisation involved only vibrational assignments in the mid-infrared region (140-500  $\text{cm}^{-1}$ ). An X-ray structure determination has shown pyrazine to bond in a unidentate fashion in  $\text{Fe}(\text{CO})_4(\text{pyz})$ ;<sup>65</sup> whereas, a linear chain polymer is formed through bridging pyrazine in  $\text{Fe}(\text{pyz})(\text{dmg})_2$  (where  $\text{dmg}$  is

dimethylglyoximate).<sup>66</sup>

In the present study, two groups of pyrazine complexes have been prepared and characterised in an attempt to correlate their magnetic and structural properties. The first group are the iron(II) pyrazine halide and pseudohalide complexes and comprises the following:  $\text{Fe}(\text{pyz})_n\text{X}_2$ , where  $n$  is 1 and  $\text{X}^-$  is  $\text{Cl}^-$  and  $\text{NCO}^-$ ; and where  $n$  is 2 and  $\text{X}^-$  is  $\text{Cl}^-$ ,  $\text{Br}^-$ ,  $\text{I}^-$  and  $\text{NCS}^-$ . The feature common to compounds of the second group is a sulfonate anion,  $\text{RSO}_3^-$ , where  $\text{R}$  is either  $\text{CF}_3$ ,  $\text{CH}_3$  or  $p\text{-CH}_3\text{C}_6\text{H}_4$ . Complexes of this group which have been investigated are represented by various stoichiometries,  $\text{M}(\text{pyz})_n(\text{RSO}_3)_2$ , where  $\text{M}$  is Fe or Cu and  $n$  is either 1, 2 or 4.

Magnetic susceptibility results for iron(II) complexes are usually more difficult to interpret than those of analogous copper(II) systems. For example, the observation of a significantly temperature-dependent magnetic moment for a copper(II) species is indicative of magnetic exchange interactions, and in these  $S=1/2$  systems the magnetic exchange effects can often be modelled in terms of an isotropic Heisenberg exchange Hamiltonian. Conversely, a temperature-dependent magnetic moment is usually observed in the case of high-spin iron(II) compounds even in the absence of magnetic concentration. A temperature dependence arises from either the ground-state orbital degeneracy and/or zero-field splitting effects of an  $S=L=2$  ion. In high-spin iron(II) complexes, the problem is to distinguish single-ion effects from magnetic exchange interactions.

An attempt was made to surmount this problem in the present study, by comparing the magnetic properties of the pyrazine complexes with those of the analogous pyridine derivatives. Pyridine (Fig. 1.1) cannot act as a bridging ligand and in these complexes single-ion effects are expected to determine the magnetic properties. The pyridine halide and pseudohalide complexes,  $\text{Fe(py)}_n\text{X}_2$ , (where  $n$  is 2 and 4 and  $\text{X}^-$  is  $\text{Cl}^-$ ,  $\text{Br}^-$ ,  $\text{I}^-$ ,  $\text{NCO}^-$  and  $\text{NCS}^-$ ) have been prepared previously and investigated by a variety of techniques, including Mössbauer, infrared and electronic spectroscopy and magnetic susceptibility measurements.<sup>67</sup> The molecular structures of  $\text{Fe(py)}_4\text{Cl}_2$ <sup>68</sup> and  $\text{Fe(py)}_4(\text{NCS})_2$ <sup>69</sup> have been determined by single-crystal X-ray diffraction. Both of these compounds have octahedral coordination about the metal involving a square-planar arrangement of nitrogen atoms and the anions occupy axial coordination sites. No magnetic exchange effects are observed in these tetrakis(pyridine) complexes, as expected for systems in which the paramagnetic centres are isolated from each other.<sup>67</sup> In contrast, the corresponding bis(pyridine)iron(II) halide and pseudohalide derivatives are proposed to be polymeric and contain bridging anions; the chloride and thiocyanate derivatives exhibit magnetic moments which increase with decreasing temperature; a result of ferromagnetic exchange interactions propagating through the bridging anions.<sup>70-73</sup>

The present study provides a comparison between the magnetic and structural properties of the bis- and tetrakis(pyridine)iron(II) halide and pseudohalide complexes and

the corresponding mono- and bis(pyrazine)iron(II) derivatives. A similar comparison involving the  $M(\text{pyz})_n(\text{RSO}_3)_2$  complexes required the synthesis and characterisation of the analogous tetrakis(pyridine) complexes,  $M(\text{py})_n(\text{RSO}_3)_2$ , where M is Fe or Cu.

The final part of this study involved measuring the magnetic properties of the anhydrous sulfonate compounds,  $\text{Fe}(\text{RSO}_3)_2$ , (where R is F,  $\text{CF}_3$ ,  $\text{CH}_3$ , and  $p\text{-CH}_3\text{C}_6\text{H}_4$ ) in order to further investigate magnetic interactions through the O-S-O bridging unit. These complexes have been previously studied in this laboratory;<sup>23-26</sup> the proposed structure involves a two-dimensional layered array, with each anion bonded to three different metal centres. Magnetic interactions are possible through the O-S-O bridging units and for  $\beta\text{-Fe}(\text{CH}_3\text{SO}_3)_2$  these interactions have been observed by Mössbauer spectroscopy.<sup>26</sup> Our earlier research on these compounds involved the measurement of magnetic properties to 80 K;<sup>25</sup> in the present study, additional magnetic susceptibility measurements were made at lower temperatures to further investigate the possibility of magnetic exchange and to corroborate the low-temperature Mössbauer spectral data.

### 1.3 METHODS OF COMPOUND CHARACTERISATION

The measurement of the magnetic susceptibilities of the complexes was one of the main focal points of this study. For magneto-structural correlations to be made a range of spectroscopic tools was required. These techniques are now

briefly introduced.

The magnetic properties of transition-metal compounds, when recorded as a function of temperature, provide information on the nature of the ground state of the metal. The magnitude and temperature dependence of the magnetic moment data of magnetically-dilute complexes are determined by several factors, for example, d-orbital occupancy and degeneracy, ligand-field symmetry, spin-orbit coupling and electron-delocalisation effects. The theory of magnetic susceptibility of transition-metal complexes is well covered in several texts.<sup>74</sup> In magnetically-concentrated systems, the factors mentioned above are also present, and any magnetic interaction is superimposed upon these single-ion phenomena. Qualitatively, magnetic exchange interactions may be thought of as arising from unpaired spin densities on neighbouring paramagnetic centres being aligned either parallel or opposed to each other, resulting in ferromagnetism or antiferromagnetism respectively. Magneto-structural correlations emphasise the importance of the stereochemistry around the metal, the efficiency of metal-ligand orbital overlap, the geometry of the bridging ligands, the type of substituent on the bridging group and the nature of any non-bridging ligands. The theoretical aspects of magnetic exchange interactions in transition-metal compounds and the models used to interpret the empirical data have been the subject of extensive investigations.<sup>75</sup> Some of the mathematical relations developed in previous studies are used in this study to model the magnetic susceptibility data.

In order for magneto-structural correlations to be made, structure determinations by X-ray crystallography are particularly relevant. This technique provides precise details of bond lengths and angles, and establishes the exact nature of the bridging system and the arrangement of non-bridging ligands. In the present study, several materials were obtained in a crystalline form and the crystal and molecular structures were solved. From these data the interactions between the metal, neutral ligands and anions have been investigated.

One distinct advantage of iron-containing compounds is that  $^{57}\text{Fe}$  exhibits a Mössbauer resonance. Mössbauer spectroscopy is capable of elucidating the electronic properties about the iron centre. From a Mössbauer spectrum two chemically important parameters are obtained, namely, the isomer shift and quadrupole splitting. The isomer shift is determined by the total s-electron density at the nucleus and has been found to be useful in determining the oxidation state of the metal.

The ability to measure quadrupole splittings is one of the more useful features of Mössbauer spectroscopy; The quadrupole splitting is related to the electric field gradient (E.F.G.) at the iron nucleus, established when the distribution of the surrounding electrons and/or ligands has lower than cubic symmetry. In the case of  $^{57}\text{Fe}$ , a transition occurs between the ground state ( $I=1/2$ ) and the excited state ( $I=3/2$ ) of the iron nucleus. The presence of a quadrupole interaction results in the splitting of the excited state and Mössbauer transitions occur between the singly-degenerate ground state and the

doubly-degenerate excited state.

Mössbauer spectroscopy is a powerful technique for probing the nature of magnetic exchange interactions, particularly when the interactions result in a transition to a magnetically-ordered state. In such a system the nuclear energy levels are split further to produce a complex magnetic hyperfine spectrum. It has been in this manner that magnetic exchange interactions have been observed for  $\beta$  iron(II) methanesulfonate in this laboratory.<sup>26</sup> The combined uses of Mössbauer spectroscopy and magnetic susceptibility measurements are complementary for probing magnetic interactions.

The thermal properties of materials can be measured by differential scanning calorimetry (D.S.C.). This technique, when applied to transition-metal complexes, provides a means of determining thermal stabilities. Enthalpies and temperatures at which chemical and physical changes occur can also be established quantitatively by such measurements. In addition, thermolysis has been shown to be a valuable preparative technique; for example, some bis(pyridine)iron(II) halide and pseudohalide complexes have been prepared from the corresponding tetrakis(pyridine) complexes by thermolysis.<sup>67</sup> In the present study, differential scanning calorimetry has proven a useful aid to synthesis by assessing the feasibility of a particular thermolysis reaction.

The use of D.S.C. combined with thermogravimetric analysis (T.G.A.) allows reactions to be monitored not only by changes in enthalpy but also by the weight changes associated with a



thermolysis reaction. In this study, a T.G.A. accessory was not available; however, improvised T.G.A. experiments were performed and this method has provided information concerning the intermediates produced during thermolysis.

The coordination geometry of transition-metal complexes can be determined from the number of absorptions and their frequencies in the ultra-violet and visible regions of the electromagnetic spectrum. Electronic absorption spectroscopy has been used throughout the study as a means of probing the ligand-field environment of the central metal ion. The correlations between the spectra and the chromophore were especially important when the nature of the chromophore had been determined by X-ray crystallography; the results obtained for complexes of known structures were then extended to probe the nature of the chromophore in compounds of undetermined structures.

Vibrational spectroscopy plays a role in structure determination as well. Infrared spectroscopy provides information on the coordination of neutral and anionic ligands through the analysis of the number of diagnostic bands and their energies. Infrared criteria have been developed to determine the mode of sulfonate anion coordination.<sup>23, 76</sup> In the case of the neutral ligands employed here, coordinated pyridine exhibits significant shifts in the positions of several bands when compared to free pyridine<sup>77</sup> and the infrared spectra of pyrazine and its complexes are particularly applicable for assigning either a unidentate or bidentate bridging mode of coordination.

Free pyrazine and coordinated bidentate pyrazine possess a centre of symmetry, hence, the infrared and Raman bands are mutually exclusive. By coordination through only one nitrogen atom, however, the symmetry in terminally coordinated pyrazine ligands is reduced to at least  $C_{2v}$  and some of the Raman active modes become infrared active.<sup>44</sup> The infrared spectral results obtained in the present study were then used in conjunction with X-ray structural data to support the use of infrared criteria in assessing the nature of anion and ligand coordination modes.

Elemental analyses of C, H, N, and in some cases O, were obtained routinely as a means of determining the stoichiometry and purity of the complexes isolated.

#### 1.4 ORGANISATION OF THE THESIS

The iron(II) and copper(II) complexes prepared in the present study contain chromophores with a combination of N and X donor sets (where N is from pyrazine or pyridine, and X arises from a halide, pseudohalide, sulfonate or perchlorate anion). For these complexes, the chromophore is either  $MN_4X_2$  or  $MN_2X_4$  and the complexes containing these chromophores are discussed separately in Chapters 3 and 4 respectively. In some cases the chromophore was clearly identified by an X-ray structure determination. In the absence of such conclusive evidence, the classification was based upon spectroscopic methods, for example, infrared, Mössbauer and electronic spectroscopy.

Chapters 3 and 4 are similarly organised. Each chapter begins with a discussion of the experimental procedures used for

the preparation of the complexes. Following this, the results arising from the characterisation are presented and interpreted, and a brief summary is given at the end of each section. General experimental procedures and techniques are described in Chapter 2. Results of magnetic susceptibility measurements performed on the anhydrous iron(II) sulfonate compounds are presented in Chapter 5. In Chapter 6, a classification of complexes based upon their magnetic and structural properties is given and some general conclusions are presented.

## CHAPTER 2

### EXPERIMENTAL PROCEDURES

#### 2.1 GENERAL SYNTHETIC METHODS

All chemicals used in this study were at least of reagent grade quality and obtained from commercial sources. Solvents were dried prior to use by the following procedures. Methanol and ethanol were refluxed in the presence of the corresponding magnesium alkoxide, diethyl ether was refluxed over sodium benzophenone ketyl, acetonitrile and dichloromethane were refluxed in the presence of calcium hydride, acetone was refluxed in the presence of potassium carbonate, and pyridine was refluxed over barium oxide. After drying, solvents were distilled under a dry nitrogen atmosphere. Most iron(II) compounds prepared were air- and moisture-sensitive and hence care was taken to avoid their exposure to the atmosphere. Standard vacuum-line techniques for the manipulation of air-sensitive compounds were used;<sup>7,8</sup> in addition, compounds were handled in an inert nitrogen atmosphere dry box, (D.L. Herring Corporation Dri-Lab (model HE-43)) equipped with a dry train (model HE-93). These precautions were found to be unnecessary for the preparation of the copper(II) compounds.

## 2.2 PHYSICAL EXPERIMENTAL TECHNIQUES

### 2.2.1 Infrared Spectroscopy

Infrared spectra were recorded on samples mulled in Nujol sandwiched between KRS-5 plates (58% TlI, 42% TlBr, Harshaw Chemical Co.). A Perkin Elmer model 598 spectrophotometer was used in the region of 250-4000  $\text{cm}^{-1}$ . All spectra were calibrated by using a polystyrene film (907 and 1601  $\text{cm}^{-1}$ ). Tabulated frequencies are considered accurate to  $\pm 5 \text{ cm}^{-1}$  for broad bands and  $\pm 2 \text{ cm}^{-1}$  for sharp bands.

### 2.2.2 Electronic Spectroscopy

Solid-state electronic spectra were obtained at room temperature by using Nujol mulls pressed between silica glass windows. A Cary model 14 spectrophotometer was used over the frequency range of 4,000-30,000  $\text{cm}^{-1}$ . Due to the broad nature of these absorptions, electronic spectral frequencies quoted are considered accurate to  $\pm 200 \text{ cm}^{-1}$ .

### 2.2.3 Magnetic Susceptibility Measurements

Three techniques were used to measure magnetic susceptibilities. Routine temperature-dependent studies from 4.2-130 K were made using a Princeton Applied Research model 155 vibrating sample magnetometer.<sup>20</sup> A magnetic field of 7.50 or 9.63 T was employed for the iron(II) and copper(II) complexes respectively. Magnetic fields were set to an accuracy of 0.5% and measured by using an F.W. Bell model 620 gaussmeter.

Accurately weighed samples of approximately 100 mg, contained in gelatin capsules, were attached to a Kel-F holder with an epoxy resin. Corrections were made for the diamagnetic background of the holder. Ultrapure nickel metal was used to calibrate the instrument. Temperature measurement was achieved with a chromel versus Au-0.02% Fe thermocouple<sup>7,9</sup> located in the sample holder immediately above the sample. The thermocouple was calibrated by using the known susceptibility versus temperature behaviour of tetramethylenediammonium tetrachlorocuprate(II) and checked with mercury(II) tetrathiocyanatocobaltate(II).<sup>80</sup> From the scatter in the data points from four separate calibrations, the temperatures are estimated to be accurate to  $\pm 1\%$  over the range studied, 2-130 K. The accuracy of the magnetic susceptibility values as measured by this technique is estimated to be  $\pm 1\%$ .

A Gouy balance<sup>81</sup> was used in the temperature region 80-300 K to measure the magnetic susceptibility of the iron(II) complexes. Samples were packed in a Pyrex tube which had been previously calibrated to correct for its diamagnetism. Measurements were made in a nitrogen atmosphere at a magnetic field strength of 0.45 T.  $\text{HgCo}(\text{NCS})_4$  was again used as a calibrant.<sup>80</sup> The accuracy of the magnetic susceptibility values obtained using the Gouy method is estimated as approximately  $\pm 5\%$ .

A Faraday balance<sup>82</sup> was used to measure magnetic susceptibilities at room temperature, free from any packing error. The Gouy method is prone to such errors. Measurements were made at magnetic field gradients of 0.0253, 0.0526 and

0.0869 T<sup>2</sup> cm<sup>-1</sup> in the case of the iron(II) complexes, and for the copper(II) species measurements were made only at the two higher field gradients. The accuracy of the magnetic susceptibility values obtained by this technique is better than  $\pm 1\%$ .

Molar magnetic susceptibilities were corrected for the diamagnetism of the metal ions and ligands.<sup>83</sup> The diamagnetic corrections (units of 10<sup>-6</sup> cm<sup>3</sup> mol<sup>-1</sup>) are: Fe<sup>2+</sup>, 13; Cu<sup>2+</sup>, 11; CF<sub>3</sub>SO<sub>3</sub><sup>-</sup>, 46; CH<sub>3</sub>SO<sub>3</sub><sup>-</sup>, 35; p-CH<sub>3</sub>C<sub>6</sub>H<sub>4</sub>SO<sub>3</sub><sup>-</sup>, 89; AsF<sub>6</sub><sup>-</sup>, 97; NCO<sup>-</sup>, 21; NCS<sup>-</sup>, 35; ClO<sub>4</sub><sup>-</sup>, 34; Cl<sup>-</sup>, 26; Br<sup>-</sup>, 36; I<sup>-</sup>, 52; H<sub>2</sub>O, 13; CH<sub>3</sub>OH, 34; pyridine, 49; pyrazine, 45; 2-methylpyrazine, 57. In addition, the copper(II) complexes were corrected for the temperature-independent-paramagnetism of Cu<sup>2+</sup>, 60.

#### 2.2.4 Mössbauer Spectroscopy

<sup>57</sup>Fe Mössbauer spectra were obtained as reported previously.<sup>84</sup> To alleviate problems of sample decomposition nylon cells, containing the finely powdered sample, were sealed with an epoxy glue. Spectra were recorded in transmission geometry, the radiation source was <sup>57</sup>Co in a Cu or Rh matrix. The Doppler velocity scale was calibrated by using a metallic iron foil absorber, and isomer shifts are quoted relative to the centre of an iron foil spectrum.

Temperature-dependent (8-300 K) Mössbauer studies were carried out in a Janis model DT-6 cryostat. The temperature was set and maintained to within  $\pm 0.02$  K with a Cryogenic Research model TC-101 temperature controller. Temperatures were measured

with calibrated Ge and Pt resistance thermometers.

Spectra were fitted to Lorentzian curves with a least-squares treatment of the data points. The programme treats the positions, line widths and areas as unconstrained fitting parameters. The estimated precision of the quadrupole splitting and isomer shift parameters is considered to be  $\pm 0.01$  mm s<sup>-1</sup>.

Low-temperature Mössbauer spectra of Fe(pyz)<sub>2</sub>(NCS)<sub>2</sub>, Fe(pyz)(CF<sub>3</sub>SO<sub>3</sub>)<sub>2</sub> and Fe(pyz)(NCO)<sub>2</sub> were measured by Dr. J.R. Sams at the Nuclear Research Centre, Demokritos, Greece.

#### 2.2.5 X-Ray Crystallography

All X-ray structure determinations were performed by Dr. S.J. Rettig of this department. Crystals suitable for X-ray analysis were obtained as described in the relevant experimental sections. The complexes whose crystal structures were determined in the present study are named in the appropriate experimental sections according to I.U.P.A.C. nomenclature. In subsequent discussions, however, a less rigorous naming system is used; for example, trans-bis(methanesulfonato-O)tetrakis(pyridine)iron(II) becomes tetrakis(pyridine)iron(II) methanesulfonate.

#### 2.2.6 Differential Scanning Calorimetry (D.S.C.)

Typical D.S.C. runs were performed in an inert atmosphere of nitrogen at a nitrogen flow rate of 50 mL min<sup>-1</sup>. Finely powdered samples of approximately 5-10 mg were accurately



weighed into aluminum crucibles and the temperature range (308-723 K) was programmed by using a Mettler TC-10A processor in conjunction with a Mettler DSC-20 cell; a rate of temperature increase of 4 K per minute was used. The temperature calibration of the Pt sensor was achieved by using the known fusion temperatures of indium, lead and zinc. The heat flow was calibrated by using an exactly known quantity of indium. For each determination an empty crucible was placed on the reference sensor.

The temperature and enthalpy of a particular thermal event were obtained from the maximum (or minimum) in the D.S.C. curve and the integrated area underneath the curve respectively. The accuracy of these values is determined somewhat by the nature of the peak. For example, two poorly resolved peaks are difficult to analyse, as are asymmetrical peaks. These difficulties may be caused by the physical characteristics of the sample or the distribution of the sample in the pan.

For a series of calibrations using indium metal, it was found that the fusion temperature was accurate to  $\pm 0.1$  K and the integrated peak area was accurate to  $\pm 2$  J g<sup>-1</sup>, which generally represents an error of approximately  $\pm 1\%$  in both measurements. These values are considered to be the upper limits of accuracy for the instrument and where broad or overlapping curves occur the temperatures and enthalpy values are considered accurate to  $\pm 5$  K and  $\pm 5\%$  respectively.

Thermogravimetric analysis was possible by removal of the aluminum crucible prior to and following a thermal event and

weighing by analytical balance. The weight changes were small and the accuracy of the weight loss figure is approximately  $\pm 5\%$ .

#### 2.2.7 Elemental Analysis

Carbon, hydrogen, nitrogen and, in some cases oxygen analyses were performed by P. Borda of this department. Analytical data are considered accurate to  $\pm 0.3\%$ . Oxygen analysis was not possible for samples containing the combination of fluorine and hydrogen.

### CHAPTER 3

#### COMPLEXES CONTAINING AN $MN_4X_2$ CHROMOPHORE

##### 3.1 INTRODUCTION

The synthesis and characterisation of several groups of complexes having an  $MN_4X_2$  chromophore are described in this chapter. The first group consists of the tetrakis(pyridine) complexes,  $M(py)_4(RSO_3)_2$ , (where M is Cu and R is  $CF_3$  or  $CH_3$ ; and where M is Fe and R is  $CF_3$ ,  $CH_3$  or  $p-CH_3C_6H_4$ ). These compounds were synthesised for two major reasons. Complexes of this type have been proposed to have structures involving an  $MN_4O_2$  chromophore in which the four nitrogen atoms of the pyridine ligands are coordinated in a square plane around the metal and the sulfonate anions occupy axial coordination sites.<sup>76</sup> Magnetic exchange interactions are expected to be non-existent or weak in such complexes, and indeed, no interactions have been observed in the previously studied tetrakis(pyridine)iron(II) compounds,  $Fe(py)_4X_2$ , (where  $X^-$  is a halide or pseudohalide).<sup>67</sup> A second reason for investigating these compounds is that their magnetic moment data served as a baseline from which magnetic exchange interactions in the analogous bis(pyrazine) complexes could be measured. In addition, the structural properties of the tetrakis(pyridine) complexes are interesting in their own right. Several of the tetrakis(pyridine) complexes were suitable for X-ray structure determination and the crystal and molecular structures of

$\text{Fe}(\text{py})_4(\text{RSO}_3)_2$ , (where R is  $\text{CF}_3$ ,  $\text{CH}_3$  or  $p\text{-CH}_3\text{C}_6\text{H}_4$ ) and  $\text{Cu}(\text{py})_4(\text{CF}_3\text{SO}_3)_2$ , were solved. These structures provide an opportunity to examine not only the bonding parameters of the pyridine ligands, but also the coordination mode of the sulfonate anions as a function of the group R and the metal. With accurate structural data available for these compounds it was possible to test previously developed infrared and other spectroscopic criteria for structure in  $\text{M}(\text{py})_4(\text{RSO}_3)_2$  complexes.<sup>7 6</sup>

The second group of compounds comprises the bis(pyrazine) derivatives containing sulfonate anions. The following complexes were isolated:  $\text{Fe}(\text{pyz})_2(\text{CF}_3\text{SO}_3)_2 \cdot \text{CH}_3\text{OH}$ ,  $\text{Fe}(\text{pyz})_2(\text{CH}_3\text{SO}_3)_2$  and the copper species  $\text{Cu}(\text{pyz})_2(\text{CH}_3\text{SO}_3)_2$ . The stereochemistry around the metal is again dependent upon the mode of coordination of the pyrazine ligand and the sulfonate anion. In the case of the copper derivative, the chromophore and the bridging system were determined by X-ray crystallography; however, both bis(pyrazine)iron(II) compounds were isolated in forms unsuitable for single-crystal X-ray diffraction studies and thus characterisation of the iron species was solely by spectroscopic methods. The magnetic properties of the bis(pyrazine) complexes were compared to those of the analogous tetrakis(pyridine) derivatives in order to explore the effects of bridging pyrazine groups on magnetic exchange interactions.

A third group of complexes to be discussed in this chapter are the bis(pyrazine)iron(II) species,  $\text{Fe}(\text{pyz})_2\text{X}_2$ , (where  $\text{X}^-$  is

a halide,  $\text{Cl}^-$ ,  $\text{Br}^-$  or  $\text{I}^-$ ; pseudohalide,  $\text{NCS}^-$ ; or perchlorate,  $\text{ClO}_4^-$ ). In the case of the halide and pseudohalide anions listed above, the corresponding tetrakis(pyridine)iron(II) derivatives have been synthesised and characterised by other researchers.<sup>67</sup> This previous work provided a data set for comparing structural, spectroscopic and magnetic properties of the pyrazine-bridged complexes, prepared in the present work, with the properties of analogous tetrakis(pyridine) compounds which contain no bridging ligands.

The bis(pyrazine) derivatives prepared in the present study represent a range of compounds in which the anion varies from being rather weakly coordinating (for example, sulfonate or perchlorate) to more strongly coordinating (for example, halide or pseudohalide). Such a series permitted an examination of possible correlations between spectroscopic and magnetic properties and anion basicity.

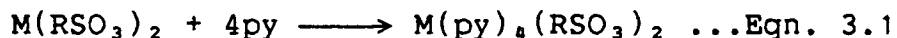
As described in Chapter 1 (Section 1.2), one of the main objectives of the present study was to prepare pyrazine complexes in which the pyrazine group would occupy a bridging position, and subsequently to investigate the efficiency of this ligand for the propagation of magnetic exchange interactions. During the course of the present research, however, several compounds were isolated in which the neutral pyrazine ligand to metal ratio was 4:1; these complexes are  $\text{Fe}(\text{2-mepyz})_4(\text{CH}_3\text{SO}_3)_2$ ,  $\text{Cu}(\text{pyz})_4(\text{CF}_3\text{SO}_3)_2 \cdot \text{H}_2\text{O}$  and  $\text{Fe}(\text{pyz})_4(\text{AsF}_6)_2 \cdot 2\text{H}_2\text{O}$ . Spectroscopic evidence, to be presented in this chapter, suggested that the complexes contain unidentate pyrazine ligands resulting in an

$MN_4X_2$  chromophore and a discussion of these complexes is relevant here. The magnetic and spectroscopic properties of  $Cu(py)_4(CF_3SO_3)_2 \cdot H_2O$  and  $Fe(2-mepy)_4(CH_3SO_3)_2$  are also of interest in relation to the properties of the tetrakis(pyridine) and bis(pyrazine) compounds. For example, these tetrakis(pyrazine) complexes provide a means of testing the infrared criteria which have been developed for determining either the bridging or terminal nature of pyrazine in its complexes.<sup>37, 44</sup>  $Cu(py)_4(CF_3SO_3)_2 \cdot H_2O$  proved a useful starting material for the preparation of the mono(pyrazine) complex  $Cu(py)(CF_3SO_3)_2$  (Section 4.2.2.4). The isolation of  $Fe(py)_4(AsF_6)_2 \cdot 2H_2O$  resulted from attempts to prepare the bis(pyrazine) derivative,  $Fe(py)_2(AsF_6)_2$ . The bis(pyrazine) complex could not be isolated in the present study and attempts to produce the desired bis(pyrazine) compound by thermolysis of  $Fe(py)_4(AsF_6)_2 \cdot 2H_2O$  were unsuccessful.

### 3.2 SYNTHETIC METHODS

#### 3.2.1 Tetrakis(pyridine) Complexes

Compounds of formula  $M(py)_4(RSO_3)_2$ , where M is Fe and R is  $CF_3$ ,  $CH_3$  and  $p-CH_3C_6H_4$ , and M is Cu and R is  $CF_3$  and  $CH_3$  were prepared by the reaction of the appropriate anhydrous metal(II) sulfonate dissolved in methanol, with an excess of pyridine.



The iron(II) complexes were prepared in an inert atmosphere dry

box to avoid oxidation. No such precautions were taken for the preparation of the copper(II) derivatives.

3.2.1.1 Trans-bis(trifluoromethanesulfonato-O)tetrakis-(pyridine)iron(II),  $\text{Fe}(\text{py})_4(\text{CF}_3\text{SO}_3)_2$

Iron(II) trifluoromethanesulfonate<sup>25</sup> (0.486 g, 1.37 mmol) was dissolved in methanol (5 mL). This resulted in a pale-green solution. An excess of pyridine (4 mL, 50 mmol) was added dropwise and the colour of the solution intensified. Overnight, pale-green, needle-shaped crystals formed; this solid product was isolated in 64% yield after filtration and washing with small quantities of methanol and diethyl ether. Anal. calcd for  $\text{FeC}_{22}\text{H}_{20}\text{N}_4\text{F}_6\text{S}_2\text{O}_6$ : C, 39.41; H, 3.01; N, 8.36; found: C, 39.41; H, 3.10; N, 8.28.

3.2.1.2 Trans-bis(methanesulfonato-O)tetrakis(pyridine)iron(II),  $\text{Fe}(\text{py})_4(\text{CH}_3\text{SO}_3)_2$

An excess of pyridine (5 mL, 62 mmol) was added to the pale-green solution resulting from the dissolution of either  $\alpha$ - or  $\beta$ - $\text{Fe}(\text{CH}_3\text{SO}_3)_2$ <sup>25</sup> (0.98 g, 4.0 mmol) in hot methanol (5 mL). Overnight, green, plate-like crystals formed; this solid product was isolated by filtration and washed with small quantities of methanol and diethyl ether (yield 70%). Anal. calcd for  $\text{FeC}_{22}\text{H}_{26}\text{N}_4\text{S}_2\text{O}_6$ : C, 46.98; H, 4.67; N, 9.96; O, 17.07; found: C, 46.70; H, 4.67; N, 9.72; O, 17.01.

### 3.2.1.3 Trans-bis(p-toluenesulfonato-O)tetrakis-(pyridine)iron(II), $\text{Fe}(\text{py})_4(\text{p-CH}_3\text{C}_6\text{H}_4\text{SO}_3)_2$

Iron(II) p-toluenesulfonate<sup>25</sup> (0.83 g, 2.1 mmol) was dissolved in methanol (18 mL). Pyridine (4 mL, 50 mmol) was added dropwise to this solution and a yellow precipitate formed immediately. Upon standing for 30 minutes this solid became an oil. In an attempt to crystallise this oil, diethyl ether (10 mL) was added and overnight, green, triangular crystals formed. The material was isolated by filtration, and washed with small amounts of methanol and diethyl ether (yield 25%). The total yield was increased to 60% by allowing the filtrate to evaporate slowly to approximately one half of its original volume; subsequently a microcrystalline solid was isolated from this solution by filtration. Anal. calcd for  $\text{FeC}_{34}\text{H}_{34}\text{N}_4\text{S}_2\text{O}_6$ : C, 57.13; H, 4.80; N, 7.84; O, 13.43; found (for first crop): C, 56.87; H, 4.82; N, 7.64; O, 13.20.

### 3.2.1.4 Tetrakis(pyridine)iron(II) fluorosulfonate, $\text{Fe}(\text{py})_4(\text{FSO}_3)_2$

The general method used to prepare the tetrakis(pyridine)iron(II) sulfonate complexes failed to produce the desired product when the anion was  $\text{FSO}_3^-$ . This was thought to be due to the hydrolysis of the S-F bond which is extremely susceptible to trace amounts of moisture. When the general route was followed (Eqn. 3.1) a yellow product was obtained whose infrared spectrum lacked absorptions in the region of 1260-1340  $\text{cm}^{-1}$ , where the asymmetric  $\text{SO}_3$  stretching vibrations



are expected to occur; the presence of a medium intensity band at  $1540\text{ cm}^{-1}$  indicated the presence of the pyridinium cation.<sup>77</sup> These observations indicate decomposition of the anion and protonation of the neutral ligand.

Paul et al.<sup>85</sup> prepared bis(pyridine)iron(II) fluorosulfonate by suspending  $\text{Fe}(\text{FSO}_3)_2$  in carbon tetrachloride and subsequently adding pyridine. This reaction could not be successfully repeated here, and, after their procedure was followed the infrared spectrum of the product indicated the presence of the pyridinium cation.<sup>77</sup>

Difficulties in synthesising  $\text{Fe}(\text{py})_4(\text{FSO}_3)_2$  have been encountered previously. The complexes,  $\text{M}(\text{py})_4(\text{FSO}_3)_2$ , (where M is Ni, Cu and Zn) have been prepared in this laboratory<sup>76</sup> and it was noted that the iron(II) complex was not isolable.<sup>86</sup>

In the present study several other methods were investigated in an attempt to synthesise the iron derivative from  $\text{Fe}(\text{FSO}_3)_2$ ; <sup>23</sup> they are as follows:

- (i) Direct addition of pyridine to  $\text{Fe}(\text{FSO}_3)_2$ .
- (ii) Addition of pyridine to a suspension of  $\text{Fe}(\text{FSO}_3)_2$  in dichloromethane.
- (iii) Addition of pyridine to a suspension of  $\text{Fe}(\text{FSO}_3)_2$  in nitromethane.
- (iv) Addition of excess pyridine (5 mL, 62 mmol) to iron(II) fluorosulfonate (0.16 g, 0.63 mmol) dissolved in warm acetonitrile (20 mL). This resulted in the formation of a yellow solid which was isolated by filtration and washed with diethyl

ether.

Attempts (i) to (iii) resulted in solids which have an infrared absorption around  $1540\text{ cm}^{-1}$ , indicative of the pyridinium cation,<sup>77</sup> and microanalytical data which do not relate to any value of  $n$  in the complex  $\text{Fe}(\text{py})_n(\text{FSO}_3)_2$ . The yellow solid obtained by method (iv) has the following microanalytical results: C, 50.26; H, 4.29; N, 11.54. These data eliminate the possibility of the complex being  $\text{Fe}(\text{py})_4(\text{FSO}_3)_2$ , for which the anal. calcd is C, 42.12; H, 3.53; N, 9.82. These experimental analytical data suggest that either the hexakis(pyridine) complex,  $\text{Fe}(\text{py})_6(\text{FSO}_3)_2$  is formed; anal. calcd for  $\text{FeC}_{30}\text{H}_{30}\text{N}_6\text{F}_2\text{S}_2\text{O}_6$ : C, 49.46; H, 4.15; N, 11.53; or  $\text{Fe}(\text{py})_4\text{SO}_4$  is formed; anal. calcd for  $\text{FeC}_{20}\text{H}_{20}\text{N}_4\text{SO}_4$ : C, 51.30; H, 4.30; N, 11.96. Infrared data (1185s, 1119sh, 1111s, 1040sh, 1029s  $\text{cm}^{-1}$ ) indicate the complex isolated from method (iv) is  $\text{Fe}(\text{py})_4\text{SO}_4$  which results from the decomposition of the fluorosulfonate anion. The complex also showed infrared absorptions which were attributable to coordinated pyridine (1598m, 630m, 625m, 620m, 434m  $\text{cm}^{-1}$ ); whereas, no absorption was present at  $1540\text{ cm}^{-1}$  indicating the absence of the pyridinium ion.<sup>77</sup>

### 3.2.1.5 Trans-bis(trifluoromethanesulfonato-O)tetrakis-(pyridine)copper(II), $\text{Cu}(\text{py})_4(\text{CF}_3\text{SO}_3)_2$

$\text{Cu}(\text{CF}_3\text{SO}_3)_2$ <sup>87</sup> (0.994 g, 2.75 mmol) was dissolved in hot methanol (11 mL). An excess of pyridine (5 mL, 62 mmol) was added dropwise, whereupon, an intense blue-coloured solution

formed. On cooling, a blue, crystalline solid resulted which was isolated by filtration. The product was recrystallised from a solution of pyridine in methanol (1:4 v/v) and isolated in 82% yield. Anal. calcd for  $\text{CuC}_{22}\text{H}_{20}\text{N}_4\text{F}_2\text{S}_2\text{O}_6$ : C, 38.97; H, 2.97; N, 8.26; found: C, 38.99; H, 2.97; N, 8.29.

### 3.2.1.6 Tetrakis(pyridine)copper(II) methanesulfonate, $\text{Cu}(\text{py})_4(\text{CH}_3\text{SO}_3)_2$

$\text{Cu}(\text{CH}_3\text{SO}_3)_2^{87}$  (1.051 g, 4.139 mmol) was dissolved in hot methanol (8 mL) yielding a pale-blue solution. On addition of an excess of pyridine (5 mL, 62 mmol) the blue colour of the solution intensified. Overnight, dark-blue rectangular crystals formed; the product was isolated by filtration in 73% yield. Anal. calcd for  $\text{CuC}_{22}\text{H}_{26}\text{N}_4\text{S}_2\text{O}_6$ : C, 46.35; H, 4.60; N, 9.83; found: C, 46.60; H, 4.70; N, 9.80.

### 3.2.2 Tetrakis(pyrazine) and Tetrakis(2-methylpyrazine) Complexes

The synthesis of two tetrakis(pyrazine) species and  $\text{Fe}(2\text{-mepyz})_4(\text{CH}_3\text{SO}_3)_2$  are now described.  $\text{Fe}(2\text{-mepyz})_4(\text{CH}_3\text{SO}_3)_2$  was prepared and handled in an inert atmosphere dry box, whilst for the synthesis of  $\text{Fe}(\text{pyz})_4(\text{AsF}_6)_2 \cdot 2\text{H}_2\text{O}$  all manipulations were performed under a nitrogen atmosphere by using standard Schlenk techniques. No such precautions were taken for the preparation of  $\text{Cu}(\text{pyz})_4(\text{CF}_3\text{SO}_3)_2 \cdot \text{H}_2\text{O}$ .

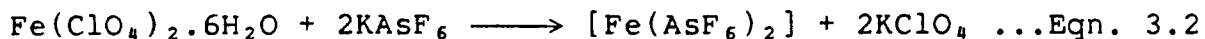
3.2.2.1 Tetrakis(2-methylpyrazine)iron(II) methanesulfonate,  
 $\text{Fe}(\text{2-mepyz})_4(\text{CH}_3\text{SO}_3)_2$

Iron(II) methanesulfonate<sup>25</sup> (0.319 g, 1.30 mmol of either the  $\alpha$  or  $\beta$  form) was dissolved in hot methanol (10 mL) and an excess of 2-methylpyrazine (5 mL, 55 mmol) was added to the pale-green solution. Green, plate-like crystals contaminated by brown flecks formed overnight. The solid was isolated by filtration and washed with a small quantity of methanol (the product appeared highly soluble in this solvent). The crystals were then washed with diethyl ether and isolated in 61% yield. Anal. calcd for  $\text{FeC}_{22}\text{H}_{30}\text{N}_8\text{S}_2\text{O}_6$ : C, 42.45; H, 4.86; N, 18.00; found: C, 42.09; H, 4.63; N, 18.20.

The slight discoloration of the product and the analytical data suggested a small amount of impurity, hence the product was recrystallised from 2-methylpyrazine. Anal. found: C, 42.47; H, 4.84; N, 17.77.

3.2.2.2 Tetrakis(pyrazine)iron(II) hexafluoroarsenate dihydrate,  
 $\text{Fe}(\text{pyz})_4(\text{AsF}_6)_2 \cdot 2\text{H}_2\text{O}$

Potassium hexafluoroarsenate (0.975 g, 4.27 mmol) was dissolved in methanol (10 mL) and added to a methanolic solution (10 mL) of iron(II) perchlorate hexahydrate (0.720 g, 1.98 mmol). The potassium perchlorate which formed (Eqn. 3.2) was removed by filtration. To remove any remaining  $\text{ClO}_4^-$ , a second addition of  $\text{KAsF}_6$  was made (0.500 g, 2.19 mmol; in methanol, 5 mL) and the solution stirred for 3 h.



$\text{KClO}_4$  was again removed by filtration and the filtrate was added to a solution of pyrazine (2.10 g, 26.3 mmol) in methanol (5 mL). Overnight, a yellow, microcrystalline solid formed; this was isolated by filtration and washed with a small amount of methanol (yield 63%). Anal. calcd for  $\text{FeC}_{16}\text{H}_{20}\text{N}_8\text{As}_2\text{F}_{12}\text{O}_2$ : C, 24.32; H, 2.55; N, 14.18; found: C, 24.30; H, 2.58; N, 14.24.

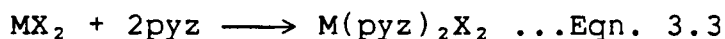
Attempts were made to prepare the bis(pyrazine) complex by using a ratio of  $\text{Fe}(\text{ClO}_4)_2 \cdot 6\text{H}_2\text{O}$  to pyrazine of 1:2; under these conditions, however, no complex was isolated and employing a ratio of 1:4 resulted in the formation of the tetrakis(pyrazine) compound. Several attempts were made to convert the tetrakis(pyrazine) complex to the analogous bis(pyrazine) derivative,  $\text{Fe}(\text{pyz})_2(\text{AsF}_6)_2$ .  $\text{Fe}(\text{pyz})_4(\text{AsF}_6)_2 \cdot 2\text{H}_2\text{O}$  was placed in a desiccator over phosphorus(V) oxide at reduced pressure; however, even after a week the infrared spectrum of the sample remained unchanged. Heating the tetrakis(pyrazine) complex in vacuo at a temperature of 323 K had no effect; heating at higher temperatures, approximately 343 K, resulted in a brown solid which exhibited strong infrared absorptions in the 600 and 450  $\text{cm}^{-1}$  regions. Absorptions in these regions are attributed to Fe-F vibrations, suggesting decomposition of the  $\text{AsF}_6^-$  anion.

### 3.2.2.3 Tetrakis(pyrazine)copper(II) trifluoromethanesulfonate monohydrate, $\text{Cu}(\text{pyz})_4(\text{CF}_3\text{SO}_3)_2 \cdot \text{H}_2\text{O}$

Copper(II) trifluoromethanesulfonate<sup>87</sup> (0.565 g, 1.55 mmol) was dissolved in hot methanol (3 mL). The copper(II) solution was then added to a hot solution of pyrazine (1.781 g, 22.3 mmol) dissolved in methanol (5 mL). A dark-blue solution resulted, and after a period of 30 min, a blue, crystalline solid formed; the product was isolated by filtration in 92% yield. Anal. calcd for  $\text{CuC}_{18}\text{H}_{18}\text{N}_8\text{F}_6\text{S}_2\text{O}_7$ : C, 30.88; H, 2.59; N, 16.01; found: C, 30.65; H, 2.57; N, 15.75.

### 3.2.3 Bis(pyrazine) Complexes

Several iron(II) complexes of stoichiometry  $\text{Fe}(\text{pyz})_2\text{X}_2$  (where  $\text{X}^-$  is  $\text{CF}_3\text{SO}_3^-$ ,  $\text{CH}_3\text{SO}_3^-$ ,  $\text{Cl}^-$ ,  $\text{Br}^-$ ,  $\text{I}^-$ ,  $\text{NCS}^-$  or  $\text{ClO}_4^-$ ), were prepared by the following general route:



The copper(II) species,  $\text{Cu}(\text{pyz})_2(\text{CH}_3\text{SO}_3)_2$  was also isolated.  $\text{Fe}(\text{pyz})_2(\text{NCS})_2$  was synthesised in the absence of oxygen by using standard Schlenk techniques; the other iron(II) complexes were prepared in an inert atmosphere dry box. No such precautions were necessary for the preparation of  $\text{Cu}(\text{pyz})_2(\text{CH}_3\text{SO}_3)_2$ .

#### 3.2.3.1 Bis(pyrazine)iron(II) trifluoromethanesulfonate methanol solvate, $\text{Fe}(\text{pyz})_2(\text{CF}_3\text{SO}_3)_2 \cdot \text{CH}_3\text{OH}$

A solution of pyrazine (0.55 g, 6.9 mmol) in methanol (5

mL) was added to iron(II) trifluoromethanesulfonate<sup>25</sup> (0.741 g, 2.09 mmol) dissolved in methanol (5 mL). A yellow solution resulted and after 24 h, precipitation of a yellow solid was facilitated by the addition of diethyl ether (30 mL). The product was removed by filtration and washed with diethyl ether and isolated in 72% yield. Anal. calcd for  $\text{FeC}_{11}\text{H}_{12}\text{N}_4\text{F}_6\text{S}_2\text{O}_7$ : C, 24.19; H, 2.21; N, 10.26; found: C, 24.12; H, 2.34; N, 10.27.

Attempts were made to remove the solvent of crystallisation by thermolysis; however, differential scanning calorimetry results (Section 3.3.6) indicate that the methanol is strongly held and that one mole of pyrazine, as well as the methanol solvent molecule are removed simultaneously. Attempts to prepare the anhydrous bis(pyrazine) complex in other solvents, for example, acetone, acetonitrile, dichloromethane and ethanol were all unsuccessful. The infrared spectrum of each of the products indicates either inclusion of solvent which could not be removed by heating at low temperatures, or, in the case of dichloromethane, it shows the product as the mono(pyrazine) complex,  $\text{Fe}(\text{pyz})(\text{CF}_3\text{SO}_3)_2$ .

### 3.2.3.2 Bis(pyrazine)iron(II) methanesulfonate, $\text{Fe}(\text{pyz})_2(\text{CH}_3\text{SO}_3)_2$

Pyrazine (1.28 g, 16.0 mmol) was dissolved in methanol (5 mL) and this solution was added to a solution of iron(II) methanesulfonate<sup>25</sup> (1.09 g, 4.43 mmol) in methanol (20 mL). A yellow precipitate formed immediately. The product was isolated in 83% yield after filtration and washing with methanol and

diethyl ether. Anal. calcd for  $\text{FeC}_{10}\text{H}_{14}\text{N}_4\text{S}_2\text{O}_6$ : C, 29.56; H, 3.48; N, 13.79; O, 23.63; found: C, 29.47; H, 3.66; N, 13.50; O, 23.95.

### 3.2.3.3 Trans-bis(methanesulfonato-O)bis( $\mu$ -pyrazine)copper(II), $\text{Cu}(\text{pyz})_2(\text{CH}_3\text{SO}_3)_2$

Copper(II) methanesulfonate<sup>87</sup> (0.535 g, 2.11 mmol) was dissolved in hot methanol (3mL). This copper(II) solution was added to a hot solution of pyrazine (2.298 g, 28.7 mmol) dissolved in methanol (5 mL). The pale-blue precipitate which formed immediately was removed by filtration. The filtrate was left to stand and over a period of several hours a grey-blue crystalline solid started to form. The small crystals which grew overnight were subsequently isolated by filtration. Both products gave identical infrared spectra and similar microanalytical data. The total yield of product was 81%. Anal. calcd for  $\text{CuC}_{10}\text{H}_{14}\text{N}_4\text{S}_2\text{O}_6$ : C, 29.02; H, 3.41; N, 13.54; found, for the crystalline material: C, 28.56; H, 3.52; N, 13.04. These poor analytical data and the infrared spectrum of the product (Section 3.3.2.3) suggest the presence of water, although this was undetected in the X-ray structure determination (Section 3.3.1.3).

### 3.2.3.4 Bis(pyrazine)iron(II) chloride, $\text{Fe}(\text{pyz})_2\text{Cl}_2$

The synthesis of the bis(pyrazine) complex was described previously although few details were given. Beech and Mortimer<sup>61</sup> obtained the anhydrous compound by mixing ethanolic



or aqueous solutions of hydrated iron(II) chloride and pyrazine. Ferraro et al.<sup>62</sup> described the synthesis of a hydrated species,  $\text{Fe}(\text{pyz})_2\text{Cl}_2 \cdot \text{H}_2\text{O}$ ; by mixing  $\text{FeCl}_2$  and the ligand in a 1:2 ratio, the solvent being ethanol.

In this study a hydrate was isolated from ethanol when the ratio of  $\text{FeCl}_2$  to pyrazine was 1:2. The presence of water was indicated by infrared absorptions in the 3500 and 1600  $\text{cm}^{-1}$  regions, and by microanalytical data. When the ligand to iron(II) chloride ratio was increased to 11:1 the product obtained showed no infrared absorptions in either the O-H stretching or bending regions indicating the absence of any OH containing species. The synthetic procedure involved the addition of an ethanolic solution (20 mL) of  $\text{FeCl}_2$  (0.503 g, 3.97 mmol) to pyrazine (3.54 g, 44.3 mmol) dissolved in ethanol (10 mL). The deep-red solid which formed was isolated by filtration and washed with ethanol and diethyl ether (yield 62%). Anal. calcd for  $\text{FeC}_8\text{H}_8\text{N}_4\text{Cl}_2$ : C, 33.49; H, 2.81; N, 19.53; found: C, 33.28; H, 2.89; N, 19.65.

#### 3.2.3.5 Bis(pyrazine)iron(II) bromide, $\text{Fe}(\text{pyz})_2\text{Br}_2$

The preparation of this complex was briefly described in an earlier report.<sup>62</sup> The following method was used in the present study. Anhydrous iron(II) bromide (0.490 g, 2.27 mmol) was dissolved in methanol (15 mL). The resulting solution was filtered into a solution of pyrazine (0.80 g, 10 mmol) dissolved in methanol (5 mL). A red precipitate started to form after several minutes; the solution was left to stand for three hours

and subsequently the product was isolated by filtration and washed with portions of methanol and diethyl ether (yield 74%).

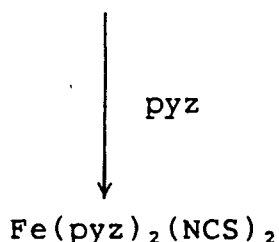
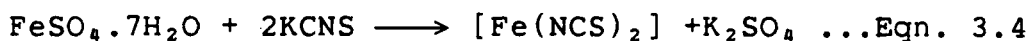
Anal. calcd for  $\text{FeC}_8\text{H}_8\text{N}_4\text{Br}_2$ : C, 25.57; H, 2.15; N, 14.91; found: C, 26.06; H, 2.41; N, 14.51.

### 3.2.3.6 Bis(pyrazine)iron(II) iodide, $\text{Fe}(\text{pyz})_2\text{I}_2$

Iron(II) iodide (0.524 g, 1.69 mmol) was dissolved in methanol (10 mL) and filtered into a methanolic solution (10 mL) of pyrazine (0.62 g, 7.75 mmol). The solution first turned yellow, then orange and after five minutes an orange cloudiness formed. Overnight, a lustrous, maroon solid formed; the product was isolated by filtration, and washed with methanol and diethyl ether (yield 44%). Anal. calcd for  $\text{FeC}_8\text{H}_8\text{N}_4\text{I}_2$ : C, 20.45; H, 1.72; N, 11.92; found: C, 20.41; H, 1.75; N, 12.09.

### 3.2.3.7 Bis(pyrazine)iron(II) thiocyanate, $\text{Fe}(\text{pyz})_2(\text{NCS})_2$

The procedure may be represented by the following scheme:



Iron(II) sulfate heptahydrate (0.672 g, 4.84 mmol) and potassium thiocyanate (0.470 g, 4.84 mmol) were dissolved in water (10 and 5 mL respectively; immediately prior to use the solvent was

degassed by several freeze-pump-thaw cycles). The potassium thiocyanate solution was added to the iron(II) solution and the resulting mixture was filtered directly into a solution of pyrazine (0.535 g, 6.69 mmol) dissolved in water (10 mL). An orange-brown precipitate resulted; the solution was stirred for 3/4 h and the product was isolated by filtration and washed with water and methanol (yield 67%). Anal. calcd for  $\text{FeC}_{10}\text{H}_8\text{N}_6\text{S}_2$ : C, 36.18; H, 2.43; N, 25.31; found: C, 35.82; H, 2.30; N, 25.10.

### 3.2.3.8 Bis(pyrazine)iron(II) perchlorate, $\text{Fe}(\text{pyz})_2(\text{ClO}_4)_2$

The preparation of the dihydrate,  $\text{Fe}(\text{pyz})_2(\text{ClO}_4)_2 \cdot 2\text{H}_2\text{O}$ , has been reported recently.<sup>60</sup> The method involved the addition of a solution of hydrated iron(II) perchlorate to a solution of the ligand, both reagents being dissolved in the minimum amount of water. In the previous report, it was noted that drying the product over silica gel at reduced pressure failed to produce the anhydrous species. The same procedure was followed in the present study and the hydrate was isolated; this was subsequently dehydrated by applying more stringent conditions. The dihydrate was heated in an Aberhalden drying pistol at a temperature of approximately 390 K for a period of 46 h at reduced pressure, in the presence of phosphorus(V) oxide. Due to the unpredictably explosive nature of perchlorates, caution should be taken when handling this material. The anhydrous compound was isolated in 72% yield. Anal. calcd for  $\text{FeC}_8\text{H}_8\text{N}_4\text{Cl}_2\text{O}_8$ : C, 23.16; H, 1.94; N, 13.50; O, 30.85; found: C, 23.13; H, 1.92; N, 13.46; O, 31.00.

### 3.2.4 Attempted Preparations

During the course of the present study attempts were made to prepare the bis(pyrazine) complexes,  $\text{Fe}(\text{pyz})_2(\text{p-CH}_3\text{C}_6\text{H}_4\text{SO}_3)_2$  and  $\text{Fe}(\text{pyz})_2(\text{NCO})_2$ . Attempts involved the addition of " $\text{FeX}_2$ " (where  $\text{X}^-$  is  $\text{p-CH}_3\text{C}_6\text{H}_4\text{SO}_3^-$  or  $\text{NCO}^-$ ), to an excess of pyrazine ( $\text{FeX}_2$  to pyrazine ratio of 1:20); in both cases, however, only the mono(pyrazine) complex was isolated (Section 4.2.2). For the cyanate derivative this may be related to the extreme insolubility of  $\text{Fe}(\text{pyz})(\text{NCO})_2$  in most solvents, for example, water, methanol, acetone and dichloromethane. In the case of the p-tosylate, however, the reason for the non-isolation of a bis(pyrazine) species is not apparent.

### 3.3 RESULTS AND DISCUSSION

#### 3.3.1 X-ray Structure Determinations

Several of the complexes containing an  $MN_4O_2$  chromophore were isolated in a form suitable for single-crystal X-ray analysis. The crystal and molecular structures of  $Fe(py)_4(RSO_3)_2$  ( $R=CF_3$ ,  $CH_3$  and  $p-CH_3C_6H_4$ ),  $Cu(py)_4(CF_3SO_3)_2$  and  $Cu(py)_2(CH_3SO_3)_2$  were determined and the crystallographic data are presented below.

##### 3.3.1.1 X-ray structure determination of $Fe(py)_4(RSO_3)_2$ complexes

It was of interest to solve the structures of the tetrakis(pyridine) iron(II) compounds and to obtain the relevant bonding parameters for two reasons:

(i) Previous research in this laboratory resulted in spectroscopic evidence indicating unidentate anion coordination in  $M(py)_4(FSO_3)_2$  complexes.<sup>76</sup> In the present study, single-crystal X-ray structure analysis has provided definitive evidence on the nature of the anion-cation interaction, and provided a qualitative basis for assessing the relative basicities of the different sulfonate anions.

(ii) Sulfonate anions, in particular the triflate anion, have been used extensively in both organic and inorganic chemistry as counter ions, as they are weakly coordinating and act as good leaving

groups.<sup>88-91</sup> This has resulted in a large number of X-ray structure reports on compounds containing ionic sulfonate groups (see for example, references 92-95), but relatively little structural data where the anion is coordinated in a uni-,<sup>96-100</sup> bi-,<sup>101-104</sup> or tridentate mode<sup>16, 105, 106</sup> or chelating fashion.<sup>107</sup>

Views of the molecular structures of the  $\text{Fe}(\text{py})_4(\text{RSO}_3)_2$  complexes and the atom numbering schemes are shown in Figs. 3.1-3.3. Selected intramolecular bond distances and angles are given in Table 3.1 and a complete compilation of structural parameters is given in Appendix I. These structural analyses show all three complexes as having an octahedral geometry with trans-coordinated monodentate sulfonate groups. With the possible exception of weak hydrogen bonds, each of the three structures consists of discrete molecules separated by normal van der Waals distances. Two distinct molecular units are observed in the  $\text{R}=\text{CH}_3$  compound, the difference between them involves slightly different orientations of the  $\text{CH}_3\text{SO}_3^-$  groups with respect to the O-Fe-O vector. The two independent  $\text{R}=\text{CH}_3$  molecules and the  $\text{R}=\text{CF}_3$  molecule have approximate  $\text{C}_2$  symmetry and for  $\text{R}=\text{p-CH}_3\text{C}_6\text{H}_4$  the molecule possesses exact  $\text{C}_2$  symmetry. In each case the two-fold axis lies in the  $\text{FeN}_4$  plane and bisects cis N-Fe-N angles.

Table 3.1 Selected Mean Bond Distances (Å) and Angles (°) for  
some  $\text{Fe}(\text{py})_4(\text{RSO}_3)_2$  Complexes

	R GROUP		
	$\text{CF}_3$	$\text{CH}_3$	$\text{p-CH}_3\text{C}_6\text{H}_4$
Bond Distances			
Fe-O	2.11	2.06	2.08
Fe-N	2.21	2.23	2.24
S-O (linking)	1.47	1.48	1.49
S-O (terminal)	1.44	1.45	1.44
S-C	1.82	1.78	1.78
Bond Angles			
O-Fe-O	175	173	175
N-Fe-N	179	179	173
O-S-O	115	112	113
O-S-C	104	106	106

Fig. 3.1 ORTEP Plot of the Structure of  $\text{Fe}(\text{py})_4(\text{CF}_3\text{SO}_3)_2$

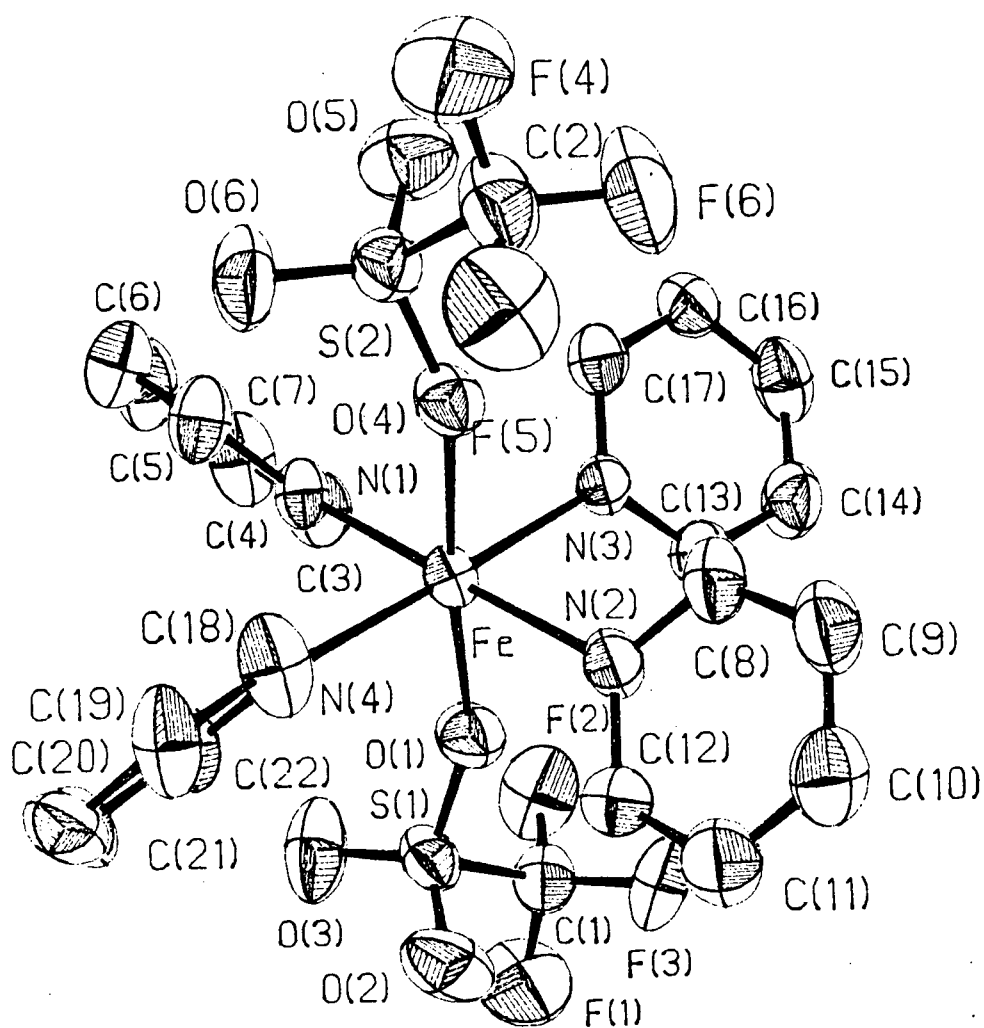




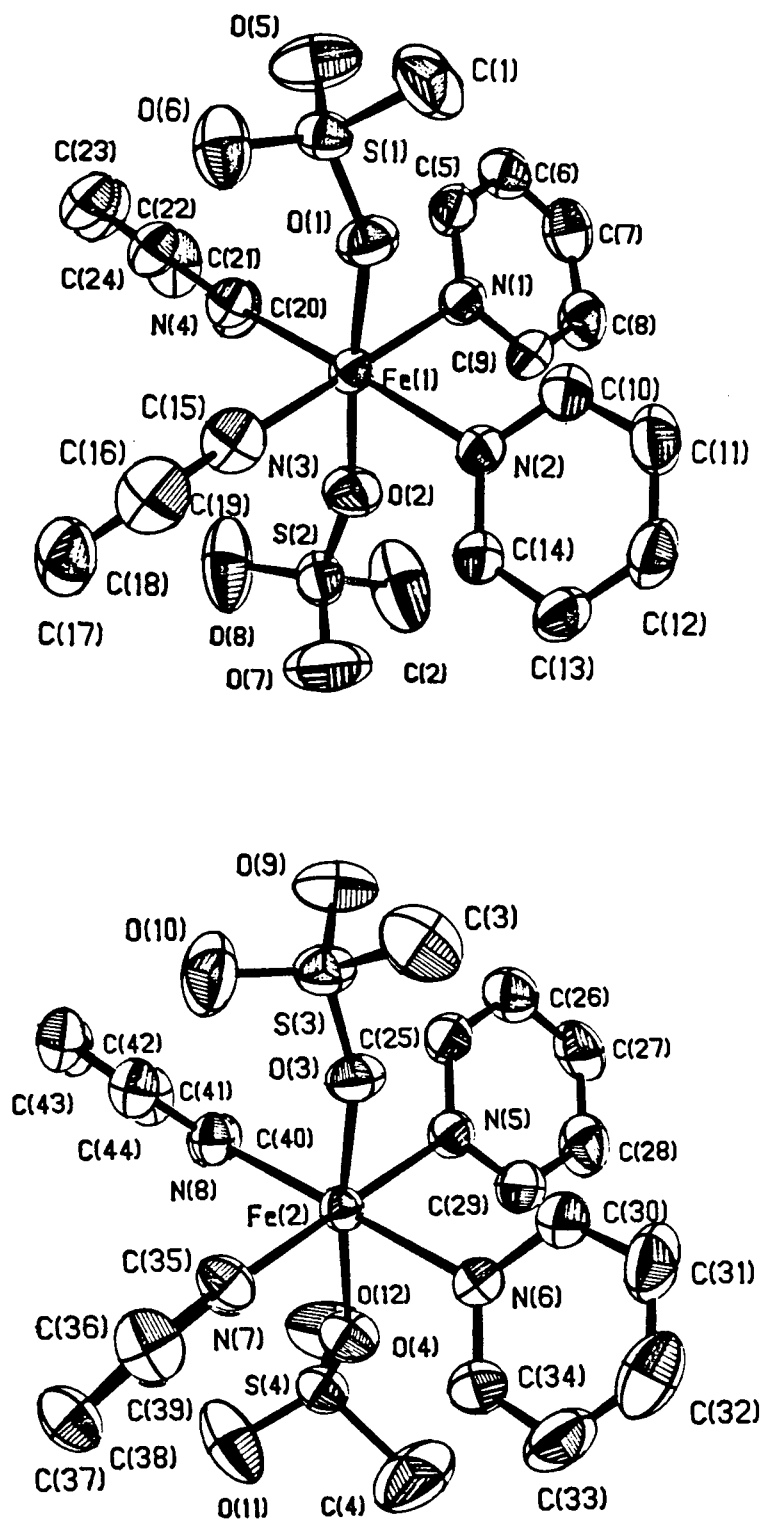
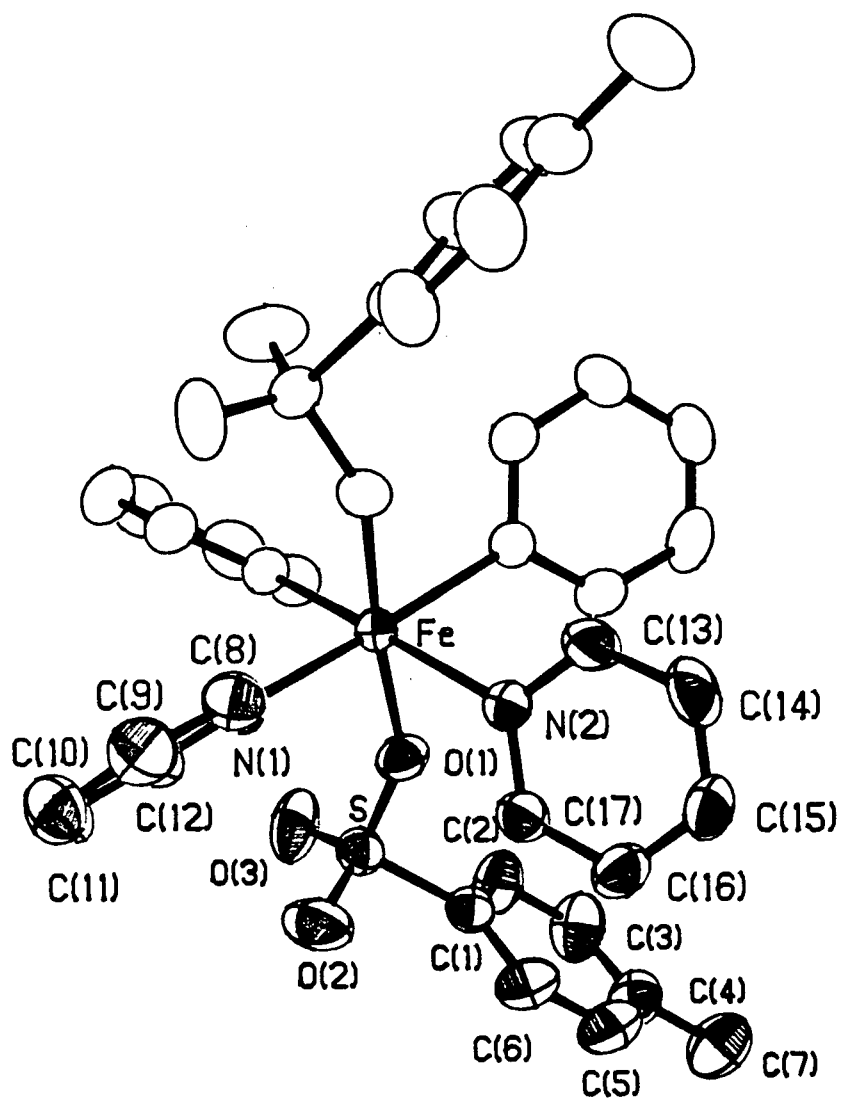
Fig. 3.2 ORTEP Plots of the Structure of  $\text{Fe}(\text{py})_4(\text{CH}_3\text{SO}_3)_2$ 

Fig. 3.3 ORTEP Plot of the Structure of  $\text{Fe}(\text{py})_4(\text{p-CH}_3\text{C}_6\text{H}_4\text{SO}_3)_2$



The  $\text{FeN}_4$  groups are non-planar in all three compounds. For the  $\text{R}=\text{CH}_3$  and  $\text{CF}_3$  compounds, the maximum deviation from the mean plane is  $0.284(4)$  Å. In the  $\text{R}=\text{CF}_3$  compound, the four pyridine nitrogen atoms are coplanar, the Fe atom being displaced  $0.015(1)$  Å from the  $\text{N}_4$  plane. The pyridine rings are generally planar to within experimental error; while the pyridine rings containing N(1), N(4) and N(6) in the  $\text{R}=\text{CH}_3$  compound and N(2) in the  $\text{R}=\text{p-CH}_3\text{C}_6\text{H}_4$  structure are non-planar, no atom deviates by more than  $0.0154(4)$  Å from the mean plane. The bond distances and angles around the pyridine rings are similar to those found for pyridine by electron diffraction studies<sup>108</sup> and microwave spectroscopy.<sup>109</sup>

An interesting structural feature present in all three compounds is the arrangement of the pyridine ligands in a propeller configuration; the trans-pyridine rings are nearly orthogonal to one another. This configuration appears to minimise interactions between adjacent pyridine rings as well as interactions between pyridine rings and sulfonate anions. This propeller-like arrangement has been previously observed in  $\text{Fe}(\text{py})_4\text{Cl}_2$ <sup>68</sup> and  $\text{Fe}(\text{py})_4(\text{NCS})_2$ .<sup>69</sup> In all three tetrakis(pyridine)iron(II) sulfonate complexes, the O-Fe-O angles deviate from linearity by no more than  $7^\circ$ . In the triflate and methanesulfonate derivatives, the trans-pyridine N-Fe-N bond angles are very close to  $180^\circ$ ; whereas, in the p-tosylate derivative, this angle is  $173^\circ$  (Table 3.1). In all three examples, the overall distortion of the  $\text{FeN}_4\text{O}_2$  chromophore is not great and the environment around the iron atom may be

approximated as  $D_{4h}$ .

The mean Fe-N distances for the  $CF_3$ ,  $CH_3$  and  $p-CH_3C_6H_4$  derivatives are 2.21, 2.23 and 2.24 Å respectively. These values are comparable to the mean Fe-N distance of 2.23 Å reported for  $Fe(py)_4Cl_2$ ,<sup>68</sup> 2.26 Å for  $Fe(py)_4(NCS)_2$ ,<sup>69</sup> and 2.26 Å for  $[Fe(py)_6][Fe_4(CO)_{13}]$ .<sup>110</sup> The mean Fe-O distances range from 2.11 Å in the trifluoromethanesulfonate complex, to 2.06 Å in the methanesulfonate analogue. Of the three complexes studied,  $Fe(py)_4(CF_3SO_3)_2$  has the longest Fe-O bonds and the shortest Fe-N bonds. This may be a consequence of the relatively weaker coordinating strength of the triflate anion compared to the other sulfonate anions in these complexes. Assuming that the Fe-O bond distance in sulfonate complexes provides a good measure of the strength of the metal-anion interaction, then it is interesting to note that in  $[\eta^5-C_5(CH_3)_5](CO)_2FeOSO_2CF_3$  the Fe-O distance is only 2.007(3) Å.<sup>100</sup> The presence of the strong  $\pi$ -acid ligands in this complex makes the iron centre strongly electrophilic and a "strong electrostatic iron-triflate interaction" ensues which results in a shorter Fe-O bond than observed in the triflate derivative studied here.

The internal bonding parameters for the triflate anion in  $Fe(py)_4(CF_3SO_3)_2$  show that the bond distances and angles observed for the  $CF_3SO_3^-$  part of the molecule appear comparable to those of other unidentate triflate groups.<sup>97-100</sup> The anion assumes a staggered-ethane configuration about the S-C bond and whilst the mean C-F bond length is greater than usual for ionic  $CF_3SO_3^-$  containing compounds<sup>92-95</sup> it is typical for a unidentate

triflate anion.<sup>97-100</sup> Repulsions between oxygen atoms are greater than those between oxygen atoms and the trifluoromethyl group; as a result, the O-S-O angles are consistently greater than the C-S-O angles. The effect of unidentate anion coordination is most evident in range of S-O bond distances. The S-O bond involving the oxygen coordinated to iron is the longest such distance in the compound and the mean bond length for the terminal S-O bonds (1.44 Å) is close to the value found in ionic triflate complexes.

The methanesulfonate anion in  $\text{Fe}(\text{py})_4(\text{CH}_3\text{SO}_3)_2$  exhibits similar structural features to those found for the anion in  $\text{Fe}(\text{py})_4(\text{CF}_3\text{SO}_3)_2$ . For example, the methanesulfonate anion has a staggered-ethane configuration and the O-S-O angles are greater than, whilst the C-S-O angles are smaller than, the tetrahedral angle. The mean S-C bond distance (1.78 Å) is intermediate between those observed in  $\text{Fe}(\text{py})_4(\text{CF}_3\text{SO}_3)_2$  and in  $\text{Ca}(\text{CH}_3\text{SO}_3)_2$ <sup>16</sup> (where the S-C bond lengths are 1.82 and 1.75 Å respectively).

In  $\text{Fe}(\text{py})_4(\text{CH}_3\text{SO}_3)_2$ , where the anions act as unidentate ligands, the range of S-O bond lengths (1.439-1.490 Å) is, as expected, somewhat greater than where the sulfonate anion acts as a tridentate bridging ligand with each oxygen atom involved in equivalent coordination to a metal centre. For example,  $\text{Ca}(\text{CH}_3\text{SO}_3)_2$ <sup>16</sup> and  $\text{Cu}(\text{CO})(\text{C}_2\text{H}_5\text{SO}_3)$ <sup>105</sup> contain tridentate anions and the S-O bond lengths range from 1.429-1.456 Å and 1.444-1.462 Å respectively.

Two other methanesulfonate complexes with known structures are relevant to the present study,  $\text{Cu}(\text{H}_2\text{O})_4(\text{CH}_3\text{SO}_3)_2$ <sup>96</sup> and

$\text{Cd}(\text{H}_2\text{O})_2(\text{CH}_3\text{SO}_3)_2$ .<sup>102</sup> In the copper complex, the water molecules form the equatorial plane of a tetragonally elongated octahedron with the unidentate  $\text{CH}_3\text{SO}_3^-$  anions occupying the two axial positions. Somewhat surprisingly, and in contrast to what is found for the pyridine complexes studied here, the S-O bonds involving the terminal oxygen atoms in  $\text{Cu}(\text{H}_2\text{O})_4(\text{CH}_3\text{SO}_3)_2$ , are longer than those involving the oxygen atoms coordinated to the metal. This has been attributed to intermolecular hydrogen bonding interactions between terminal oxygen atoms and hydrogen atoms from water molecules on adjacent  $\text{Cu}(\text{H}_2\text{O})_4(\text{CH}_3\text{SO}_3)_2$  molecules.  $\text{Cd}(\text{H}_2\text{O})_2(\text{CH}_3\text{SO}_3)_2$  consists of cadmium atoms bridged by bidentate methanesulfonate groups to form an infinite chain structure.<sup>102</sup> In this case, the mean terminal S-O bond (1.44 Å) is slightly shorter than these bonds in  $\text{Fe}(\text{py})_4(\text{CH}_3\text{SO}_3)_2$  (1.45 Å). This result is expected, since, in the cadmium complex, the sulfur to oxygen  $\pi$ -bonding primarily involves only one terminal S-O bond; whereas, in  $\text{Fe}(\text{py})_4(\text{CH}_3\text{SO}_3)_2$ , the two terminally bonded oxygen atoms are involved in  $\pi$ -bonding to sulfur.

For the p-tosylate anion in  $\text{Fe}(\text{py})_4(\text{p-CH}_3\text{C}_6\text{H}_4\text{SO}_3)_2$ , the geometry around the sulfur is approximately tetrahedral and the benzene ring is planar within experimental error; the bond lengths and angles around this ring show no unusual features.<sup>111</sup> The effect of unidentate anion coordination is readily seen in the S-O bond distances; for example, the S-O distances for the bonds involving terminal oxygen atoms are shorter (1.44 Å) than the distances involving the coordinated oxygen atoms (1.49 Å). In organic p-toluenesulfonates,<sup>112-114</sup> the S-O distances of the

S-O-R group are even longer, being approximately 1.5-1.6 Å. This clearly illustrates the difference in the mode of bonding between p-tosylate and a metal ion on the one hand, and carbon on the other; the former is a more ionic interaction which does not perturb the anion as significantly as does the formation of a covalent bond to carbon. In fact, the S-O bond distances in the pyridine complex more closely resemble those found in  $\text{H}_3\text{O}^+(\text{p-CH}_3\text{C}_6\text{H}_4\text{SO}_3^-)$ .<sup>115</sup> This compound exists as an oxonium salt with all the S-O bonds approximately equivalent, with a mean S-O bond distance of 1.45 Å.

#### 3.3.1.2 X-ray structure determination of $\text{Cu}(\text{py})_4(\text{CF}_3\text{SO}_3)_2$

The structure of  $\text{Cu}(\text{py})_4(\text{CF}_3\text{SO}_3)_2$  shows many similarities with the structure of the analogous iron complex discussed above; however, some significant differences are also noted. A view of the molecular structure of  $\text{Cu}(\text{py})_4(\text{CF}_3\text{SO}_3)_2$  is shown in Fig. 3.4 and selected intramolecular bond distances and angles are given in Table 3.2. A complete compilation of X-ray structural data is given in Appendix I.

Table 3.2 Selected Bond Distances (Å) and Angles (°) for  
 $\text{Cu}(\text{py})_4(\text{CF}_3\text{SO}_3)_2^1$

---

Bond Distances	
Cu-O(1)	2.425(4)
Cu-N(1)	2.045(6)
Cu-N(2)	2.053(6)
Cu-N(3)	2.020(5)
S-O(1) linking	1.439(5)
S-O(2) terminal	1.422(4)

---

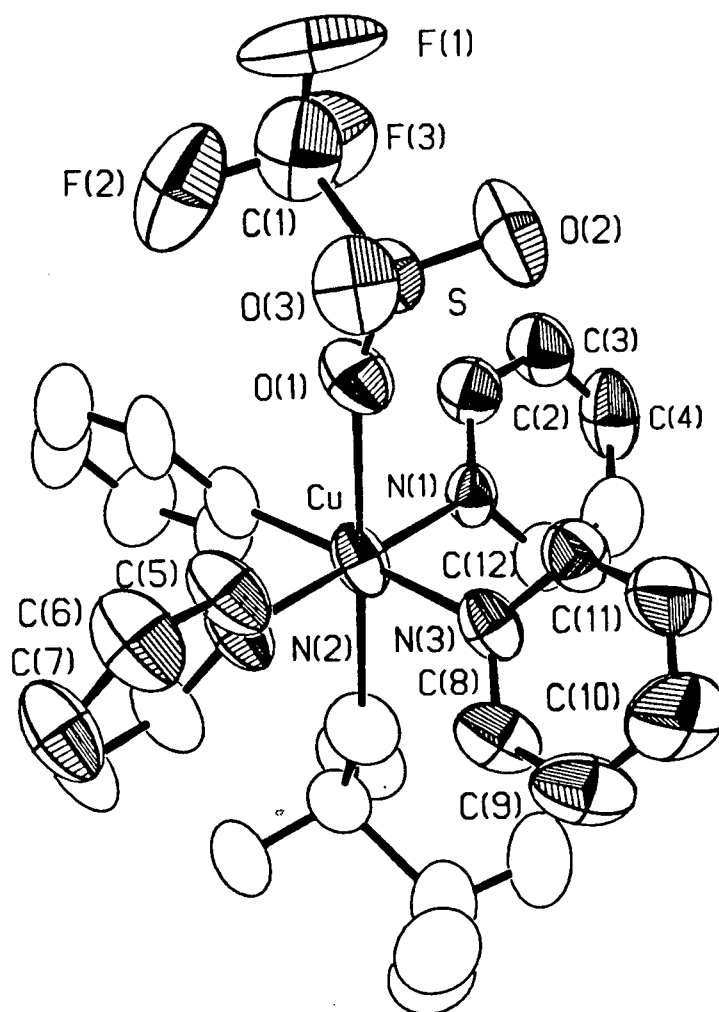
Bond Angles	
O(1)-Cu-O(1)	179.8(2)
N(1)-Cu-N(2)	180.0
O-S-O	115
O-S-C	103

---

1). Estimated standard deviations in parenthesis



Fig. 3.4 ORTEP Plot of the Structure of  $\text{Cu}(\text{py})_4(\text{CF}_3\text{SO}_3)_2$



As found for the analogous iron derivative, the coordination sphere around copper consists of a square-planar array of nitrogen atoms from four pyridine moieties and axial coordination sites occupied by oxygen atoms from trans-coordinated unidentate triflate anions. Unlike the coordination sphere about the metal in the analogous iron derivative, the coordination sphere in the copper complex is strongly distorted from regular octahedral geometry. The difference between the Cu-O (2.425(4)Å) and Cu-N (2.05 Å) bond distances reflects the large tetragonal distortion of the coordination sphere. This situation is often found in six-coordinate copper(II) compounds and is attributed to the Jahn-Teller effect.<sup>116</sup>

$\text{Cu}(\text{py})_4(\text{CF}_3\text{SO}_3)_2$  possesses a two-fold axis of symmetry, but unlike the analogous iron(II) derivative in which the two-fold axis bisects the cis N-Fe-N angle, the two-fold axis in  $\text{Cu}(\text{py})_4(\text{CF}_3\text{SO}_3)_2$  lies along the Cu-N(3) vector. The four nitrogen atoms and the copper atom lie in one plane and the pyridine rings are planar within experimental error. The pyridine rings are canted out of the  $\text{CuN}_4$  plane (56.7-64.7°) in a propeller-like arrangement as found for the analogous iron(II) derivative.

In  $\text{Cu}(\text{py})_4(\text{CF}_3\text{SO}_3)_2$ , the mean Cu-N distance (2.04 Å) is typical for a Cu-N bond in which the nitrogen-containing ligand is bound in the equatorial plane. For example the Cu-N bond distances in  $\text{Cu}(\text{pyz})_2(\text{ClO}_4)_2$ <sup>43</sup> and  $\text{Cu}(\text{NH}_3)_4\text{SO}_4 \cdot \text{H}_2\text{O}$ <sup>117</sup> are 2.06 and 2.05 Å respectively. The Cu-O bond distance in

$\text{Cu}(\text{py})_4(\text{CF}_3\text{SO}_3)_2$  (2.425(4) Å) and in two related structures provide for an interesting comparison. The inner coordination sphere in  $\text{Cu}(\text{pyz})_2(\text{ClO}_4)_2$ <sup>43</sup> and  $\text{Cu}(\text{H}_2\text{O})_4(\text{CH}_3\text{SO}_3)_2$ <sup>96</sup> are both distorted by a tetragonal elongation and anions are weakly bonded in the axial positions; the Cu-O bond lengths are 2.373(12) and 2.381(8) Å for the perchlorate and methanesulfonate complexes respectively. The longer Cu-O bond length in the triflate compound studied here, signifies a weaker cation-anion interaction in this complex which may reflect the more weakly basic nature of the triflate anion in comparison to perchlorate and methanesulfonate anions.

The bonding parameters for the triflate anion are similar to those found for the analogous iron(II) derivative (Section 3.3.1.1). For example, the triflate anion adopts a staggered-ethane configuration about the S-C bond and the O-S-O angles are greater than the C-S-O angles. The S-O bond lengths are similar to those found in  $\text{Fe}(\text{py})_4(\text{CF}_3\text{SO}_3)_2$ , the S-O(1) bond involving the oxygen bound to copper being longer than S-O(2), involving the terminally bound oxygen atom.

### 3.3.1.3 X-ray structure determination of $\text{Cu}(\text{pyz})_2(\text{CH}_3\text{SO}_3)_2$

The X-ray structure determination of  $\text{Cu}(\text{pyz})_2(\text{CH}_3\text{SO}_3)_2$  was relevant to the present study for several reasons. It established the mode of coordination of pyrazine and the orientation of the pyrazine  $\pi$ -system with respect to the d-orbitals of the copper ion. This particular  $d\pi$ - $p\pi$  interaction has been proposed as playing an important role in determining

the nature of the magnetic exchange interaction in copper(II)-pyrazine complexes.<sup>54</sup> The present study also established the mode of coordination of the methanesulfonate anion and permitted the bonding parameters for this part of the molecule to be compared to those in other  $\text{CH}_3\text{SO}_3^-$  containing species.

Complete structural parameters for  $\text{Cu}(\text{pyz})_2(\text{CH}_3\text{SO}_3)_2$  are given in Appendix I. The X-ray structure analysis revealed the complex to be made up of parallel sheets each consisting of an infinite square array of copper(II) ions bridged by bidentate pyrazine ligands; one such sheet is illustrated in Fig. 3.5. The inner coordination sphere around each copper ion is made up of two nitrogen atoms (Cu-N(1) distance of 2.058(2) Å), and two oxygen atoms (Cu-O(1) distance of 1.9559(13) Å); the axial coordination sites are occupied by pyrazine groups with significantly longer Cu-N bond lengths (Cu-N(2) bond distances of 2.692(2) Å). This is illustrated in Fig. 3.6 together with the atom numbering scheme and selected bond distances and angles are presented in Table 3.3.

In spite of being coordinated to copper at different distances, the pyrazine rings in  $\text{Cu}(\text{pyz})_2(\text{CH}_3\text{SO}_3)_2$  have similar internal bonding parameters. Both types of pyrazine ring are planar within experimental error and the bond lengths and angles within the pyrazine rings are similar to those found in free pyrazine.<sup>118</sup> The dimensions of the pyrazine rings compare well with those reported for other metal complexes containing bidentate bridging pyrazine ligands. For example, in the

Table 3.3 Selected Bond Distances (Å) and Angles (°) for  
 $\text{Cu}(\text{pyz})_2(\text{CH}_3\text{SO}_3)_2$ <sup>1</sup>

---

Bond Distances	
Cu-O(1)	1.9559(13)
Cu-N(1)	2.058(2)
Cu-N(2)	2.692(2)
S-O(1) (linking)	1.4832(13)
S-O(2) (terminal)	1.4423(13)
S-C(1)	1.765(2)

---

Bond Angles	
O(1)-S-O(1)	180
N(1)-Cu-N(1)	180
N(2)-Cu-N(2)	180
O-S-O	112
O-S-C	106

---

1). Estimated standard deviations in parenthesis

Fig. 3.5 View of a Single Layer in  $\text{Cu}(\text{pyz})_2(\text{CH}_3\text{SO}_3)_2$

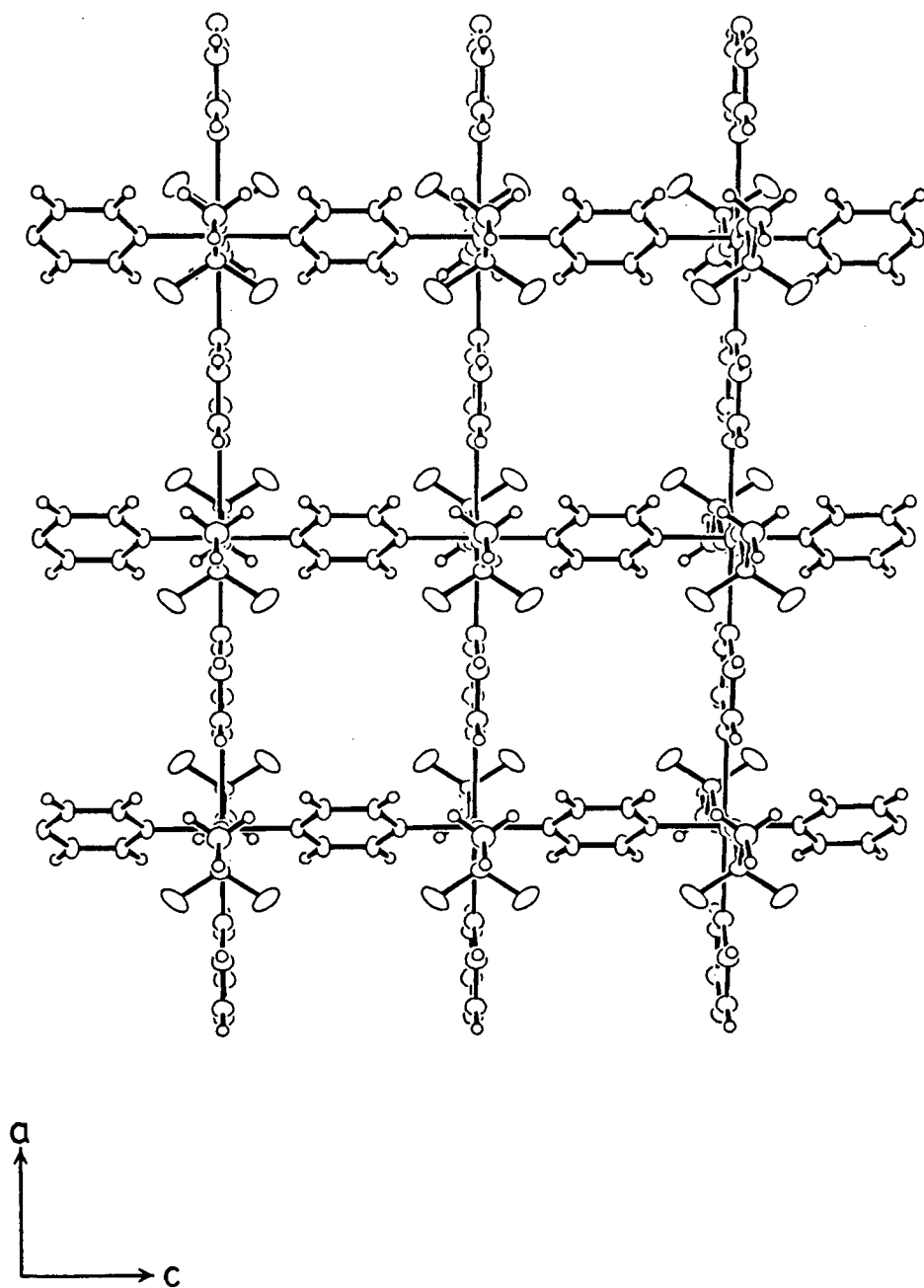
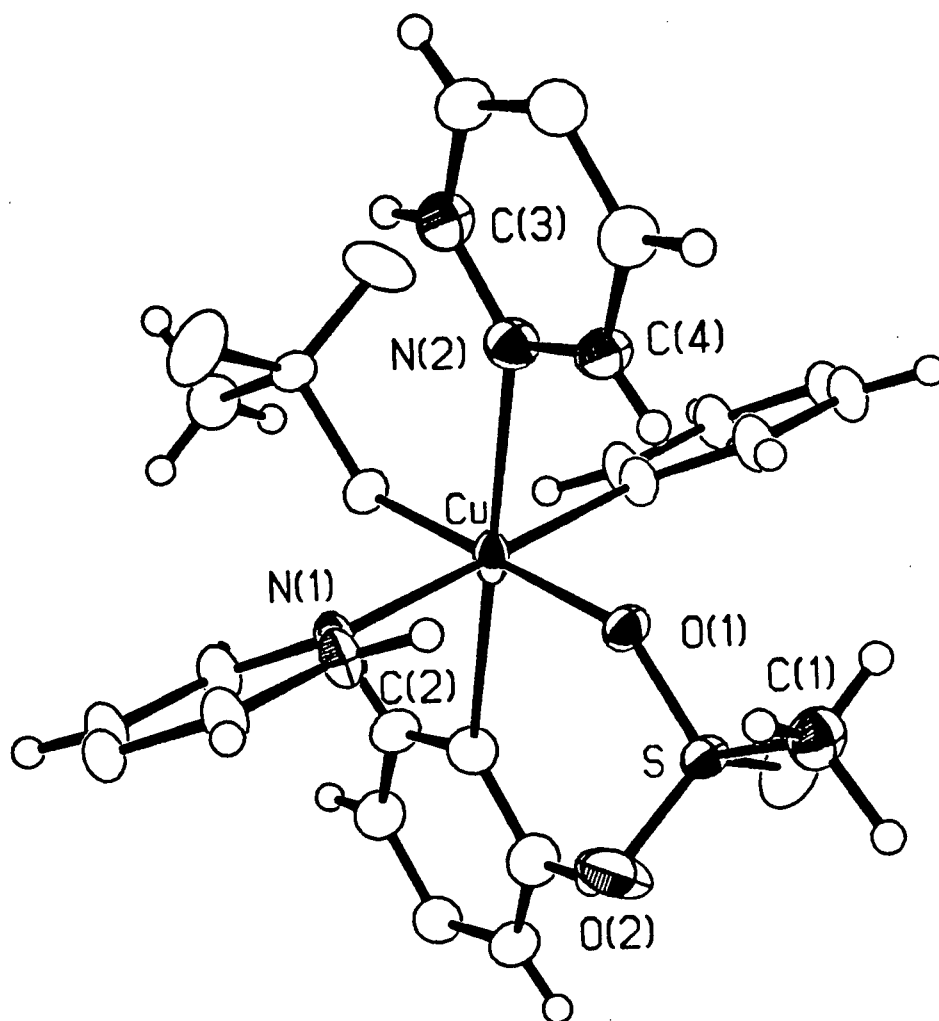


Fig. 3.6 ORTEP Plot of the Inner Coordination Sphere About the Copper Ion in  $\text{Cu}(\text{pyz})_2(\text{CH}_3\text{SO}_3)_2$



Creutz-Taube complex the mean C-N bond length is 1.348(9) Å and the C-C distance is 1.382(10) Å;<sup>46</sup> in  $\text{Cu}(\text{pyz})_2(\text{CH}_3\text{SO}_3)_2$  these distances are 1.341 and 1.390 Å respectively.

The pyrazine rings involved in the stronger bonding to copper (hereafter called the equatorially bound pyrazine ligands) are canted at an angle of  $28.50(8)^\circ$  to the  $\text{CuN}_2\text{O}_2$  (xy) plane; whereas, the pyrazine rings bonded weakly to copper (hereafter called the axially bound pyrazine ligands) lie in the  $\text{CuN}_2\text{O}_2$  (xz) plane.

The methanesulfonate anion in  $\text{Cu}(\text{pyz})_2(\text{CH}_3\text{SO}_3)_2$  adopts a staggered-ethane configuration as found for  $\text{Fe}(\text{py})_4(\text{CH}_3\text{SO}_3)_2$  (Section 3.3.1.1). The S-O(1) bond length (1.4832(13) Å) is significantly longer than the distance of 1.4423(13) Å found for the terminally bound S-O(2) bond as a result of coordination of oxygen atom O(1) to copper. The remaining bonding parameters for the anion, for example, the S-C bond length and the O-S-O and O-S-C bond angles, are of a comparable magnitude to those found in  $\text{Fe}(\text{py})_4(\text{CH}_3\text{SO}_3)_2$  (Section 3.3.1.1).

The Cu-O bond distance in  $\text{Cu}(\text{pyz})_2(\text{CH}_3\text{SO}_3)_2$  (1.9959(13) Å) is typical for an oxygen atom bound to copper in the equatorial plane; for example in  $\text{Cu}(\text{pyz})(\text{NO}_3)_2$  the equatorial Cu-O bond distance is 2.010(4) Å.<sup>42</sup> The Cu-N(1) distance (2.062(3) Å) is almost identical to the value of 2.058(2) Å found in  $\text{Cu}(\text{pyz})_2(\text{ClO}_4)_2$ ;<sup>43</sup> whereas, the Cu-N(2) distance (2.692(2) Å) in  $\text{Cu}(\text{pyz})_2(\text{CH}_3\text{SO}_3)_2$  is much longer. This axial pyrazine group is further removed from the copper atom than the axial pyrazine groups in  $\text{Cu}(\text{pyz})(\text{hfac})_2$ ,<sup>53</sup> (Cu-N of 2.529(9) Å) and

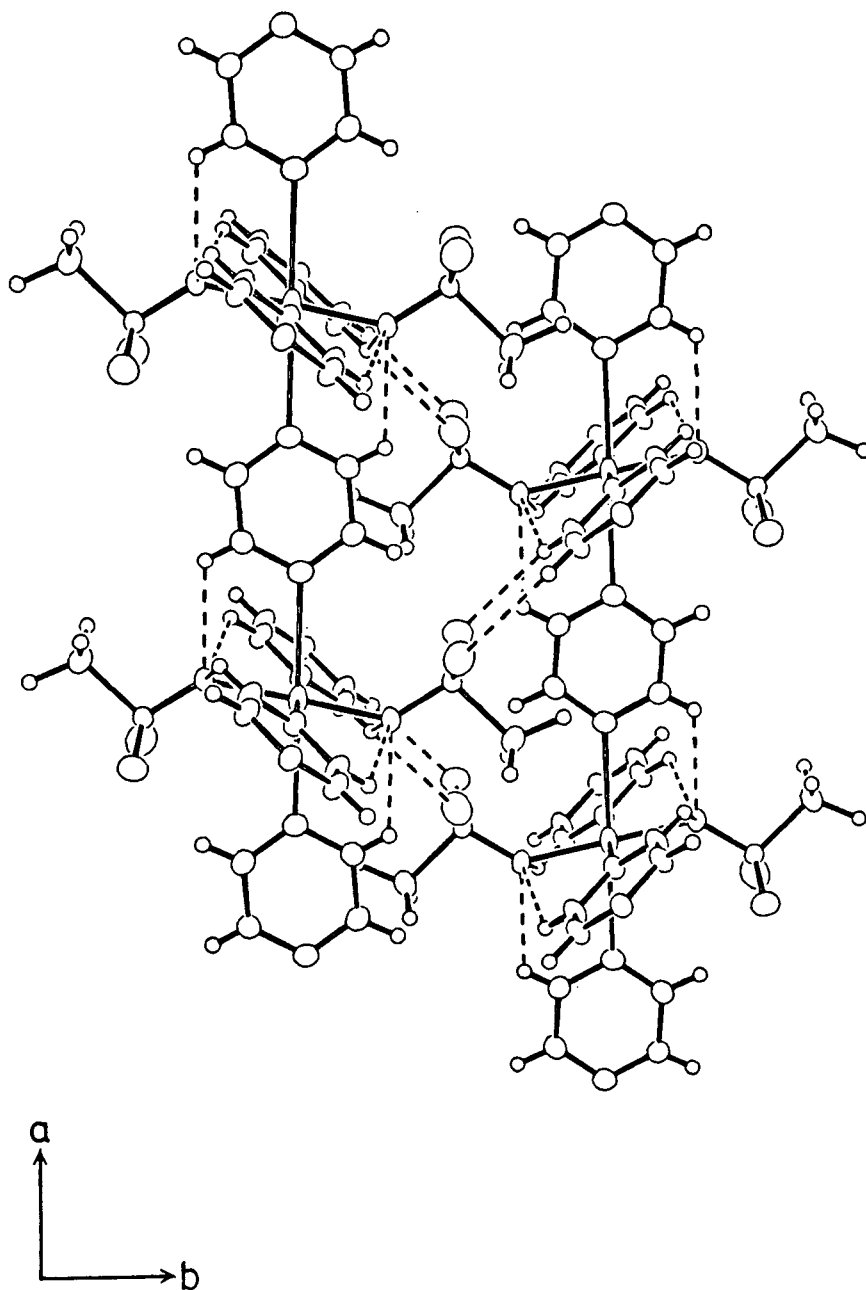


$\text{Cu}_2(\text{OAc})_4(\text{pyz})^{55}$  (Cu-N of 2.171(6) Å), indicating a much weaker copper axial-pyrazine interaction in the methanesulfonate complex.

There are several hydrogen-bonding interactions which may play a role in determining the overall structure of  $\text{Cu}(\text{pyz})_2(\text{CH}_3\text{SO}_3)_2$  (Figs. 3.7-3.8). Intralayer hydrogen-bonding interactions between the sulfonate oxygen atom O(1) and the hydrogen atoms attached to the pyrazine rings appear to influence the canting of the pyrazine rings. The hydrogen-bond distances, H(4)-O(1) and H(2)-O(1) are 2.50 and 2.46 Å respectively. The first of these interactions holds the axial pyrazine group in the  $\text{CuN}_2\text{O}_2$  plane; whereas, the second interaction may partially result in the observation that the equatorially bound pyrazine ligand is canted at an angle of  $28^\circ$  to the  $\text{CuN}_2\text{O}_2$  plane.

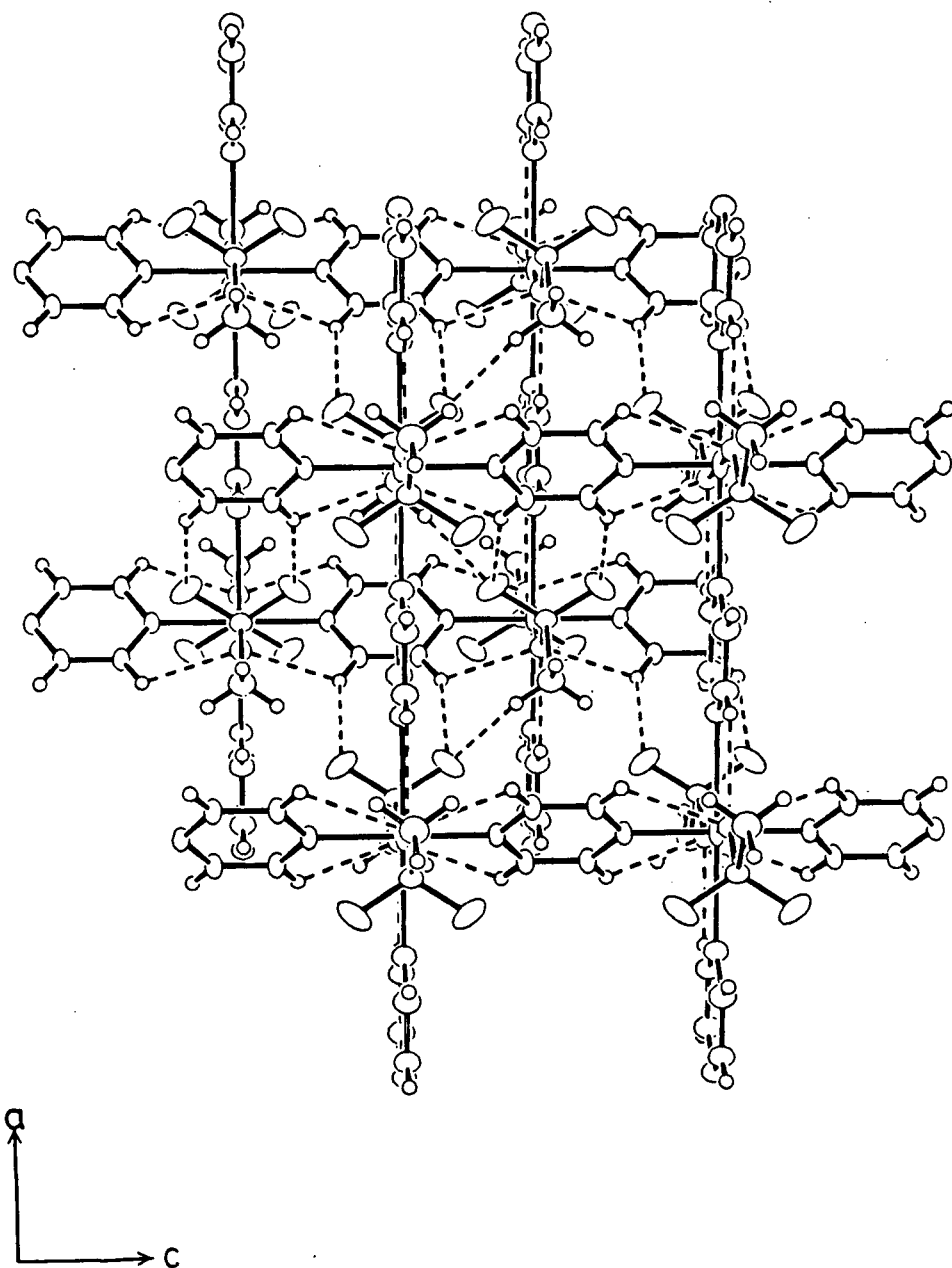
In  $\text{Cu}(\text{pyz})_2(\text{CH}_3\text{SO}_3)_2$ , the layers are separated by a distance of 6.565 Å. In comparison, the interlayer separation in  $\text{Cu}(\text{pyz})_2(\text{ClO}_4)_2^{43}$  is 7.012 Å. The proximity of adjacent layers in the methanesulfonate complex may result from intralayer hydrogen-bonding interactions. There are two such interactions, H(1b)-O(2) (2.38 Å) and H(2)-O(2) (2.50 Å), which may be significant. Both involve the terminally bound sulfonate oxygen atom, O(2), which interacts with a hydrogen atom of a methanesulfonate anion on an adjacent layer, and a hydrogen atom on the equatorially bound pyrazine ligand.

Fig. 3.7 Two Adjacent Layers in  $\text{Cu}(\text{pyz})_2(\text{CH}_3\text{SO}_3)_2$  Viewed Along the c-Axis



Hydrogen bonding interactions shown by broken lines

Fig. 3.8 Two Adjacent Layers in  $\text{Cu}(\text{pyz})_2(\text{CH}_3\text{SO}_3)_2$  Viewed Along the b-Axis



Hydrogen bonding interactions shown by broken lines

It is informative to compare the similarities and differences between the structures of  $\text{Cu}(\text{pyz})_2(\text{CH}_3\text{SO}_3)_2$  and  $\text{Cu}(\text{pyz})_2(\text{ClO}_4)_2$ .<sup>43</sup> Both complexes contain bidentate bridging pyrazine groups resulting in a two-dimensional lattice. For  $\text{Cu}(\text{pyz})_2(\text{ClO}_4)_2$ , the copper ions are surrounded by a square-planar array of nitrogen atoms. In contrast, the square plane in  $\text{Cu}(\text{pyz})_2(\text{CH}_3\text{SO}_3)_2$  consists of two trans-pyrazine groups and two trans-oxygen donor atoms from unidentate methanesulfonate anions. For  $\text{Cu}(\text{pyz})_2(\text{ClO}_4)_2$ , it is the perchlorate anions which are weakly coordinated in axial sites; whereas, in the methanesulfonate derivative two pyrazine groups weakly interact with the copper centre and are coordinated along the z-axis; the methanesulfonate anions being coordinated strongly in the equatorial plane. In  $\text{Cu}(\text{pyz})_2(\text{CH}_3\text{SO}_3)_2$ , this type of anion coordination does not appear to be related to the weakly basic nature of the anion. From a consideration of anion basicity, it might be expected that the anion would coordinate weakly in the axial sites, as is the case in  $\text{Cu}(\text{H}_2\text{O})_4(\text{CH}_3\text{SO}_3)_2$ .<sup>96</sup> One possible explanation for strong methanesulfonate anion coordination in this case, may be that in this coordination mode a significant hydrogen-bonding interaction takes place between the coordinated sulfonate oxygen atom, O(1) and the hydrogen atom, H(4) on the axially bound pyrazine ring, O(1)-H(4) distance is 2.50 Å. In  $\text{Cu}(\text{H}_2\text{O})_4(\text{CH}_3\text{SO}_3)_2$ ,<sup>96</sup> this type of hydrogen-bonding interaction cannot take place. In  $\text{Cu}(\text{pyz})_2(\text{ClO}_4)_2$ ,<sup>43</sup> the canting of the pyrazine rings effectively eliminates this interaction.

In summary, the X-ray diffraction studies described in Sections 3.3.1.1-3.3.1.3 permitted the determination of the structure of some iron and copper complexes containing pyridine, pyrazine and sulfonate anions as ligands. The tetrakis(pyridine)iron(II) and copper(II) sulfonate complexes exist as isolated molecular units, containing square-planar arrangements of pyridine ligands and axially coordinated unidentate sulfonate anions.  $\text{Cu}(\text{pyz})_2(\text{CH}_3\text{SO}_3)_2$  is a two-dimensional sheet-like polymer containing two distinct types of bridging pyrazine moieties and unidentate methanesulfonate anions. In the tetrakis(pyridine)iron(II) complexes, the coordination sphere about the metal shows a small tetragonal compression; whereas, in both copper complexes studied, the coordination sphere is distorted by a significant tetragonal elongation, as a result of the Jahn-Teller effect. The following sections of this chapter discuss the spectroscopic and magnetic properties of these compounds in view of their known structures. These spectroscopic and magnetic properties are also compared with those of other complexes for which detailed structural analyses have not yet been possible.

### 3.3.2 Infrared Spectroscopy

Infrared spectral results for complexes with an  $MN_4X_2$  chromophore are presented in this section. The spectra have been assigned in terms of vibrations which arise separately from the neutral ligand and the anion. In the light of their known structures, the tetrakis(pyridine)iron(II) complexes and  $Cu(py)_4(CF_3SO_3)_2$  are discussed first; the infrared spectrum of  $Cu(py)_4(CH_3SO_3)_2$  is also considered in Section 3.3.2.1. Following this, the infrared data for the  $Fe(pyz)_2X_2$  compounds (where  $X^-$  is  $Cl^-$ ,  $Br^-$ ,  $I^-$  or  $NCS^-$ ) are considered (Section 3.3.2.2), and because of the simplicity of the anion spectra, these examples are presented prior to discussion of the infrared data for the bis(pyrazine) complexes containing sulfonate or perchlorate anions (Section 3.3.2.3). Finally, the infrared spectral data for  $Fe(2-mepyz)_4(CH_3SO_3)_2$ ,  $Cu(pyz)_4(CF_3SO_3)_2 \cdot H_2O$  and  $Fe(pyz)_4(AsF_6)_2 \cdot 2H_2O$  are analysed (Section 3.3.2.4).

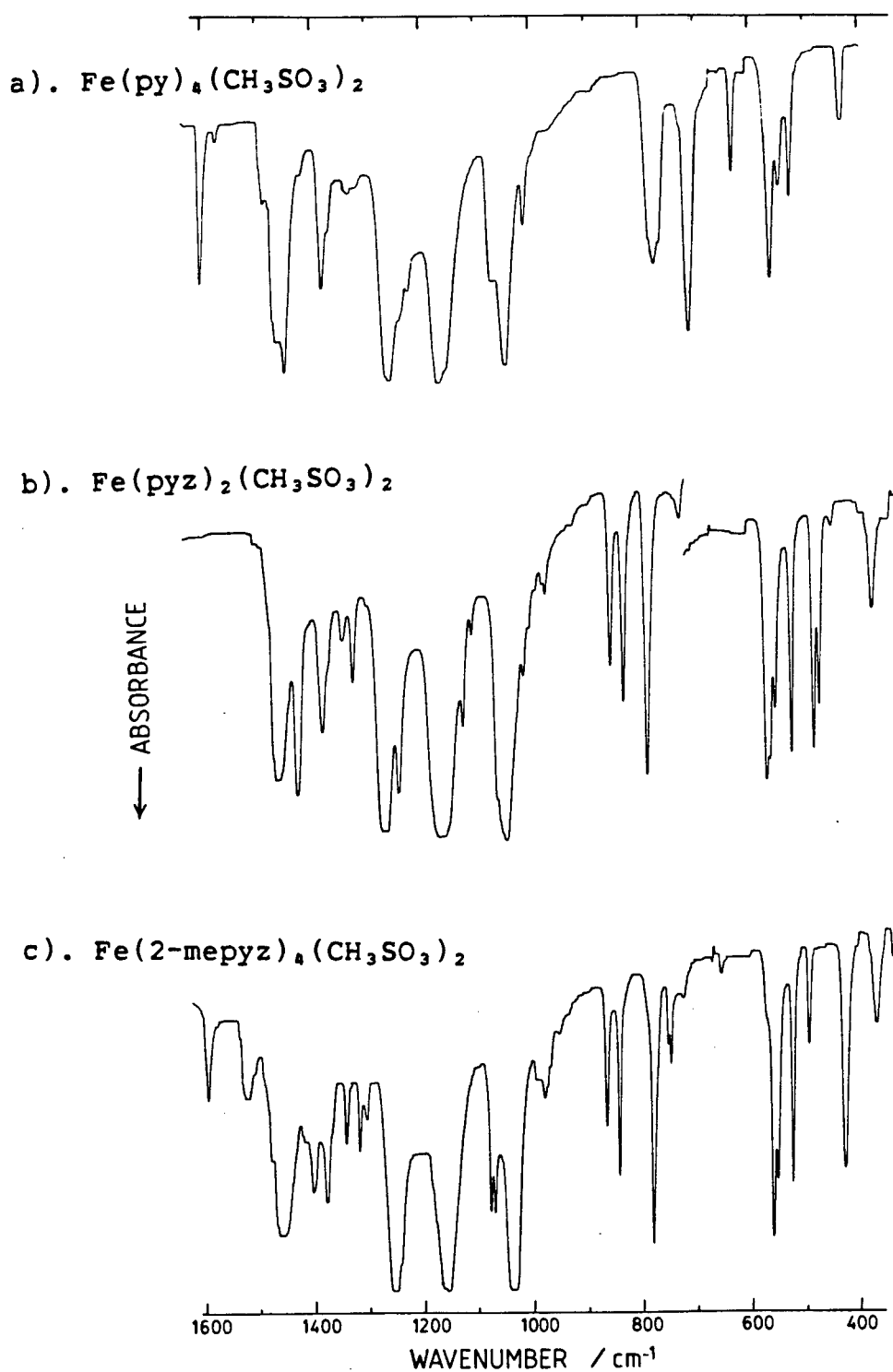
The spectral bands assigned to pyridine vibrations in the tetrakis(pyridine) compounds are compiled in Appendix II and sulfonate anion vibrations and unassigned bands are listed in Appendix III. To facilitate comparisons between complexes containing the same sulfonate anion, Appendix III is divided into Parts A, B and C. Each part tabulates the infrared assignments of the anions for the compounds containing triflate, methanesulfonate and p-tosylate anions respectively. Vibrational assignments for pyrazine in the bis(pyrazine) complexes are given in Appendix IV.

### 3.3.2.1 Infrared spectral results for tetrakis(pyridine) complexes

The  $M(\text{py})_4(\text{RSO}_3)_2$  complexes have vibrational bands in the infrared region which are assigned separately to the pyridine ligand and the sulfonate anion (Appendices II and III respectively). A representative spectrum of this class of compound, that of  $\text{Fe}(\text{py})_4(\text{CH}_3\text{SO}_3)_2$ , is shown in Fig. 3.9a. Previous research<sup>77</sup> has suggested that each band in the infrared spectrum of pyridine is reproduced in pyridine complexes with only minor shifts or splittings. Such a 1:1 correspondence is also observed in this study and allowed the coordinated pyridine vibrations to be ascertained by a direct comparison with the spectrum of the uncomplexed base. The assignments of the normal vibrational modes of liquid pyridine, made by Kline and Turkevich<sup>119</sup> and the more recent assignment of overtones<sup>120</sup> are given in Appendix II. Upon coordination of pyridine, most bands shift in frequency by up to  $10\text{ cm}^{-1}$ . As observed previously,<sup>77</sup> the 8a, 6a and 16b vibrations show a more pronounced coordination dependence and shift by  $20\text{--}30\text{ cm}^{-1}$  to higher frequency upon coordination. Some of the pyridine bands exhibit small splittings which, in this and earlier studies, are attributed to interactions between adjacent pyridine rings.<sup>121</sup>

In the free sulfonate anion,  $\text{RSO}_3^-$ , the symmetry is  $C_{3v}$  and six infrared-active bands ( $3E$  and  $3A_1$ ) are expected to arise from the  $\text{CSO}_3^-$  fragment of the anion; these fundamental vibrations have been designated  $\nu_1$  to  $\nu_6$ .

Fig. 3.9 Infrared Spectra of  $\text{Fe}(\text{py})_4(\text{CH}_3\text{SO}_3)_2$ ,  
 $\text{Fe}(\text{pyz})_2(\text{CH}_3\text{SO}_3)_2$  and  $\text{Fe}(\text{2-mepyz})_4(\text{CH}_3\text{SO}_3)_2$

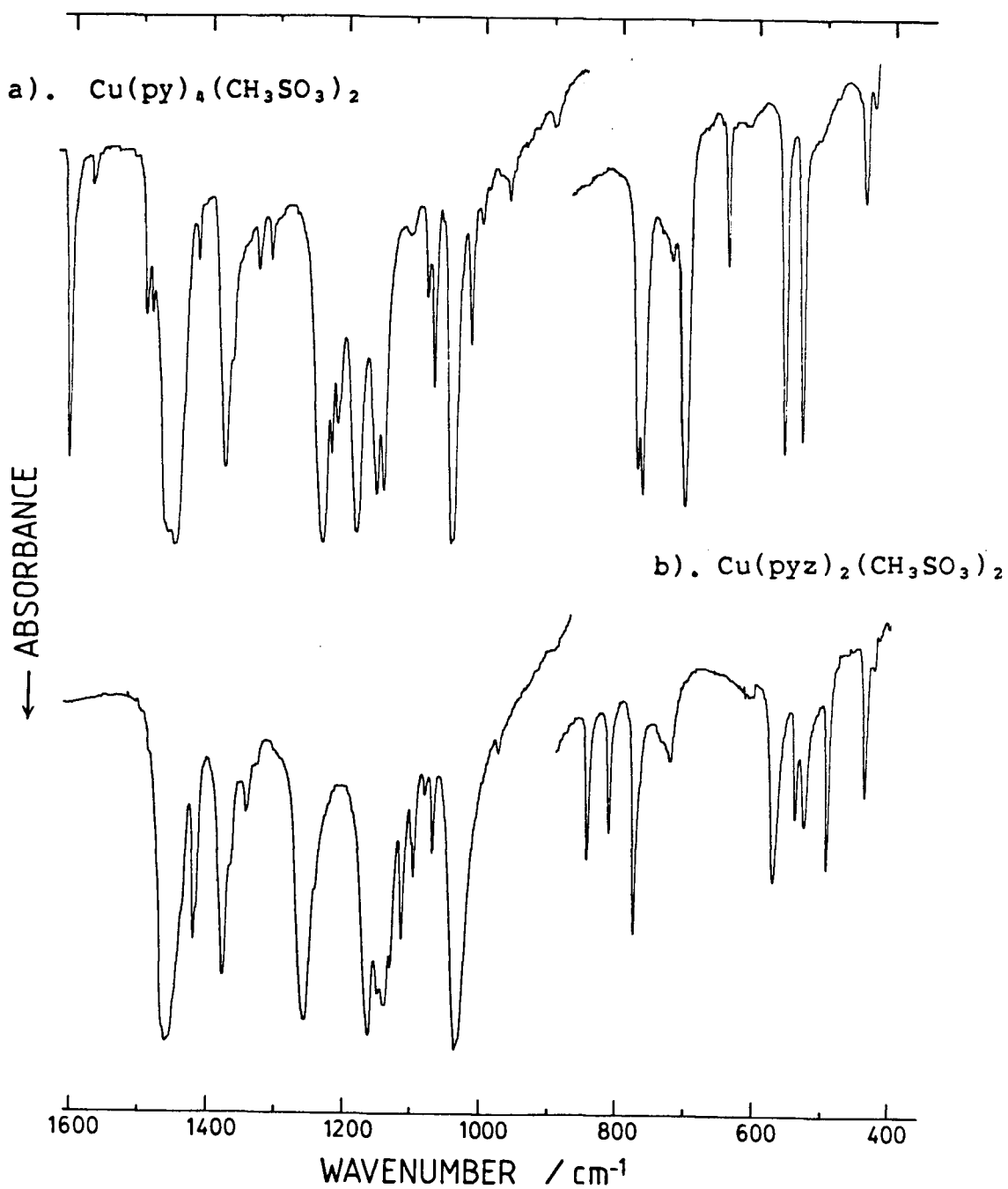




These bands have been assigned in a number of anhydrous metal sulfonate complexes,  $M(\text{RSO}_3)_2$ ,<sup>23, 25, 87</sup> where the anion retains  $C_{3v}$  symmetry by adopting a tridentate mode of coordination. If the anion coordinates in any other way than by using three oxygen atoms in an equivalent fashion, then the anion symmetry is reduced to either  $C_s$  or  $C_i$ ; the degenerate E modes ( $\nu_4$ ,  $\nu_5$  and  $\nu_6$ ) are expected to split and a total of nine infrared-active vibrations should be observed. For the  $\text{Fe}(\text{py})_4(\text{RSO}_3)_2$  complexes, a splitting of some of the doubly degenerate anion bands is evident. In particular, the splitting of  $\nu_4$ , the asymmetric  $\text{SO}_3$  stretching vibration, is the largest (approximately  $80 \text{ cm}^{-1}$ ) and most clearly observed in all cases; whereas, splitting of  $\nu_5$ , the asymmetric  $\text{SO}_3$  deformation, when observed, is much smaller (approximately  $10 \text{ cm}^{-1}$ ). In the present study,  $\nu_6$ , the S-C deformation mode, is difficult to assign due to its weak nature and the possibility that it is obscured by the 16b vibration of pyridine. The splittings of the doubly degenerate modes, in particular the splitting of  $\nu_4$ , indicate that the anion symmetry is reduced below  $C_{3v}$  which is consistent with unidentate anion coordination as revealed by X-ray crystallography (Section 3.3.1.1).

The infrared spectra of  $\text{Cu}(\text{py})_4(\text{CF}_3\text{SO}_3)_2$  and  $\text{Cu}(\text{py})_4(\text{CH}_3\text{SO}_3)_2$  (Appendices II and III) exhibit both similarities and differences with those of the analogous iron(II) derivatives. The infrared spectrum of  $\text{Cu}(\text{py})_4(\text{CH}_3\text{SO}_3)_2$  is shown in Fig. 3.10a and may be compared with that of  $\text{Fe}(\text{py})_4(\text{CH}_3\text{SO}_3)_2$  (Fig. 3.9a).

Fig. 3.10 Infrared Spectra of  $\text{Cu}(\text{py})_4(\text{CH}_3\text{SO}_3)_2$  and  $\text{Cu}(\text{pyz})_2(\text{CH}_3\text{SO}_3)_2$



The similarities between the infrared spectra of the copper and iron derivatives are clearly seen. In the copper complexes, three absorptions are observed in the  $\text{SO}_3$  stretching region ( $1000\text{--}1280\text{ cm}^{-1}$ ) as expected upon reduction of anion symmetry below  $\text{C}_{3v}$ . The other anion bands occur at frequencies similar to those observed for the iron analogues. Vibrational assignments for the neutral ligand also show similarities in the two groups of compounds. Pyridine ligand absorptions are reproduced in the copper complexes with some shifts and splittings when compared to the spectrum of pyridine. These infrared spectral data indicate that the basic structure of the copper and iron derivatives is similar and this has been confirmed by X-ray crystallography (Sections 3.3.1.1 and 3.3.1.2).

Several important differences are noted, however, between the infrared spectra of the copper and iron derivatives. Firstly, for the copper(II) derivatives the magnitude of the splitting of the  $\text{SO}_3$  asymmetric stretching mode,  $\nu_4$ , is approximately half the value found for the iron(II) compounds, i.e., approximately  $90$  and  $50\text{ cm}^{-1}$  for the iron and copper complexes respectively. Secondly, the infrared spectra of both tetrakis(pyridine)copper(II) derivatives have the asymmetric  $\text{SO}_3$  deformation mode,  $\nu_5$ , remaining as one single unsplit band; whereas, in the analogous iron(II) complexes this band is split by approximately  $10\text{ cm}^{-1}$ . Finally, an additional difference between the copper and iron complexes, is the extent to which the  $8a$ ,  $6a$  and  $16b$  vibrations of pyridine are shifted from those

observed in the spectrum of free pyridine. For example, for the  $M(\text{py})_4(\text{CF}_3\text{SO}_3)_2$  complexes, the 16b vibration occurs at 428 and 443  $\text{cm}^{-1}$ , where M is Fe and Cu respectively. These spectral differences indicate structural differences between the two groups of compounds. For the copper complexes, the smaller degree of splitting of  $\nu_4$ , when compared to the iron compounds, and the lack of splitting of  $\nu_5$ , indicate that there is a weaker cation-anion interaction in the copper complexes. This decrease in strength of the cation-anion interaction appears to correlate with an increase of the copper-pyridine interaction, as measured by the greater frequency increase of the 16b band in the copper(II) derivatives. These infrared results are consistent with the findings of the X-ray structure determinations for the  $M(\text{py})_4(\text{CF}_3\text{SO}_3)_2$  complexes (where M is Fe and Cu, Sections 3.3.1.1 and 3.3.1.2 respectively). For example, the Cu-O bond distance (2.425 Å) in  $\text{Cu}(\text{py})_4(\text{CF}_3\text{SO}_3)_2$  is considerably longer than the mean Fe-O bond distance (2.11 Å) in the iron complex and the mean M-N distances are 2.04 and 2.21 Å for the copper and iron derivatives respectively. The Jahn-Teller distortion in the copper(II) complexes accounts for the weak cation-anion and strong cation-pyridine interaction when compared to the iron(II) complexes.

For  $M(\text{py})_4(\text{RSO}_3)_2$  compounds, the bands which are not assigned to either the pyridine ligand or the sulfonate anion vibrations are listed in Appendix III, Parts A-C. These "unassigned" bands may include the  $\nu_6$  vibration of the anion and also the internal vibrations of the anion associated with the

$\text{CF}_3$ ,  $\text{CH}_3$  or  $p\text{-CH}_3\text{C}_6\text{H}_4$  groups. These bands are not generally useful in determining the mode of coordination of the anion.

For compounds containing trifluoromethyl groups, absorption bands in the  $1150\text{-}1250\text{ cm}^{-1}$  region have been previously assigned to C-F stretching vibrations.<sup>122</sup> In the present study, these bands occur in the same region as the intense S-O stretching vibrations. In the triflate complexes,  $\text{Fe}(\text{py})_4(\text{CF}_3\text{SO}_3)_2$  and  $\text{Cu}(\text{py})_4(\text{CF}_3\text{SO}_3)_2$ , several bands, in addition to the  $\text{SO}_3$  symmetric and asymmetric stretching vibrations, are present in this region and are proposed to arise from C-F stretching vibrations. Likewise, the C-F deformation modes have been previously observed around  $580\text{ cm}^{-1}$  in  $\text{AgCF}_3\text{SO}_3$ ,<sup>122</sup> and the triflate derivatives prepared in this study exhibit weak absorptions in this region which may be attributed to these vibrations (Appendix III, Part A).

Methanesulfonate derivatives are expected to show bands characteristic of the methyl group, for example, bands arising from C-H deformation modes in the  $1300\text{-}1350\text{ cm}^{-1}$  region.<sup>122</sup> In this study the methanesulfonate-containing compounds exhibit weak absorptions in this part of the spectrum which may be assigned to these vibrational modes (Appendix III, Part B).

Of the tetrakis(pyridine) derivatives studied here,  $\text{Fe}(\text{py})_4(p\text{-CH}_3\text{C}_6\text{H}_4\text{SO}_3)_2$  exhibits the most complex infrared spectrum. No attempt has been made to assign the internal vibrations of the  $p\text{-CH}_3\text{C}_6\text{H}_4$  group.

Anion spectra very similar to those reported here have been used previously to infer unidentate sulfonate anion

coordination.<sup>76</sup> The combination of X-ray diffraction and infrared spectroscopy which were used in this study, has validated these earlier conclusions and supports the use of infrared criteria for the determination of anion coordination and pyridine bonding in such complexes. Furthermore, the current study has shown that the magnitude of the splitting of  $\text{SO}_3$  asymmetric stretching mode, ( $\nu_4$ ), is a particularly good measure of the degree of interaction between the sulfonate anion and the metal, and the shifts in the pyridine 6a and 16b vibrations correlate well with the strength of the metal-pyridine interaction.

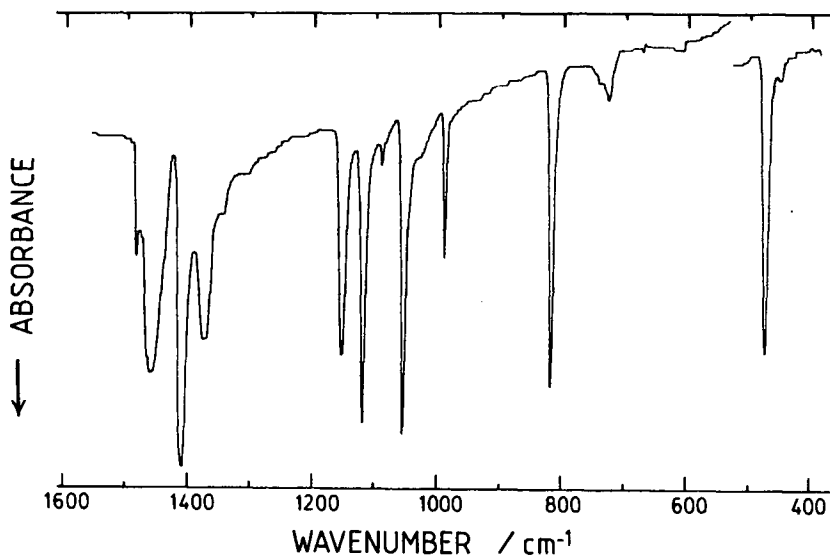
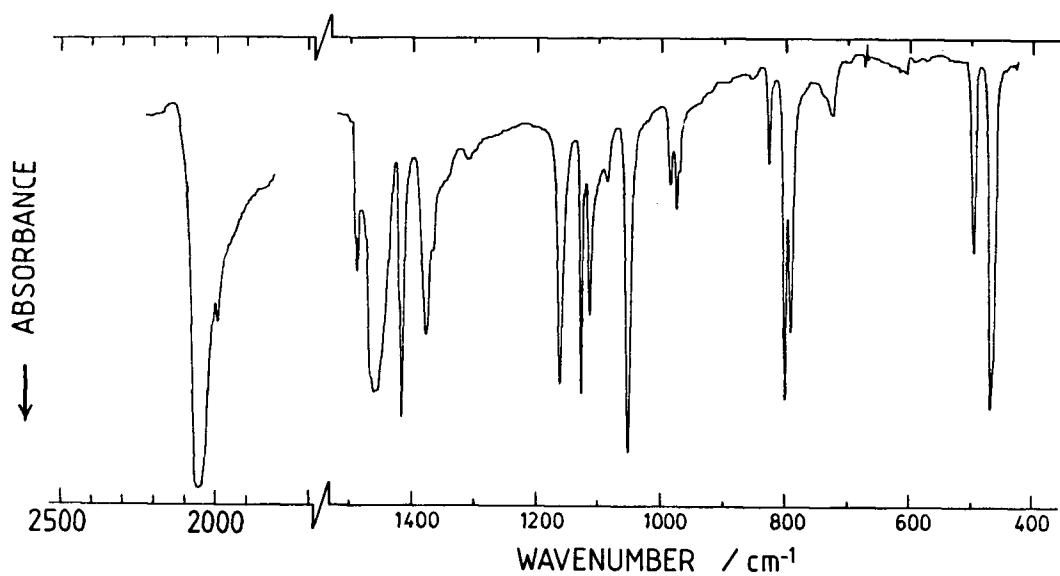
### 3.3.2.2 Infrared spectral results for bis(pyrazine)iron(II) halide and thiocyanate complexes

Previous studies on the infrared spectra of pyrazine complexes of cobalt(II) and nickel(II) halides have used the presence or absence of a single band in the  $980\text{ cm}^{-1}$  region as a basis for determining whether pyrazine coordinates in a uni- or bidentate mode.<sup>32, 33, 38</sup> Later studies have demonstrated this mid-infrared criterion to be sometimes misleading; however, by using a combination of infrared and Raman spectroscopy, Goldstein et al. were able to unambiguously determine the mode of pyrazine bonding in a series of  $\text{M}(\text{pyz})_2\text{X}_2$ <sup>37</sup> and  $\text{Sn}(\text{pyz})_n\text{X}_4$ <sup>44</sup> compounds. Their approach considered the different symmetries of unidentate and bidentate pyrazine groups and the effect of ligand symmetry on the infrared and Raman spectra of pyrazine complexes. Electron diffraction results<sup>123</sup> indicate that

pyrazine is planar; the symmetry may be represented by the  $D_{2h}$  point group and infrared assignments have been made and subsequently discussed on this basis.<sup>124</sup> When both nitrogen atoms of pyrazine coordinate equivalently to metal centres in a bridging mode, then the symmetry remains the same as in the uncomplexed ligand and a mutual exclusion of infrared and Raman bands occurs. When pyrazine coordinates through only one nitrogen atom, in a unidentate mode, the symmetry is reduced to at least  $C_{2v}$  and vibrational bands formally forbidden in  $D_{2h}$  symmetry become active in the infrared spectrum of the complex. Infrared spectra were routinely recorded in the present study, but the intense red-brown colour of the halide and thiocyanate complexes has precluded any characterisation by Raman spectroscopy.

The infrared spectra of the bis(pyrazine) complexes,  $Fe(pyz)_2X_2$  are tabulated in Appendix IV. The assignments of free pyrazine are those of Lord et al.<sup>124</sup> A representative spectrum of this class of complex, that of  $Fe(pyz)_2I_2$ , is shown in Fig 3.11. Previously reported infrared spectral data<sup>62 63</sup> for the chloro- and bromo derivatives are comparable to the data presented in this study.

The infrared activity of the pyrazine vibrational modes in these complexes is similar to that observed in known pyrazine-bridged complexes, for example,  $Sn(pyz)X_4$ ,<sup>44</sup> and  $M(pyz)_2X_2$ <sup>37</sup> (where  $X^-$  is  $Cl^-$ ,  $Br^-$  or  $I^-$ ); but is markedly different from that of  $Sn(pyz)_2X_4$ <sup>44</sup> (where  $X^-$  is  $Cl^-$  or  $Br^-$ ), in which pyrazine coordinates in a unidentate mode.

Fig. 3.11 Infrared Spectra of  $\text{Fe}(\text{pyz})_2\text{I}_2$  and  $\text{Fe}(\text{pyz})_2(\text{NCS})_2$  $\text{Fe}(\text{pyz})_2\text{I}_2$  $\text{Fe}(\text{pyz})_2(\text{NCS})_2$ 



The infrared spectra of complexes containing unidentate pyrazine groups and the Raman spectrum of free pyrazine<sup>124</sup> exhibit bands at approximately 1230, 920 and 750  $\text{cm}^{-1}$ . For the bis(pyrazine)iron(II) compounds there are no absorption bands in these regions, indicating that the pyrazine ligand retains  $D_{2h}$  symmetry upon complex formation by acting as a bidentate bridge between metal centres.

Most of the pyrazine absorptions exhibit shifts upon coordination of pyrazine. The most coordination sensitive of these absorption bands, at 417  $\text{cm}^{-1}$  in the uncoordinated ligand,<sup>124</sup> is shifted to considerably higher frequency (30-40  $\text{cm}^{-1}$ ) upon complex formation. Small splittings of some of the pyrazine vibrations are observed upon coordination and this may arise from interactions between adjacent pyrazine rings, as has been proposed for pyridine complexes.<sup>121</sup> Different orientations of the pyrazine rings about their N-N axes may result in different environments for the pyrazine groups, another possible cause of the splittings.

The infrared spectrum of  $\text{Fe}(\text{pyz})_2(\text{NCS})_2$  provides insight not only on pyrazine coordination but also on anion coordination. Infrared criteria have been developed<sup>125-128</sup> to determine the mode of coordination of the thiocyanate anion. Several alternatives exist: coordination to the metal through nitrogen only (thiocyanato-N), coordination to the metal through sulfur only (thiocyanato-S), or bridging two metal ions to form M-NCS-M' units. These three types of coordination are well known.<sup>127</sup> Other modes of bridging such as  $>\text{NCS}^-$  or  $>\text{SCN}^-$  are

also possible.

The vibrational modes of the anion are appreciably mixed but can be designated:  $\nu_1$  as  $\nu_{\text{CN}}$ ,  $\nu_2$  as  $\delta_{\text{CNS}}$  and  $\nu_3$  as  $\nu_{\text{CS}}$ . The infrared spectrum of the free anion in  $\text{KCNS}^{129}$  exhibits three bands, as expected for a linear triatomic ion, which have been assigned (values are in  $\text{cm}^{-1}$ ) as follows:

$\nu_1$	$\nu_2$	$\nu_3$
2053s	486m	746m
	471m	

The splitting of  $\nu_2$  is attributed to a solid-state effect.

The infrared spectrum of  $\text{Fe}(\text{pyz})_2(\text{NCS})_2$  is illustrated in Fig. 3.11. The anion bands are assigned as follows:

$\nu_1$	$\nu_2$	$\nu_3$
2060s	493m	824m
2000sh		

The intense C-N stretching vibration,  $\nu_1$ , occurs at  $2060 \text{ cm}^{-1}$  which is similar to the value of  $2065 \text{ cm}^{-1}$  observed in the thiocyanato-N complex,  $\text{Fe}(\text{py})_4(\text{NCS})_2$ .<sup>67</sup> Empirical data<sup>127</sup> indicate that thiocyanato-N coordination results in little change in the position of this band from the free-ion value of  $2053 \text{ cm}^{-1}$ , while S-bonding results in an increase to approximately  $2100 \text{ cm}^{-1}$ . In bridging thiocyanate ( $-\text{NCS}-$ ) complexes, this band occurs well above  $2100 \text{ cm}^{-1}$ .<sup>127</sup> The value of  $2060 \text{ cm}^{-1}$  observed for  $\text{Fe}(\text{pyz})_2(\text{NCS})_2$  is consistent with the presence of an N-terminally bonded  $\text{NCS}^-$  anion.

The frequency of the carbon-sulfur stretching vibration, ( $\nu_3$ ), also has been used to diagnose thiocyanate

coordination.<sup>127</sup> The intensity of this absorption is often low and in some cases is difficult to identify. Frequencies in the  $700\text{ cm}^{-1}$  region are taken as indicative of S-bonding, while those at approximately  $800\text{ cm}^{-1}$  indicate N-bonding. The infrared spectrum of  $\text{Fe}(\text{pyz})_2(\text{NCS})_2$  lacks absorption bands in the  $650\text{--}750\text{ cm}^{-1}$  region and hence S-bonding is not suspected. There are three bands near  $800\text{ cm}^{-1}$ , two of which are assigned to pyrazine, and a third weak band at  $824\text{ cm}^{-1}$  which is assigned to the carbon-sulfur stretching vibration. This value compares favourably with the value of  $810\text{ cm}^{-1}$  found in  $\text{Fe}(\text{py})_4(\text{NCS})_2$ <sup>67</sup> and hence, the value of  $824\text{ cm}^{-1}$  supports an N-coordination mode for the anion.

Another criterion of thiocyanate coordination is based upon the frequency and multiplicity of the anion deformation mode ( $\nu_2$ ). A single sharp band in the region of  $480\text{ cm}^{-1}$  is indicative of N-bonding, while several bands of low intensity near  $400\text{ cm}^{-1}$  indicates S-bonding.<sup>127</sup>  $\text{Fe}(\text{pyz})_2(\text{NCS})_2$  exhibits two sharp bands of medium intensity in the  $450\text{--}500\text{ cm}^{-1}$  region. Pyrazine is expected to show one absorption in this region (which may be split) and assignment of either of these bands to either pyrazine or the anion is difficult. Both bands, however, are certainly well above the range observed for S-bonded thiocyanate and thus thiocyanato-N is indicated. The band at  $493\text{ cm}^{-1}$  is tentatively assigned to this anion vibration. These vibrational assignments provide a substantial indication for the coordination of the anion through the nitrogen donor atom.

To summarise these infrared data: the pyrazine groups

retain the symmetry of the free ligand by functioning as bidentate bridging ligands; a polymeric structure is formed, with halide anions or nitrogen atoms from  $\text{NCS}^-$  anions completing the coordination sphere around the iron centre.

### 3.3.2.3 Infrared spectral results for bis(pyrazine) complexes containing sulfonate or perchlorate anions

Vibrational assignments for the pyrazine ligand are listed in Appendix IV, whilst the infrared spectral data pertaining to the sulfonate anion and any unassigned vibrations are tabulated in Appendix III, Parts A and B.

For  $\text{Fe}(\text{pyz})_2(\text{CF}_3\text{SO}_3)_2 \cdot \text{CH}_3\text{OH}$ ,  $\text{Fe}(\text{pyz})_2(\text{CH}_3\text{SO}_3)_2$  and  $\text{Cu}(\text{pyz})_2(\text{CH}_3\text{SO}_3)_2$  the intense, broad anion vibrations, particularly in the S-O stretching region between 1000 and 1200  $\text{cm}^{-1}$ , make it advantageous to discuss these vibrations prior to the neutral ligand vibrations. The various modes of sulfonate anion coordination, the concomitant anion symmetry and the resulting effects on the infrared spectra were discussed in Section 3.3.2.1.

Vibrational assignments for  $\text{Cu}(\text{pyz})_2(\text{CH}_3\text{SO}_3)_2$  are readily made in terms of monodentate  $\text{CH}_3\text{SO}_3^-$  anion coordination (Appendix III, Part B). Coordination results in the splitting of the doubly degenerate  $\text{SO}_3$  asymmetric stretching and bending modes ( $\nu_4$  and  $\nu_5$ ) by 95 and 13  $\text{cm}^{-1}$  respectively (Fig. 3.10b). It has been noted (Section 3.3.2.1) that in  $\text{Cu}(\text{py})_4(\text{CH}_3\text{SO}_3)_2$  the splitting of these bands is significantly less, for example,  $\nu_4$  is split by 49  $\text{cm}^{-1}$  and  $\nu_5$  is not observed to split (Section

3.3.2.1). These results indicate that the cation-anion interaction in  $\text{Cu}(\text{pyz})_2(\text{CH}_3\text{SO}_3)_2$  is stronger than that in  $\text{Cu}(\text{py})_4(\text{CH}_3\text{SO}_3)_2$ . These infrared data for  $\text{Cu}(\text{pyz})_2(\text{CH}_3\text{SO}_3)_2$  are consistent with the X-ray structure result which shows the anion to be coordinated strongly in the equatorial plane.

In both of these copper-methanesulfonate compounds, the metal achieves one of its preferred coordination geometries by having four short (equatorial) and two long (axial) interactions. In the pyrazine compound, the relatively weak basicity of the pyrazine ligand precludes an equatorial geometry in which the pyrazine ligands fulfill all four strong interactions. In this case, the four strong interactions are provided by the two sulfonate oxygen atoms plus two bonds to pyrazine, while the two weaker interactions are provided by two bonds to pyrazine (Section 3.3.1.3). In the pyridine complex, the four neutral ligands coordinate strongly in the equatorial plane and the anions adopt axial coordination sites.

The infrared spectrum of  $\text{Cu}(\text{pyz})_2(\text{CH}_3\text{SO}_3)_2$  exhibits a broad absorption in the  $2800\text{--}3500\text{ cm}^{-1}$  region, indicating the presence of an O-H containing species. This is somewhat surprising since the X-ray analysis showed no evidence for such a species. It seems possible that small amounts of water or methanol may be present on the crystal surface and lead to this infrared absorption.

The infrared spectra of  $\text{Fe}(\text{pyz})_2(\text{CF}_3\text{SO}_3)_2 \cdot \text{CH}_3\text{OH}$  and  $\text{Fe}(\text{pyz})_2(\text{CH}_2\text{SO}_3)_2$  are similar to that of the copper complex. A splitting of the  $\text{SO}_3$  asymmetric stretching and bending modes ( $\nu_4$

and  $\nu_5$ ) is clearly observed indicating a reduction of anion symmetry to below  $C_{3v}$  which presumably arises from a unidentate mode of sulfonate anion coordination. A comparison of the number and position of the anion vibrations for the bis(pyrazine)iron(II) sulfonate species and the analogous tetrakis(pyridine) complexes gave the following results. The methanesulfonate anion spectra are virtually identical for  $Fe(py)_4(CH_3SO_3)_2$  and  $Fe(pyz)_2(CH_3SO_3)_2$  (Fig. 3.9a,b and Appendix III, Part B). In view of the X-ray structural data for  $Fe(py)_4(CH_3SO_3)_2$ , in which the anion is clearly demonstrated as coordinating in a unidentate mode, it is concluded that the anion is coordinated to the metal in a similar fashion in  $Fe(pyz)_2(CH_3SO_3)_2$ . The splittings of the  $SO_3$  asymmetric stretching and bending modes are virtually of the same magnitude which may indicate a similar degree of cation-anion interaction for both complexes. Similarly, for  $Fe(pyz)_2(CF_3SO_3)_2 \cdot CH_3OH$  the mode of anion coordination was ascertained by a comparison with the anion bands of  $Fe(py)_4(CF_3SO_3)_2$  (Appendix III, Part A). Both complexes show a close correlation for the bands assigned to the anion, and unidentate anion coordination in the bis(pyrazine) complex is inferred. The splittings of the  $SO_3$  asymmetric stretching and bending modes also indicate a similar degree of cation-anion interaction in the two compounds. In  $Fe(pyz)_2(CF_3SO_3)_2 \cdot CH_3OH$  the broad absorption between  $3400-2500\text{ cm}^{-1}$  clearly demonstrates the presence of an O-H containing species, in agreement with the microanalytical data which suggest the presence of one mole of methanol per mole of

complex.

Before a discussion of the vibrational assignments for the anion in  $\text{Fe}(\text{pyz})_2(\text{ClO}_4)_2$ , it is relevant to comment on the relationship between the number and frequency of the anion vibrational bands and perchlorate anion symmetry. The free perchlorate anion belongs to the symmetry point group  $T_d$ . There are four normal vibrational modes (Table 3.4) and of these only the asymmetric stretching and bending modes ( $\nu_3$  and  $\nu_4$ , respectively) are infrared active.

Table 3.4 Vibrations of the Perchlorate Anion as a Function of Symmetry

SYMMETRY		(R=RAMAN, I=INFRARED ACTIVE)			
$T_d$	$\nu_1$	$A(R)$	$\nu_2$	$E(R)$	
	$\nu_3$	$F_2(I, R)$	$\nu_4$	$F_2(I, R)$	
$C_{3v}$	$\nu_1$	$A_1(I, R)$	$\nu_2$	$E(I, R)$	
	$\nu_3$	$A(I, R)$	$\nu_4$	$E(I, R)$	

In the infrared spectra of ionic perchlorate-containing compounds, these bands generally occur at approximately 1110 and 630  $\text{cm}^{-1}$  respectively;<sup>130</sup> the former appearing as a very broad strong band which is occasionally split. Upon coordination through a single oxygen atom, the symmetry is reduced at least to  $C_{3v}$ , a splitting of the two triply degenerate normal vibrational modes results and the two symmetric modes become infrared active (Table 3.4).

There are two features in the infrared spectrum of  $\text{Fe}(\text{pyz})_2(\text{ClO}_4)_2$  which indicate that the symmetry of the anion is

not  $T_d$ . The splittings of the triply degenerate modes ( $\nu_3$  and  $\nu_4$  in  $T_d$  symmetry) indicate a lowering of anion symmetry and the presence of a strong absorption at  $918\text{ cm}^{-1}$  would not be expected if the anion retained  $T_d$  symmetry. Assuming  $C_{3v}$  anion symmetry for the perchlorate anion in  $\text{Fe}(\text{pyz})_2(\text{ClO}_4)_2$ , the following assignments are made:

$\nu_2(\text{A})$	$\nu_1(\text{A})$	$\nu_4(\text{E})$	$\nu_3(\text{A})$ and $\nu_5(\text{E})$
918s	1026s	1145s	637m, 626s, 617s

$\nu_6$  is not observed.

These vibrational assignments are very similar to those made for some  $\text{M}(\text{py})_4(\text{ClO}_4)_2$  complexes where unidentate anion coordination has been proposed.<sup>86</sup> The infrared spectral data presented here indicate a similar mode of anion coordination in  $\text{Fe}(\text{pyz})_2(\text{ClO}_4)_2$ .

Vibrational assignments for pyrazine in these bis(pyrazine)iron(II) sulfonate and perchlorate complexes are made more difficult by the strong absorptions of the sulfonate and perchlorate anions; as a result, some of the pyrazine bands are obscured. Some assignments have been made by a comparison of the infrared spectra of the  $\text{M}(\text{pyz})_2(\text{RSO}_3)_2$  complexes with those of the neutral ligand<sup>124</sup> and of the  $\text{Fe}(\text{pyz})_2\text{X}_2$  complexes (Section 3.3.2.2); these are given in Appendix IV.

The infrared spectrum of  $\text{Cu}(\text{pyz})_2(\text{CH}_3\text{SO}_3)_2$  is illustrated in Fig. 3.10b and it may be seen that the  $1000\text{--}1300\text{ cm}^{-1}$  region of the spectrum is not particularly useful for assessing the coordination mode of pyrazine. The occurrence of two bands at  $813$  and  $846\text{ cm}^{-1}$  and two absorptions at  $440$  and  $494\text{ cm}^{-1}$ ,



however, is informative. For comparison, in free pyrazine these infrared absorptions are observed at 804 and 417  $\text{cm}^{-1}$  respectively,<sup>124</sup> and upon coordination, minor shifts are expected which are sometimes accompanied by small splittings of usually less than 10  $\text{cm}^{-1}$ . The magnitudes of the splittings of these bands in  $\text{Cu}(\text{pyz})_2(\text{CH}_3\text{SO}_3)_2$ , by 33 and 54  $\text{cm}^{-1}$ , appear too large to be associated with interactions between adjacent pyrazine rings but are consistent with the X-ray structural result which shows two distinct pyrazine groups. Presumably, the absorptions at the two higher frequencies (494 and 846  $\text{cm}^{-1}$ ) are associated with the ligand more strongly bonded to copper, whilst for the more weakly bound pyrazine group, the shifts to higher frequency are of a lesser extent (to 440 and 804  $\text{cm}^{-1}$ ).

The infrared spectra of  $\text{Fe}(\text{pyz})_2(\text{CF}_3\text{SO}_3)_2 \cdot \text{CH}_3\text{OH}$  and  $\text{Fe}(\text{pyz})_2(\text{CH}_3\text{SO}_3)_2$  show differences and similarities in the absorptions assigned to pyrazine, when compared to  $\text{Cu}(\text{pyz})_2(\text{CH}_3\text{SO}_3)_2$ . Both bis(pyrazine)iron(II) derivatives exhibit only small splittings (of less than 10  $\text{cm}^{-1}$ ) of the absorption in the 470  $\text{cm}^{-1}$  region which may indicate the presence of only one type of pyrazine ligand in the iron compounds. The bands assigned to pyrazine in  $\text{Fe}(\text{pyz})_2(\text{CF}_3\text{SO}_3)_2 \cdot \text{CH}_3\text{OH}$  are more numerous than in  $\text{Fe}(\text{pyz})_2(\text{CH}_3\text{SO}_3)_2$ , and this may be a result of additional interactions between the pyrazine and methanol in the triflate compound. Such interactions are absent in  $\text{Fe}(\text{pyz})_2(\text{CH}_3\text{SO}_3)_2$ .

It is difficult to use the previously established infrared criteria to determine the mode of neutral ligand coordination in

these complexes. If unidentate pyrazine groups are present, then absorption bands may be activated in the infrared spectrum at approximately 1230, 1020 and 750  $\text{cm}^{-1}$ . For the complexes under investigation here, it is likely that if these bands are present, then they are obscured by the presence of the strong anion vibrations in these regions.

The similarities between the spectra of the three bis(pyrazine) sulfonate complexes, together with the X-ray structural evidence for the copper derivative, strongly suggest that  $\text{Fe}(\text{pyz})_2(\text{CF}_3\text{SO}_3)_2 \cdot \text{CH}_3\text{OH}$  and  $\text{Fe}(\text{pyz})_2(\text{CH}_3\text{SO}_3)_2$  contain unidentate sulfonate anions; however, evidence for bidentate bridging pyrazine groups is rather weak.

The assignment of infrared absorptions arising from pyrazine in  $\text{Fe}(\text{pyz})_2(\text{ClO}_4)_2$  is beset by problems similar to those encountered for the sulfonate derivatives, i.e., strong absorptions of  $\text{ClO}_4^-$  in the 900-1200  $\text{cm}^{-1}$  region. The pyrazine bands which are assigned (Appendix IV) provide inconclusive evidence for pyrazine coordination.

#### 3.3.2.4 Infrared spectral results for tetrakis(pyrazine) complexes

The infrared spectrum of  $\text{Fe}(2\text{-mepyz})_4(\text{CH}_3\text{SO}_3)_2$  is illustrated in Fig 3.9c, the spectra of  $\text{Fe}(\text{py})_4(\text{CH}_3\text{SO}_3)_2$  and  $\text{Fe}(\text{pyz})_2(\text{CH}_3\text{SO}_3)_2$  are shown for comparison (Figs. 3.9a and 3.9b respectively). The vibrations assigned to the sulfonate anion are listed in Appendix III, Part B. The similarities between the anion spectra of the 2-methylpyrazine complex and the other

two methanesulfonate derivatives (Section 3.3.2.1 and 3.3.2.3 respectively), are readily apparent. For example, the splittings of the asymmetric  $\text{SO}_3$  stretching and bending modes (by 95 and 17  $\text{cm}^{-1}$  respectively) are of a similar magnitude to those found in the other iron(II) methanesulfonate complexes, and a unidentate mode of anion coordination is proposed for  $\text{Fe}(\text{2-mepyz})_4(\text{CH}_3\text{SO}_3)_2$ ; a similar degree of cation-anion interaction is also indicated.

The absorptions arising from the 2-methylpyrazine ligand in the complex are given in Appendix V, and these bands are similar to those previously observed in other 2-methylpyrazine derivatives.<sup>33</sup> The free ligand lacks a centre of symmetry, and criteria which are sometimes useful in determining the mode of pyrazine coordination cannot be applied to 2-methylpyrazine complexes.

The infrared spectrum of  $\text{Cu}(\text{pyz})_4(\text{CF}_3\text{SO}_3)_2 \cdot \text{H}_2\text{O}$  is characterised by absorptions from pyrazine groups, triflate anions and water moieties. The absorptions of the triflate anion and unassigned vibrations are given in Appendix III, Part A. Several bands occur in the  $\text{SO}_3$  stretching region and three of these were tentatively assigned to the asymmetric and symmetric  $\text{SO}_3$  stretching modes by comparison with the spectral data for the other triflate-containing compounds prepared in this study (it is likely that the other absorptions in this region arise from the  $\text{CF}_3$  stretching vibrations). A reduction in anion symmetry to below  $\text{C}_{3v}$  is indicated and suggests a unidentate mode of anion coordination. Vibrations assigned to

pyrazine are listed in Appendix V and due to the complex nature of the infrared spectrum in the  $900\text{--}1300\text{ cm}^{-1}$  region it is difficult to conclusively identify pyrazine bands; hence, no definite conclusions are drawn concerning the nature of pyrazine coordination. The broad absorptions centred at  $3400$  and  $1630\text{ cm}^{-1}$  indicate the presence of an OH-containing species, presumably water.

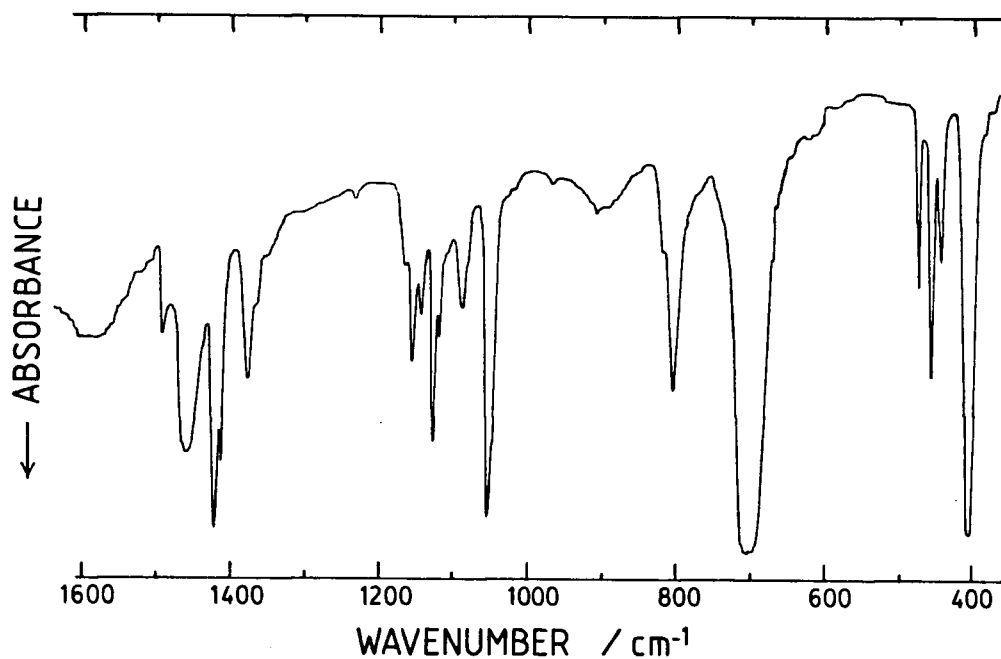
Classification of  $\text{Fe}(\text{pyz})_4(\text{AsF}_6)_2 \cdot 2\text{H}_2\text{O}$  as having an  $\text{FeN}_4\text{X}_2$  chromophore is dependent upon two criteria. Firstly, the pyrazine ligands must be coordinated in a unidentate fashion; and secondly, either the water molecules or the hexafluoroarsenate anions must occupy the remaining coordination sites. Infrared spectroscopy is capable of determining whether these conditions pertain.

The infrared spectrum of the complex is shown in Fig. 3.12 and the vibrations assigned to the pyrazine ligand are given in Appendix V. The presence of bands near  $3000$  and  $1600\text{ cm}^{-1}$  clearly indicate the presence of water. Their broad nature suggests that the water molecules may be coordinated to the metal centre.

The free  $\text{AsF}_6^-$  anion has  $\text{O}_h$  symmetry and is expected to exhibit two infrared active vibrations. In the ionic salt,  $\text{CsAsF}_6$ ,<sup>131</sup> these vibrations are observed at  $699$  and  $392\text{ cm}^{-1}$ . When anion coordination occurs the symmetry of the anion is reduced below  $\text{O}_h$  and this results in band splittings and the appearance of infrared absorptions which are forbidden in octahedral symmetry. For  $\text{Fe}(\text{pyz})_4(\text{AsF}_6)_2 \cdot 2\text{H}_2\text{O}$ , anion bands are

assigned at 700 and 400  $\text{cm}^{-1}$ . The occurrence of only two anion bands and the fact that these bands show no splitting indicate that the anion retains octahedral symmetry and is not coordinated to the metal, as expected for this very weakly basic ligand.

Fig. 3.12 Infrared Spectrum of  $\text{Fe}(\text{pyz})_4(\text{AsF}_6)_2 \cdot 2\text{H}_2\text{O}$



Because of the presence of only two anion bands, vibrational assignments for pyrazine are made more easily than those for the sulfonate complexes (Section 3.3.2.3). The assignments are given in Appendix IV and from these it appears that a number of pyrazine bands are split; this could arise either from there being two different environments for the ligand or interactions between neighbouring pyrazine rings. Weak absorptions are observed at 1232 and 920  $\text{cm}^{-1}$ ; bands are observed at comparable frequencies in the Raman spectrum of free pyrazine<sup>124</sup> and in the infrared spectra of unidentate-pyrazine containing compounds.<sup>44</sup> The activation of these bands in the infrared spectrum of  $\text{Fe}(\text{pyz})_4(\text{AsF}_6)_2 \cdot 2\text{H}_2\text{O}$  is proposed to arise from a reduction in ligand symmetry below  $D_{2h}$  which may indicate a unidentate mode of pyrazine coordination. Further evidence for this mode of pyrazine coordination comes from the observation that  $\text{Cu}(\text{pyz})_4(\text{AsF}_6)_2$ <sup>132</sup> exhibits similar infrared spectral features as those described here and unidentate pyrazine coordination has been proposed in this copper complex. These infrared spectral results suggest ionic hexafluoroarsenate anions, terminal unidentate pyrazine groups and coordinated water molecules which supports the proposal of an  $\text{FeN}_4\text{O}_2$  chromophore and the absence of a bridging network in this complex.

In summary, infrared spectroscopy indicates unidentate anion coordination in  $\text{Fe}(2\text{-mepyz})_4(\text{CH}_3\text{SO}_3)_2$  and  $\text{Cu}(\text{pyz})_4(\text{CF}_3\text{SO}_3)_2 \cdot \text{H}_2\text{O}$ ; whereas, ionic non-coordinated anions are proposed for  $\text{Fe}(\text{pyz})_4(\text{AsF}_6)_2 \cdot 2\text{H}_2\text{O}$ . The infrared spectral data

are inconclusive as to the mode of 2-methylpyrazine and pyrazine coordination in the methanesulfonate and triflate derivatives respectively; on the other hand, infrared spectroscopy indicates unidentate pyrazine coordination in the hexafluoroarsenate compound.

### 3.3.3 Electronic Spectroscopy

Electronic spectra over the frequency range 4,000-30,000  $\text{cm}^{-1}$  were recorded for all of the complexes investigated in this study. It was anticipated that such studies would not only provide confirmatory evidence regarding the nature of the metal chromophore but also could be used to further investigate the differences in the coordinating tendencies of the various ligands involved.

#### 3.3.3.1 Electronic spectral results for complexes containing an $\text{FeN}_4\text{O}_2$ chromophore

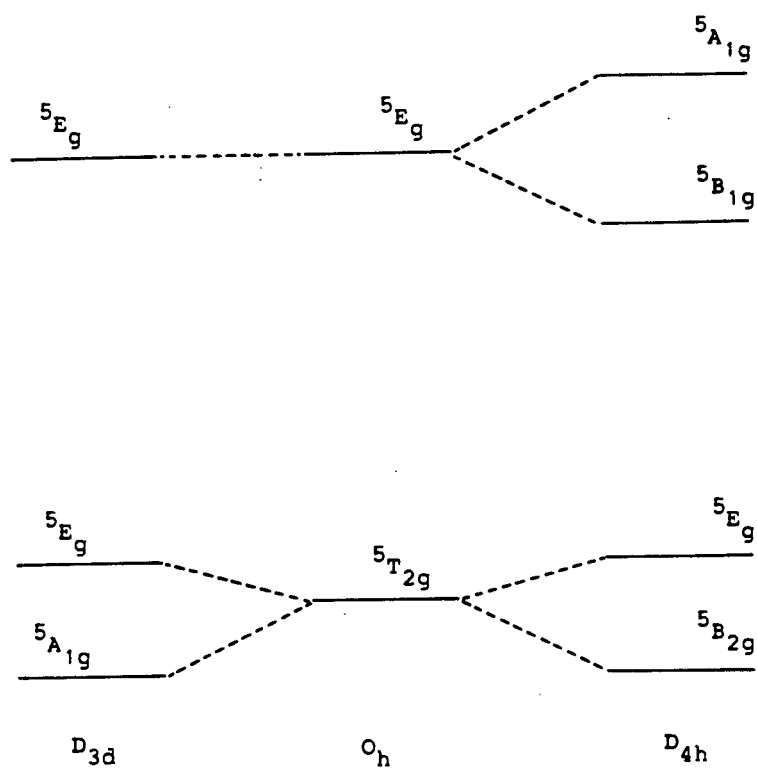
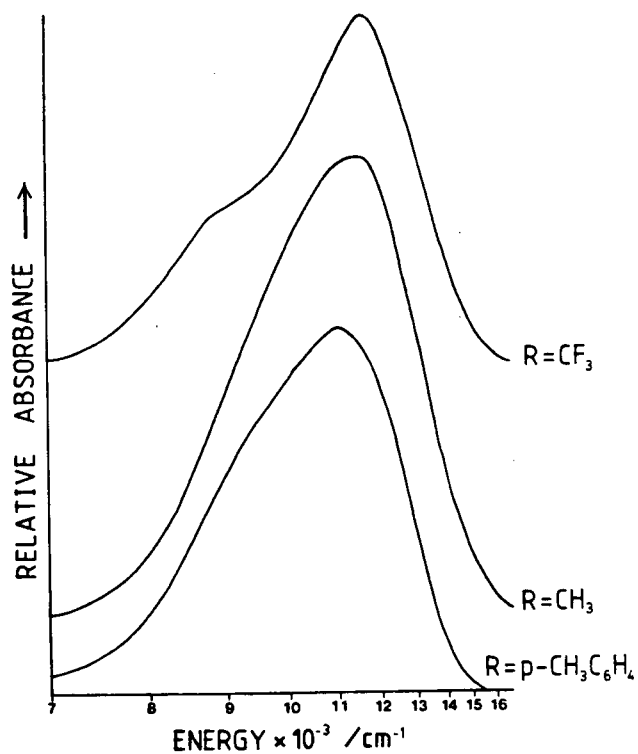
The electronic ground state for high-spin  $\text{Fe}^{2+}$  is represented by the  $^5\text{D}$  term symbol. In ligand fields of cubic symmetry the ground state splits to give  $^5\text{T}_{2g}$  and  $^5\text{E}_g$  states separated by  $10\text{D}_q$ . In octahedral symmetry the  $^5\text{T}_{2g}$  state lies lowest in energy and one spin-allowed d-d transition is expected and is usually observed as a broad band in the near-infrared region of the electromagnetic spectrum. The band is often asymmetric in character, whilst sometimes it is clearly resolved into two components. These observations are attributed to the splitting of the excited state in ligand fields of less than  $\text{O}_h$  symmetry. The electronic energy level diagram for high-spin iron(II) complexes in ligand fields of octahedral, tetragonal and trigonal symmetry is shown in Fig. 3.13. The ordering of the energy levels on the right-hand side of this figure is for a tetragonal compression, and takes into account the  $\sigma$ -bonding effects of the ligands. This ordering is expected for the



$\text{Fe}(\text{py})_4(\text{RSO}_3)_2$  complexes because of the presence of a tetragonally compressed coordination sphere about the metal (Section 3.3.1.1).

The electronic spectral parameters for the  $\text{Fe}(\text{py})_4(\text{RSO}_3)_2$  complexes are presented in Appendix VII, Part A, and the spectra are illustrated in Fig. 3.14. In all three cases, a principal absorption band is observed around  $11,000 \text{ cm}^{-1}$  and for the  $\text{R}=\text{CH}_3$  and  $p\text{-CH}_3\text{C}_6\text{H}_4$  compounds, the band shows a small degree of asymmetry at low energy. For the triflate derivative, a more distinct shoulder ( $9,000 \text{ cm}^{-1}$ ) is observed at low-energy. Of the  $\text{Fe}(\text{py})_4(\text{RSO}_3)_2$  complexes studied by X-ray diffraction (Section 3.3.3.1), the coordination sphere about the metal is least distorted in the triflate complex. The greater tetragonal compression in the methanesulfonate and  $p$ -tosylate complexes would be expected to produce larger splittings of the excited state than that produced by the triflate complex, which would result in the observation of band splitting in the former two complexes; this, however, is not observed. The relatively small tetragonal compression in the triflate complex would not be expected to lead to band splitting. Thus, it appears likely that the shoulder at  $9,000 \text{ cm}^{-1}$  in  $\text{Fe}(\text{py})_4(\text{CF}_3\text{SO}_3)_2$ , is not caused by the splitting of the excited state but may be due to a vibrational band, possibly an overtone. This band is not observed in the other two complexes and this may be because the absorption bands are considerably broadened.

Fig. 3.13 Electronic Energy Levels for High-Spin Iron(II)

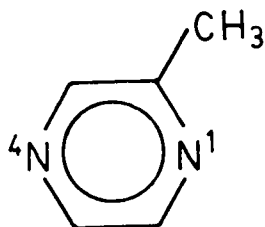
Fig. 3.14 Electronic Spectra for  $Fe(py)_4(RSO_3)_2$  Complexes

The tetrakis(pyridine)iron(II) complexes show only small differences in the frequencies of the maximum absorption,  $\nu_{\max}$ . For these complexes, the values of  $10D_q$  (of approximately 11,000  $\text{cm}^{-1}$ , as measured by  $\nu_{\max}$ ) are significantly higher than the value of 8,000  $\text{cm}^{-1}$ , observed for the anhydrous sulfonate species,  $\text{Fe}(\text{RSO}_3)_2$ .<sup>24, 25</sup> This is consistent with the stronger ligand field associated with the  $\text{FeN}_4\text{O}_2$  chromophore in the pyridine complexes, compared to the ligand field associated with the  $\text{FeO}_6$  chromophore present in the sulfonate complexes.

Electronic spectral data for the bis(pyrazine)iron(II) complexes,  $\text{Fe}(\text{pyz})_2(\text{CF}_3\text{SO}_3)_2 \cdot \text{CH}_3\text{OH}$  and  $\text{Fe}(\text{pyz})_2(\text{CH}_3\text{SO}_3)_2$  are given in Appendix VII, Part A. Both complexes exhibit electronic spectra which are very similar to those of the tetrakis(pyridine)iron(II) sulfonate complexes. This observation supports the assignment of an  $\text{FeN}_4\text{O}_2$  chromophore in the bis(pyrazine) derivatives and also the conclusion that pyridine and pyrazine occupy positions close to each other in the spectrochemical series.

The electronic spectrum of  $\text{Fe}(2\text{-mepyz})_4(\text{CH}_3\text{SO}_3)_2$  exhibits one broad band at 9,800  $\text{cm}^{-1}$ , which is in the range expected for high-spin octahedral iron(II) compounds. This value indicates the presence a weaker ligand field than that which exists in the analogous tetrakis(pyridine) or bis(pyrazine)iron(II) complexes. From these observations an  $\text{FeN}_4\text{O}_2$  chromophore seems likely and this would require the neutral ligand to be coordinated in a terminal unidentate manner. Two alternatives exist: coordination through either N(1) or N(4) (Fig. 3.15).

Fig. 3.15 2-Methylpyrazine

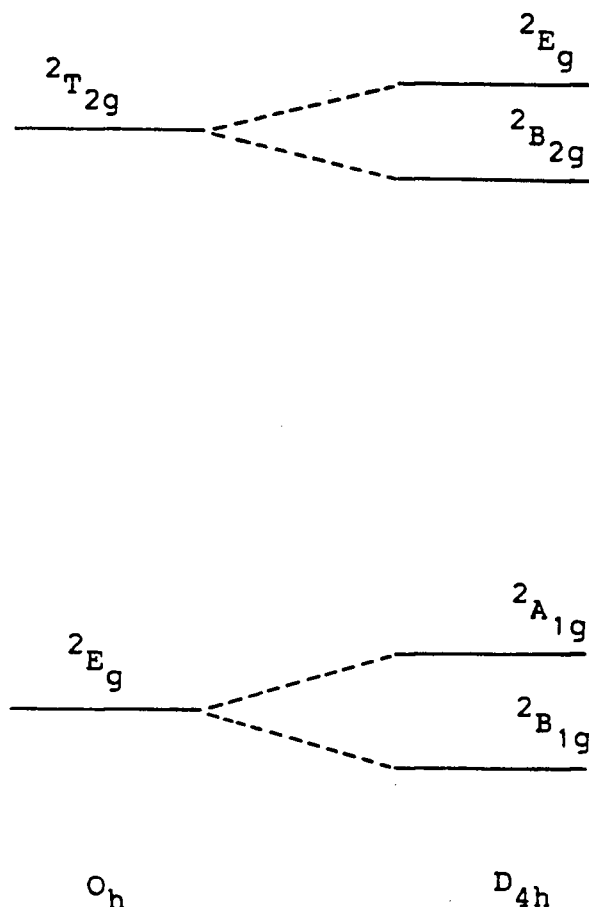


The former nitrogen atom is more basic than that of pyrazine ( $pK_a$  values of 1.45 and -0.6 respectively<sup>28</sup>) and coordination through this nitrogen atom might be expected to produce a stronger ligand field. By judging from the  $\nu_{\max}$ , a stronger ligand field is not present which suggests that this mode of coordination is either hindered by the presence of the methyl group or that coordination takes place through the less basic nitrogen atom N(4).

### 3.3.3.2 Electronic spectral results for complexes containing an $\text{CuN}_4\text{O}_2$ chromophore

The copper(II) ion has a  $d^9$  electron configuration which gives rise to a  $^2D$  free-ion ground term. The energy level diagram for a copper(II) ion in crystal fields of  $O_h$  and  $D_{4h}$  symmetry is shown in Fig. 3.16. Since the ground state in an octahedral ligand field is the  $^2E_g$  state, it is subject to a considerable Jahn-Teller instability, and as a result the majority of octahedral copper(II) complexes are tetragonally distorted with four short copper-ligand bonds in one plane ( $xy$ ) and two longer copper-ligand bonds lying along the  $z$ -axis above and below this plane.

Fig. 3.16 Electronic Energy Levels for Copper(II)



In  $D_{4h}$  symmetry, three absorptions are expected, but often in the case of tetragonally distorted copper(II) compounds only one broad asymmetric band is observed in the visible region; the position of this band may be taken to represent the average ligand field,  $10D_q$ .

The electronic spectral parameters for the tetrakis(pyridine)copper(II) complexes and  $Cu(pyz)_2(CH_3SO_3)_2$  are given in Appendix VII, Part B. For comparison, the results from a previous study on  $Cu(py)_4(FSO_3)_2$  and  $Cu(py)_4(p-CH_3C_6H_4SO_3)_2$  are also included.<sup>76</sup> The tetrakis(pyridine)copper(II) sulfonate

complexes all exhibit a single broad asymmetric band which presumably is of a composite nature. For a large number of bis(ethylenediamine)copper(II) complexes,<sup>133</sup> the position of the visible band has been correlated with the degree of tetragonality of the copper chromophore; these previous studies demonstrated that the position of the band shifts to higher energies with increasing tetragonal distortion. Hathaway et al.<sup>134</sup> have shown from polarised radiation single-crystal electronic spectral studies, that the highest energy component in the visible band of these complexes arises from the  ${}^2B_{1g} \longrightarrow {}^2E_g$  transition and it is largely the shift of this transition to higher energies on increasing tetragonal distortion that accounts for the overall shift of the visible band. For the tetrakis(pyridine)copper(II) complexes, as the R group of the anion changes from  $CH_3$  to  $p-CH_3C_6H_4$  to F to  $CF_3$ ,  $\nu_{max}$  is observed to increase. This indicates a greater degree of tetragonality in the same order and this would be predicted on the basis of relatively weaker anion basicities for  $FSO_3^-$  and  $CF_3SO_3^-$  when compared to those of the methanesulfonate and p-tosylate.

The absorption bands for the copper-pyridine complexes are at significantly higher frequencies (approximately  $17,000\text{ cm}^{-1}$ ) than those for the corresponding anhydrous sulfonate compounds,  $Cu(RSO_3)_2$ ,<sup>87</sup> where absorption bands are present in the range of  $8,000\text{--}14,000\text{ cm}^{-1}$ . As described for the iron complexes, this is attributable to a stronger ligand field afforded by four pyridine ligands and two sulfonate oxygen atoms in the pyridine

complexes, in comparison to six sulfonate oxygen atoms in the anhydrous sulfonates.

The electronic spectral data for  $\text{Cu}(\text{py})_4(\text{CF}_3\text{SO}_3)_2$  are entirely consistent with the X-ray structure result which revealed a pseudooctahedral coordination geometry distorted by a tetragonal elongation (Section 3.3.1.2).

The electronic spectrum of  $\text{Cu}(\text{pyz})_2(\text{CH}_3\text{SO}_3)_2$  shows a broad absorption at  $14,000\text{ cm}^{-1}$ ; this is at a considerably lower energy than that observed for  $\text{Cu}(\text{py})_4(\text{CH}_3\text{SO}_3)_2$ ,  $16,800\text{ cm}^{-1}$ . An X-ray structure determination shows  $\text{Cu}(\text{pyz})_2(\text{CH}_3\text{SO}_3)_2$  to possess a  $\text{CuN}_2\text{O}_2\text{N}'_2$  chromophore (Section 3.3.1.3); whereas, infrared and electronic spectroscopy suggest that  $\text{Cu}(\text{py})_4(\text{CH}_3\text{SO}_3)_2$  has a  $\text{CuN}_4\text{O}_2$  chromophore (Section 3.3.2.1). The difference in the electronic spectra of the two complexes possibly reflects the greater degree of tetragonality associated with the  $\text{CuN}_4\text{O}_2$  chromophore in  $\text{Cu}(\text{py})_4(\text{CH}_3\text{SO}_3)_2$  as well as the slightly higher position of pyridine over pyrazine in the spectrochemical series and also the fact that in the pyrazine complex, one of the bridging ligands is only very weakly bonded to copper.

The electronic spectrum of  $\text{Cu}(\text{pyz})_4(\text{CF}_3\text{SO}_3)_2 \cdot \text{H}_2\text{O}$  exhibits a broad absorption band at  $16,100\text{ cm}^{-1}$ . This is at a slightly lower energy than that observed for  $\text{Cu}(\text{py})_4(\text{CF}_3\text{SO}_3)_2$  ( $17,400\text{ cm}^{-1}$ ). Again, the lower frequency of the absorption band in the pyrazine complex is consistent with a weaker ligand field and/or a lesser degree of tetragonality in the tetrakis(pyrazine) complex.

### 3.3.3.3 Electronic spectral results for complexes containing an $\text{FeN}_4\text{X}_2$ chromophore

The electronic spectral parameters for the bis(pyrazine)iron(II) halide, thiocyanate and perchlorate derivatives, and  $\text{Fe}(\text{pyz})_4(\text{AsF}_6)_2 \cdot 2\text{H}_2\text{O}$  are listed in Appendix VII, Part C. The perchlorate and hexafluoroarsenate compounds are yellow; whereas, the colours of the halide and thiocyanate complexes are particularly intense and range from maroon for  $\text{Fe}(\text{pyz})_2\text{I}_2$  to red for the chloro- and bromo derivatives;  $\text{Fe}(\text{pyz})_2(\text{NCS})_2$  is brown. In comparison, the iron(II) complexes with sulfonate anions (Section 3.3.3.1) are pale green or yellow.

Absorption bands are seen in the near-infrared region ( $11,000\text{--}13000\text{ cm}^{-1}$ ); these band positions are diagnostic of high-spin octahedral iron(II) complexes. The absorptions are of a broad nature and evidence for band splitting is observed in the spectra of  $\text{Fe}(\text{pyz})_2\text{I}_2$  and  $\text{Fe}(\text{pyz})_2(\text{NCS})_2$ . As was done for the tetrakis(pyridine) complexes,<sup>67</sup> the average ligand field in the pyrazine complexes is represented by taking either the centre of the unsplit absorption band or, in the case where band splitting is observed, by taking the average position of the two bands.



These values ( $\text{cm}^{-1}$ ) together with those for the tetrakis(pyridine) complexes<sup>6,7</sup> are as follows:

X	$\text{Fe}(\text{pyz})_2\text{X}_2$	$\text{Fe}(\text{py})_4\text{X}_2$
Cl	11,800	9620
Br	11,200	9280
I	9,200	8620
NCS	11,500	10,670

These data indicate that pyrazine provides a slightly stronger ligand field than does pyridine. This apparently stronger ligand field afforded by pyrazine may be a consequence of the stabilisation of the  $^5\text{T}_{2g}$  levels as a result of the better  $\pi$ -acceptor properties of pyrazine over pyridine.

The intense colours of the bis(pyrazine)iron(II) halide and thiocyanate complexes are presumably a consequence of charge-transfer bands in the visible region of the spectrum (Appendix VII, Part C). Charge-transfer spectra have been observed in other iron(II) complexes<sup>135</sup> and in view of the relative ease of oxidation of iron(II) to iron(III) these spectra are proposed to be predominantly metal to ligand in character. Previously in metal-pyrazine complexes, charge transfer has been proposed to be from the metal to a low-lying empty  $\pi$ -antibonding orbital of the pyrazine moiety<sup>34</sup> and this is probably the case here. The colour of the tetrakis(pyridine)iron(II) halides and thiocyanate complexes are

pale-yellow;<sup>6,7</sup> and the metal to ligand charge-transfer band presumably occurs at higher energy in the ultraviolet region. These results are consistent with the better  $\pi$ -acceptor properties of pyrazine over pyridine.

In this study, it was noted that for the complexes to be intensely coloured the combined presence of pyrazine and either halide or pseudohalide was necessary. Complexes which lacked this combination of ligands were found to be pale in colour. For example,  $\text{Fe}(\text{pyz})_2(\text{CH}_3\text{SO}_3)_2$  and  $\text{Fe}(\text{py})_4\text{Cl}_2$ <sup>6,7</sup> are pale yellow; whereas,  $\text{Fe}(\text{pyz})_2\text{Cl}_2$  is deep-red. This suggests that the halide or pseudohalide anions also play a role in the charge-transfer process; presumably a role which the sulfonate anions cannot engage in. Because of the ease of oxidation of halide and pseudohalide anions it is likely that the role of the anion in the charge-transfer process is ligand to metal in nature which then facilitates metal to pyrazine charge transfer.

Before considering the magnetic properties, it is worthwhile summarising the structural evidence for these compounds. Electronic spectral data indicate that the complexes contain pseudooctahedrally coordinated metal centres resulting in an  $\text{MN}_4\text{X}_2$  chromophore. For the bis(pyrazine) complexes, infrared spectroscopy strongly suggests unidentate anion coordination and in some cases bidentate bridging pyrazine moieties. The tetrakis(pyridine) complexes also contain anions coordinated in a unidentate fashion as well as coordinated pyridine ligands. The major difference between the bis(pyrazine) and tetrakis(pyridine) compounds is that a

two-dimensional lattice is present in the former group; whereas, monomeric species are present in the tetrakis(pyridine) complexes. X-ray crystallography has confirmed both of these structural types. Discussions in subsequent sections (3.3.5-3.3.6) of this chapter attempt to probe the effects that these structural differences have on the magnetic, Mössbauer and thermal properties of these materials.

### 3.3.4 Magnetic Properties

One of the initial objectives of this work was the study of the magnetic properties of pyrazine-bridged metal complexes in an effort to determine the magnitude of magnetic exchange propagation via this ligand and to investigate correlations between magnetic exchange and structural features of such complexes. As described earlier in this chapter, for both divalent iron and copper, it was possible to obtain and characterise not only complexes with bridging pyrazine groups but also analogous complexes with identical chromophores but without bridging ligands. It was anticipated that a better evaluation of exchange effects via bridging pyrazine would be possible by comparing the magnetic properties of these two groups of compounds.

The magnetic susceptibility data from the vibrating-sample magnetometer, Gouy and Faraday techniques for the copper and iron complexes are given in Appendices VIII and IX respectively.

#### 3.3.4.1 Magnetic susceptibility results for complexes containing a $\text{CuN}_4\text{O}_2$ chromophore

At all temperatures studied,  $\text{Cu}(\text{py})_4(\text{CF}_3\text{SO}_3)_2$ ,  $\text{Cu}(\text{py})_4(\text{CH}_3\text{SO}_3)_2$  and  $\text{Cu}(\text{pyz})_4(\text{CF}_3\text{SO}_3)_2 \cdot \text{H}_2\text{O}$  have magnetic moments within the range of 1.7-2.1 B.M., there being only a slight variation with temperature for all three examples (Appendix VIII). For copper(II) complexes, a temperature-independent magnetic moment is expected for magnetically-dilute systems and such complexes often exhibit room-temperature magnetic moment

values close to the spin-only value of 1.73 B.M. The magnetic moment data for  $\text{Cu}(\text{py})_4(\text{CF}_3\text{SO}_3)_2$  indicate the lack of magnetic exchange interactions and this is in accord with the X-ray structure result (Section 3.3.1.2) which shows the paramagnetic centres well isolated from each other. The magnetic moment data for  $\text{Cu}(\text{py})_4(\text{CH}_3\text{SO}_3)_2$  are consistent with a structure similar to that of the triflate derivative. The temperature-independent magnetic moment observed for the  $\text{Cu}(\text{pyz})_4(\text{CF}_3\text{SO}_3)_2 \cdot \text{H}_2\text{O}$  compound is consistent with the conclusion that the pyrazine groups are coordinated to the copper ion in a unidentate fashion. Bridging pyrazine groups may be expected to lead to magnetic concentration effects at low temperatures (see later). The magnitude and temperature dependence of the magnetic moment data presented here are similar to those previously observed for some related  $\text{Cu}(\text{py})_4\text{X}_2$  compounds (where  $\text{X}^-$  is  $\text{FSO}_3^-$ ,  $\text{p-CH}_3\text{C}_6\text{H}_4\text{SO}_3^-$ ,  $\text{ClO}_4^-$  and  $\text{BF}_4^-$ ).<sup>76</sup> In this previous study, however, magnetic measurements were limited to the temperature range of 80-300 K.

The magnetic properties of the bis(pyrazine) complex,  $\text{Cu}(\text{pyz})_2(\text{CH}_3\text{SO}_3)_2$ , were found to be quite different from those of the complexes discussed above. Although the room-temperature moment is of a similar magnitude to those of the other complexes, the data exhibit a strong temperature dependence,  $\mu_{\text{eff}}$  ranging from 1.87 B.M. at room temperature, to 0.85 B.M. at 4.2 K. For a comparison, the temperature dependencies of the magnetic moments of the bis(pyrazine) and tetrakis(pyridine)copper(II) methanesulfonate complexes are depicted in Fig. 3.17. The strong temperature dependence of

$\mu_{\text{eff}}$  for the bis(pyrazine) derivative is almost certainly due to the presence of antiferromagnetic exchange. The effect of magnetic concentration is more clearly seen in the magnetic susceptibility data, where the susceptibility exhibits a maximum at approximately 6.2 K (Fig. 3.18). Such behaviour can only be accounted for by invoking antiferromagnetic exchange effects. Rather long Cu-Cu distances (6.1934(2) and 8.1991(4) Å) tend to rule out direct exchange interactions between metal centres and the presence of pyrazine bridges suggests superexchange through the bridging ligands.

Fig. 3.17 Magnetic Moments vs Temperature for  $\text{Cu}(\text{py})_4(\text{CH}_3\text{SO}_3)_2$  and  $\text{Cu}(\text{pyz})_2(\text{CH}_3\text{SO}_3)_2$

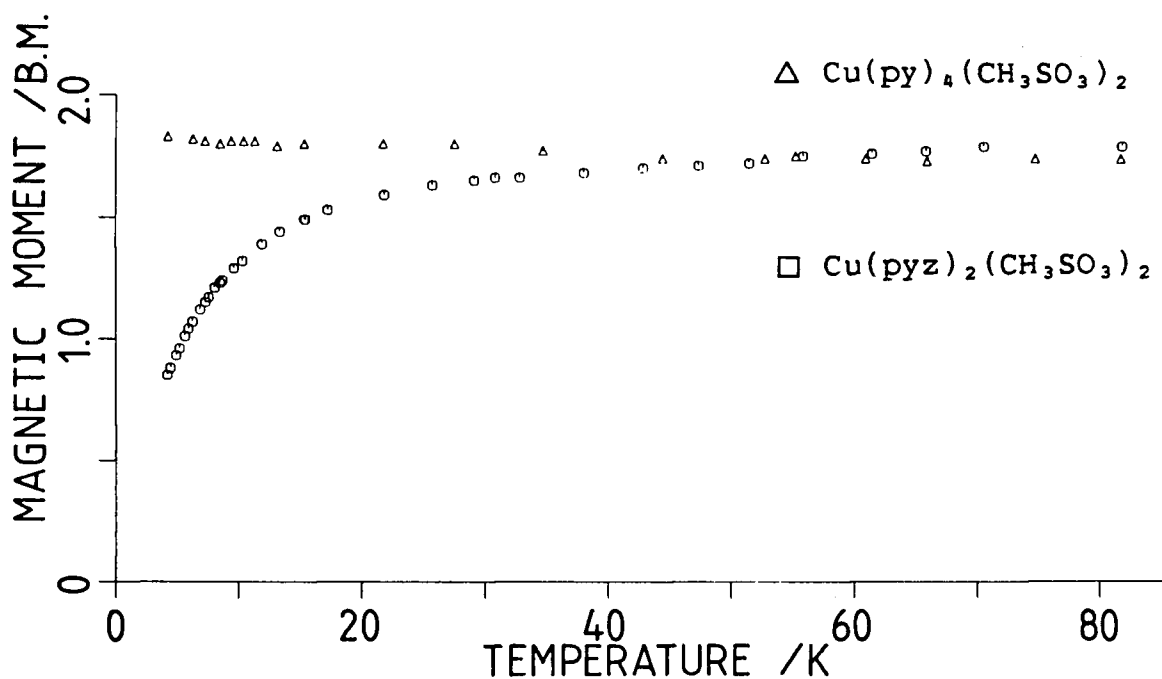
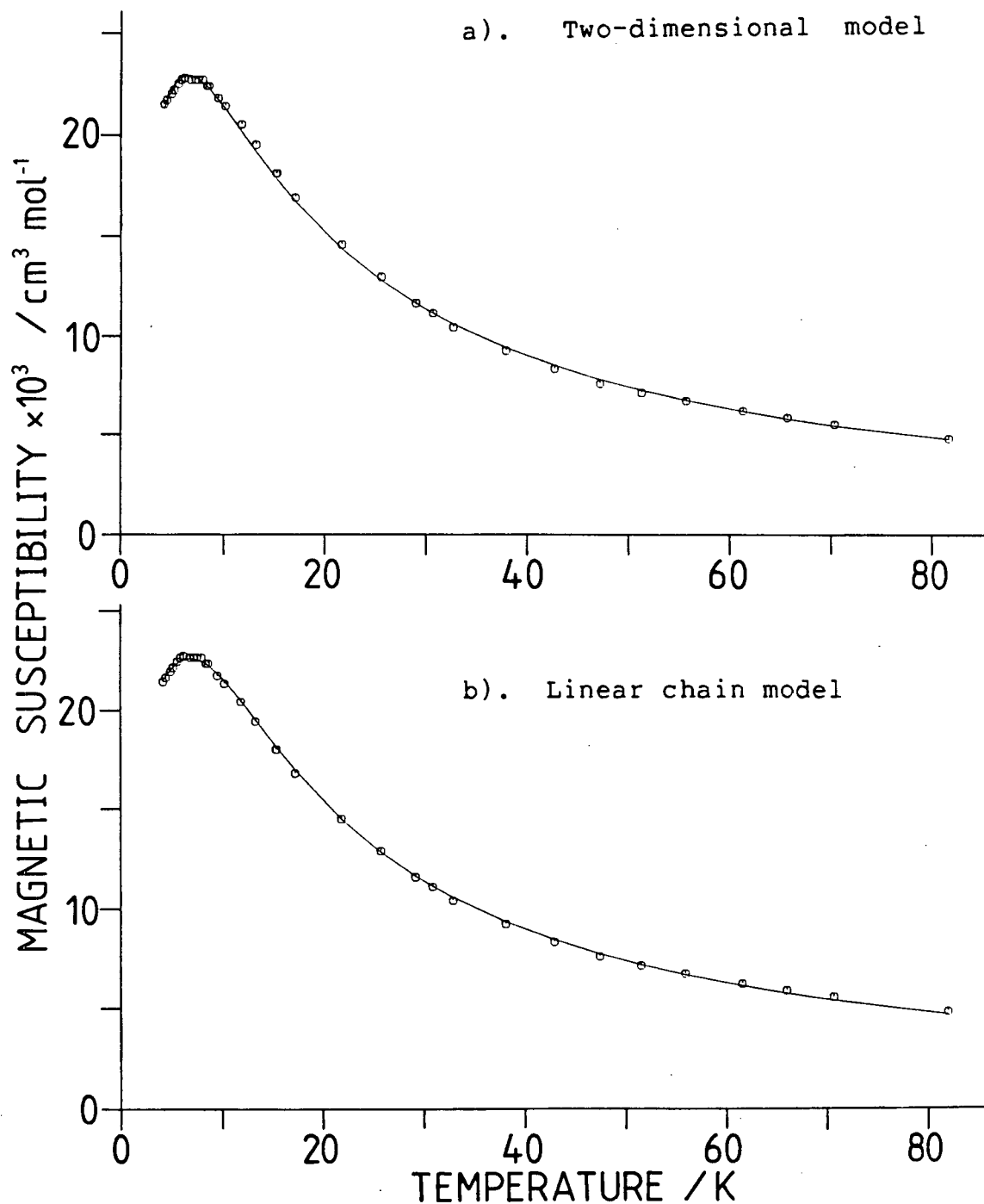


Fig. 3.18 Magnetic Susceptibility vs Temperature for  $\text{Cu}(\text{pyz})_2(\text{CH}_3\text{SO}_3)_2$

a). Two-dimensional model; solid line generated from  $J=-2.48 \text{ cm}^{-1}$ ,  $g=2.15$

b). Linear chain model; solid line generated from  $J=-3.82 \text{ cm}^{-1}$ ,  $g=2.13$



Magneto-structural correlations have been made for several related copper(II)-pyrazine complexes. Particularly relevant are the studies on  $\text{Cu}(\text{pyz})_2(\text{ClO}_4)_2$ .<sup>43, 52</sup> X-ray crystallography has revealed important structural similarities and differences between  $\text{Cu}(\text{pyz})_2(\text{ClO}_4)_2$  and  $\text{Cu}(\text{pyz})_2(\text{CH}_3\text{SO}_3)_2$  (Section 3.3.1.3). It was of interest to determine whether these structural characteristics were manifested in the magnetic properties of the two compounds. The magnetic susceptibility of  $\text{Cu}(\text{pyz})_2(\text{ClO}_4)_2$  exhibits a maximum value at 12.1 K<sup>52</sup> and Darriet *et al.*<sup>43</sup> successfully modelled these data by using Lines' high-temperature series-expansion expression for a two-dimensional square-planar antiferromagnet in the Heisenberg limit.<sup>136</sup> In general terms, the expression for the magnetic susceptibility is given by the following:

$$\frac{N g^2 \beta^2}{\chi J} = 3\theta + \sum_{n=1}^{\infty} \frac{C_n}{\theta^{n-1}} \quad \dots \text{Eqn. 3.5}$$

where  $\theta = kT/JS(S+1)$ ,  $g$  is the Lande  $g$  factor,  $N$  is the number of spins in the lattice and the coefficients,  $C_n$ , have been determined for spin  $S=1/2$  for values of  $n$  up to 6. For  $S=1/2$  these coefficients are as follows:  $C_1, 4$ ;  $C_2, 2.667$ ;  $C_3, 1.185$ ;  $C_4, 0.149$ ;  $C_5, -0.191$ ;  $C_6, 0.001$ .<sup>136</sup>

The parameters obtained from the fit of the magnetic susceptibility data to this expression for  $\text{Cu}(\text{pyz})_2(\text{ClO}_4)_2$  are the exchange coupling constant,  $J = -5.3 \text{ cm}^{-1}$  and  $g = 2.107$ .<sup>43</sup> Before the single-crystal X-ray analysis revealed the two-dimensional nature of  $\text{Cu}(\text{pyz})_2(\text{ClO}_4)_2$ , the magnetic



susceptibility data had been fit reasonably well to a model based on a tetrameric structure.<sup>52</sup> The small differences between calculated and experimental values for the two models indicate that it is not always possible to determine the nature of the polymeric structure merely by the fact that the magnetic susceptibility data are well represented by a particular model and emphasises the importance of X-ray structure determination in the study of magneto-structural correlations.

Based on the structure of  $\text{Cu}(\text{pyz})_2(\text{CH}_3\text{SO}_3)_2$  the magnetic susceptibility data for this compound were analysed by using the two-dimensional model as represented by Eqn. 3.5. A good fit between the experimental and calculated susceptibilities was obtained (the solid line in Fig. 3.18a represents the best fit). The parameters obtained from this fit are  $J = -2.48 \text{ cm}^{-1}$  and  $g = 2.15$ . These values were obtained from a least-squares fitting procedure by allowing both  $J$  and  $g$  to vary until a minimum value was obtained for the function  $F$  (Eqn. 3.6). In this case  $F$  is 0.0118.

$$F = \left[ \frac{1}{NT} \sum \left( \frac{x_{\text{calc}}^i - x_{\text{obs}}^i}{x_{\text{obs}}^i} \right)^2 \right]^{1/2} \quad \dots \text{Eqn. 3.6}$$

In Eqn. 3.4,  $NT$  is the number of data points, and  $x_i^{\text{obs}}$  and  $x_i^{\text{calc}}$  are the experimental and calculated molar magnetic susceptibilities, respectively.

As measured by the exchange coupling parameter  $J$ , the magnitude of the magnetic exchange in the methanesulfonate complex is approximately one half of that calculated for

$\text{Cu}(\text{pyz})_2(\text{ClO}_4)_2$ . Several possibilities exist to explain this relative diminution of  $J$  in  $\text{Cu}(\text{pyz})_2(\text{CH}_3\text{SO}_3)_2$ . The first is that the methanesulfonate anion, by acting as a stronger Lewis base than the perchlorate anion towards copper, effectively decreases the acidity of the copper(II) ions towards the bridging pyrazine groups and hence, lowers the intralayer exchange interaction. A second alternative mechanism is related to the fact that in the perchlorate derivative the pyrazine groups are equivalent and oriented in a way so as to interact effectively with the unpaired electron density on the copper(II) ions, resulting in an equal contribution from each pyrazine ligand to the overall exchange interaction. In  $\text{Cu}(\text{pyz})_2(\text{CH}_3\text{SO}_3)_2$ , however, there are two distinct pyrazine ligands and the exchange integral for each bridging pyrazine is likely to be dependent upon two factors: the degree of separation of the two copper ions and the orientation of the pyrazine  $\pi$ -system with respect to the copper d-orbitals. In  $\text{Cu}(\text{pyz})_2(\text{CH}_3\text{SO}_3)_2$ , adjacent copper(II) ions are separated by either 6.1934(2) Å, when the intervening pyrazine group is strongly bound in the equatorial plane, or 8.1991(4) Å, when the intervening pyrazine group is weakly bound in an axial position. Considering bond lengths alone, it would be expected that the shorter the Cu-Cu separation is, then the greater would be the magnetic exchange effect. Thus, the equatorially bound pyrazine groups may transmit exchange coupling effects more efficiently than the axially bound pyrazine groups.

In  $\text{Cu}(\text{pyz})_2(\text{CH}_3\text{SO}_3)_2$ , the two different orientations of the

pyrazine groups with respect to the copper d-orbitals may also play an important role in determining the nature of the exchange interaction. Electronic spectral results (Section 3.3.3.2) combined with the presence of a tetragonally elongated pseudooctahedral environment about copper (Section 3.3.1.3) indicate that the unpaired electron is in the  $d_{x^2-y^2}$  orbital. Previous research<sup>54</sup> has demonstrated that for copper-pyrazine complexes with this electronic configuration and structure, the magnitude of the antiferromagnetic exchange is determined from the overlap of the  $d_{x^2-y^2}$  orbital and the pyrazine  $\pi$ -system. This interaction, however, is only possible when the pyrazine ring is canted out of the xy plane. For example, the pyrazine rings in  $\text{Cu}(\text{pyz})_2(\text{ClO}_4)_2$ <sup>43</sup> and  $\text{Cu}(\text{pyz})(\text{NO}_3)_2$ <sup>42</sup> are canted out of the xy plane by an angle of 66.1 and 50° respectively and significant magnetic exchange interactions are observed.<sup>43, 49</sup> On the other hand, in  $\text{Cu}(\text{pyzA})_2(\text{ClO}_4)_2$  (where pyzA is pyrazine-2-carboxamide), the pyrazine rings lie in the xy plane<sup>137</sup> resulting in orthogonal overlap and a magnetically-dilute system.<sup>138</sup> These previous studies<sup>42, 43, 137, 138</sup> and the X-ray structure result for  $\text{Cu}(\text{pyz})_2(\text{CH}_3\text{SO}_3)_2$  (Section 3.3.1.3) suggest that the equatorially bound pyrazine group in the methanesulfonate compound, which is canted out of the xy plane by 28.5°, is suitably oriented to present a  $\pi$ -pathway for magnetic interactions between copper centres.

The pyrazine coordinated further away from copper is oriented in a substantially different fashion with respect to

the copper d-orbitals than the equatorial pyrazine ligand. The plane of the axial pyrazine ring lies in the xz plane of the  $\text{CuN}_2\text{O}_2$  unit; this type of pyrazine ligand orientation has been observed previously in  $\text{Cu}(\text{pyz})(\text{hfac})_2$ <sup>53</sup> (where hfac is 1,1,1,5,5,5-hexafluoropentane-2,4-dionate). In spite of the presence of bridging pyrazine ligands no magnetic exchange interactions were observed in this compound.<sup>54</sup> It was argued that the only symmetry-allowed overlap between the copper d-orbitals and the pyrazine  $\pi$ -system arises from  $d_{xy}-\pi(b_{1g})$  overlap and a combination of the small amount of unpaired spin density in the  $d_{xy}$  orbital and poor effective overlap results in a poor  $\pi$ -pathway for magnetic exchange. The structural similarities between the pyrazine ligand in  $\text{Cu}(\text{pyz})(\text{hfac})_2$  and the axially bound pyrazine group in  $\text{Cu}(\text{pyz})_2(\text{CH}_3\text{SO}_3)_2$  suggest that this group may also be ineffective in propagating magnetic exchange interactions.

The comparison of the pyrazine group orientations in  $\text{Cu}(\text{pyz})_2(\text{CH}_3\text{SO}_3)_2$  with those in other copper(II)-pyrazine complexes suggests that the magnetic exchange interaction in the methanesulfonate derivative proceeds via two different routes, with the exchange interaction through the equatorially bound pyrazine,  $J_{\text{eq}}$ , proposed to be significantly stronger than the exchange,  $J_{\text{ax}}$ , through the pyrazine bound in the axial position. In the extreme case where  $J_{\text{eq}} \gg J_{\text{ax}}$ , the magnetic properties may be more closely represented by a one-dimensional linear chain model. A model has been proposed for the analysis of the magnetic susceptibility of a Heisenberg linear chain for  $S=1/2$

ions. Hall<sup>139</sup> and Hatfield<sup>140</sup> developed the model proposed by Bonner and Fisher;<sup>141</sup> this resulted in an expression for the molar susceptibility of a linear chain of interacting  $S=1/2$  spins as a polynomial expansion:

$$\chi_m = \frac{Ng^2\beta^2}{kT} \left[ \frac{0.250+0.14995x^{-1}+0.30094x^{-2}}{1+1.9862x^{-1}+0.68854x^{-2}+6.0626x^{-3}} \right] \dots \text{Eqn. 3.7}$$

where  $x=kT/|J|$ .

The best fit of the data for  $\text{Cu}(\text{pyz})_2(\text{CH}_3\text{SO}_3)_2$  to this expression is equally as good as the best fit to the two-dimensional model; for the one-dimensional model the parameters obtained from the best fit are  $J=-3.82 \text{ cm}^{-1}$  and  $g=2.13$ , with  $F=0.0118$ . The best fit is represented by the solid line in Fig. 3.18b. The data for  $\text{Cu}(\text{pyz})_2(\text{ClO}_4)_2$ , however, gave a fit to the one-dimensional model which was poorer ( $F=0.0460$ ) than that for the two-dimensional model, as expected on the basis of the equivalent pyrazine ligands present in this compound. From these observations the methanesulfonate compound may be considered as consisting of linear chains of  $-\text{Cu-pyz-Cu}-$  units, in which there are relatively strong intrachain magnetic exchange interactions and although these linear chains are crosslinked through the weakly bound axial pyrazine groups the interchain interactions appear to be of a much smaller magnitude.

The results provided in this section demonstrate that there are significant differences between the magnetic properties of the complexes studied. The tetrakis(pyridine) and

tetrakis(pyrazine)copper(II) complexes are magnetically dilute as is consistent with their monomeric (non-bridged) structures involving isolated  $\text{CuN}_4\text{O}_2$  chromophores.  $\text{Cu}(\text{pyz})_2(\text{CH}_3\text{SO}_3)_2$  has two distinct types of bridging pyrazine groups one of which may be oriented in such a way so as to provide a more effective overlap with the  $d_{x^2-y^2}$  orbital of copper and hence be more efficient in propagating magnetic exchange interactions. The magnetic susceptibility data are well represented by a two-dimensional model in spite of the inequivalence of the bridging pyrazine ligands. The data are also well represented by a linear chain model which may present a more realistic picture of the exchange interaction being along one unique direction of the two-dimensional material.

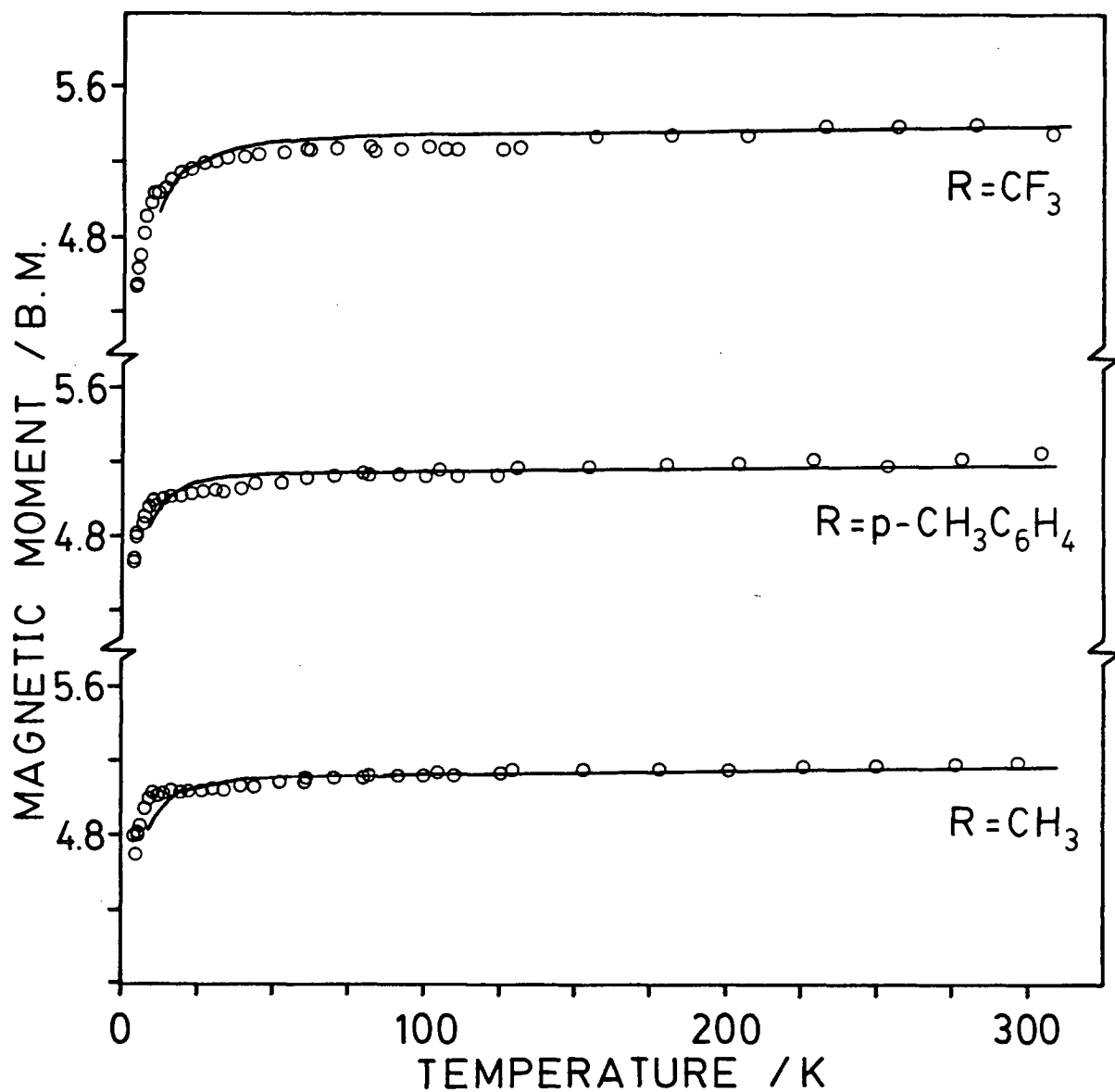
#### 3.3.4.2 Magnetic susceptibility results for complexes containing an $\text{FeN}_4\text{O}_2$ chromophore

Magnetic susceptibility data for the tetrakis(pyridine) and bis(pyrazine)iron(II) sulfonate complexes are presented in Appendix IX, Part A. The magnetic susceptibilities for  $\text{Fe}(2\text{-mepyz})_4(\text{CH}_3\text{SO}_3)_2$  (Appendix IX, Part A) are also discussed in this section.

The magnetic moment data for the  $\text{Fe}(\text{py})_4(\text{RSO}_3)_2$  complexes and  $\text{Fe}(2\text{-mepyz})_4(\text{CH}_3\text{SO}_3)_2$  all show a similar temperature dependence. At room temperature the magnetic moment values for these complexes are in the range of 5.2-5.4 B.M. which is consistent with their formulation as high-spin iron(II) compounds. The magnetic moment values remain fairly constant as

the temperature is decreased and it is not until below 15 K that a more significant decrease in  $\mu_{\text{eff.}}$  is observed. The magnetic moment temperature dependencies for the  $\text{Fe}(\text{py})_4(\text{RSO}_3)_2$  complexes are shown in Fig. 3.19.

Fig. 3.19 Magnetic Moments vs Temperature for  $\text{Fe}(\text{py})_4(\text{RSO}_3)_2$  Complexes



For these complexes, the observed temperature dependence of  $\mu_{\text{eff}}$  may arise from a combination of several factors. A temperature-dependent magnetic moment is expected for  $\text{Fe}^{2+}$  compounds ( $d^6$ ) with a triply degenerate  $^5T_{2g}$  ground state. Small zero-field splitting effects may also be invoked to explain such a temperature dependence. The X-ray structural data for the  $\text{Fe}(\text{py})_4(\text{RSO}_3)_2$  complexes show the paramagnetic centres well isolated from each other. Hence, the small decrease in  $\mu_{\text{eff}}$  at low temperatures is unlikely to be associated with any magnetic exchange effects. Further indirect evidence in support of the magnetically dilute nature of these iron complexes comes from the results presented in the preceeding section which indicate the absence of magnetic interactions in the analogous copper complexes. For the monomeric  $\text{Fe}(\text{py})_4(\text{RSO}_3)_2$  complexes, no magnetic concentration was expected and the temperature dependence of  $\mu_{\text{eff}}$  for  $\text{Fe}(\text{2-mepyz})_4(\text{CH}_3\text{SO}_3)_2$  (similar to that observed for  $\text{Fe}(\text{py})_4(\text{CH}_3\text{SO}_3)_2$ ) indicates that the 2-methylpyrazine ligand coordinates in a terminal unidentate mode resulting in a monomeric species. Bridging 2-methylpyrazine groups may be expected to give rise to magnetic exchange effects.

The magnetic properties of the  $\text{Fe}(\text{py})_4(\text{RSO}_3)_2$  complexes studied are proposed to arise from single-ion effects and hence, the magnetic moment data were analysed by two different methods which take into account such phenomena. The first method was initially proposed by Figgis and Lewis<sup>64</sup> and simultaneously developed by König and Chakravarty.<sup>142</sup> The Figgis model has been



applied to a number of transition-metal complexes<sup>64, 143-146</sup> and the approach used may be illustrated by high-spin iron(II) compounds having a  $^5T_{2g}$  ground term. The model involves simultaneous perturbation of the 15-fold degenerate  $^5T_{2g}$  basis set by the effects of spin-orbit coupling and an axially symmetric ligand-field distortion (either tetragonal or trigonal). The temperature dependence of the magnetic moment is analysed in terms of three parameters. Firstly, the axial-distortion parameter  $\Delta$  (sometimes called 3Ds). This is the separation between the  $^5B_{2g}$  and  $^5E_g$  states arising from the cubic field  $^5T_{2g}$  ground state, in the presence of an axially symmetric ligand field (Fig. 3.13). A positive value of  $\Delta$  corresponds to the orbitally non-degenerate  $^5B_{2g}$  state lying lowest. The spin-orbit coupling constant,  $\lambda$ , is the second parameter and, in complexes, its value is expected to be reduced somewhat below the free-ion value of  $-100 \text{ cm}^{-1}$ .<sup>147</sup> The third parameter is the orbital reduction factor,  $\kappa$ . This variable allows for electron delocalisation from the  $t_{2g}$  orbital set.

The Figgis model has several drawbacks which have been previously pointed out. Firstly, it is difficult to unambiguously determine the sign of  $\Delta$  from magnetic susceptibility data obtained on powdered polycrystalline samples. In fact, Gregson and Mitra<sup>148</sup> contend that the measurement of the average magnetic susceptibility is incapable of giving reliable results for either  $\Delta$  or  $\kappa$  and that measurements on single crystals are required to deduce meaningful values for these ligand-field parameters. Another

shortcoming of the model has been pointed out by Figgis:<sup>149</sup> the relationship between observed  $\kappa$  values and the electronegativity and  $\pi$ -bonding characteristics of various ligands is unclear.

The following method was used to fit the magnetic moment data for the  $\text{Fe}(\text{py})_4(\text{RSO}_3)_2$  complexes to this model. Figgis et al.<sup>64</sup> have tabulated magnetic moment data as a function of  $\Delta/\lambda$  and  $\kappa$ ; in the present study, these data were used to produce plots of  $\mu_{\text{eff}}$  as a function of  $kT/\lambda$  which were then compared visually with the experimental data. The best fits between calculated and experimental data are obtained by using the parameter values given in Table 3.5 and the best fits are represented by the solid lines in Fig. 3.19. While reasonable fits are obtained in the temperature region of 25-300 K, care must be taken not to place too much emphasis on interpreting these parameter values, due to the inherent limitations of the model. At temperatures below 25 K the agreement between experimental and calculated magnetic moment values is not as good and this is not unexpected because the model ignores zero-field splitting effects which may be significant for  $\text{Fe}^{2+}$  under these conditions.

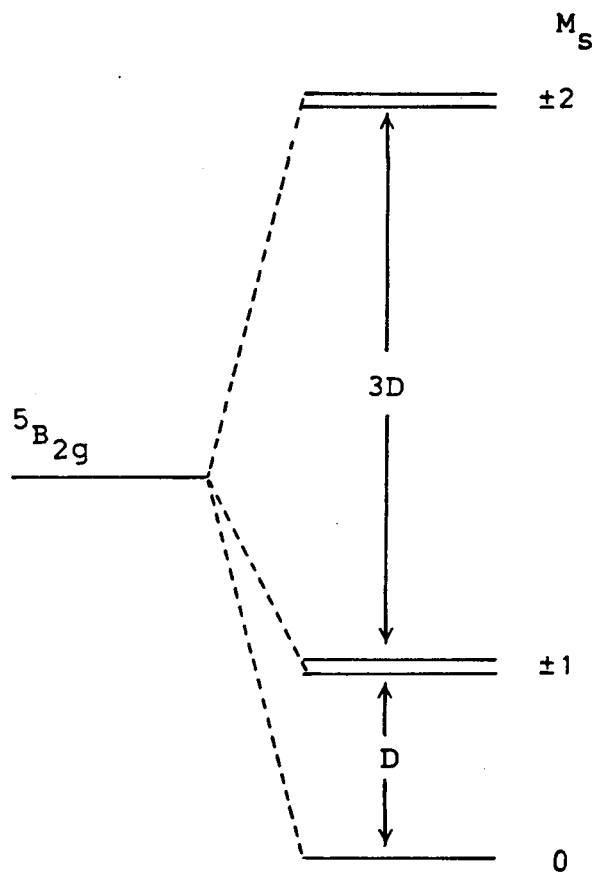
Table 3.5 Crystal Field Parameters for  $\text{Fe}(\text{py})_4(\text{RSO}_3)_2$   
Complexes

R	$\Delta/\text{cm}^{-1}$	$\lambda / \text{cm}^{-1}$	$\kappa$
$\text{CF}_3$	600	-80	1.0
$\text{CH}_3$	700	-70	0.7
$p\text{-CH}_3\text{C}_6\text{H}_4$	600	-60	0.8

As mentioned above, the information contained in magnetic susceptibility data from powdered polycrystalline samples is insufficient to determine the sign of  $\Delta$  unambiguously. Interpretation of the Mössbauer spectral data (Section 3.3.5.1), however, suggests strongly that the ground state in each of the tetrakis(pyridine)iron(II) sulfonate species must be nondegenerate. Hence, only positive values of  $\Delta$  were considered when fitting the magnetic moment data. From the values of  $\Delta$  in Table 3.5, it appears that the axial distortions are of approximately the same magnitude in all three cases. The values of  $\lambda$  are, as expected upon complex formation, reduced from the free-ion value of  $-100 \text{ cm}^{-1}$ . For the methanesulfonate derivative,  $\lambda$  and  $\kappa$  are reduced by corresponding amounts which is clearly fortuitous as such a correlation does not exist in the other two cases.

The second model considers zero-field splitting. This phenomenon results when spin-orbit coupling induces mixing in of higher energy levels and leads to partial removal of the ground-state degeneracy and thus to a temperature-dependent magnetic moment. Spin-orbit coupling has the effect of partially lifting the degeneracy of the  $M_s$  levels (Fig. 3.20).

Fig. 3.20 Zero-Field Splitting for High-spin Iron(II)



The relative energies of the three zero-field levels of 0, D and 4D are shown for a positive value of D. The level sequence is reversed where D is less than zero. When the zero-field splitting parameter is non-zero and positive and the magnitude of D is of the order of kT, then as the sample temperature is decreased the  $M_s=\pm 2$  and  $M_s=\pm 1$  levels are depopulated and this is manifested in a decrease in the magnetic moment. In the present study, the axial zero-field splitting parameter D, and the g values were found by least-squares fits of the temperature dependence of the molar magnetic susceptibility to the following expression:<sup>150</sup>

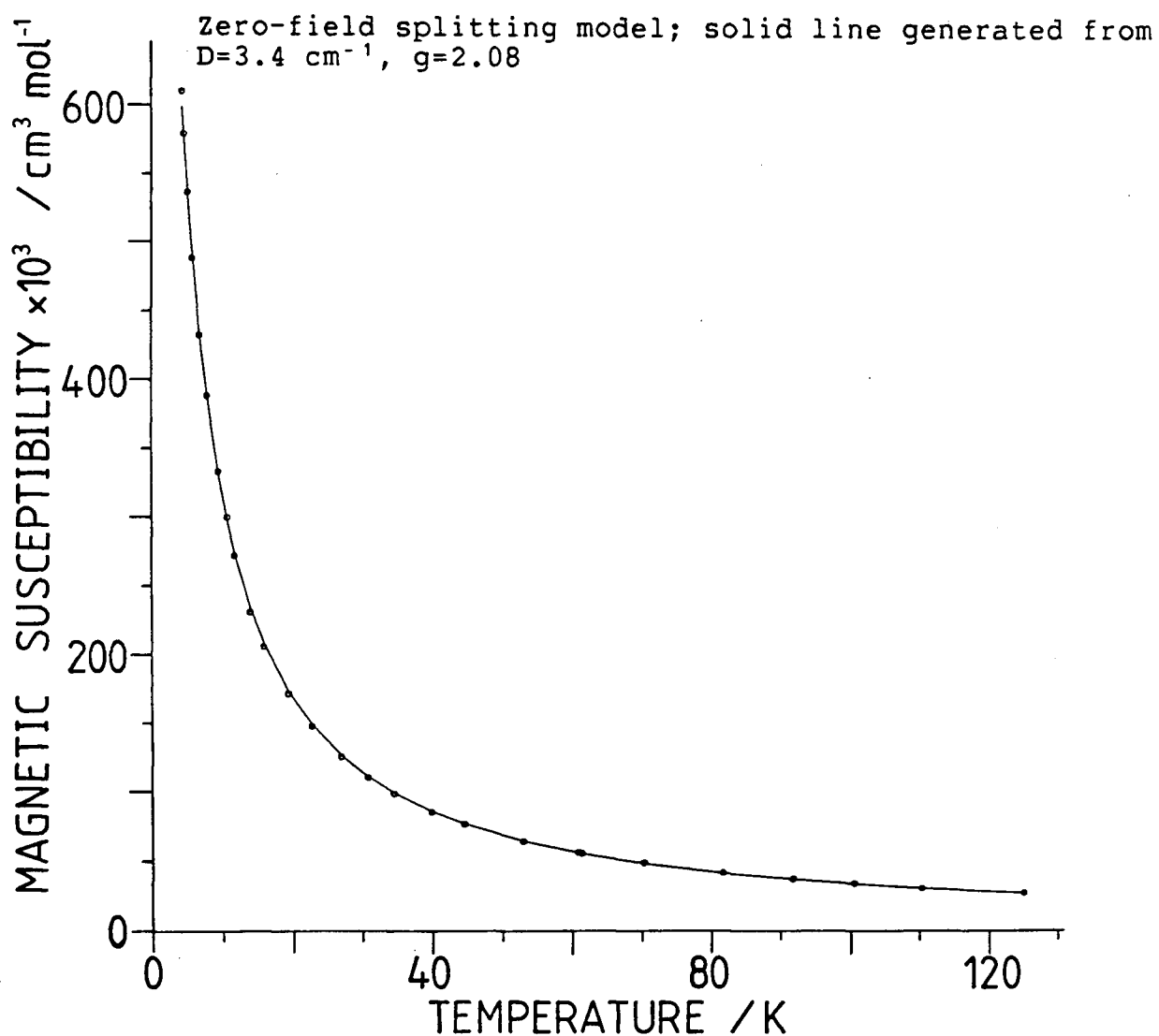
$$\chi_{\parallel} = C \frac{2e^{-x} + 8e^{-4x}}{1 + 2e^{-x} + 2e^{-4x}} \quad \chi_{\perp} = C \frac{\frac{6}{x}(1 - e^{-x}) + \frac{4}{3x}(e^{-x} - e^{-4x})}{1 + 2e^{-x} + 2e^{-4x}} \quad \dots \text{Eqn. 3.8}$$

where  $x=D/kT$ ,  $C=Ng^2\beta^2/kT$  and  $\chi_p=[(\chi_{\parallel}+2\chi_{\perp})/3]$ .

When isotropic g values are used it was found that the minima in the fitting function, F, are shallow, making it difficult to obtain unique values of g, g and D. When isotropic g values are employed, an approach used previously by Klein et al.,<sup>150</sup> the minima in F are steeper and g and D values were obtained and are shown in Table 3.6. The solid line in Fig. 3.21 represents the best fit of this model to the magnetic susceptibility data for  $\text{Fe}(\text{py})_4(\text{CH}_3\text{SO}_3)_2$ .

Table 3.6 Zero-Field Splitting Parameters

COMPOUND	$D/\text{cm}^{-1}$	$g_{\text{iso}}$	F
$\text{Fe}(\text{py})_4(\text{CF}_3\text{SO}_3)_2$	6.1	2.15	0.0076
$\text{Fe}(\text{py})_4(\text{CH}_3\text{SO}_3)_2$	3.4	2.08	0.0122
$\text{Fe}(\text{py})_4(\text{p-CH}_3\text{C}_6\text{H}_4\text{SO}_3)_2$	3.9	2.09	0.0108
$\text{Fe}(\text{pyz})_2(\text{CF}_3\text{SO}_3)_2 \cdot \text{CH}_3\text{OH}$	14.5	2.11	0.0353
$\text{Fe}(\text{pyz})_2(\text{CH}_3\text{SO}_3)_2$	13.5	2.03	0.0354

Fig. 3.21 Magnetic Susceptibility vs Temperature for  $\text{Fe}(\text{py})_4(\text{CH}_3\text{SO}_3)_2$ 

Information contained in the powder magnetic susceptibility data is insufficient to determine the sign of D and equally good fits are obtained using either positive or negative D values. The value of D is largest for the triflate derivative and somewhat smaller for the p-tosylate and methanesulfonate compounds. Previously the zero-field splitting parameter has been approximated from the following expression:<sup>151</sup>

$$D = \frac{\xi^2}{16} \frac{1}{E(^5E) - E(^5B)} \quad \dots \text{Eqn 3.9}$$

Thus, the magnitude of the zero-field splitting is expected to be inversely proportional to the separation of the  $^5E_g$  and  $^5B_{2g}$  states (arising from the  $^5T_{2g}$  ground state) and proportional to the square of the single-electron spin-orbit coupling constant,  $\xi$ . The magnitude of the D values in Table 3.6 indicates that the separation of the  $^5E_g$  and  $^5B_{2g}$  states is smallest for the triflate derivative and of a comparable magnitude in the other two cases. This is in contrast to the Figgis model where the axial distortion parameter,  $\Delta$ , was found to be approximately the same in all three cases.

To summarise, the magnetic properties of the  $\text{Fe}(\text{py})_4(\text{RSO}_3)_2$  complexes and of  $\text{Fe}(\text{2-mepyz})_4(\text{CH}_3\text{SO}_3)_2$  are consistent with their formulation as high-spin iron(II) compounds. The temperature dependence of  $\mu_{\text{eff}}$  arises from single-ion effects. There is no evidence for magnetic concentration, this being entirely consistent with their monomeric molecular nature. These complexes then serve as a baseline from which magnetic exchange

effects in the related bis(pyrazine) derivatives were measured.

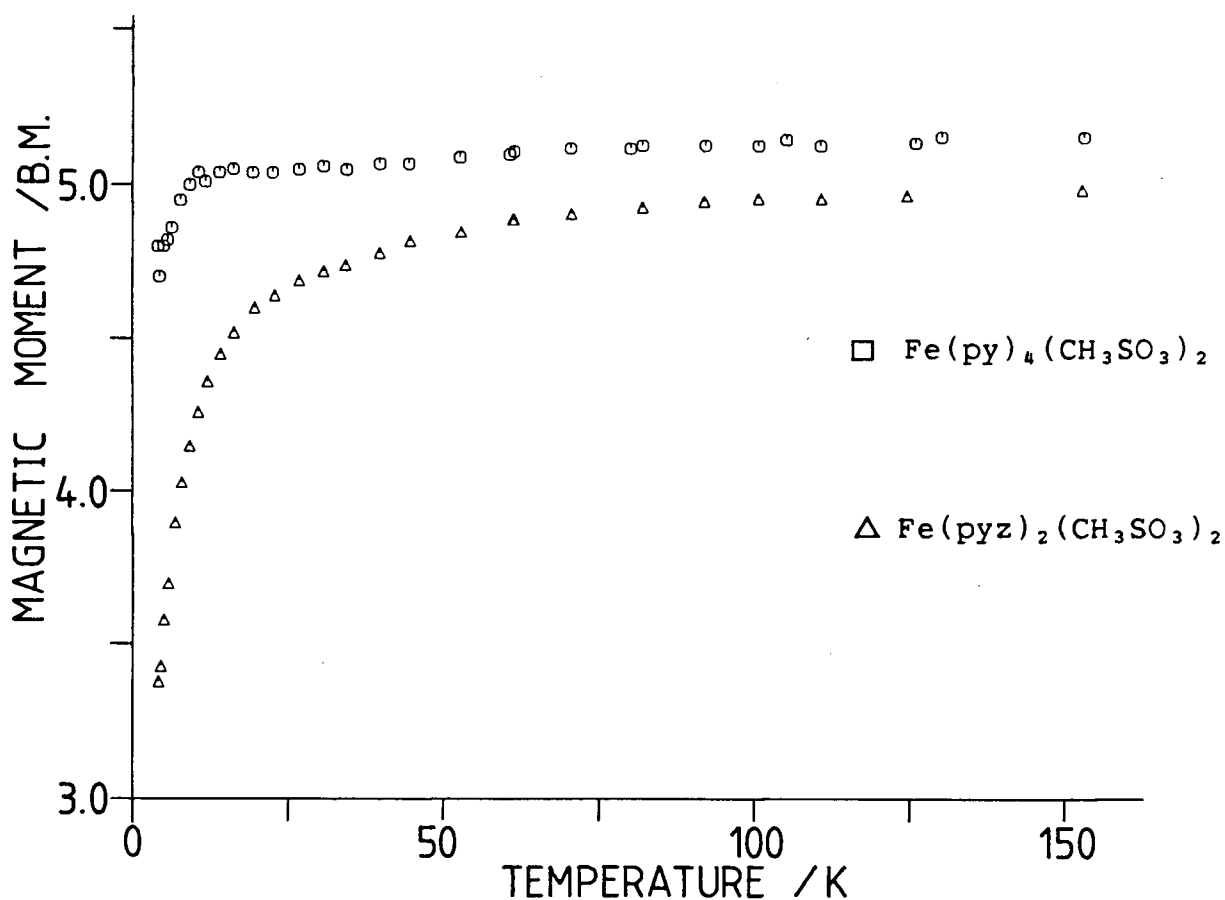
The magnetic properties of the bis(pyrazine) complexes  $\text{Fe}(\text{pyz})_2(\text{CF}_3\text{SO}_3)_2 \cdot \text{CH}_3\text{OH}$  and  $\text{Fe}(\text{pyz})_2(\text{CH}_3\text{SO}_3)_2$  are significantly different from those of the  $\text{Fe}(\text{py})_4(\text{RSO}_3)_2$  compounds. The differences are not significant at room temperature, where the magnetic moment values for the tetrakis(pyridine) and bis(pyrazine)iron(II) compounds are very similar (within the range of 5.1-5.4 B.M.), indicative of the high-spin nature of the complexes. The bis(pyrazine) complexes, however, exhibit much stronger temperature dependencies in their  $\mu_{\text{eff}}$  values than do the tetrakis(pyridine) complexes and at liquid helium temperatures the magnetic moments for the two groups of compounds diverge by about 1.3 B.M. A comparison of the temperature dependence of magnetic moment data for  $\text{Fe}(\text{pyz})_2(\text{CH}_3\text{SO}_3)_2$  and  $\text{Fe}(\text{py})_4(\text{CH}_3\text{SO}_3)_2$  is shown in Fig. 3.22. A similar comparison can be made for the bis(pyrazine) and tetrakis(pyridine) triflate derivatives (Appendix IX, Part A). Unlike  $\text{Cu}(\text{pyz})_2(\text{CH}_3\text{SO}_3)_2$ , the bis(pyrazine)iron(II) species exhibit no maxima in their magnetic susceptibility versus temperature plots down to 4.2 K, and hence, no conclusive evidence for antiferromagnetic exchange interactions in the iron complexes can be obtained from the  $\chi_m$  versus temperature plots.

Comparing bis(pyrazine) to tetrakis(pyridine) complexes, the greater temperature dependence of the magnetic moment data for the former group may arise from either weak antiferromagnetism or a larger zero-field splitting effect. Further support for this conclusion is provided by the fact that



the Figgis model, which provides a satisfactory fit for the magnetic properties of the tetrakis(pyridine) compounds, proves to be entirely unsatisfactory for the bis(pyrazine) derivatives. The parameters tried are quite incapable of reproducing the observed magnetic moment behaviour. The experimental  $\mu_{\text{eff}}$  values are always substantially below any values which the model generates. The unsatisfactory results for the bis(pyrazine) compounds gives further support for the proposal that zero-field and/or magnetic exchange effects play a significant role in determining their magnetic properties.

Fig. 3.22 Magnetic Moments vs Temperature for  $\text{Fe}(\text{py})_4(\text{CH}_3\text{SO}_3)_2$  and  $\text{Fe}(\text{pyz})_2(\text{CH}_3\text{SO}_3)_2$

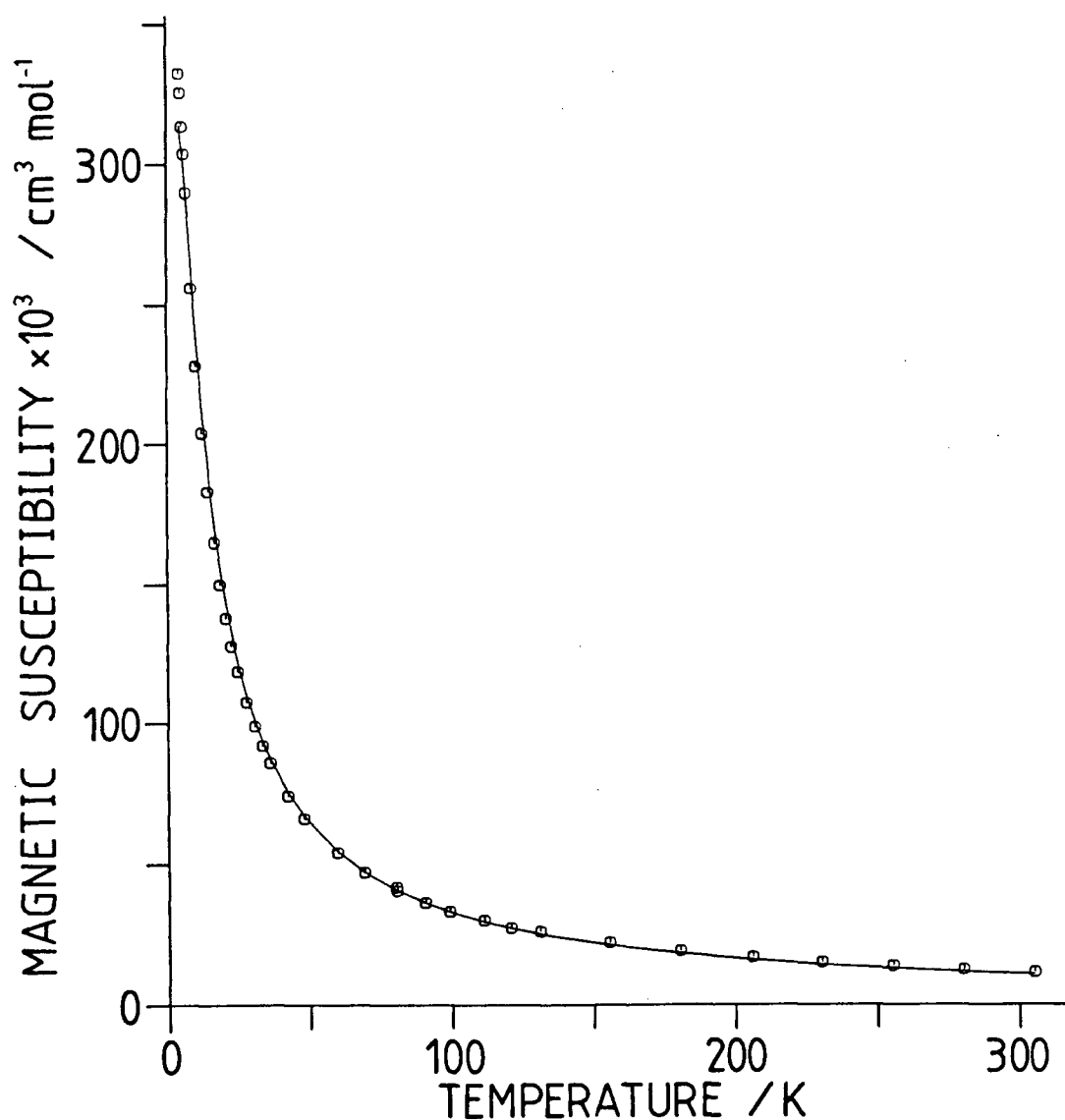


To take into account zero-field effects, the model which was used previously to analyse the magnetic properties of the tetrakis(pyridine) complexes was applied to the bis(pyrazine) compounds. The parameters obtained from the least-squares fits are given in Table 3.6. For  $\text{Fe}(\text{pyz})_2(\text{CF}_3\text{SO}_3)_2 \cdot \text{CH}_3\text{OH}$  the best fit of the data is shown in Fig. 3.23.

Fig. 3.23

Magnetic Susceptibility vs Temperature for  $\text{Fe}(\text{pyz})_2(\text{CF}_3\text{SO}_3)_2 \cdot \text{CH}_3\text{OH}$

Zero-field splitting model; solid line generated from  $D=14.5 \text{ cm}^{-1}$ ,  $g=2.11$



To reproduce the magnetic susceptibility data of the bis(pyrazine) complexes it is necessary to employ a significantly larger  $D$  value than that used for the analogous tetrakis(pyridine) complexes. It should be noted that using this model results in a rather poorer fit, as measured by the value of  $F$ , for the bis(pyrazine) complexes, compared to the  $F$  values for their tetrakis(pyridine) analogues.

The third model chosen to represent the magnetic properties of the bis(pyrazine) complexes is the Lines' two-dimensional model. This model was discussed previously (Section 3.3.4.1) when applied to the magnetic properties of the two-dimensional complex,  $\text{Cu}(\text{pyz})_2(\text{CH}_3\text{SO}_3)_2$ . The choice of this model was thought to be appropriate based upon the proposed two-dimensional layer structure of these bis(pyrazine) compounds and the possibility that weak magnetic interactions may be propagated via the bridging pyrazine ligand. By substituting the following coefficients<sup>136</sup> into Eqn. 3.5 the model can be applied to  $S=2$  systems;  $C_1$ , 4;  $C_2$ , 1.500;  $C_3$ , 0.252;  $C_4$ , 0.258;  $C_5$ , 0.124;  $C_6$ , 0.015.

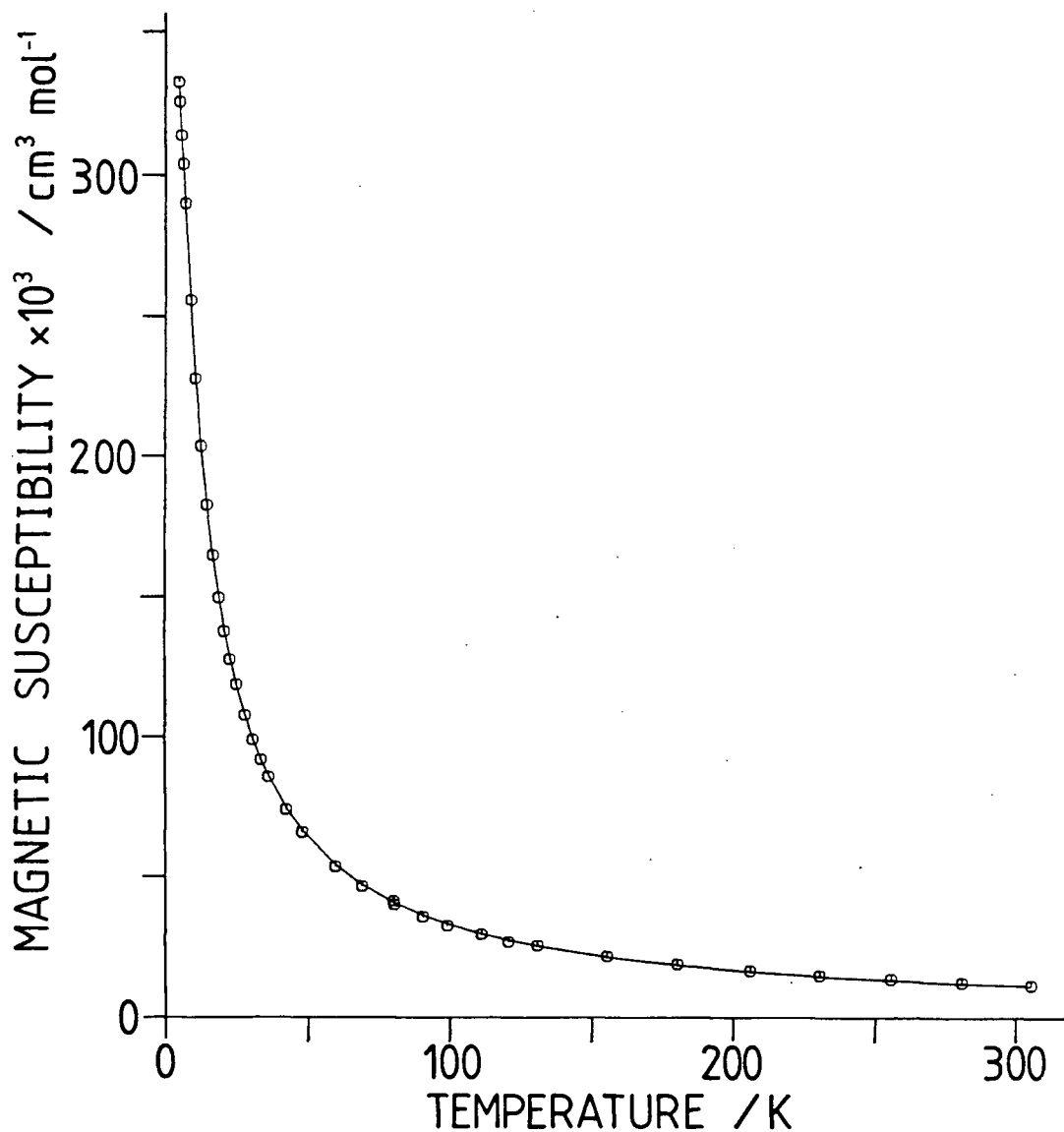
Excellent agreement between calculated and experimental data was obtained by using this model using the following parameter values:

	$-J/\text{cm}^{-1}$	$g$	$F$
$\text{Fe}(\text{pyz})_2(\text{CF}_3\text{SO}_3)_2 \cdot \text{CH}_3\text{OH}$	0.20	2.16	0.0122
$\text{Fe}(\text{pyz})_2(\text{CH}_3\text{SO}_3)_2$	0.18	2.07	0.0143

The best fit of the data for the methanesulfonate complex is shown as the solid line in Fig. 3.24.

Fig. 3.24 Magnetic Susceptibility vs Temperature for  $\text{Fe}(\text{pyz})_2(\text{CH}_3\text{SO}_3)_2$

Two-dimensional model; solid line generated from  $J = -0.18 \text{ cm}^{-1}$ ,  $g = 2.07$



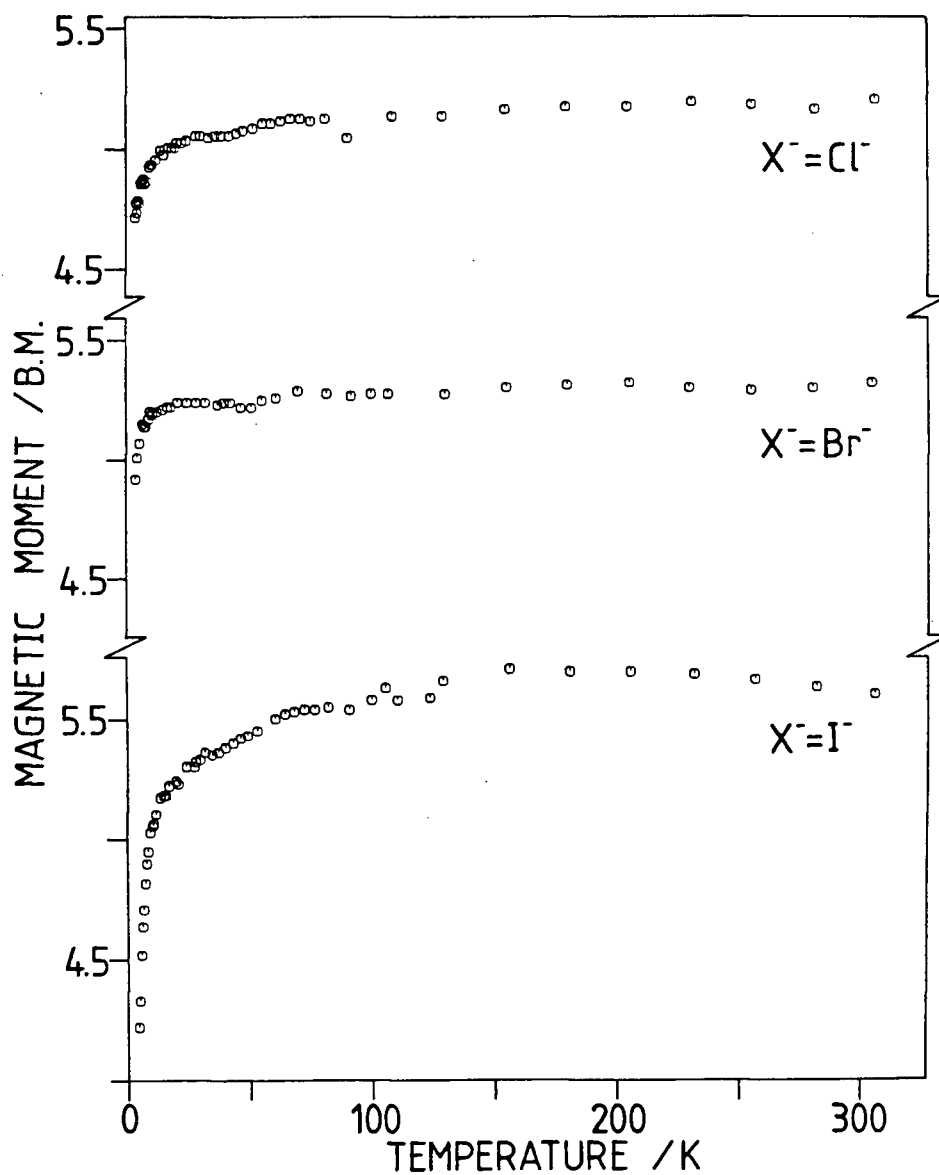
The small negative values of  $J$  indicate that if exchange interactions are present they are of a weak antiferromagnetic nature.

The treatment of the magnetic properties of the bis(pyrazine) compounds by using the two-dimensional and the zero-field splitting models, together with the parameters from the zero-field splitting model for the tetrakis(pyridine) complexes, provide a rationale for the different magnetic properties of the two groups of compounds. Both groups have an  $\text{FeN}_4\text{O}_2$  chromophore and would be expected to possess similar single-ion effects, resulting in similar  $D$  values. However, treating the bis(pyrazine) complexes using the zero-field splitting model only, and ignoring magnetic exchange effects, generates  $D$  values which we believe are unrealistically large compared to those for the tetrakis(pyridine) complexes. Ignoring zero-field splitting effects, and treating the bis(pyrazine) complexes using the two-dimensional magnetic exchange model, generates better fits to experiment than for the zero-field splitting model, giving strong support to the conclusion that weak exchange effects are present in these complexes. Therefore, it is proposed that the differences in the magnetic properties of the two groups are most likely a consequence of the major structural difference between the two groups; i.e., the presence of bridging pyrazine ligands in the pyrazine compounds. Such groups could provide a suitable pathway for antiferromagnetic exchange coupling, as in the copper complex discussed above.

### 3.3.4.3 Magnetic susceptibility results for complexes containing an $\text{FeN}_4\text{X}_2$ chromophore

The results of the magnetic measurements are tabulated in Appendix IX, Part A. The magnetic moment data for the three bis(pyrazine)iron(II) halide derivatives are illustrated in Fig. 3.25.

Fig. 3.25 Magnetic Moments vs Temperature For  $\text{Fe}(\text{pyz})_2\text{X}_2$  Complexes



The chloro- and bromo species have magnetic moments which remain fairly constant down to approximately 50 K and then decrease more significantly, especially at temperatures less than 20 K. At room temperature the magnitudes of the magnetic moments follow the order  $I > Br > Cl$  and of the three compounds  $Fe(pyz)_2I_2$  exhibits the largest temperature dependence, the magnetic moment plot passing through a broad maximum at approximately 160 K before falling to 4.2 B.M. at 4.2 K. The magnetic susceptibility versus temperature plot for each of the three compounds implies Curie-Weiss behaviour and the absence of a maximum in this plot indicates a lack of strong magnetic exchange interactions.

Magnetic moments for  $Fe(pyz)_2Br_2$  and the monohydrate,  $Fe(pyz)_2Cl_2 \cdot H_2O$  have been measured at room temperature (Gouy technique) by other researchers.<sup>62</sup> For  $Fe(pyz)_2Cl_2 \cdot H_2O$ ,<sup>62</sup> a room temperature magnetic moment of 4.7 B.M. was reported. Whilst in the present study for  $Fe(pyz)_2Cl_2$ , a considerably higher value of 5.20 B.M. is found at room temperature. The bromide<sup>62</sup> was found to have a room temperature moment of 4.4 B.M. which does not compare well with the value of 5.3 B.M. obtained in this study. Ferraro *et al.*<sup>62</sup> surmised that the low magnetic moment value was a result of magnetic exchange interactions, but from the more extensive data set obtained here this appears unlikely. The reason for the large discrepancy for the room temperature magnetic moment of  $Fe(pyz)_2Br_2$  is not fully understood, but it appears that the Gouy measurements of Ferraro *et al.*<sup>62</sup> were not corrected for any packing errors. On the

other hand, in the present study, packing errors were found to be no more than 5%, a possible source of error too small to account for the disagreement.

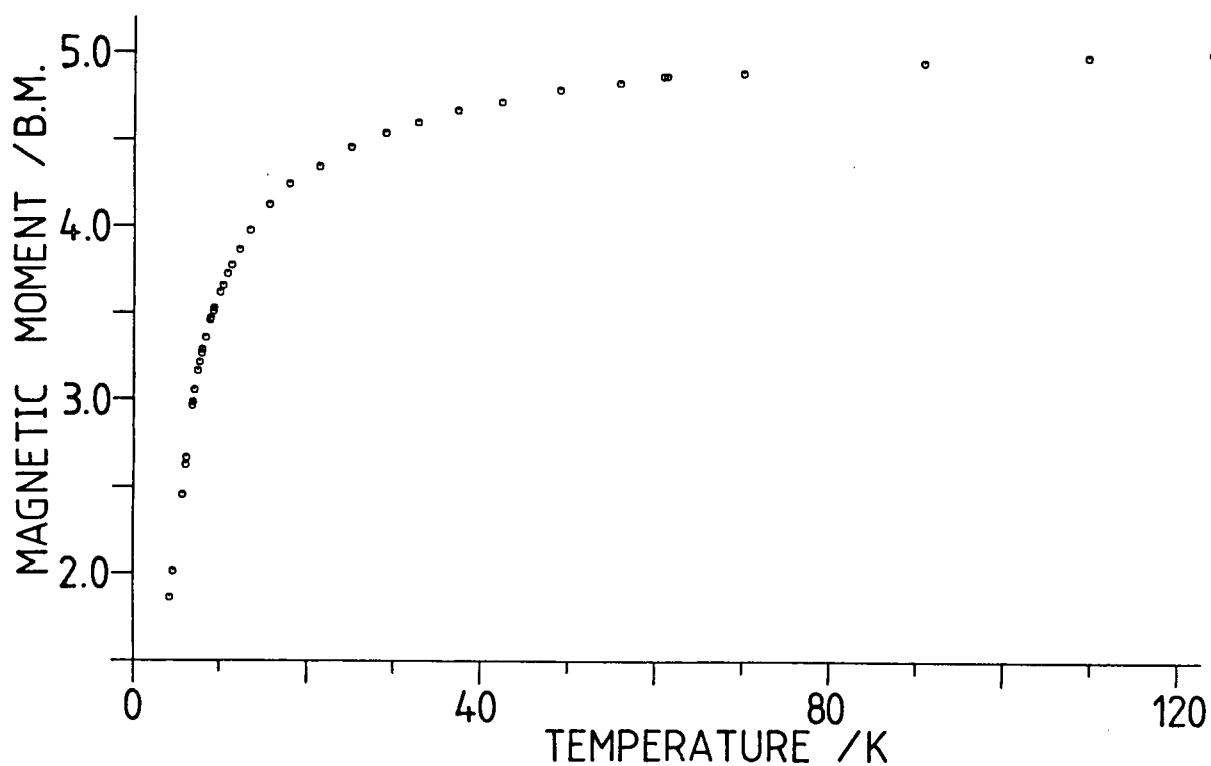
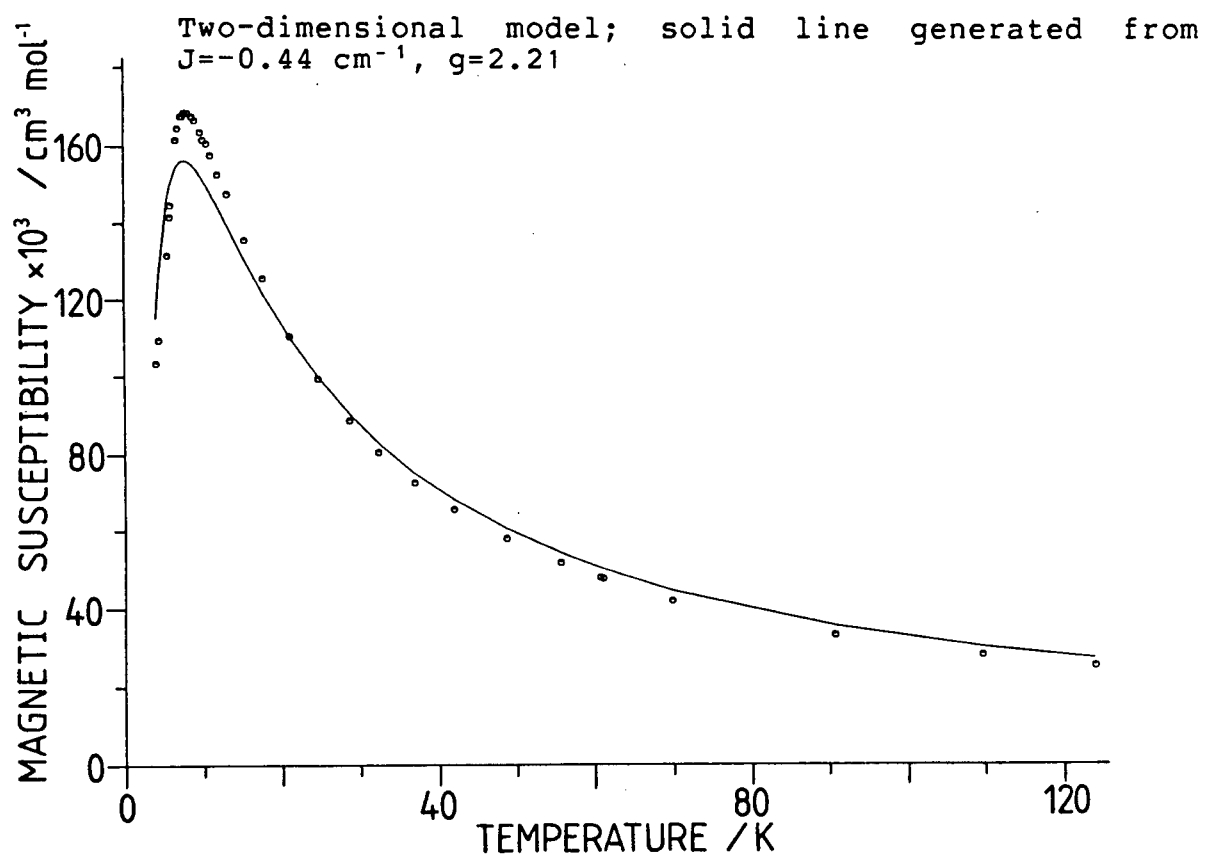
The temperature dependence of the magnetic moments for the bis(pyrazine)iron(II) halides may be compared with data obtained by other researchers for the tetrakis(pyridine) complexes, investigated over the temperature range 20-300 K.<sup>67</sup> The results show a similar temperature dependence for both groups of compounds; i.e., for the  $\text{Fe}(\text{py})_4\text{X}_2$  compounds, the magnetic moment remains fairly constant from room temperature down to 60 K. Below this temperature, a slight decrease in magnetic moment is observed. Compared to the magnetic properties of the bis(pyrazine) and tetrakis(pyridine)iron(II) sulfonate derivatives, much smaller differences are found for the analogous halide complexes. The implication is that magnetic exchange interactions, if present at all, are of an extremely weak nature in the bis(pyrazine)iron(II) halide complexes. A similar conclusion was reached for the cobalt(II)<sup>58</sup> and nickel(II)<sup>37</sup> pyrazine halide derivatives.

The results of the magnetic susceptibility measurements for  $\text{Fe}(\text{pyz})_2(\text{ClO}_4)_2$  and  $\text{Fe}(\text{pyz})_4(\text{AsF}_6)_2 \cdot 2\text{H}_2\text{O}$  (Appendix IX, Part A) also indicate a lack of strong magnetic exchange effects. Both complexes exhibit a magnetic moment which decreases with decreasing temperature. No maximum is observed in the susceptibility data; thus, magnetic exchange interactions in both compounds are, at most, weak. This may be expected for  $\text{Fe}(\text{pyz})_4(\text{AsF}_6)_2 \cdot 2\text{H}_2\text{O}$  as spectroscopic evidence indicates



monodentate pyrazine ligands. Magnetic exchange interactions might be expected in the perchlorate complex; spectroscopic evidence suggests a structure which is similar to that of the copper analogue<sup>43</sup> and, if this is the case, then magnetic exchange may be expected through the bridging pyrazine groups. If exchange interactions are present in  $\text{Fe}(\text{pyz})_2(\text{ClO}_4)_2$ , it is clear that they are substantially weaker than in the copper derivative.

These results indicate the lack of any substantial magnetic interactions through pyrazine in a number of  $\text{Fe}(\text{pyz})_2\text{X}_2$  complexes. On the other hand, this clearly does not apply generally to pyrazine-bridged iron(II) complexes, as illustrated by the magnetic moment data for  $\text{Fe}(\text{pyz})_2(\text{NCS})_2$ . The results of the magnetic measurements for  $\text{Fe}(\text{pyz})_2(\text{NCS})_2$  are given in Appendix IX, Part A and a plot of magnetic moment versus temperature is shown in Fig. 3.26. The magnetic moment shows a large temperature dependence, falling monotonically from a value of 5.2 B.M. at room temperature, to 4.8 B.M. at 50 K, and then decreasing more rapidly to 1.87 B.M. at 4.2 K. This behaviour is almost certainly due to the presence of antiferromagnetic interactions, a fact more clearly revealed by a maximum in the magnetic susceptibility plot at approximately 8.0 K (Fig. 3.27).

Fig. 3.26 Magnetic Moment vs Temperature for  $\text{Fe}(\text{pyz})_2(\text{NCS})_2$ Fig. 3.27 Magnetic Susceptibility vs Temperature for  $\text{Fe}(\text{pyz})_2(\text{NCS})_2$ 

Magnetic susceptibility data in the temperature range 80-300 K have been reported previously<sup>64</sup> for this complex. The agreement between the reported data and those obtained in the present study is poor. Magnetic susceptibility data reported here were recorded over the temperature range 4.2-300 K on two separate occasions using two independently prepared samples of  $\text{Fe}(\text{pyz})_2(\text{NCS})_2$ . The agreement between each of the data sets was excellent. The reason for poor agreement between the data obtained here and those obtained previously is not understood; however, in the earlier study,<sup>64</sup> neither the method of preparation nor any additional spectroscopic data were reported. This lack of information makes a comparison with the complex prepared in this study impossible, which is unfortunate. It appears likely that the two complexes, as well as possessing different magnetic properties, probably have distinctive spectroscopic properties also.

The magnetic properties, reported here, are quite different from those of the analogous tetrakis(pyridine) complex.<sup>152</sup> For  $\text{Fe}(\text{py})_4(\text{NCS})_2$ ,  $\mu_{\text{eff}}$  shows only a slight temperature dependence; however, magnetic measurements on this compound have been limited to temperatures above 90 K. A comparison suggests that the presence of bridging pyrazine ligands results in the distinctive magnetic properties of  $\text{Fe}(\text{pyz})_2(\text{NCS})_2$ . Several other thiocyanate complexes of iron(II), also exhibit unusual magnetic phenomena:  $\text{Fe}(\text{py})_2(\text{NCS})_2$ <sup>71-73</sup> undergoes a metamagnetic transition at approximately 6 K to a one-dimensional ferromagnetically ordered species and the magnetic

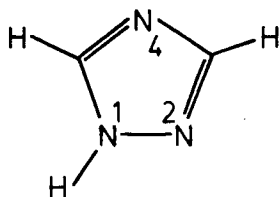
susceptibility plot of  $\text{Fe}(\text{bpy})(\text{NCS})_2$ <sup>153, 154</sup> (where bpy is 2,2'-bipyridine) shows a maximum at 18 K. It is proposed that the magnetic exchange interactions in these two cases take place through the bridging thiocyanate network. For  $\text{Fe}(\text{pyz})_2(\text{NCS})_2$ , however, spectroscopic evidence, in particular infrared data (Section 3.3.2.2), suggests strongly terminal unidentate anions and a bridging pyrazine network resulting in a two-dimensional lattice. If  $\text{Fe}(\text{pyz})_2(\text{NCS})_2$  exists in this structural form, it is reasonable to assume that the bridging pyrazine groups are responsible for the observed magnetic effects rather than superexchange through the anion.

As suggested by the proposal of a two dimensional structure, the magnetic susceptibility data were analysed in terms of the Lines' model (as described in Section 3.3.4.2). The best fit was obtained by using the parameters:  $J = -0.44 \text{ cm}^{-1}$  and  $g = 2.21$ , ( $F = 0.0221$ ). This fit is represented by the solid line in Fig 3.27. The calculated and experimental values do not correspond very closely in the region of the susceptibility maximum and the parameters obtained from the fit are, at best, semi-quantitative and should be viewed with caution. This may be attributed to inadequacies in the model for high-spin iron(II) complexes. The model describes the nearest-neighbour interactions between iron centres in the isotropic Heisenberg limit and it is usually not possible to represent the magnetic properties of iron(II) compounds accurately by either the pure isotropic or the anisotropic Ising model. There has been no solution developed for a two-dimensional Ising model applicable

to spin  $S=2$ . As well as neglecting zero-field splitting effects, the model also ignores any extended three-dimensional interactions which are not negligible in  $\text{Fe}(\text{pyz})_2(\text{NCS})_2$ , especially at temperatures below 8 K, as indicated by the low-temperature Mössbauer data (Section 3.3.5.3).

Magneto-structural correlations previously reported for  $\text{Fe}(\text{trz})_2(\text{NCS})_2$  (where trz is 1,2,4-triazole, see Fig. 3.28) are relevant to these studies on  $\text{Fe}(\text{pyz})_2(\text{NCS})_2$ .

Fig. 3.28 1,2,4-Triazole



Powder diffraction studies<sup>155</sup> have shown the triazole complex to be isomorphous with  $\text{Co}(\text{trz})_2(\text{NCS})_2$ <sup>156</sup> which exists as a two-dimensional sheet-like polymer, formed by the triazole ligand using nitrogen atoms N(2) and N(4) to bridge adjacent metal centres. The thiocyanate groups are N-bonded in axial positions to complete the  $\text{MN}_6$  chromophore. A similar structure is proposed for  $\text{Fe}(\text{pyz})_2(\text{NCS})_2$ . For the triazole compound, powder susceptibility data<sup>155</sup> reveal a maximum at a temperature of 8.8 K while single-crystal measurements<sup>157</sup> reveal a maximum in the susceptibility at 12.2 K. In the present study, the

magnetic susceptibility data for the pyrazine-bridged species show a maximum at a temperature of approximately 8.0 K. The similarity in these two sets of magnetic data indicates that pyrazine and 1,2,4-triazole propagate magnetic exchange effects to about the same degree in both complexes.

It is useful to summarise the results for the bis(pyrazine) halide and thiocyanate complexes. The magnetic properties of the bis(pyrazine)iron(II) halide complexes are similar to those of the analogous tetrakis(pyridine) derivatives. It is concluded that in complexes of this type pyrazine is a poor ligand for propagating magnetic exchange interactions, however, in  $\text{Fe}(\text{pyz})_2(\text{NCS})_2$ , the neutral ligand is shown to be effective in propagating magnetic interactions. As a result, the magnetic properties of  $\text{Fe}(\text{pyz})_2(\text{NCS})_2$  are substantially different from those of the monomeric  $\text{Fe}(\text{py})_4(\text{NCS})_2$  compound. From these results, it appears that the nature of the anionic ligand (for example,  $\sigma$ - and  $\pi$ -donor properties) may play a role in influencing the strength of the superexchange interaction through the neutral ligand. Changes in pyrazine ligand orientation and interlayer separation also have an effect upon the magnetic exchange interactions and X-ray structural results are necessary before these effects can be investigated. It would be worthwhile to investigate further magneto-structural correlations in  $\text{M}(\text{pyz})_2(\text{NCS})_2$  compounds by choosing M to be either Cu or Mn. In the present study, the cyanate derivative  $\text{Fe}(\text{pyz})_2(\text{NCO})_2$  was not isolated. Further attempts should be made to isolate this complex as its magnetic properties may also

provide for an interesting comparison with the results reported in the present study.

### 3.3.5 Mössbauer Spectroscopy

Two parameters routinely measured in a Mössbauer experiment are the isomer shift,  $\delta$ , and the quadrupole splitting,  $\Delta E_q$ . Before the Mössbauer spectra of the complexes prepared in the present study are discussed, a brief summary of the interactions responsible for isomer shift and quadrupole splitting and their chemical interpretation is worthwhile.<sup>158</sup>

The isomer shift arises from the electrostatic interaction between charge density at the nucleus and those electrons which have a finite probability of being located in the region of the nucleus, i.e., the s-electrons. During a nuclear  $\gamma$ -transition the effective nuclear size usually changes, thereby slightly altering the nucleus-electron interaction energy. Assuming spherical electron distribution, this interaction does not lead to a splitting of nuclear energy levels but results in a shift in energy which, in general, is different for the source and absorber. It is this difference in relative energies between source and absorber which is the isomer shift (Fig. 3.29). An expression which relates the isomer shift to nuclear and electronic factors is:

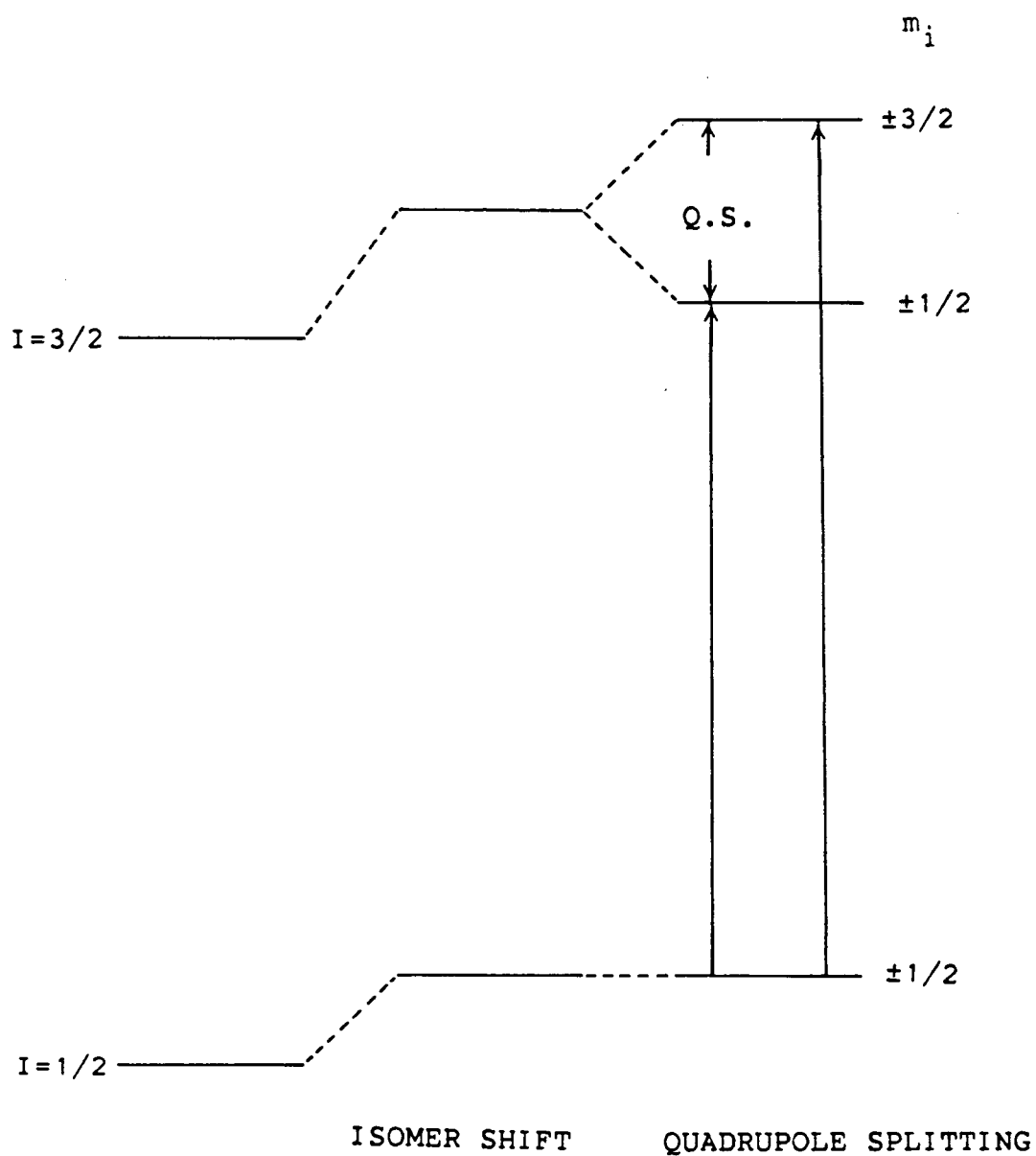
$$\delta = \frac{4}{5} \pi Z e^2 r^2 (\delta r / r [ |\psi_s(0)_A|^2 - |\psi_s(0)_B|^2 ]) \dots \text{Eqn. 3.10}$$

where  $Z$  is the atomic number,  $e$  is the positive elementary charge,  $r$  is the mean nuclear radius,  $\delta r = r_e - r_g$ , (the difference in nuclear radii of the excited and ground states respectively) and  $|\psi_s(0)_A|^2$  and  $|\psi_s(0)_B|^2$  are the s-electron densities at the



nucleus for source and absorber respectively.

Fig. 3.29 Isomer Shift and Quadrupole Splitting



The isomer shift is dependent upon two factors: a nuclear factor which is constant for any given nucleus and a factor which arises from the s-electron density at the nucleus. If  $|\psi_s(0)_A|^2$  is kept constant by using the same source, then the isomer shift will be proportional to the s-electron density at the absorber nucleus. In the case of  $^{57}\text{Fe}$ , the nucleus expands as it emits a  $\gamma$ -ray in going from the excited to ground state and hence,  $\delta r/r$  is negative, and therefore, an increase in s-electron density leads to a decrease in isomer shift. Since p- and d-electrons can exert a screening effect on the s-electrons, changes in p- and d-orbital occupancy influence the isomer shift by effectively altering the s-electron density at the nucleus. This screening effect is clearly seen from the range of  $\delta$  values for high-spin iron compounds. Iron(III) compounds,  $d^5$ , have isomer shifts in the range 0.2-0.6 mm s $^{-1}$ , while iron(II) compounds,  $d^6$ , have isomer shifts in the range 0.7-1.5 mm s $^{-1}$  (quoted relative to iron metal). The presence of an extra d-electron in iron(II) complexes screens the s-electron density and thus the isomer shift increases.

The preceding discussion on the isomer shift applies to systems with spherical or cubic electron-density distributions. The degeneracy of the nuclear energy levels for nuclei with  $I > 1/2$  is removed by a non-cubic electron or ligand distribution.

The appropriate nuclear quadrupole coupling Hamiltonian is given by:

$$\mathcal{H} = \frac{e^2qQ}{4I(2I-1)} [3I_z^2 - I(I+1) + (\eta/2)(I_+^2 + I_-^2)] \dots \text{Eqn. 3.11}$$

where  $eQ$  is  $V_{zz}$ , the  $z$ -component of the electric field gradient (E.F.G.),  $\eta$  is the asymmetry parameter,  $I_z$  is the nuclear spin operator, and  $I_+$  and  $I_-$  are shift operators.  $^{57}\text{Fe}$  has a ground state with  $I=1/2$  and hence zero quadrupole moment and a first excited state with  $I=3/2$ . In the presence of an electric field gradient the  $I=3/2$  level is split into two substates  $m_i=\pm 3/2$  and  $\pm 1/2$ . The separation of the two substates is termed the quadrupole splitting,  $\Delta E_q$  and has units of  $\text{mm s}^{-1}$ , (Fig. 3.29) and in most cases the Mössbauer spectrum consists of two lines of equal intensities whose separation is  $|\Delta E_q|$ .

From a symmetric two-line Mössbauer spectrum of a randomly oriented polycrystalline absorber only the magnitude of  $\Delta E_q$  can be determined. No information concerning either the sign of  $V_{zz}$  or the value of  $\eta$  is gained. The magnitude of the quadrupole splitting is found to be dependent upon the oxidation state and spin multiplicity of the iron centre. For example, the high-spin iron(III) cation has a spherically symmetric  $d^5$  electronic configuration and the electric field gradient (E.F.G.) can only arise from an asymmetrical arrangement of the ligands and the value of  $\Delta E_q$  is expected to be small and temperature independent. For high-spin iron(II) the situation is somewhat more complicated. In an octahedral ligand field the

sixth d-electron is equally distributed within the  $t_{2g}$  set and in this case there is no net E.F.G. In cases of lower symmetry about the metal centre, such as a trigonal or tetragonal, the degeneracy of the  $t_{2g}$  set is removed and a non-zero E.F.G. is produced. Thermal population of the low-lying excited states then causes a variation in the electron configuration with temperature and since the 3d-orbitals have differing contributions to the E.F.G. a temperature-dependent  $\Delta E_q$  is expected.

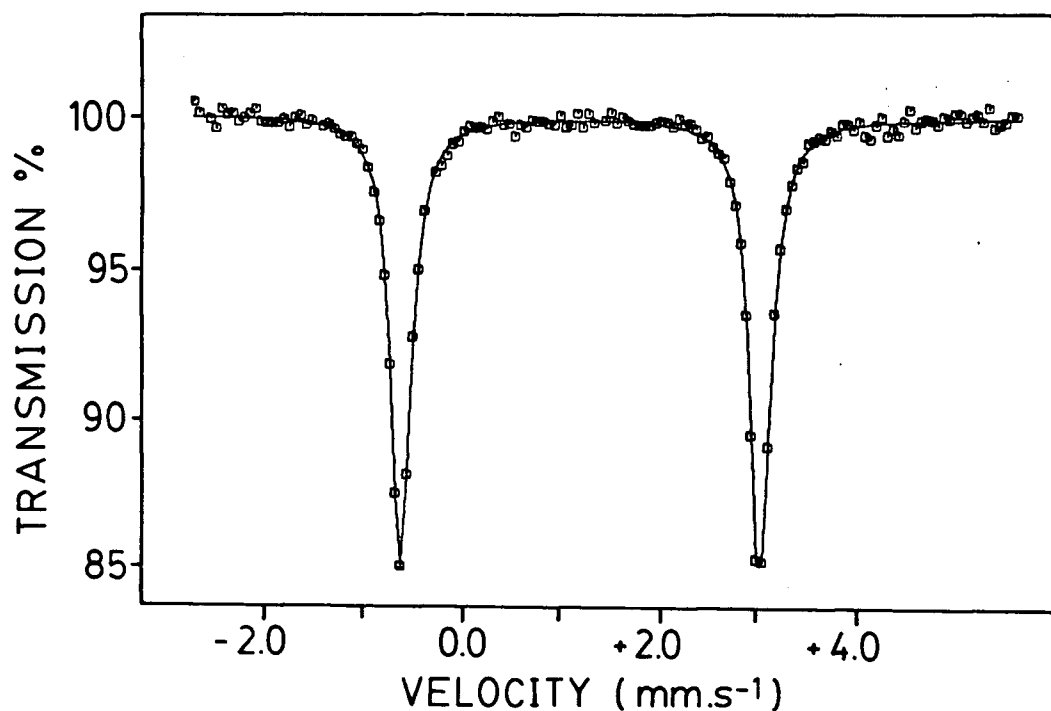
The Mössbauer spectral results for the complexes containing an  $FeN_4X_2$  chromophore are discussed under two headings. Firstly, the results for complexes containing an  $FeN_4O_2$  chromophore are considered in Section 3.3.5.1, i.e., the tetrakis(pyridine)-, tetrakis(pyrazine)- and bis(pyrazine)iron(II) sulfonate derivatives. Secondly, the results for the bis(pyrazine)iron(II) compounds, i.e.,  $Fe(pyz)_2X_2$ , where  $X^-$  is  $Cl^-$ ,  $Br^-$ ,  $I^-$ ,  $NCS^-$  and  $ClO_4^-$ , are reported in Section 3.3.5.2. Low-temperature (1.8-10 K) Mössbauer spectra for  $Fe(pyz)_2(NCS)_2$  are discussed in Section 3.3.5.3.

#### 3.3.5.1 Mössbauer spectral parameters for complexes containing an $FeN_4O_2$ chromophore

The Mössbauer spectral parameters are given in Appendix X, Part A. The spectra consist of a symmetrical quadrupole-split doublet as expected for tetragonally distorted pseudooctahedral high-spin iron(II) compounds. A typical spectrum, that of

$\text{Fe}(\text{py})_4(\text{CH}_3\text{SO}_3)_2$ , is shown in Fig. 3.30.

Fig. 3.30 Mössbauer Spectrum of  $\text{Fe}(\text{py})_4(\text{CH}_3\text{SO}_3)_2$  at 78 K



For the tetrakis(pyridine)iron(II) sulfonate species, the room-temperature isomer shifts are virtually identical and approximately  $0.3 \text{ mm s}^{-1}$  lower than those of the corresponding anhydrous iron(II) sulfonates derivatives.<sup>24, 25</sup> The lower isomer shifts for the pyridine complexes are attributable to the more covalent nature of the Fe-N bond, which leads to a greater electron density at the iron nucleus than in the more "ionic"  $\text{Fe}(\text{RSO}_3)_2$  compounds with an  $\text{FeO}_6$  chromophore. Evidently, in the sulfonate complexes with an  $\text{FeN}_4\text{O}_2$  chromophore, differences in

anion basicity are not large enough to have an appreciable effect on the isomer shift. This result contrasts with that found for the corresponding halide complexes,  $\text{Fe}(\text{py})_4\text{X}_2$ , where the room temperature isomer shift decreases slightly from 1.06  $\text{mm s}^{-1}$  for the chloride, to 0.99  $\text{mm s}^{-1}$  for the iodide.<sup>67</sup>

The room-temperature isomer shift values for the two bis(pyrazine)iron(II) sulfonate complexes and for  $\text{Fe}(\text{2-mepyz})_4(\text{CH}_3\text{SO}_3)_2$  (Appendix X, Part A) are slightly higher than those of the corresponding tetrakis(pyridine) complexes. This suggests a greater degree of covalency in the pyridine complexes which is consistent with the relative base strengths of pyridine, pyrazine and 2-methylpyrazine. With the exception of the isomer shift for  $\text{Fe}(\text{py})_4(\text{CH}_3\text{SO}_3)_2$ , a slight temperature dependence of  $\delta$  is observed. This temperature dependence is attributable to a second-order Doppler effect and has no chemical significance. On the other hand, the temperature-independent isomer shift for  $\text{Fe}(\text{py})_4(\text{CH}_3\text{SO}_3)_2$  arises because the spectra were recorded with the source and absorber at the same temperature.

At all temperatures the quadrupole splitting values exceed 3  $\text{mm s}^{-1}$ . The magnitude of  $\Delta E_q$  provides some indication of the nature of the ground state in the complexes. For these octahedral iron(II) complexes the degeneracy of the  $^5\text{T}_{2g}$  ground state is removed by the presence of a tetragonally distorted ligand field (Fig. 3.13) and a non-zero electric field gradient is produced by the sixth d-electron occupying either the singly or doubly degenerate ground state ( $^5\text{B}_{2g}$  or  $^5\text{E}_g$ ). A

non-degenerate ground state is expected to produce an E.F.G. in proportion to  $+4/7\langle r^{-3} \rangle$ , twice the value and of opposite sign to that produced by a doubly degenerate ground state. For these complexes, the observation of a quadrupole splitting value substantially greater than  $2 \text{ mm s}^{-1}$  is diagnostic evidence for the presence of a non-degenerate ground state which corresponds to the  $d_{xy}$  orbital lying lowest in energy. This is precisely as required by the molecular geometries discussed in Section 3.3.3.1, which show, in the case of the tetrakis(pyridine)iron(II) sulfonate compounds, an axially compressed octahedron of approximately  $D_{4h}$  symmetry. With this combination of a non-degenerate ground state and a tetragonal compression of the  $\text{FeN}_4\text{O}_2$  chromophore, a positive value of  $V_{zz}$  is indicated and  $V_{zz}$  is presumably directed along the pseudo-tetragonal O-Fe-O axis.

Previous research has involved the evaluation of ligand-field parameters ( $\Delta$  and  $\lambda$ ) from the temperature dependence of the quadrupole splitting data.<sup>84</sup> Except for  $\text{Fe}(\text{py})_4(\text{CH}_3\text{SO}_3)_2$ , the data set obtained in the present study is too limited for such an analysis. For  $\text{Fe}(\text{py})_4(\text{CH}_3\text{SO}_3)_2$ , the temperature dependence of  $\Delta E_q$  was analysed using this model and the parameter values obtained are  $\Delta = 650 \text{ cm}^{-1}$  and  $\lambda = -80 \text{ cm}^{-1}$ . These values are quite similar to those obtained from the analysis of the magnetic moment data using the Figgis model, in spite of the theoretical limitations of the latter treatment (Section 3.3.4.2)

### 3.3.5.2 Mössbauer spectral parameters for bis(pyrazine)iron(II) halide and thiocyanate complexes and $\text{Fe}(\text{pyz})_4(\text{AsF}_6)_2 \cdot 2\text{H}_2\text{O}$

The Mössbauer spectral parameters are presented in Appendix X, Part B. At room and liquid nitrogen temperatures the complexes show symmetric, quadrupole split Mössbauer spectra with isomer shift and quadrupole splitting values consistent with their formulation as high-spin iron(II) compounds. The bis(pyrazine)iron(II) halide complexes exhibit no appreciable differences in isomer shifts. This is unexpected considering the different  $\sigma$ -donating abilities of the halide anions. For the tetrakis(pyridine)iron(II) halide species, small changes in isomer shift values do correlate with the differences in  $\sigma$ -donating abilities of the anionic ligands.<sup>67</sup> The presence of a halide anion dependence for the isomer shifts of the pyridine complexes where there is none for the pyrazine complexes indicates that in the former group of complexes the s-electron density at the iron nucleus increases with the  $\sigma$ -donating ability of the halide anion in the order  $\text{Cl}^- > \text{Br}^- > \text{I}^-$ ; whereas, in the latter group, s-electron density at the iron nucleus remains fairly constant in spite of the increased  $\sigma$ -donation from the halide anions. This observation may be related to the fact that pyrazine is a better  $\pi$ -acceptor ligand than pyridine. Thus,  $\sigma$ -electron density from the anion is transferred to the metal in the pyridine complexes and in the pyrazine complexes, it is transferred one stage further onto the neutral ligand. This seems to suggest a rather facile charge-transfer process in the pyrazine complexes, and is



consistent with the observation of charge-transfer bands in the visible region of the spectrum (Section 3.3.2.3).

At room temperature, the isomer shift value for  $\text{Fe}(\text{pyz})_2(\text{NCS})_2$  is very similar to that reported for  $\text{Fe}(\text{py})_4(\text{NCS})_2$ <sup>67</sup> which indicates that both compounds have similar s-electron densities as a result of their identical  $\text{FeN}_4\text{N}_2$  chromophores.

The quadrupole splittings for the bis(pyrazine) halide and thiocyanate complexes are greater than  $2 \text{ mm s}^{-1}$  which indicates a non-degenerate ground state.

#### 3.3.5.3 Low-temperature Mössbauer spectra of $\text{Fe}(\text{pyz})_2(\text{NCS})_2$

It may be recalled that the magnetic susceptibilities for  $\text{Fe}(\text{pyz})_2(\text{NCS})_2$  (Section 3.3.4.3) show a maximum at approximately 8.0 K, indicating the presence of short-range magnetic interactions. Mössbauer spectra were recorded in the temperature range 1.8-10K in order to ascertain the extent of any three-dimensional magnetic ordering. The spectra are illustrated in Fig. 3.31 and the results are presented in Table 3.7. (Note, the spectra were recorded and fitted by Dr. J.R. Sams)

Table 3.7 Low-Temperature Mössbauer Spectral Parameters for  
 $\text{Fe}(\text{pyz})_2(\text{NCS})_2$

TEMP K	$\delta$ mm s <sup>-1</sup>	$\Delta E_Q$ mm s <sup>-1</sup>	$\Gamma^1$ mm s <sup>-1</sup>	$H_{\text{int}}$ T	$\theta$ deg	$\eta$
1.8	1.14	2.68	0.18	27.7	41	0.07
4.2	1.14	2.70	0.18	27.1	40	0.07
5.7	1.13	2.72	0.18	26.9	41	0.06
6.7	1.14	2.70	0.21	25.2	40	0
8.0	1.13	2.76	0.20*	22.9	40*	0*
9.8	1.13	2.65	0.29	0	-	-

1).  $\Gamma$  values are quoted for halfwidth at halfheight

\* Constrained

At 9.8 K, the Mössbauer spectrum remains a single, symmetric quadrupole doublet, and the the isomer shift and quadrupole splitting values at this temperature are similar to those found at liquid nitrogen temperature. It is concluded that no phase change takes place over this temperature range, and that the ground state is effectively isolated. Between 9.8 and 8.0 K the lines of the quadrupole doublet broaden and split. The Neel temperature is estimated to be  $9.2 \pm 0.5$  K which is unexpected as this is at a higher temperature than the maximum in the susceptibility curve (8.0 K). An interpretation of this phenomenon would be somewhat tenuous at this stage, because in this temperature region difficulties were encountered with temperature control of the Mössbauer cryostat. Below 8.0 K, a fully-resolved magnetic hyperfine spectrum resulting from the presence of a magnetic-dipole interaction in addition to the electric quadrupole interaction is observed.

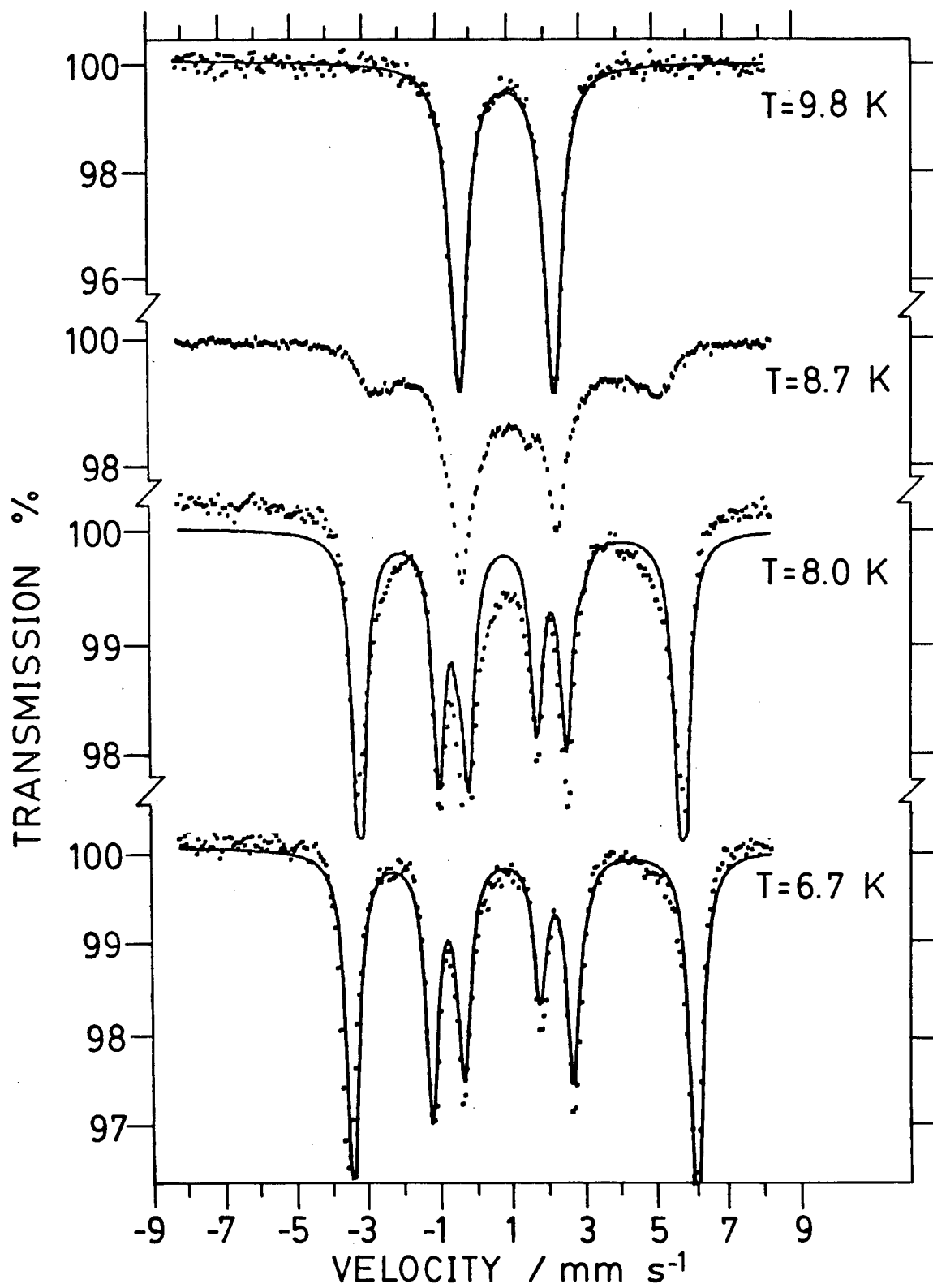
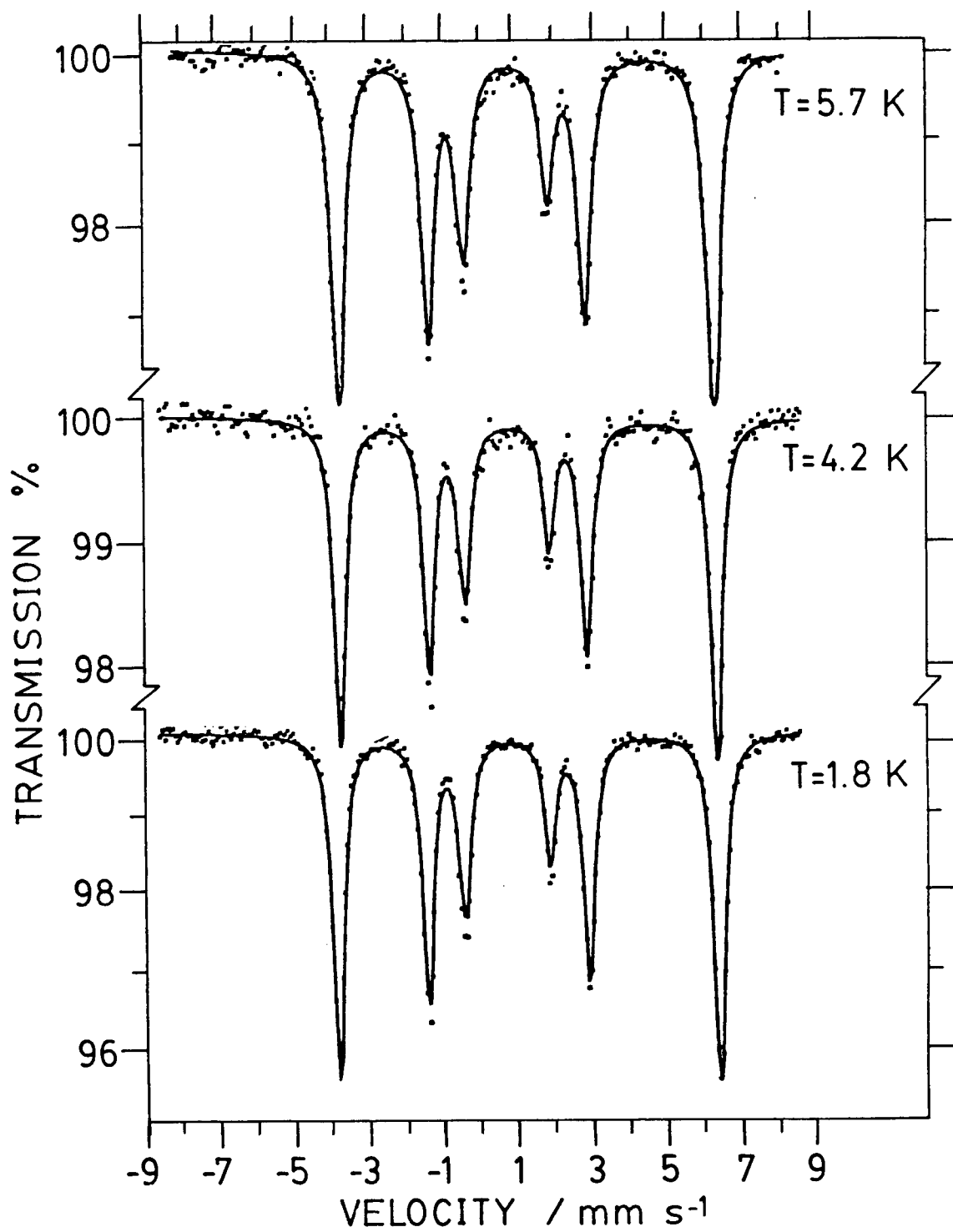
Fig. 3.31 Low-Temperature Mössbauer Spectrum of  $\text{Fe}(\text{pyz})_2(\text{NCS})_2$ 

Fig. 3.31 Continued

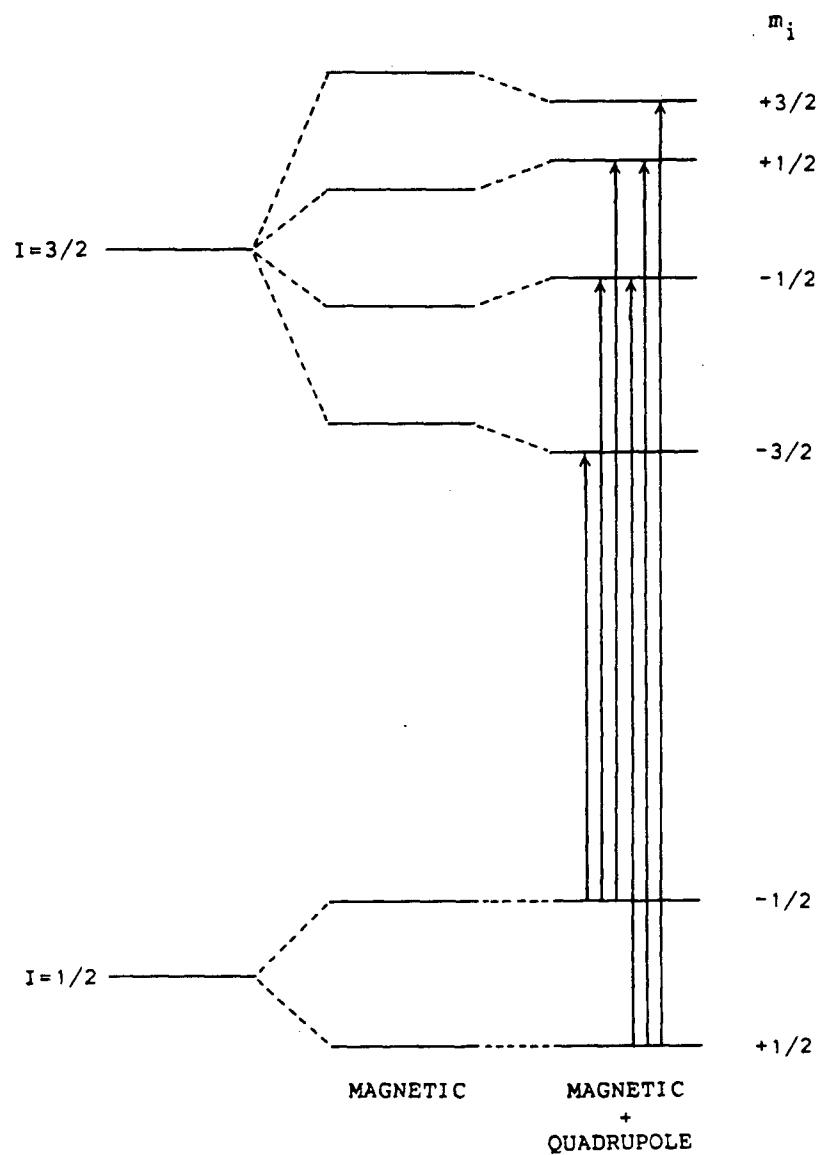


The origins of the quadrupole interaction have been previously described (Section 3.3.5) and the origin of the magnetic-dipole interaction may be thought to arise in the following manner. The  $^{57}\text{Fe}$  nucleus has a magnetic moment in the ground and excited state. These moments interact with a magnetic field at the nucleus to lift the degeneracy of the  $m_i$  states (Fig. 3.32) according to the Hamiltonian:

$$\mathcal{H} = -g_n \beta_n \mathbf{I} \cdot \mathbf{H} \dots \text{Eqn. 3.12}$$

where  $g_n$  is the nuclear gyromagnetic ratio and  $\beta_n$  is the nuclear magneton. The magnetic splitting produces  $2I+1$  levels for each state. Thus, the ground state ( $I=1/2$ ) is split into two levels ( $m_i = +1/2$  and  $-1/2$ ) and the excited state ( $I=3/2$ ) into four levels ( $m_i = +1/2, -1/2, +3/2$  and  $-3/2$ ). The selection rules restrict the allowed transitions to those for which  $\Delta m_i = 0, \pm 1$  so that a six-line spectrum results. For most paramagnetic complexes the electron spins which generate the internal magnetic field are subject to rapid electronic spin relaxation. The field is time-averaged to zero and consequently, no magnetic hyperfine spectra are observed.

Fig. 3.32 Combined Effects of Magnetic and Quadrupole Interactions

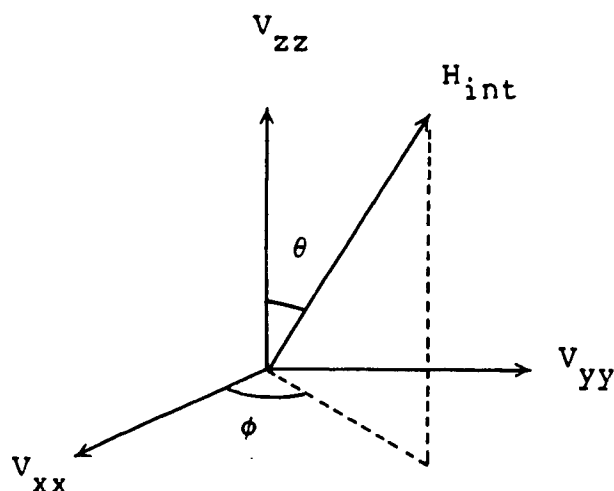


For materials which show magnetic ordering, the electronic spin-relaxation rate decreases and the iron nucleus experiences an internal magnetic field which, at temperatures below the ordering temperature, is not time-averaged to zero, resulting in a complex Mössbauer spectrum. In general, the magnetic-dipole interaction is represented by the Hamiltonian:

$$\mathcal{H} = -g\mu_n H_{\text{int}} [I_z \cos\theta + (I_x \cos\phi + I_y \sin\phi) \sin\theta] \dots \text{Eqn. 3.13}$$

For any given combination of magnetic-dipole (Eqn. 3.13) and electric-quadrupole (Eqn. 3.11) interactions a Mössbauer spectrum may be computed by constructing the energy level diagram (for example, Fig. 3.32) and calculating the transition energies and probabilities. From an analysis of a Mössbauer hyperfine spectrum the following parameters are obtained:  $H_{\text{int}}$  is the magnitude of the hyperfine field at the iron nucleus,  $\theta$  and  $\phi$  are the polar angles which specify the direction of  $H_{\text{int}}$  with respect to the E.F.G. axis system (Fig. 3.33),  $\eta$  is the asymmetry parameter, where

$$\eta = (V_{xx} - V_{yy}) / V_{zz} \dots \text{Eqn. 3.14}$$

Fig. 3.33 Relation Between  $H_{int}$  and the E.F.G. Axis System

The magnitude and sign of the quadrupole splitting,  $e^2qQ$ , and hence the sign of  $V_{zz}$  are also obtained from such an analysis. By using this type of approach and a program based upon the results of Kundig,<sup>159</sup> Mössbauer spectra were computed and compared with the spectra of  $\text{Fe}(\text{pyz})_2(\text{NCS})_2$ . The solid lines in Fig. 3.31 were generated by a least-squares fitting procedure using the parameters listed in Table 3.7. From  $T_N$  down to approximately 7 K, the spectral lines are broadened due to spin-relaxation effects, with an electronic-spin relaxation time comparable to the Mössbauer time scale ( $10^{-7}$  s). Below 7 K, the spectra are well fitted using the parameters given in Table 3.7. These values provide substantial information in support of the proposed structure of  $\text{Fe}(\text{pyz})_2(\text{NCS})_2$ . The asymmetry parameter,  $\eta$ , is found to be very small which implies the electric field gradient to have effectively axial symmetry. Because of this,



all orientations of the hyperfine field,  $H_{int}$ , relative to the xy plane (of the E.F.G. axis system) are equally probable and hence, the angle  $\phi$  (Fig. 3.33) is indeterminate. The positive value of  $e^2qQ$  indicates a tetragonal compression of the  $FeN_4N_2'$  polyhedron, with the Fe-N(anion) distance somewhat shorter than the Fe-N(pyz) length and a non-degenerate ground state ( $d_{xy}$  orbital at lower energy than  $d_{xz}$  and  $d_{xy}$ ). Axial symmetry is also suggested by the infrared spectral data (Section 3.3.2.2) which indicate a square planar array of bridged  $Fe(pyz)_2^{2+}$  units and monodentate  $NCS^-$  anions coordinated trans to each other in axial sites. The polar angle,  $\theta$  was found to be  $40^\circ$ , and assuming that the principal axis of the E.F.G. tensor ( $V_{zz}$ ) is coincident with the N(anion)-Fe-N(anion) axis, then the easy axis of magnetisation is tipped towards the xy-plane. This indicates that the magnetic exchange pathway through pyrazine is not sufficiently strong to align the spins in the xy-plane, as a value of  $\theta=90^\circ$  would then be expected.

The internal hyperfine field at the iron nucleus,  $H_{int}$ , as a function of temperature is given in Table 3.7. It can be seen that the field saturates rapidly below 9.8 K and then slowly approaches a maximum value of approximately 28 T at 1.8 K. The contributions to  $H_{int}$  are given by:

$$H_{int} = H_F + H_l + H_{dip} \dots \text{Eqn. 3.15}$$

For high-spin iron(II) complexes, the contribution to  $H_{int}$  from the Fermi contact interaction,  $H_F$ , is approximately 44 T.<sup>158</sup> The

opposing orbital contribution to  $H_{int}$  is expected to be relatively small in view of the near spin-only moment at high temperatures and the non-degenerate ground state. On the other hand, the dipolar contribution,  $H_{dip}$  is probably not negligible as  $|H_{dip}| = \beta V_{zz}^{158}$  and is usually of opposite sign to  $H_F$ . Hence, for  $Fe(pyraz)_2(NCS)_2$  the value of 25 T is not unreasonable for the expected Fermi contribution, reduced somewhat by both opposing dipolar and to a lesser extent orbital contributions.

In summary, the analysis of the low-temperature Mössbauer spectra of  $Fe(pyraz)_2(NCS)_2$  is consistent with the proposed two-dimensional layer structure and weak magnetic exchange interactions propagating through the bridging pyrazine ligands.

### 3.3.6 Thermal Studies

The range of thermal stabilities of these tetrakis(pyridine) and bis(pyrazine) complexes was established by using differential scanning calorimetry (D.S.C.). A comparison of the relative thermal stabilities for the two groups of complexes was interesting in view of their different structures (monomeric or polymeric). D.S.C. results were also informative in regard to the possibility of obtaining complexes with lower ligand to iron ratios by utilising thermolysis as a preparative technique. Gravimetric measurements made during the course of a D.S.C. experiment were particularly useful in this respect.

The thermolysis results for the tetrakis(pyridine)iron(II) and copper(II) sulfonate derivatives are given in Table 3.8. The D.S.C. curves for  $\text{Fe}(\text{py})_4(\text{CF}_3\text{SO}_3)_2$  (Fig. 3.34a) and  $\text{Fe}(\text{py})_4(\text{p-CH}_3\text{C}_6\text{H}_4\text{SO}_3)_2$  exhibit two endothermic events in the temperature range of 400-520 K. Exothermic decomposition is noted above 800 K. The D.S.C. curve for the methanesulfonate derivative (Fig. 3.34b) shows an endothermic event at 414 K; however, above this temperature several endothermic peaks are recorded, indicating a more complex thermolysis for  $\text{Fe}(\text{py})_4(\text{CH}_3\text{SO}_3)_2$  than for either the triflate or p-tosylate derivative. The weight loss data obtained after the occurrence of several of these thermal events are given in Table 3.8.

Table 3.8 Thermal parameters<sup>1</sup> for some Tetrakis(pyridine) and Bis(pyrazine) Complexes

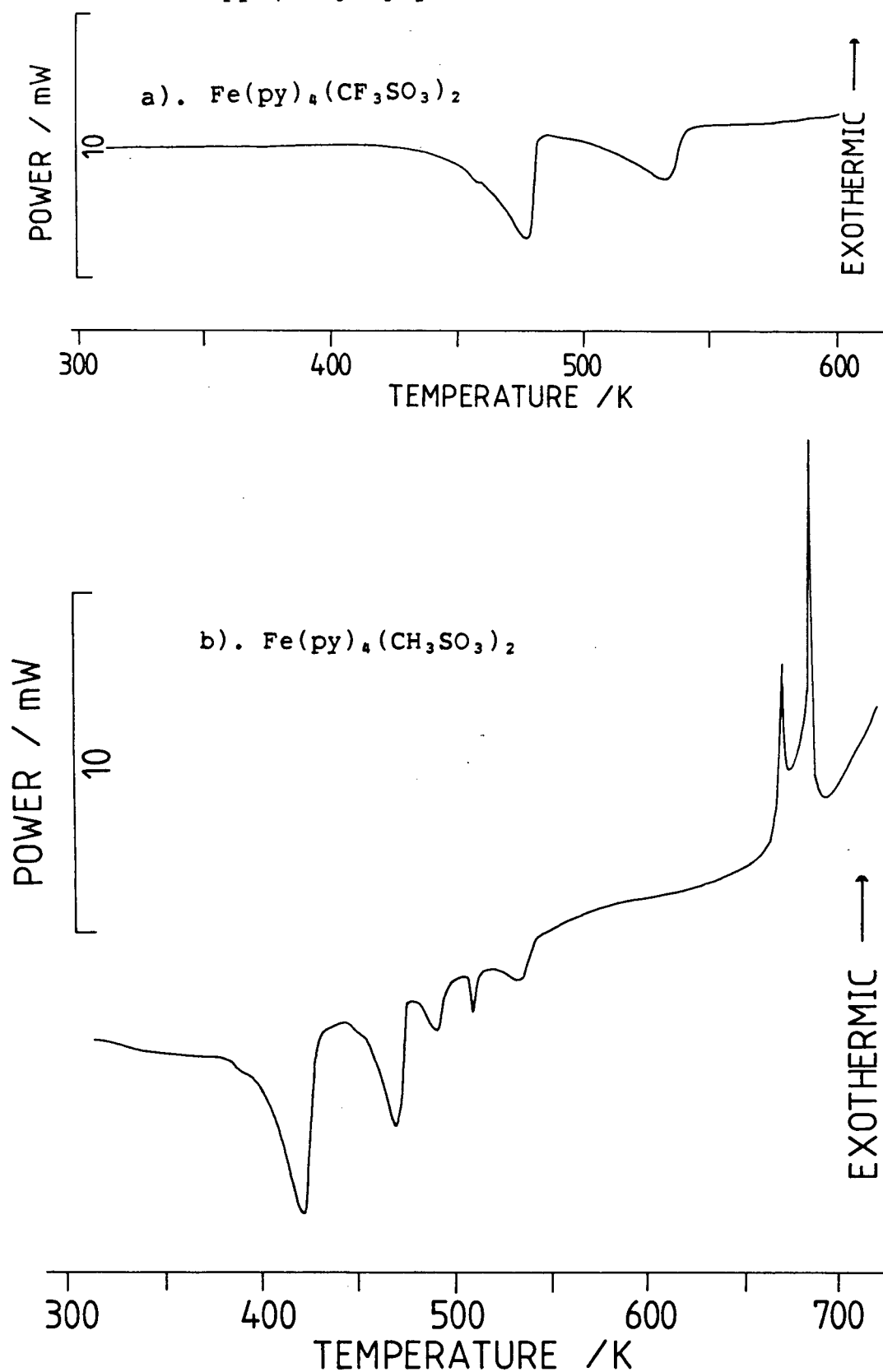
Compound	Peak Temp. K	$\Delta H$ kJ mol <sup>-1</sup>	Weight loss (%)	
			Calc. <sup>2</sup>	Obs.
$\text{Fe}(\text{py})_4(\text{CF}_3\text{SO}_3)_2$	465	95	24	26
	513	60	47	44
$\text{Fe}(\text{py})_4(\text{CH}_3\text{SO}_3)_2$	414	91	28	28
	3		56	55
$\text{Fe}(\text{py})_4(\text{p-CH}_3\text{C}_6\text{H}_4\text{SO}_3)_2$	419	94	22	24
	458	109	44	42
$\text{Cu}(\text{py})_4(\text{CF}_3\text{SO}_3)_2$	509	-	-	-
	520	-	-	-
$\text{Cu}(\text{py})_4(\text{CH}_3\text{SO}_3)_2$	453	91	-	-
	469	51	-	-
$\text{Fe}(\text{pyz})_2(\text{CF}_3\text{SO}_3)_2 \cdot \text{CH}_3\text{OH}$	415	104	21	21
	603	60	35	37
$\text{Fe}(\text{pyz})_2(\text{CH}_3\text{SO}_3)_2$	503	84	20	22
	583	40	39	42
$\text{Cu}(\text{pyz})_2(\text{CH}_3\text{SO}_3)_2$	461	62	19	19
	570	61	39	39

1). Estimated error limits: Peak Temp.  $\pm 5$  K,  $\Delta H$   $\pm 5\%$ , weight loss  $\pm 5\%$ .

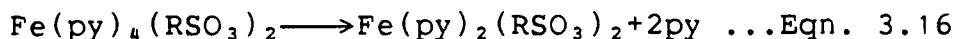
2). For explanation of calculated values see text

3). For discussion of thermolysis above 450 K see text

Fig. 3.34 D.S.C Curves for  $\text{Fe}(\text{py})_4(\text{CF}_3\text{SO}_3)_2$  and  $\text{Fe}(\text{py})_4(\text{CH}_3\text{SO}_3)_2$



For the  $\text{Fe}(\text{py})_4(\text{RSO}_3)_2$  compounds, after completion of the first thermal event, the weight loss data (Table 3.8) indicate the loss of two moles of pyridine per mole of complex, suggesting the formation of bis(pyridine) complexes according to:



where R is  $\text{CF}_3$ ,  $\text{CH}_3$  or  $p\text{-CH}_3\text{C}_6\text{H}_4$ .

For triflate and p-tosylate derivatives, the weight loss data after the second thermal event indicate the removal of the two remaining pyridine groups in one step, to form the anhydrous sulfonate species:



where R is  $\text{CF}_3$  or  $p\text{-CH}_3\text{C}_6\text{H}_4$ .

As noted above, thermolysis of the methanesulfonate complex (Fig. 3.34b) allows the observation of several additional endothermic events. A more complex thermolysis pattern than that represented by Eqn. 3.17 is indicated. After the final endothermic event, a weight loss of 55% suggests total removal of pyridine. These observations indicate that the final two moles of pyridine are removed in several steps. This is not without precedent; for example,  $\text{Fe}(\text{py})_4\text{Cl}_2$  undergoes thermal decomposition through several intermediates:  $\text{Fe}(\text{py})_2\text{Cl}_2$ ,  $\text{Fe}(\text{py})\text{Cl}_2$ ,  $\text{Fe}(\text{py})_{2/3}\text{Cl}_2$ , before  $\text{FeCl}_2$  is produced.<sup>160</sup>

For these  $\text{Fe}(\text{py})_4(\text{RSO}_3)_2$  complexes,  $\text{Fe}(\text{RSO}_3)_2$  was indicated

to be the final product of thermolysis (before exothermic decomposition) not only by gravimetric data but also by infrared spectroscopy. The infrared spectra of the thermolysis products were identical to the infrared spectra of the  $\text{Fe}(\text{RSO}_3)_2$  compounds synthesised by published methods.<sup>25</sup>

The temperature at which each thermal event occurs is measured during a D.S.C. experiment. The values indicate the thermal stability of the complexes with respect to loss of ligand. For the tetrakis(pyridine)iron(II) complexes, the temperature at which the first thermal event occurs shows only a small anion dependence (Table 3.8), with very similar thermal stability found for all three complexes.

Another parameter measured during the course of a D.S.C. experiment is the enthalpy change,  $\Delta H$ , associated with each event. The magnitude of  $\Delta H$  is likely to be dependent on a number of contributing factors.

- (i) the Fe-N bond strength as pyridine is removed
- (ii) the Fe-O bond strength as the anion changes its mode of coordination during thermolysis.
- (iii) the energy change involved when the monomeric tetrakis(pyridine) complexes convert to polymeric anhydrous sulfonates.

It is noted for the first endothermic event that  $\Delta H$  is independent of anion (Table 3.8). This observation, consistent with the gravimetric data, suggests the same process is taking place in all three compounds; i.e., the removal of the first two pyridine groups, with a similar concomitant change in the

coordinating behaviour of the anionic groups. A considerable dependence upon the sulfonate anion is noted for the enthalpy values associated with the second thermal event in the triflate and p-tosylate derivatives. This is somewhat surprising, as gravimetric results show that this event is a result of the removal of the second two pyridine moieties in both cases.

Previous researchers<sup>6,7</sup> have employed thermolysis as a preparative technique for the conversion of some tetrakis(pyridine)iron(II) complexes to their bis(pyridine) derivatives. The results obtained in this study indicate that the isolation of the bis(pyridine)iron(II) sulfonate complexes should be possible by a thermolysis route. Indeed, the  $\text{Fe}(\text{py})_2(\text{CF}_3\text{SO}_3)_2$  was obtained by thermolysis in vacuo (Section 4.2.1.1).

Thermolysis data for  $\text{Cu}(\text{py})_4(\text{CF}_3\text{SO}_3)_2$  and  $\text{Cu}(\text{py})_4(\text{CH}_3\text{SO}_3)_2$  are listed in Table 3.8 and their D.S.C. curves are shown in Fig. 3.35. The D.S.C experiments for both copper compounds exhibit two endothermic events which are separated by temperatures of 11 and 16 K for the triflate and methanesulfonate complexes respectively.

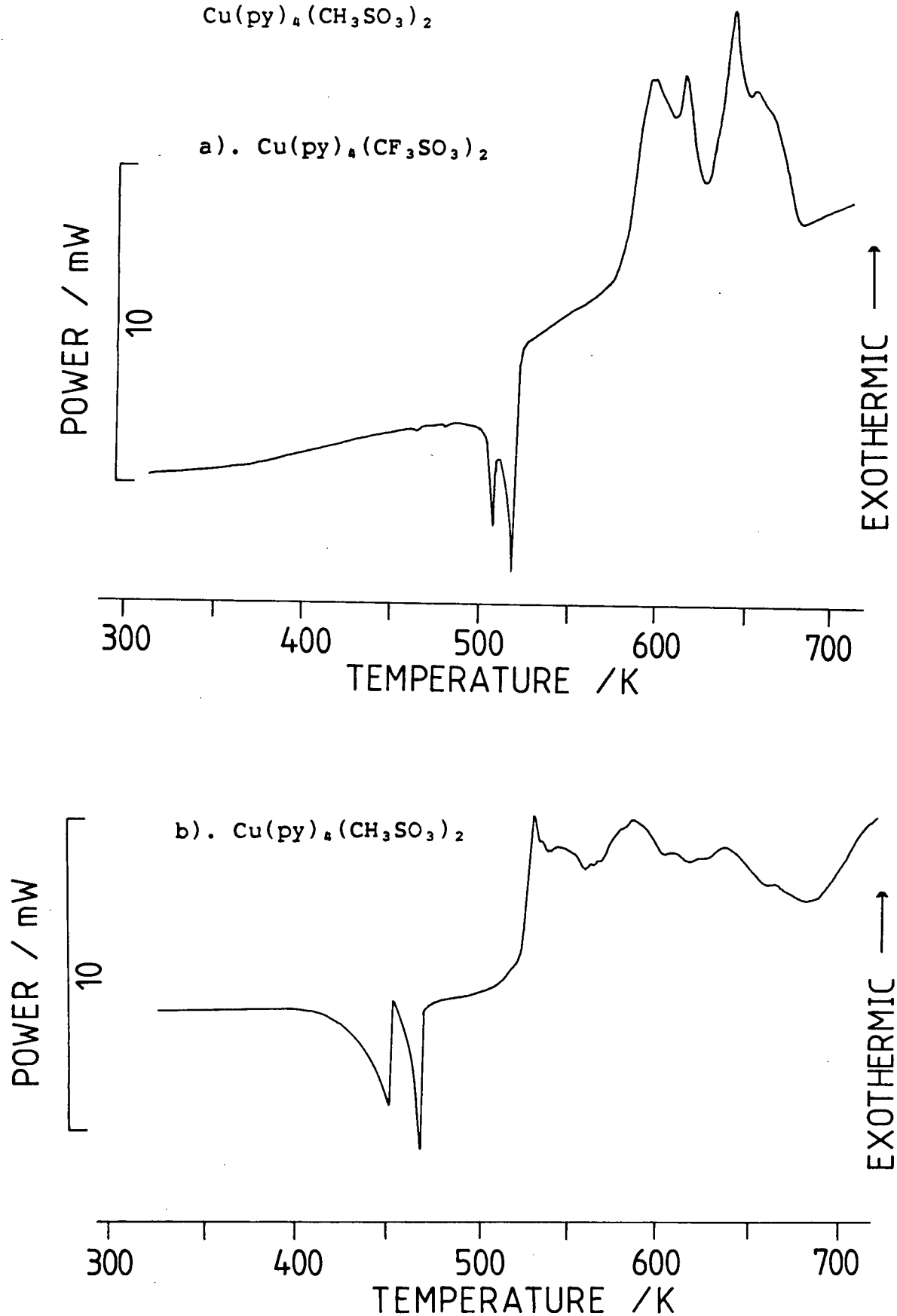
For the triflate derivative, the close proximity of the two thermal steps and the relatively broad nature of the second event make it difficult to characterise individual weight or enthalpy changes associated with each event. The peak temperature is the only parameter to be evaluated (Table 3.8). The two events are accompanied by a total weight loss of 20% which is close to that expected (23%) for the removal of two



pyridine groups from  $\text{Cu}(\text{py})_4(\text{CF}_3\text{SO}_3)_2$ . For the copper-triflate complex, the presence of two peaks suggests that the first two pyridine groups are lost in a stepwise manner rather than simultaneously as found in the thermolysis of  $\text{Fe}(\text{py})_4(\text{CF}_3\text{SO}_3)_2$ . Presumably, for  $\text{Cu}(\text{py})_4(\text{CF}_3\text{SO}_3)_2$ , the two remaining pyridine groups are lost at higher temperatures and it appears likely that these events are obscured by the exothermic decomposition of the compound above approximately 580 K (Fig. 3.35a).

$\text{Cu}(\text{py})_4(\text{CH}_3\text{SO}_3)_2$  exhibits endothermic events at 453 and 469 K and whilst the enthalpy changes associated with these events were approximated, it was difficult to establish weight changes associated with each event. The gravimetric results were found to be irreproducible from one D.S.C. experiment to another and meaningful conclusions could not be made. Information was obtained, however, by heating  $\text{Cu}(\text{py})_4(\text{CH}_3\text{SO}_3)_2$  to a temperature slightly above the temperature of the second thermal event. An overall weight loss of 36% was measured, a value which is intermediate between the weight decrease expected for the loss of two and three moles of pyridine (28 and 42% respectively). As was also noted above for  $\text{Fe}(\text{py})_4(\text{CH}_3\text{SO}_3)_2$ , a more complex decomposition route involving loss of a non-integral number of pyridine ligands is suggested. Exothermic decomposition takes place at temperatures above approximately 530 K.

Fig. 3.35 D.S.C. Curves for  $\text{Cu}(\text{py})_4(\text{CF}_3\text{SO}_3)_2$  and  $\text{Cu}(\text{py})_4(\text{CH}_3\text{SO}_3)_2$



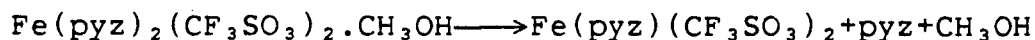
It is interesting to compare the relative thermal stabilities of  $M(\text{py})_4(\text{CF}_3\text{SO}_3)_2$  and  $M(\text{py})_4(\text{CH}_3\text{SO}_3)_2$ , where M is either Fe or Cu. The infrared spectra of these complexes (Section 3.3.2.1) show the coordination-sensitive pyridine vibrations, in particular, the 16b vibration, to shift to higher frequencies. This shift is more pronounced for the copper(II) complexes, indicating a stronger M-N(pyridine) interaction in these derivatives. For the  $M(\text{py})_4(\text{CF}_3\text{SO}_3)_2$  complexes (where M is either Fe or Cu), X-ray crystallography (Sections 3.3.1.1 and 3.3.1.2 respectively) shows a considerably shorter M-N bond length in the copper complexes. It was interesting to investigate whether these observations correlate with greater thermal stability in the copper compounds. Using the temperature of the first thermal event as a measure of thermal stability, it is noted that the copper derivatives are indeed, thermally more stable than the analogous iron derivatives by approximately 40 K.

No attempt was made to prepare the bis(pyridine)copper(II) sulfonate derivatives. The preceding data suggest that thermolysis may prove successful in isolating  $\text{Cu}(\text{py})_2(\text{CF}_3\text{SO}_3)_2$ , but would be ineffective for the synthesis of  $\text{Cu}(\text{py})_2(\text{CH}_3\text{SO}_3)_2$ .

Both the effect of a weaker Lewis base, pyrazine compared to pyridine, and its presence in a bridging configuration are expected to result in quite different thermal properties for the pyrazine compounds from those discussed above for the tetrakis(pyridine) complexes.

The data obtained from the D.S.C. measurements for the

bis(pyrazine) sulfonate compounds,  $\text{Fe}(\text{pyz})_2(\text{CF}_3\text{SO}_3)_2 \cdot \text{CH}_3\text{OH}$ ,  $\text{Fe}(\text{pyz})_2(\text{CH}_3\text{SO}_3)_2$  and  $\text{Cu}(\text{pyz})_2(\text{CH}_3\text{SO}_3)_2$ , are given in Table 3.8. All three complexes show two endothermic events in the temperature range studied and the results of gravimetric analysis again provide an insight into the thermolysis pathways. For  $\text{Fe}(\text{pyz})_2(\text{CF}_3\text{SO}_3)_2 \cdot \text{CH}_3\text{OH}$ , after the first thermal event a weight loss of 21% was measured. Removal of methanol would be accompanied by a weight change of only 6%. For the loss of pyrazine alone, a weight reduction of 15% would be expected. Hence, the observed weight loss indicates simultaneous removal of methanol and the first mole of pyrazine. The first step in thermolysis may be represented as follows:

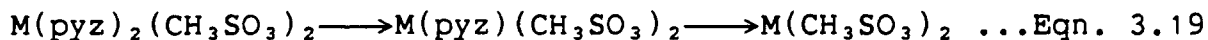


...Eqn. 3.18

An overall reduction in weight of 37% accompanies the second thermal event, consistent with the loss of the second pyrazine group and the formation of  $\text{Fe}(\text{CF}_3\text{SO}_3)_2$ .

Similar D.S.C. curves are observed for  $\text{Fe}(\text{pyz})_2(\text{CH}_3\text{SO}_3)_2$  and the analogous copper derivative.

Two endothermic events with weight losses consistent with the successive removal of pyrazine in two distinct steps are observed according to the following scheme:



where M is Fe or Cu.

Presumably for  $\text{Cu}(\text{pyz})_2(\text{CH}_3\text{SO}_3)_2$ , the more weakly bound axial pyrazine group is removed first.

A comparison of the relative thermal stability of these tetrakis(pyridine) and bis(pyrazine) complexes was made by using the temperature of an event in the D.S.C. curve. As stated, the first thermal event for the two groups of compounds corresponds to the removal of either two moles of pyridine or one mole of pyrazine per mole of complex. From the temperatures at which these events occur no stability trend is apparent. In some instances the bis(pyrazine) compounds are thermally more stable than the analogous tetrakis(pyridine) species and the opposite is also found, making a consistent interpretation hazardous. Where the second thermal event arises from loss of either the remaining pyrazine or pyridine groups, the temperature of this event is always higher by at least 100 K for the pyrazine complexes. This added thermal stability of the intermediate pyrazine complexes over the bis(pyridine) complexes may result from the type of polymer present in these thermolysis intermediates.

D.S.C. measurements were also carried out on the bis(pyrazine) complexes containing the halide anions,  $\text{Cl}^-$ ,  $\text{Br}^-$  or  $\text{I}^-$  and the pseudohalide,  $\text{NCS}^-$ . The results are presented in Table 3.9.

Table 3.9 Thermal Parameters for Bis(pyrazine)iron(II)  
Halide and Thiocyanate Complexes

Compound	Peak Temp. K	$\Delta H$ $\text{kJ mol}^{-1}$	Weight Loss (%)	
			Calc. <sup>1</sup>	Obs.
$\text{Fe}(\text{pyz})_2\text{Cl}_2$	477	70	28	34
	723	86	56	59
$\text{Fe}(\text{pyz})_2\text{Br}_2$	508	75	21	23
	742	41	43	48
$\text{Fe}(\text{pyz})_2\text{I}_2$	516	59	2	69
$\text{Fe}(\text{pyz})_2(\text{NCS})_2$	563	47	24	25
	638	40	48	60

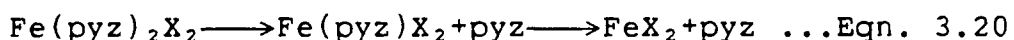
1). For explanation of calculated values see text

2). For discussion of this complex see text

Due to the well-known highly unstable nature of perchlorate compounds and the desire to maintain the fragile D.S.C. sensor intact,  $\text{Fe}(\text{pyz})_2(\text{ClO}_4)_2$  was not included in this thermal study.

The D.S.C. curves for the chloro- and bromo derivatives show two endothermic events, indicating thermolysis to take place in two stages.

From the gravimetric analyses (Table 3.9) it is tentatively suggested that the two endothermic events result from the loss of pyrazine in a stepwise fashion as observed for the bis(pyrazine) sulfonate complexes according to:



where X is  $\text{Cl}^-$  or  $\text{Br}^-$

Heating the iodo derivative produces one single endothermic event and a weight loss of 69%. The removal of one or two moles of pyrazine would correspond to weight losses of 17 and 34% respectively. The gravimetric measurements, together with the observation of a brown ring around the pin hole in the aluminum crucible after heating the compound to 540 K, indicate the loss of iodine and suggest more extensive sample decomposition in this compound. Heating the complex to 473 K, well before the onset of any detectable thermal event, results already in an observed weight loss of 7%. Thus decomposition of the complex occurs over a wide temperature range.

The D.S.C. curve for  $\text{Fe}(\text{pyz})_2(\text{NCS})_2$  shows two endothermic events and the weight loss (Table 3.9) which accompanies the first event suggests that one of the two pyrazines is removed. The second event is accompanied by a weight loss of 60%. Not only removal of the remaining pyrazine but also decomposition of the anion are implied.

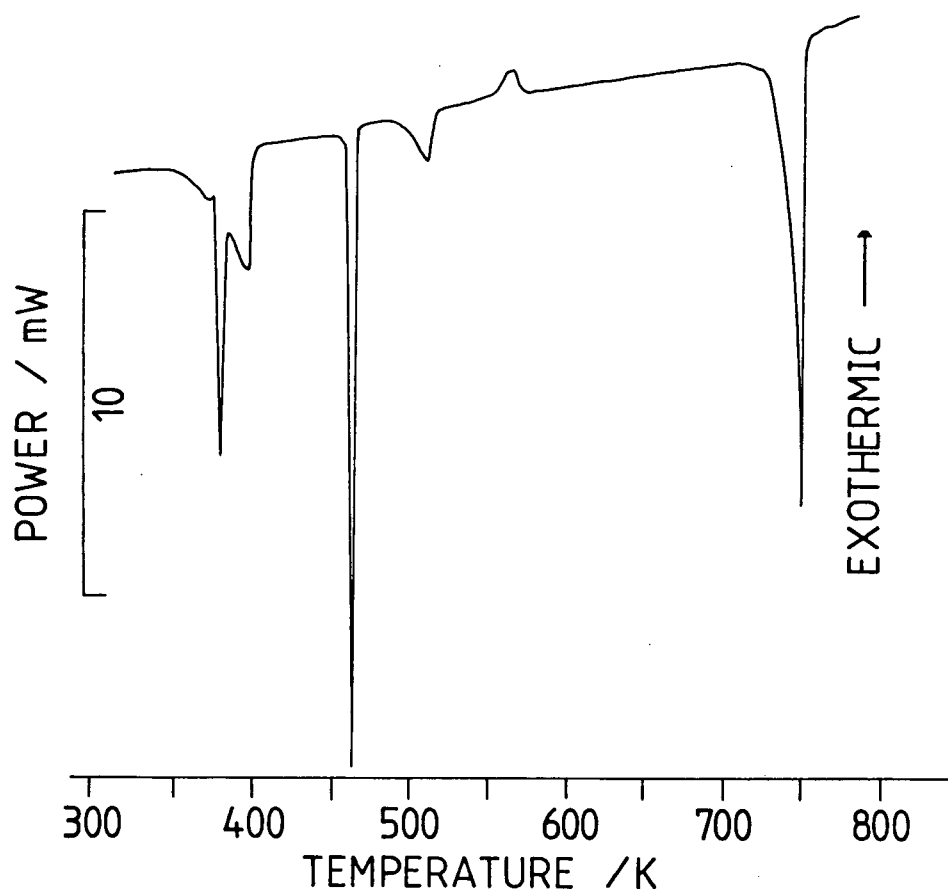
The thermolysis results for the tetrakis(pyrazine) complexes are given in Table 3.10.

$\text{Fe}(2\text{-mepyz})_4(\text{CH}_3\text{SO}_3)_2$  exhibits a complex D.S.C. thermogram as illustrated in Fig. 3.36.

Table 3.10 Thermal Parameters for  $\text{Fe}(2\text{-mepyz})_4(\text{CH}_3\text{SO}_3)_2$ ,  
 $\text{Cu}(\text{pyz})_4(\text{CF}_3\text{SO}_3)_2 \cdot \text{H}_2\text{O}$  and  $\text{Fe}(\text{pyz})_4(\text{AsF}_6)_2 \cdot 2\text{H}_2\text{O}$

Compound	Peak Temp. K	$\Delta H$ kJ mol <sup>-1</sup>
$\text{Fe}(2\text{-mepyz})_4(\text{CH}_3\text{SO}_3)_2$	382	-
	400	-
	467	81
	540	12
	570	-11
	750	180
$\text{Cu}(\text{pyz})_4(\text{CF}_3\text{SO}_3)_2 \cdot \text{H}_2\text{O}$	398	53
	460	175
	650	-
$\text{Fe}(\text{pyz})_4(\text{AsF}_6)_2 \cdot 2\text{H}_2\text{O}$	430	71
	500	40
	590	180



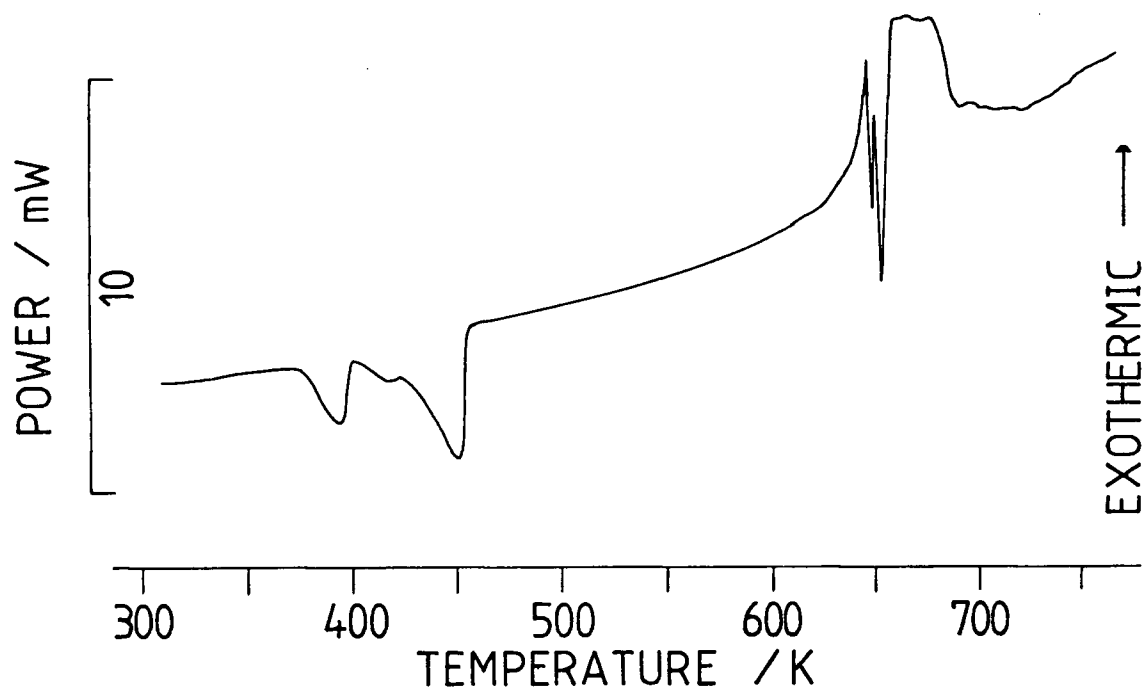
Fig. 3.36 D.S.C. Curve for  $\text{Fe}(\text{2-mepyz})_4(\text{CH}_3\text{SO}_3)_2$ 

The broad nature of the peak around 400 K and its close proximity to the first thermal event at 381 K preclude any estimation of the enthalpy changes associated with these two events. For both events a combined weight loss of 35% was recorded which is close to the expected value (30%) for the removal of two 2-methylpyrazine ligands from the tetrakis(2-methylpyrazine) complex. On further heating, a sharp endothermic peak is observed (467 K,  $\Delta H = 81 \text{ kJ mol}^{-1}$ ) and an accumulated weight loss of 54% was determined; this figure is close to that expected for the loss of three neutral ligands. When the complex is heated to approximately 560 K, about 20 K

above the temperature of the minor endothermic event at 540 K, an accumulated weight loss of 59% is observed. This loss agrees even more closely with that expected for the removal of three ligands. A major endothermic event is evident at a higher temperature, 750 K, ( $180 \text{ kJ mol}^{-1}$ ) and this is associated with a total weight loss of 85%. It is obvious from this value that other decomposition reactions are taking place as well.

Between 370 and 470 K, the D.S.C. curve for  $\text{Cu}(\text{pyz})_4(\text{CF}_3\text{SO}_3)_2 \cdot \text{H}_2\text{O}$  (Fig. 3.37) reveals two broad endothermic peaks; the event at 460 K exhibits a low temperature shoulder.

Fig. 3.37 D.S.C. Curve for  $\text{Cu}(\text{pyz})_4(\text{CF}_3\text{SO}_3)_2 \cdot \text{H}_2\text{O}$



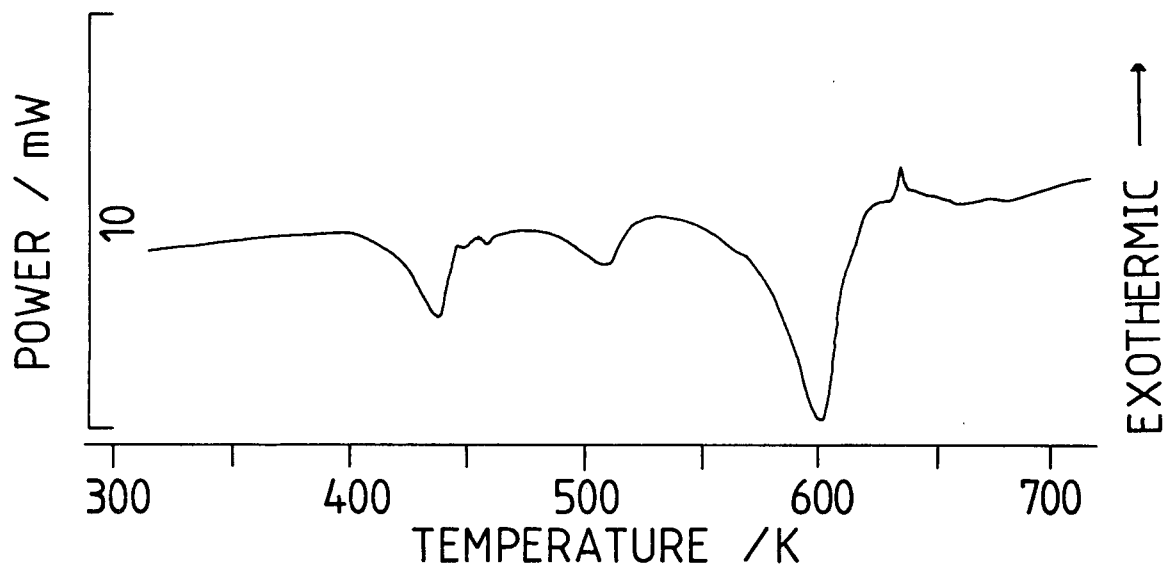
Heating the complex to 410 K, slightly above the temperature of

the first event, results in a small weight loss of approximately 5%. This appears to indicate the removal of water from the complex, expected weight loss of 3%. Further heating to 483 K, beyond the temperature of the second event, results in a weight loss of 36%. This compares favourably with 37% expected when not only water but also three pyrazine molecules are lost from the compound. The results also indicate a high thermal stability for  $\text{Cu}(\text{pyz})(\text{CF}_3\text{SO}_3)_2$ , and have specific relevance for the synthesis of the mono(pyrazine) derivative by thermolysis (Section 4.2.2.4). On additional heating to a temperature of 600 K, the D.S.C. curve shows a broad exothermic event accompanied by a weight loss of approximately 77%. Both observations are consistent with extensive sample decomposition at these temperatures.

$\text{Fe}(\text{pyz})_4(\text{AsF}_6)_2 \cdot 2\text{H}_2\text{O}$  undergoes thermolysis as illustrated in Fig. 3.38. Three events are observed. The first, at 433 K, is accompanied by a 13% weight loss, consistent with the loss of both water molecules and one pyrazine group, (expected weight loss of 15%). At 490 K, a second thermal event occurs accompanied by a total weight loss of 30%. This loss is intermediate between the values expected for the removal of one or two additional pyrazine groups (25 or 35% weight losses respectively). A third broad endotherm is centred around 590 K. At this temperature the weight loss figure of 76% indicates that extensive decomposition has set in (the loss of four pyrazine groups and both water molecules would represent a 45% weight loss). It appears that thermolysis above temperatures of 500 K

follows a more complex route than would be predicted by mere loss of neutral ligands. These results indicate that it is unlikely that  $\text{Fe}(\text{pyz})_2(\text{AsF}_6)_2$  is formed during thermolysis. Other investigations (Section 3.2.2.2) showed that heating a sample of  $\text{Fe}(\text{pyz})_4(\text{AsF}_6)_2 \cdot 2\text{H}_2\text{O}$ , in vacuo, at 320 K had no effect; whereas, heating at 340 K resulted in formation of a brown solid and sample decomposition.

Fig. 3.38 D.S.C. Curve for  $\text{Fe}(\text{pyz})_4(\text{AsF}_6)_2 \cdot 2\text{H}_2\text{O}$



## CHAPTER 4

### COMPLEXES CONTAINING AN $MN_2X_4$ CHROMOPHORE

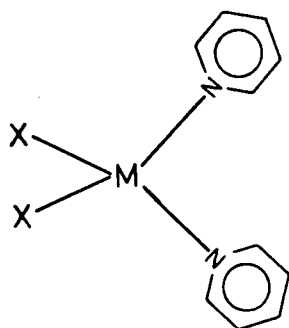
#### 4.1 INTRODUCTION

The synthesis and characterisation of complexes containing an  $MN_4X_2$  chromophore were discussed in the preceeding chapter; complexes in which two of the nitrogen donor atoms are removed from the  $MN_4X_2$  chromophore are considered in this chapter. Preparation and characterisation of mono(pyrazine) and bis(pyridine) compounds were performed because a variety of polymeric or monomeric structures may be visualised. It was found that for the complexes which contain an  $MN_4X_2$  chromophore, the anions coordinate in a unidentate fashion; upon removal of two nitrogen donors the coordination mode of the anion may be either unaltered, resulting in a four-coordinate complex ( $MN_2X_2$  chromophore), or the anion may assume bidentate coordination so as to maintain a six-coordinate metal centre ( $MN_2X_4$  chromophore). In both of these situations the structure of the complex is dependent upon the coordination mode of the neutral ligand. For the four-coordinate complex, where the ligand is pyridine, a monomeric species would result (Fig. 4.1a); whereas, incorporation of pyrazine results in the formation of a polymer (Fig. 4.1b). For the anions used in this study, however, the preferred mode of coordination is not necessarily unidentate. For example, sulfonate anions have the potential to use more than one oxygen atom to bridge metal centres, and a

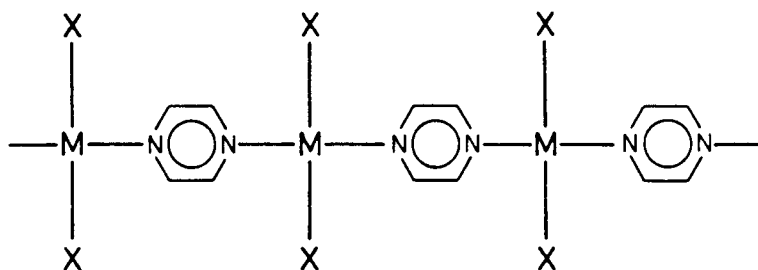
bridging mode for halide<sup>161</sup> and pseudohalide<sup>127</sup> ligands is well known. In these bis(pyridine) and mono(pyrazine) compounds, a bridging bidentate coordination mode for the anion would result in an  $MN_2X_4$  chromophore. Again, several structural modifications may exist, dependent upon the neutral ligand. In the case where the two nitrogen donor atoms are from pyridine, then the only bridging groups are the anionic ligands and polymers may be formed as shown in Fig. 4.1c (i) and (ii). For complexes where the two nitrogen atoms arise from pyrazine, a combination of bridging pyrazine and bridging anionic ligands may lead to more complex polymeric materials and possible structures are shown in Fig. 4.1d (i) and (ii). If such polymeric structures are formed for the bis(pyridine) or mono(pyrazine) complexes isolated in this study, then magnetic interactions are possible through the bridging network.

Various spectroscopic methods were employed in this study in an attempt to distinguish between the possible structures. The results of these studies enabled conclusions to be drawn concerning the coordination sphere around the metal, the nature of the bridging group or groups and the extent of any magnetic exchange interactions. Comparisons are made between the structures and properties of these complexes and those of the complexes containing an  $MN_4X_2$  chromophore.

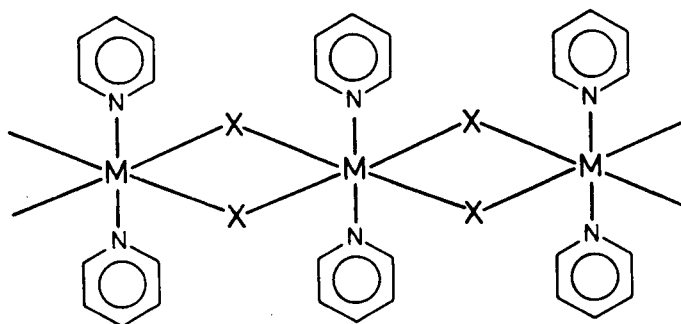
Fig. 4.1 Some Possible Structures of Mono(pyrazine) and Bis(pyridine) Complexes



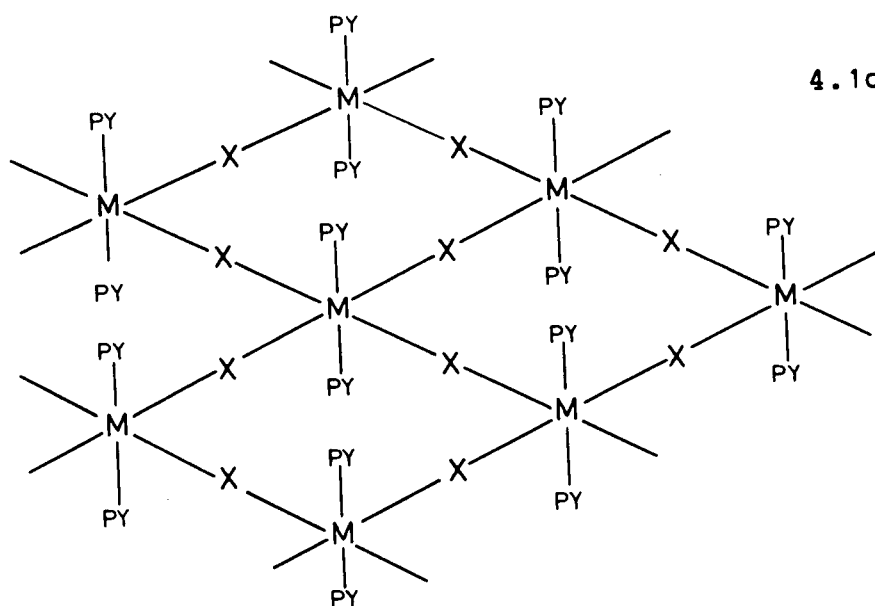
4.1a).



4.1b).



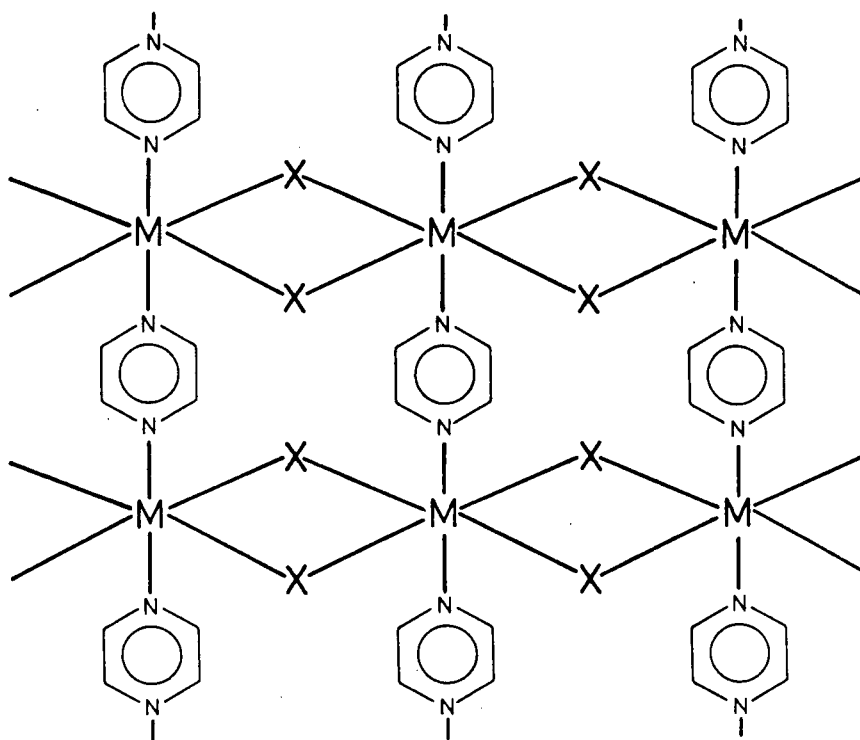
4.1c). (i)



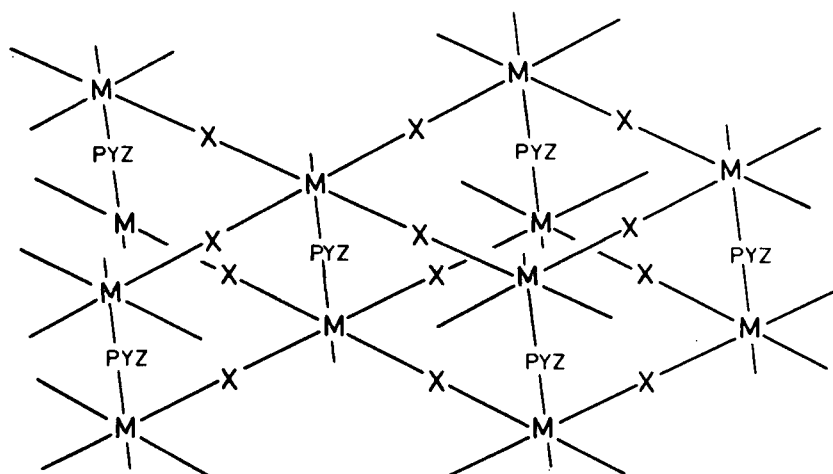
4.1c). (ii)

Fig. 4.1 Continued

4.1d). (i)



4.1d). (ii)





## 4.2 SYNTHETIC METHODS

Either a solution or a thermolysis route was used for the preparation of the mono(pyrazine) and bis(pyridine) complexes. With regard to the thermolysis method, D.S.C. results (Section 3.3.6) are useful in that they indicate thermolysis often occurs by stepwise loss of neutral ligand. These results also show that thermal events often take place at temperatures higher than those attainable in this laboratory using conventional heating methods, for example, an oil bath or a drying pistol. By heating in vacuo, temperatures required for thermolysis on a preparative scale were lower than those indicated by the D.S.C. studies. The choice of temperature for bulk thermolysis was found to be quite critical and was determined by heating at gradually increasing temperature and monitoring the changes in the infrared spectrum of the material as well as monitoring the microanalytical data. It was found that heating at too high a temperature resulted in the loss of more than the required amount of ligand (either pyrazine or pyridine), whilst heating at too low a temperature had the opposite effect. Experiment showed that in every case the compounds obtained by this route were unique materials, rather than being stoichiometric mixtures; for example, the infrared spectrum of the product obtained from thermolysis of  $\text{Fe}(\text{py})_4(\text{CF}_3\text{SO}_3)_2$  is quite different from the spectrum which would result from a 1:1 mixture of  $\text{Fe}(\text{py})_4(\text{CF}_3\text{SO}_3)_2$  and  $\text{Fe}(\text{CF}_3\text{SO}_3)_2$  (Section 4.3.1.1).

#### 4.2.1 Bis(pyridine) Complexes

Two synthetic routes for the preparation of bis(pyridine)iron(II) sulfonate complexes were attempted. The first involved thermolysis of the analogous tetrakis(pyridine) complexes. This route has been used successfully for the synthesis of several bis(pyridine)iron(II) halide and pseudohalide complexes.<sup>67</sup> D.S.C. results indicate the loss of two molecules of pyridine from the tetrakis(pyridine)iron(II) derivatives occurs as the first step. Thermolysis of  $\text{Fe}(\text{py})_4(\text{CF}_3\text{SO}_3)_2$ , in vacuo, indeed leads to the isolation of the bis(pyridine) analogue. For the methanesulfonate and p-tosylate derivatives, however, thermolysis in vacuo proved unsuccessful in isolating the desired bis(pyridine) complexes. Heating to temperatures of 360 and 350 K for the methanesulfonate and p-tosylate complexes respectively, results in no loss of pyridine, as monitored by infrared spectroscopy and microanalytical data; whereas, at the higher temperatures of 370 and 360 K respectively, the same techniques indicate loss of more than the two moles of pyridine. These observations suggest that the choice of temperature for the vacuum thermolysis of these two materials is more critical than for the corresponding triflate derivative.

The second preparative route involved the addition of pyridine to a methanolic solution of the appropriate iron(II) sulfonate in a 2 to 1 mole ratio. Slow evaporation of the resulting solution consistently gave the tetrakis(pyridine)iron(II) complexes. Attempts at obtaining

bis(pyridine) complexes by using pyridine to metal ratios of less than 2 to 1 were also unsuccessful.

#### 4.2.1.1 Bis(pyridine)iron(II) trifluoromethanesulfonate, $\text{Fe}(\text{py})_2(\text{CF}_3\text{SO}_3)_2$

On a preparative scale it was found that heating  $\text{Fe}(\text{py})_4(\text{CF}_3\text{SO}_3)_2$ , in vacuo, at a temperature of approximately 360 K for 22 h resulted in loss of two moles of pyridine and production of  $\text{Fe}(\text{py})_2(\text{CF}_3\text{SO}_3)_2$ . Anal. calcd for  $\text{FeC}_{12}\text{H}_{10}\text{N}_2\text{F}_6\text{S}_2\text{O}_6$ : C, 28.14; H, 1.97; N, 5.47; found: C, 28.15; H, 2.04; N, 5.63. Upon further heating at this temperature no further loss of pyridine was recorded.

#### 4.2.2 Mono(pyrazine) Complexes

Several mono(pyrazine) complexes were isolated during the course of this study. A thermolysis route proved successful in the isolation of  $\text{Fe}(\text{pyz})(\text{CF}_3\text{SO}_3)_2$ ,  $\text{Fe}(\text{pyz})(p\text{-CH}_3\text{C}_6\text{H}_4\text{SO}_3)_2$ ,  $\text{Cu}(\text{pyz})(\text{CF}_3\text{SO}_3)_2$  and  $\text{Fe}(\text{pyz})\text{Cl}_2$ . The mono(pyrazine) complexes:  $\text{Fe}(\text{pyz})(p\text{-CH}_3\text{C}_6\text{H}_4\text{SO}_3)_2 \cdot 2\text{CH}_3\text{OH}$ , and  $\text{Fe}(\text{pyz})(\text{NCO})_2$  were isolated via a solution method.

##### 4.2.2.1 Mono(pyrazine)iron(II) trifluoromethanesulfonate, $\text{Fe}(\text{pyz})(\text{CF}_3\text{SO}_3)_2$

Thermal analysis (Section 3.3.6) indicates the formation of the mono(pyrazine) derivative by the loss of pyrazine and methanol from  $\text{Fe}(\text{pyz})_2(\text{CF}_3\text{SO}_3)_2 \cdot \text{CH}_3\text{OH}$ . The same chemical change took place when the bis(pyrazine) complex was heated for 15 h

(in vacuo) at 380 K in the presence of  $P_2O_5$  in an Aberhalden drying pistol. The infrared spectrum of the product shows significant changes from that of the starting material and the microanalytical data are consistent with the formation of the mono(pyrazine) complex. Anal. calcd for  $FeC_6H_4N_2F_6S_2O_6$ : C, 16.60; H, 0.93; N, 6.45; found: C, 16.85; H, 0.98; N, 6.38. Heating for longer periods of time at the same temperature resulted in no further loss of pyrazine, as judged by infrared spectroscopy and microanalytical data.

#### 4.2.2.2 Mono(pyrazine)iron(II) p-toluenesulfonate bis(methanol) solvate, $Fe(pyz)(p-CH_3C_6H_4SO_3)_2 \cdot 2CH_3OH$

Iron(II) p-toluenesulfonate<sup>25</sup> (0.87 g, 2.2 mmol) was dissolved in methanol (10 mL). Pyrazine (0.77 g, 9.6 mmol), dissolved in methanol/diethyl ether (12 mL, 1:5v/v), was then added to this solution. Small, orange-yellow crystals formed after 1/2 h and after three days the solid was removed by filtration and the product was washed with a small amount of diethyl ether (yield 66%). Anal. calcd for  $FeC_{20}H_{26}N_2S_2O_8$ : C, 44.29; H, 4.83; N, 5.16; found: C, 44.05; H, 4.71; N, 4.93.

4.2.2.3 Mono(pyrazine)iron(II) p-toluenesulfonate,  
 $\text{Fe}(\text{pyz})(\text{p-CH}_3\text{C}_6\text{H}_4\text{SO}_3)_2$

The unsolvated compound was prepared by heating the solvate, prepared as described above, at approximately 340 K in vacuo for 16 h. Anal. calcd for  $\text{FeC}_{18}\text{H}_{18}\text{N}_2\text{S}_2\text{O}_6$ : C, 45.20; H, 3.79; N, 5.85; O, 20.07; found: C, 44.98; H, 3.77; N, 5.77; O, 19.86.

4.2.2.4 Mono(pyrazine)copper(II) trifluoromethanesulfonate,  
 $\text{Cu}(\text{pyz})(\text{CF}_3\text{SO}_3)_2$

D.S.C. results (Section 3.3.6) indicate the loss of not only water but also three moles of pyrazine from  $\text{Cu}(\text{pyz})_4(\text{CF}_3\text{SO}_3)_2 \cdot \text{H}_2\text{O}$ . Upon heating the tetrakis(pyrazine) complex in an Aberhalden drying pistol at a temperature of 360 K in the presence of phosphorus(V) oxide for 14 h in vacuo the mono(pyrazine) complex was produced. Anal. calcd for  $\text{CuC}_6\text{H}_4\text{N}_2\text{F}_6\text{S}_2\text{O}_6$ : C, 16.31; H, 0.91; N, 6.34; found: C, 16.33; H, 1.00; N, 6.24.

4.2.2.5 Mono(pyrazine)iron(II) chloride,  $\text{Fe}(\text{pyz})\text{Cl}_2$

The synthesis involved the thermolysis of  $\text{Fe}(\text{pyz})_2\text{Cl}_2$  for 3 days at a temperature of 380 K in an Aberhalden drying pistol. Anal. calcd for  $\text{FeC}_4\text{H}_4\text{N}_2\text{Cl}_2$ : C, 23.23; H, 1.95; N, 13.54; found: C, 23.15; H, 1.99; N, 13.36.

4.2.2.6 Mono(pyrazine)iron(II) cyanate,  $\text{Fe}(\text{pyz})(\text{NCO})_2$ 

The mono(pyrazine) complex was prepared by a similar route to that used for  $\text{Fe}(\text{pyz})_2(\text{NCS})_2$ , (Section 3.2.3.7); for the cyanate derivative,  $\text{KCNO}$  was used in place of  $\text{KCNS}$ . Iron(II) sulfate heptahydrate (1.079 g; 3.88 mmol) was dissolved in water (5 mL). To this solution was added an aqueous solution (5 mL) of potassium cyanate (0.644 g; 8.06 mmol). This solution was filtered directly into an aqueous solution (10 mL) of pyrazine (0.645 g; 7.93 mmol). A dark-purple solid formed instantly and the mixture was stirred for 2 h. The product was isolated in 77% yield after filtration and washing with a small amount of water and methanol. Anal. calcd for  $\text{FeC}_6\text{H}_4\text{N}_4\text{O}_2$ : C, 32.76; H, 1.83; N, 25.47; O, 14.55; found: C, 32.69; H, 1.89; N, 25.31; O, 14.62.

## 4.3 RESULTS AND DISCUSSION

### 4.3.1 Infrared Spectroscopy

#### 4.3.1.1 $\text{Fe}(\text{py})_2(\text{CF}_3\text{SO}_3)_2$

Vibrational assignments for the bis(pyridine) derivative were made on the basis that the absorption bands originate from two constituent parts, namely, the pyridine groups and the triflate anions. Vibrational assignments for the pyridine ligands are given in Appendix II for comparison with those of the tetrakis(pyridine) complexes. The 8a and 16b pyridine ligand vibrations are shifted considerably, by approximately  $20\text{ cm}^{-1}$ , from those of the free ligand; the 6a pyridine vibration is probably obscured by the anion band at  $635\text{ cm}^{-1}$ . The shifts and splittings of the pyridine vibrations are similar to those present in the infrared spectrum of  $\text{Fe}(\text{py})_4(\text{CF}_3\text{SO}_3)_2$  and indicate the coordination of pyridine.

The vibrational assignments for the anion are given in Appendix III, Part A. The bands assigned to the triflate anion show many similarities with the corresponding absorption bands in  $\text{Fe}(\text{py})_4(\text{CF}_3\text{SO}_3)_2$  and the anion spectra for the bis(pyridine) complex are assigned on the basis of a reduction of anion symmetry below that of the free ion (i.e., below  $C_{3v}$ ). For example, the splitting of the asymmetric  $\text{SO}_3$  stretching mode,  $\nu_4$ , is a clear indication of this reduction of anion symmetry. The magnitude of the splitting of this band is, however, different in the two triflate derivatives and this provides

information on the mode of anion coordination. For  $\text{Fe}(\text{py})_2(\text{CF}_3\text{SO}_3)_2$ , the splitting of this band is  $111\text{ cm}^{-1}$ ; whereas, in the tetrakis(pyridine) complex the splitting is significantly lower,  $85\text{ cm}^{-1}$ . The degree of splitting of the  $\nu_4$  band has been used to indicate bidentate anion coordination in  $(\text{CH}_3)_2\text{Sn}(\text{FSO}_3)_2$ .<sup>162</sup> In this tin complex, bidentate anion coordination was proposed on the basis of spectroscopic measurements including infrared data. It was noted that the splitting of the anion band,  $\nu_4$ , was substantially larger than in complexes where the anion is coordinated in a unidentate mode. A bidentate mode of coordination was subsequently established by X-ray crystallography.<sup>163</sup> The larger splitting of  $\nu_4$  in the bis(pyridine) complex, when compared to  $\text{Fe}(\text{py})_4(\text{CF}_3\text{SO}_3)_2$ , suggests a bidentate mode of anion coordination in the former compound.

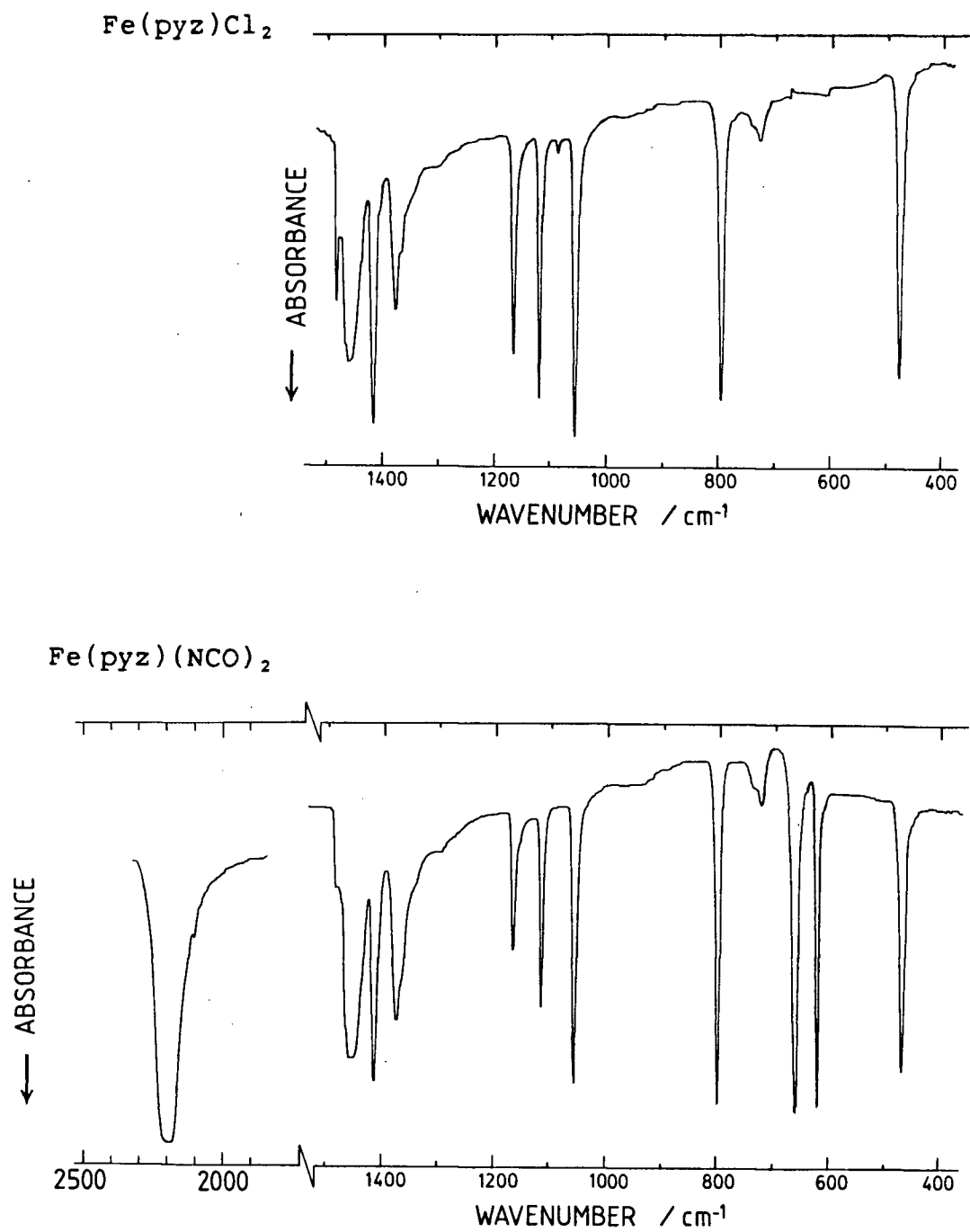
The remaining absorption bands assigned to the anion show only small differences with the assignments made for  $\text{Fe}(\text{py})_4(\text{CF}_3\text{SO}_3)_2$  (Appendix III, Part A) and indicate that these bands are insensitive to the mode of anion coordination. These infrared spectral data clearly eliminate the possibility that the product of the thermolysis of  $\text{Fe}(\text{py})_4(\text{CF}_3\text{SO}_3)_2$  is an equimolar mixture of the tetrakis(pyridine) compound and  $\text{Fe}(\text{CF}_3\text{SO}_3)_2$ . In particular, infrared spectroscopy would detect the anhydrous sulfonate compound through the presence of an intense band at  $1239\text{ cm}^{-1}$  (the asymmetric  $\text{SO}_3$  stretching vibration<sup>25</sup>) and this is not observed in the spectrum of  $\text{Fe}(\text{py})_2(\text{CF}_3\text{SO}_3)_2$ .



#### 4.3.1.2 $\text{Fe}(\text{pyz})\text{Cl}_2$ and $\text{Fe}(\text{pyz})(\text{NCO})_2$

The infrared spectra of these complexes are illustrated in Fig. 4.2 and the absorptions assigned to pyrazine are tabulated in Appendix VI. The infrared spectrum of  $\text{Fe}(\text{pyz})\text{Cl}_2$  is relatively simple, especially in comparison to that of  $\text{Fe}(\text{pyz})_2\text{Cl}_2$  (Section 3.3.2.2). The pyrazine vibrations in  $\text{Fe}(\text{pyz})\text{Cl}_2$  show no evidence for band splitting in contrast to the splitting observed in the infrared spectrum of  $\text{Fe}(\text{pyz})_2\text{Cl}_2$  (Appendix IV). For the bis(pyrazine) complex, the splitting was attributed to interactions between adjacent pyrazine rings and in the mono(pyrazine) compounds these interactions are likely to be absent if the pyrazine rings are trans-disposed to one another (Fig. 4.1c). The infrared activity of the pyrazine vibrations in  $\text{Fe}(\text{pyz})\text{Cl}_2$  is similar to that in known pyrazine-bridged species<sup>37, 44</sup> and is consistent with the ligand retaining  $D_{2h}$  symmetry by coordinating in an equivalent manner to two metal centres.

The infrared spectrum of  $\text{Fe}(\text{pyz})(\text{NCO})_2$  is illustrated in Fig. 4.2 and the spectral data assigned to pyrazine are tabulated in Appendix VI. From Fig. 4.2 the similarities and differences between the infrared spectrum of  $\text{Fe}(\text{pyz})(\text{NCO})_2$  and  $\text{Fe}(\text{pyz})\text{Cl}_2$  are immediately apparent. In particular, the absorptions assigned to pyrazine are virtually identical for the two complexes and a bidentate bridging mode of coordination for pyrazine is proposed for both complexes. The differences between the two spectra are attributed to the strong absorptions of the cyanate anion in the infrared spectrum of  $\text{Fe}(\text{pyz})(\text{NCO})_2$ .

Fig. 4.2 Infrared Spectra of  $\text{Fe}(\text{pyz})\text{Cl}_2$  and  $\text{Fe}(\text{pyz})(\text{NCO})_2$ 

Previous research<sup>126, 127, 164, 165</sup> on the nature of  $\text{NCO}^-$  coordination suggests several modes are possible and these include: terminal bonding, through either oxygen or nitrogen; and bridging, either  $\text{M-NCO-M'}$  or  $\text{M-N-M'}$ . Infrared criteria have been established for determining some of these coordination modes.<sup>126, 127, 164</sup>

The three normal vibrations of the triatomic  $\text{NCO}^-$  anion are the asymmetric stretching vibration,  $\nu_{\text{CN}}$ , ( $\nu_1$ ); the bending vibration,  $\delta_{\text{NCO}}$ , ( $\nu_2$ ), and the pseudo-symmetric stretching vibration,  $\nu_{\text{CO}}$  ( $\nu_3$ ). In cyanate compounds, these vibrational modes are appreciably mixed. From the infrared spectrum of  $\text{KNCO}$ <sup>166</sup> the following vibrational assignments ( $\text{cm}^{-1}$ ) have been made for the anion:

$\nu_1$	$\nu_2$	$\nu_3$
2170	629	1254

The value of  $\nu_3$  was calculated from the Fermi resonance interaction.<sup>167</sup> From the infrared spectrum of  $\text{Fe}(\text{pyz})(\text{NCO})_2$ , the following assignments ( $\text{cm}^{-1}$ ) are made:

$\nu_1$	$\nu_2$
2200s	658s
2100sh	620s

The  $\nu_1$  and  $\nu_2$  vibrations appear to be split and  $\nu_3$  was not observed. It has been noted previously, that upon coordination of the cyanate anion the frequency of  $\nu_1$  increases when compared to the free-ion value<sup>126, 127, 164</sup> and this also occurs for  $\text{Fe}(\text{pyz})(\text{NCO})_2$ . For this complex, the value of  $2200 \text{ cm}^{-1}$  falls within the range for either a terminally N-bonded or bridging

cyanate anion, and this absorption is not useful in distinguishing these two coordination modes.

The magnitude of the splitting of the  $\nu_2$  vibration has been found to be a good indicator for the presence of bridging  $\text{NCO}^-$  anions.<sup>126, 127, 164</sup> In terminally N-bonded cyanate complexes, this band is often split but the magnitude of the splitting is usually of the order of a few wavenumbers. The splitting of the  $\nu_2$  vibration in  $\text{Fe}(\text{pyz})(\text{NCO})_2$ , by  $38\text{ cm}^{-1}$ , indicates a bridging mode for the anionic ligand. The  $>\text{NCO}$  mode of cyanate bridging has been observed by X-ray crystallography in  $\text{AgNCO}$ <sup>168</sup> and is the most common bridging mode. In this silver salt, which contains zig-zag chains of  $-\text{Ag}-\text{N}-\text{Ag}-\text{N}-$  units, the  $\nu_2$  vibration is split by  $59\text{ cm}^{-1}$ .<sup>164</sup> The magnitude of the splitting of the  $\nu_2$  vibration in  $\text{Fe}(\text{pyz})(\text{NCO})_2$  suggests an anion bridging mode in this complex, possibly similar to that observed in  $\text{AgNCO}$ .

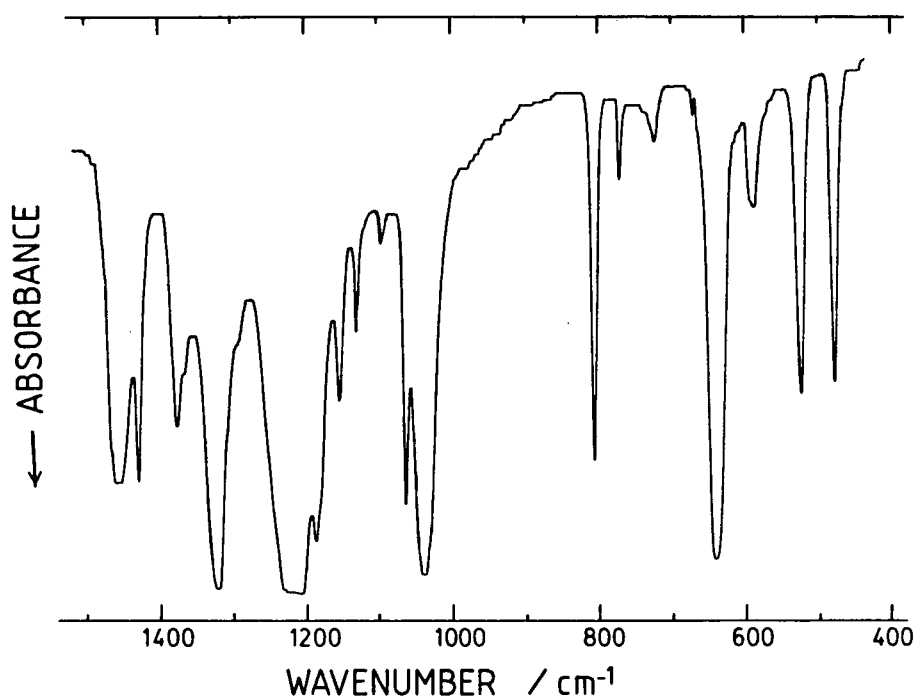
The  $\nu_3$  vibration is not observed in the infrared spectrum of  $\text{Fe}(\text{pyz})(\text{NCO})_2$ . This is not unexpected and in other complexes containing bridging cyanate groups this band is often of a much-reduced intensity.<sup>127</sup>

#### 4.3.1.3 Mono(pyrazine) sulfonate complexes.

Infrared spectral assignments for the neutral ligand (Appendix VI) and the sulfonate anions (Appendix III, Parts A and C) are discussed for the following complexes:  $\text{Fe}(\text{pyz})(\text{CF}_3\text{SO}_3)_2$ ,  $\text{Fe}(\text{pyz})(p\text{-CH}_3\text{C}_6\text{H}_4\text{SO}_3)_2$  (and its bis(methanol) solvate), and  $\text{Cu}(\text{pyz})(\text{CF}_3\text{SO}_3)_2$ . The spectrum of a representative member of this class of compound, that of

$\text{Fe}(\text{pyz})(\text{CF}_3\text{SO}_3)_2$ , is illustrated in Fig. 4.3.

Fig. 4.3 Infrared Spectrum of  $\text{Fe}(\text{pyz})(\text{CF}_3\text{SO}_3)_2$



In general, it is noted that the vibrational assignments made for the anions in these compounds (Appendix III, Parts A and C) bear a strong resemblance to those made for the sulfonate anions in the analogous tetrakis(pyridine) and bis(pyrazine) complexes (Section 3.3.2.1 and 3.3.2.3). For example, three absorption bands are observed in the  $\text{SO}_3$  stretching region and the splitting of the asymmetric  $\text{SO}_3$  stretching vibration,  $\nu_4$ , is conclusive evidence for the reduction of anion symmetry to below  $C_{3v}$ . Such a reduction, either to  $C_s$  or  $C_i$ , can result from either uni- or bidentate anion coordination. It was hoped that these infrared data would provide evidence for the mode of anion

coordination. From the results for  $\text{Fe}(\text{py})_2(\text{CF}_3\text{SO}_3)_2$  (Section 4.3.1.1) it was suggested that an increase in the splitting of the anion band,  $\nu_4$ , may arise from a bidentate mode of coordination. For the mono(pyrazine) complexes, the magnitude of this band splitting is, in general, larger (i.e., greater than  $100\text{ cm}^{-1}$ ) than for either the bis(pyrazine) or tetrakis(pyridine) compounds (i.e., less than  $100\text{ cm}^{-1}$ ). This may indicate a bidentate mode of anion coordination in these mono(pyrazine) complexes. It is interesting to note that the splitting of  $\nu_4$  of  $115\text{ cm}^{-1}$  for  $\text{Fe}(\text{pyz})(\text{CF}_3\text{SO}_3)_2$  is of a similar magnitude to the value of  $111\text{ cm}^{-1}$  observed for  $\text{Fe}(\text{py})_2(\text{CF}_3\text{SO}_3)_2$ ; this would be expected if both complexes have a similar mode of anion coordination possibly of a bidentate nature. A large splitting of  $\nu_4$  indicates bidentate sulfonate anion coordination but it should also be pointed out that the lack of a large splitting of this band does not necessarily eliminate the possibility of bidentate anion coordination, as the following example has demonstrated. X-ray crystallography demonstrated the presence of bidentate bridging methanesulfonate anions in an indium porphyrin complex;<sup>104</sup> anions link the porphyrin units to form an infinite linear chain compound. The infrared spectrum was assigned and the symmetric  $\text{SO}_3$  stretching vibration ( $\nu_1$ ) occurs at  $1040\text{ cm}^{-1}$  and the asymmetric stretching vibrations ( $\nu_4$ ) are at  $1130$ ,  $1150$ ,  $1250$  and  $1260\text{ cm}^{-1}$ . The  $\nu_4$  vibration shows additional small splittings but the positions of the bands are similar to those observed for unidentate methanesulfonate anions (for example, see the data for

$\text{Fe}(\text{py})_4(\text{CH}_3\text{SO}_3)_2$  in Appendix III, Part B).

It should be noted that the other vibrational assignments for the anions in the mono(pyrazine) sulfonate complexes studied here are similar to those made for the sulfonate anions which were shown to be coordinated in a unidentate manner, (Section 3.3.2.1) and it appears that these absorption bands are insensitive to the mode of anion coordination.

The absorption bands assigned to the neutral ligand are listed in Appendix VI. Many of the pyrazine absorptions are obscured by the strong absorptions of the anions ( $1000\text{--}1200\text{ cm}^{-1}$  region) but some information concerning the coordination of the neutral ligand was obtained from the bands which were assigned. As observed for  $\text{Fe}(\text{pyz})(\text{NCO})_2$  and  $\text{Fe}(\text{pyz})\text{Cl}_2$ , the pyrazine vibrations in the mono(pyrazine) sulfonate compounds show no splittings; in contrast to the bis(pyrazine) complexes for which pyrazine band splitting was found to be the rule rather than the exception. The relatively simple nature of these pyrazine-ligand spectra (with the exception of  $\text{Fe}(\text{pyz})(\text{p-CH}_3\text{C}_6\text{H}_4\text{SO}_3)_2 \cdot 2\text{CH}_3\text{OH}$ ), may be a result of there only being one distinct type of pyrazine ligand; moreover, an interaction between pyrazine groups which can lead to band splitting would be expected to be non-existent when the pyrazine moieties are trans-disposed to one another. The vibrational assignments for pyrazine in  $\text{Fe}(\text{pyz})(\text{p-CH}_3\text{C}_6\text{H}_4\text{SO}_3)_2 \cdot 2\text{CH}_3\text{OH}$ , however, do show additional splittings which may be due to interactions of the pyrazine groups with the methanol solvent molecules present in the lattice. A similar explanation was

proposed for the complex infrared spectrum of  $\text{Fe}(\text{pyz})_2(\text{CF}_3\text{SO}_3)_2 \cdot \text{CH}_3\text{OH}$  (Section 3.3.2.3).

For these mono(pyrazine) complexes, the remaining unassigned absorptions are listed in Appendix III, Parts A and C. No useful information concerning the coordination modes of the either the anionic or neutral ligands was obtained from these absorptions which primarily arise from either the  $\text{CF}_3$ ,  $\text{CH}_3$  or  $p\text{-CH}_3\text{C}_6\text{H}_4$  groups and, in one case, solvent molecules.

It is useful to summarise the infrared spectral results for these mono(pyrazine) and bis(pyridine) complexes. There is evidence to suggest bidentate bridging pyrazine and terminally coordinated pyridine ligands respectively. There is strong evidence for bridging cyanate anions in  $\text{Fe}(\text{pyz})(\text{NCO})_2$ ; whereas, the evidence for the mode of anion coordination is not as conclusive in the sulfonate complexes. The splitting of  $\nu_4$  indicates either  $C_s$  or  $C_i$  anion symmetry and a bidentate mode of anion coordination is suggested by the magnitude of this splitting.



### 4.3.2 Electronic Spectroscopy

In this section the electronic spectral data are reported and from the analysis of this data the chromophore determined. The complexes are considered in two categories. The results for mono(pyrazine) and bis(pyridine) sulfonate compounds are presented in Section 4.3.2.1, and in Section 4.3.2.2 the electronic spectral results for  $\text{Fe}(\text{pyz})\text{Cl}_2$  and  $\text{Fe}(\text{pyz})(\text{NCO})_2$  are discussed.

#### 4.3.2.1 $\text{Fe}(\text{pyz})(\text{CF}_3\text{SO}_3)_2$ , $\text{Fe}(\text{pyz})(p\text{-CH}_3\text{C}_6\text{H}_4\text{SO}_3)_2$ (and its bis(methanol) solvate), $\text{Fe}(\text{py})_2(\text{CF}_3\text{SO}_3)_2$ and $\text{Cu}(\text{pyz})(\text{CF}_3\text{SO}_3)_2$

Electronic spectral data are given in Appendix VII, Parts A and B, for the iron and copper complexes respectively. The colour of the iron complexes ranges from pale-yellow to orange, and all exhibit a broad absorption band in the near-infrared region of the electromagnetic spectrum. The position of the absorption maximum occurs at approximately the same frequency ( $10,800\text{--}10,900\text{ cm}^{-1}$ ) which is strong evidence to suggest the same chromophore in all instances. In general, the mono(pyrazine) and bis(pyridine)iron(II) complexes exhibit an absorption maximum at slightly lower frequency than do the corresponding bis(pyrazine) or tetrakis(pyridine) derivatives. Since pyrazine and pyridine are both higher in the spectrochemical series than the weakly basic sulfonate anions, the observation of a shift in the absorption maxima to lower frequency is consistent with the removal of either two terminal pyridine ligands or one bidentate bridging pyrazine group and

conversion of the sulfonate anion from a uni- to a bidentate mode of coordination resulting in an  $\text{FeN}_2\text{O}_4$  chromophore. The results are also consistent with a distorted pseudooctahedral arrangement since geometries such as square-planar or tetrahedral are expected to exhibit a different number of absorptions occurring at different frequencies from those observed here.

$\text{Cu}(\text{pyz})(\text{CF}_3\text{SO}_3)_2$  is a pale-blue colour and shows a broad absorption band in the visible region of the spectrum, the frequency of this band ( $13,900\text{ cm}^{-1}$ ) is similar to that of  $\text{Cu}(\text{pyz})_2(\text{CH}_3\text{SO}_3)_2$  ( $14,000\text{ cm}^{-1}$ ). This observation is consistent with  $\text{Cu}(\text{pyz})(\text{CF}_3\text{SO}_3)_2$  possessing a distorted pseudooctahedral chromophore.

It is concluded on the basis of this electronic spectral analysis that the mono(pyrazine) and bis(pyridine) sulfonate complexes contain an  $\text{MN}_2\text{O}_4$  chromophore. For  $\text{Fe}(\text{py})_2(\text{CF}_3\text{SO}_3)_2$ , this would involve bidentate bridging triflate anions and coordinated pyridine groups. In addition to containing bridging anions, the mono(pyrazine) compounds are considered to possess bridging pyrazine ligands. Possible structures which fulfill these coordination requirements for both the neutral ligand and the anions are shown in Figs. 4.1c and 4.1d.

#### 4.3.2.2 $\text{Fe}(\text{pyz})\text{Cl}_2$ and $\text{Fe}(\text{pyz})(\text{NCO})_2$

Both compounds exhibit absorptions in the near-infrared region at approximately  $11,000\text{ cm}^{-1}$  which is a typical value for distorted pseudooctahedral iron(II) complexes. The close

similarity between the band positions for the mono(pyrazine) and bis(pyrazine) chloride complexes indicates the equivalent ligand field strengths associated with the two complexes.

During the course of the present study, it was observed that several of the complexes are intensely coloured (brown, red or purple). For complexes containing an  $\text{FeN}_4\text{X}_2$  chromophore, the combined presence of pyrazine and either halide or thiocyanate appear to be a prerequisite for an intense colouration (Section 3.3.3.3). For the iron complexes discussed here a similar observation was made. For example,  $\text{Fe}(\text{pyz})\text{Cl}_2$  and  $\text{Fe}(\text{pyz})(\text{NCO})_2$  are red-brown and dark-purple respectively. On the other hand, the mono(pyrazine) sulfonate complexes (Section 4.3.2.1) are either pale-yellow or orange and the pyridine complexes  $\text{Fe}(\text{py})_2\text{Cl}_2$  and  $\text{Fe}(\text{py})_2(\text{NCO})_2$  are pale yellow.<sup>67</sup> An explanation for the origins of these colours was made in Section 3.3.3.3 and may also apply here; i.e., the intense colour is due to charge-transfer absorption bands which involve not only metal to neutral ligand but also anionic ligand to metal. For the complexes which contain sulfonate anions or pyridine ligands, the charge-transfer transition is of high energy and is not observed in the visible region of the spectrum.

### 4.3.3 Magnetic Properties

For these mono(pyrazine) and bis(pyridine) complexes there are no X-ray structural data; however, structural information was obtained from the techniques of infrared and electronic spectroscopy (Sections 4.3.1 and 4.3.2 respectively). These data indicate that the metal centre maintains six coordination and an  $MN_2X_4$  chromophore results from the coordination of four donor atoms from bidentate anionic ligands, together with two nitrogen donor atoms from either a single bidentate bridging pyrazine or two terminal pyridine ligands. It appears likely that these materials are polymeric and possible structures for these complexes are shown in Fig. 4.1c and d. The magnetic susceptibilities of these complexes were measured in an attempt to determine the presence of magnetic exchange interactions and to correlate the magnetic properties with structure. For the purpose of this discussion, the complexes are divided into two categories according to the metal. The magnetic properties of  $Cu(pyz)(CF_3SO_3)_2$  are discussed prior to the results for the iron(II) compounds,  $Fe(py)_2(CF_3SO_3)_2$ ,  $Fe(pyz)(CF_3SO_3)_2$ ,  $Fe(pyz)(p-CH_3C_6H_4SO_3)_2$  (and its bis(methanol) solvate),  $Fe(pyz)Cl_2$  and  $Fe(pyz)(NCO)_2$ .

#### 4.3.3.1 $Cu(pyz)(CF_3SO_3)_2$

Results of the magnetic measurements are presented in Appendix VIII. The magnetic moment of  $Cu(pyz)(CF_3SO_3)_2$  shows a significant temperature dependence; at room temperature the magnetic moment is 1.9 B.M. and this decreases to 1.7 B.M. at

100 K, at 4.2 K the moment is reduced further to 0.85 B.M. The temperature dependence is shown in Fig. 4.4, along with the plot for the magnetically-dilute complex,  $\text{Cu}(\text{pyz})_4(\text{CF}_3\text{SO}_3)_2 \cdot \text{H}_2\text{O}$  for comparison. The magnetic susceptibility (Fig. 4.5) increases with decreasing temperature until a maximum is observed at approximately 7 K. Below this temperature, down to 4.2 K, the magnetic susceptibility decreases. These temperature dependencies of  $\mu_{\text{eff.}}$  and  $\chi_m$  are clearly a consequence of antiferromagnetic exchange interactions propagated through the bridging ligands.

Fig. 4.4 Magnetic Moments vs Temperature for  $\text{Cu}(\text{pyz})(\text{CF}_3\text{SO}_3)_2$  and  $\text{Cu}(\text{pyz})_4(\text{CF}_3\text{SO}_3)_2 \cdot \text{H}_2\text{O}$

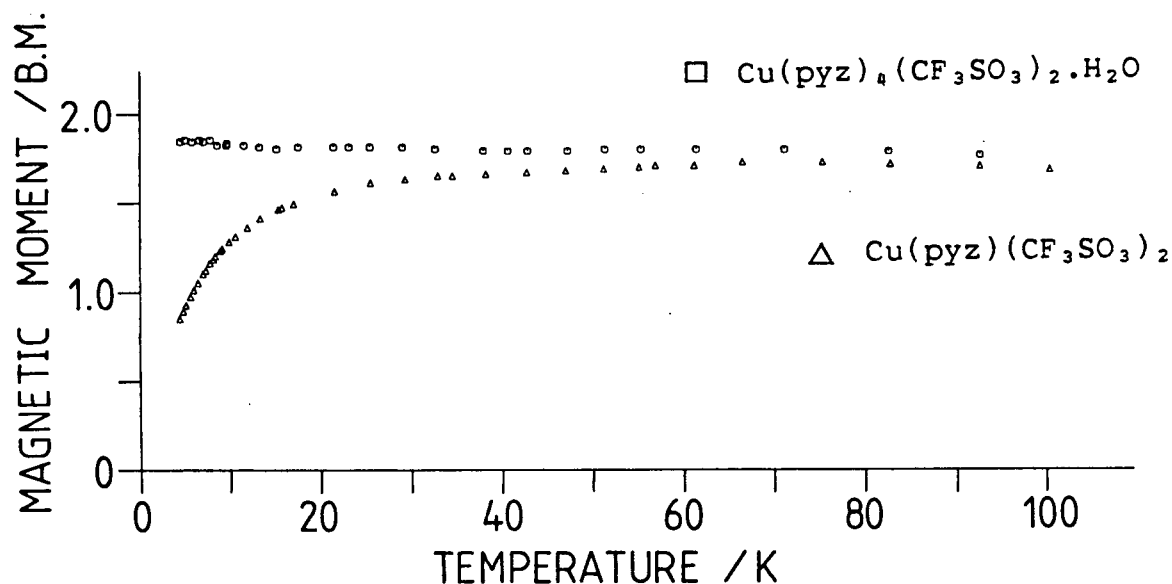
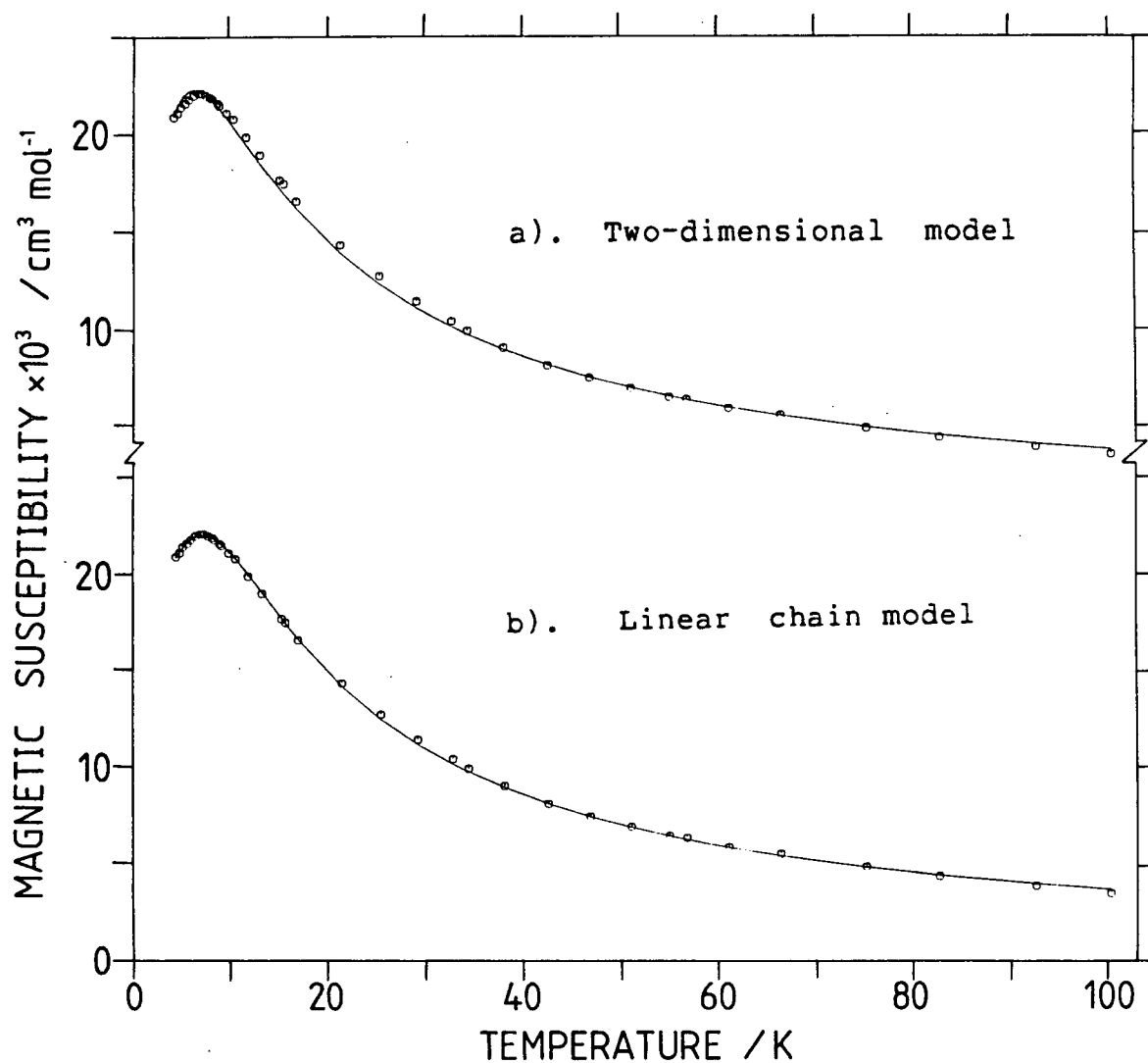


Fig. 4.5 Magnetic Susceptibility vs Temperature for  $\text{Cu}(\text{pyz})(\text{CF}_3\text{SO}_3)_2$

a). Two-dimensional model, solid line generated from  $J=-2.43 \text{ cm}^{-1}$ ,  $g=2.10$

b). Linear chain model, solid line generated from  $J=-3.78 \text{ cm}^{-1}$ ,  $g=2.08$



Infrared and electronic spectroscopic results (Sections 4.3.2 and 4.3.3 respectively) suggest that  $\text{Cu}(\text{pyz})(\text{CF}_3\text{SO}_3)_2$  contains bridging pyrazine and bridging triflate anions and hence, a polymeric structure is likely (Fig 4.1d). From the spectroscopic data presented above, it is difficult to distinguish between the possible structures shown in Fig. 4.1d. The magnetic susceptibility data for the triflate derivative and  $\text{Cu}(\text{pyz})_2(\text{CH}_3\text{SO}_3)_2$  exhibit similar temperature dependencies which suggests that the dominant magnetic exchange pathway may be similar in both compounds. Considering this proposal, the Lines' two-dimensional model (Eqn. 3.5) was employed to represent the magnetic susceptibility data of  $\text{Cu}(\text{pyz})(\text{CF}_3\text{SO}_3)_2$  and the best fit is represented by the solid line in Fig. 4.5a which was generated from the following parameters:  $J = -2.43 \text{ cm}^{-1}$ ,  $g = 2.10$ , ( $F = 0.0216$ ).

The susceptibility data for  $\text{Cu}(\text{pyz})_2(\text{CH}_3\text{SO}_3)_2$  were analysed equally as well using a one-dimensional linear chain model (Section 3.3.4.1); this was explained by the presence of two inequivalent exchange pathways through pyrazine. Spectroscopic evidence indicates that  $\text{Cu}(\text{pyz})(\text{CF}_3\text{SO}_3)_2$  has a structure which may be represented by one of those shown in Fig. 4.1d. From these structures it is clear that there are at least two distinct pathways for magnetic exchange, one route through bridging pyrazine rings and the second route through bridging triflate anions. These pathways are unlikely to be equivalent and indeed, the magnetic properties of the mono(pyrazine) derivative are also successfully represented by the linear chain

model (Eqn. 3.7). The parameters obtained with this model are as follows:  $J = -3.78 \text{ cm}^{-1}$ ,  $g = 2.08$ , ( $F = 0.0126$ ); the best fit is shown as the solid line in Fig. 4.5b. In fact, for  $\text{Cu}(\text{pyz})(\text{CF}_3\text{SO}_3)_2$ , the fit of the magnetic susceptibility data to the one-dimensional model is slightly improved over that for the two-dimensional model as measured by the relative values of  $F$  and judged visually. The similarity between the magnetic properties of  $\text{Cu}(\text{pyz})(\text{CF}_3\text{SO}_3)_2$  and  $\text{Cu}(\text{pyz})_2(\text{CH}_3\text{SO}_3)_2$  suggests that the feature common to both complexes is strongly bridging pyrazine groups along one dimension. This ligand may provide a more facile route for magnetic exchange interactions than other bridging entities (the axial pyrazine group in one case and the triflate anion in the other).

#### 4.3.3.2 Mono(pyrazine) and bis(pyridine)iron(II) complexes

The magnetic susceptibility measurements for compounds of these two types are listed in Appendix IX, Part B. The mono(pyrazine) compounds,  $\text{Fe}(\text{pyz})(\text{CF}_3\text{SO}_3)_2$  and  $\text{Fe}(\text{pyz})(\text{NCO})_2$  exhibit particularly interesting magnetic properties, with both compounds showing strongly temperature-dependent magnetic moments (Fig. 4.6). At room temperature both complexes exhibit a magnetic moment value of approximately 5 B.M., as expected for high-spin iron(II) compounds; whereas, at 4.2 K the magnetic moment value decreases to 0.88 and 2.94 B.M. for the cyanate and triflate derivatives respectively. Both species exhibit a maximum in their magnetic susceptibility data (Figs. 4.7 and 4.8), a clear indication of antiferromagnetic exchange



interactions. The maximum for the cyanate derivative occurs at approximately 38 K indicating a much stronger interaction than in the triflate where the maximum is at the lower temperature of approximately 4.4 K. A further difference between the two magnetic susceptibility curves is that down to the lowest temperature studied the triflate derivative has a susceptibility which decreases and tends to zero; whereas, the susceptibility for the cyanate derivative remains fairly constant below a temperature of approximately 11 K. This low-temperature magnetic behaviour for the cyanate complex may be attributed to the presence of a small amount of material which remains paramagnetic and is not converted to the antiferromagnetic phase. This is suggested by the Mössbauer spectral data (Section 4.3.4.1).

Structural evidence from spectroscopic data (Sections 4.3.1 and 4.3.2) indicates that both complexes possess bridging pyrazine moieties and either bridging triflate or bridging cyanate anions. It is likely that both of these bridging units contribute to some extent to the superexchange between metal centres.

Fig. 4.6 Magnetic Moments vs Temperature for  $\text{Fe}(\text{pyz})(\text{NCO})_2$  and  $\text{Fe}(\text{pyz})(\text{CF}_3\text{SO}_3)_2$

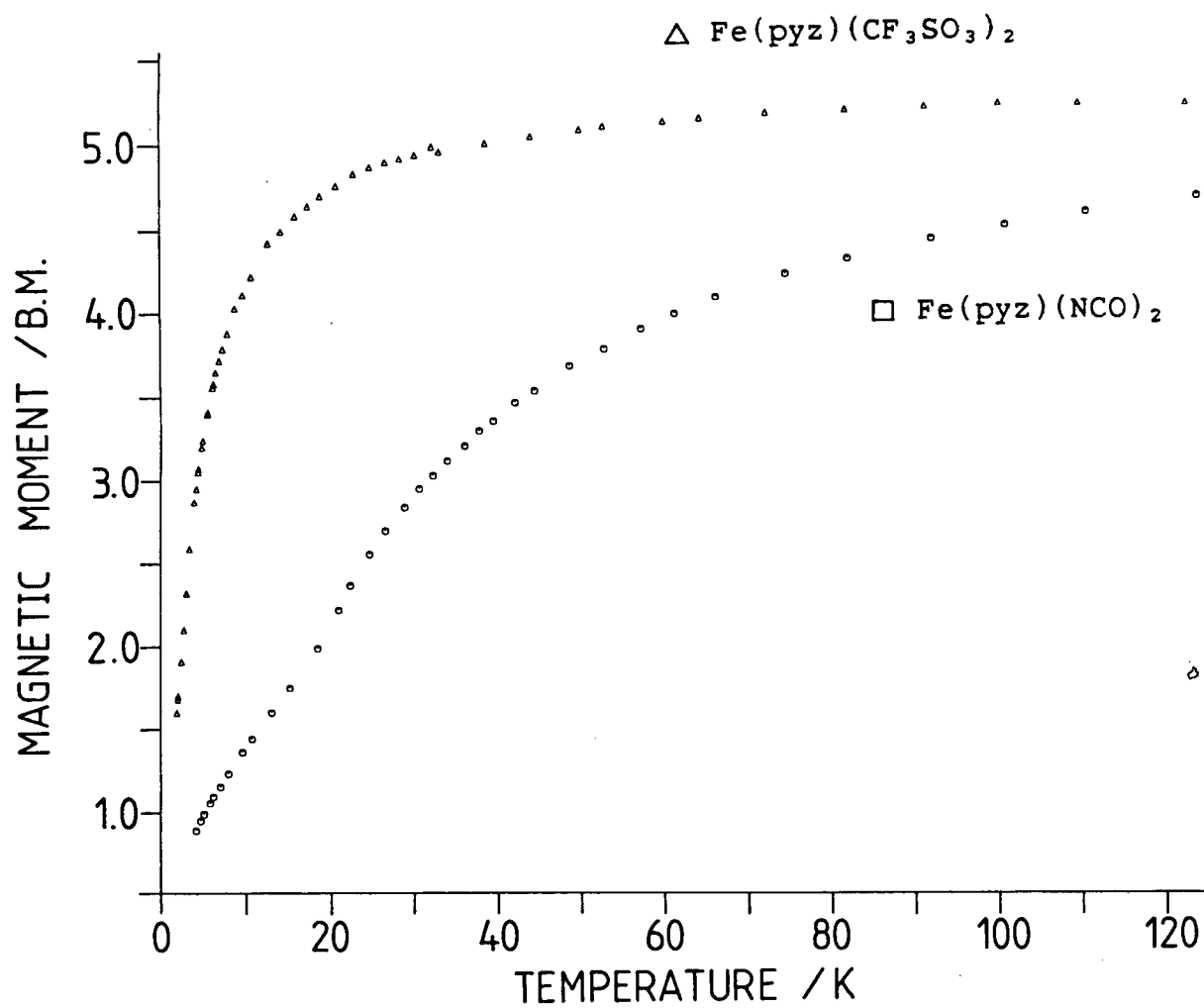


Fig. 4.7 Magnetic Susceptibility vs Temperature for  $\text{Fe}(\text{pyz})(\text{NCO})_2$

a). Weng linear chain model, solid line generated from  $J = -5.18 \text{ cm}^{-1}$ ,  $g = 2.28$

b). Two-dimensional model, solid line generated from  $J = -3.94 \text{ cm}^{-1}$ ,  $g = 2.31$

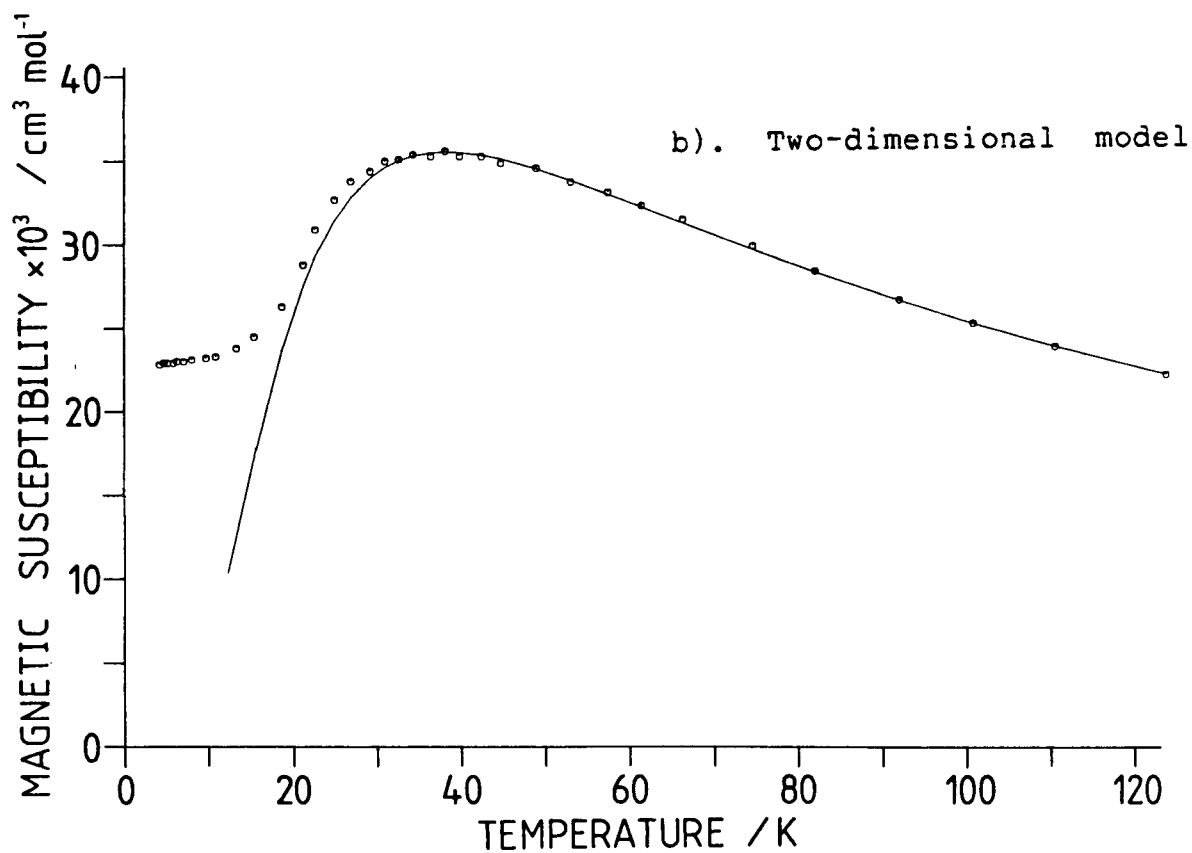
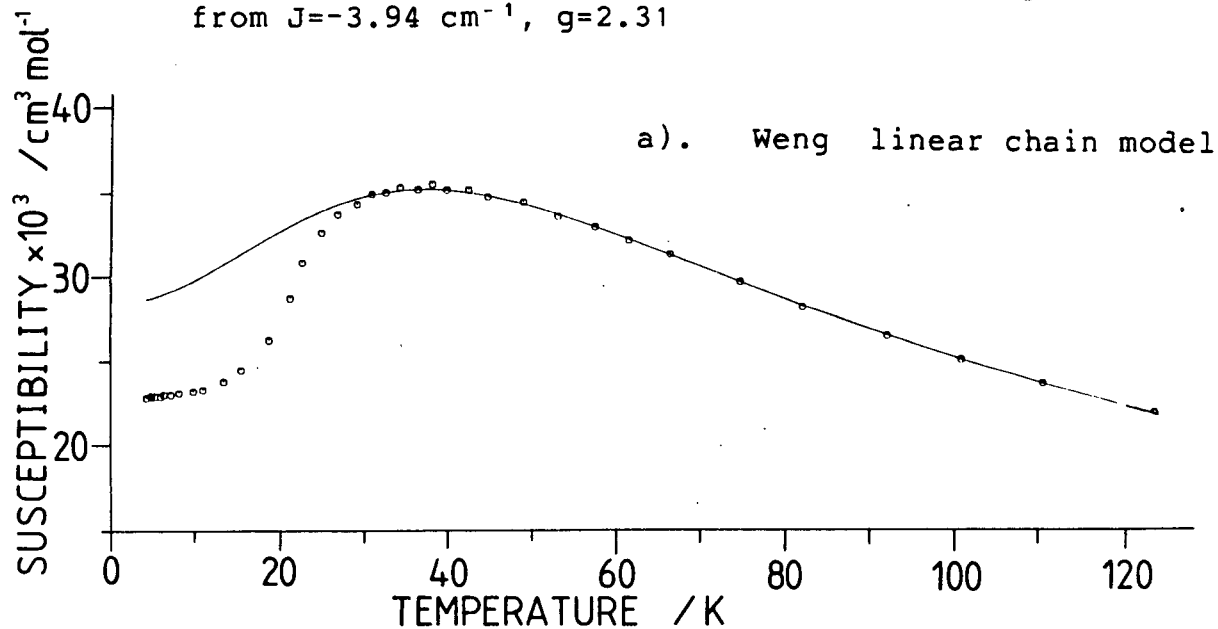
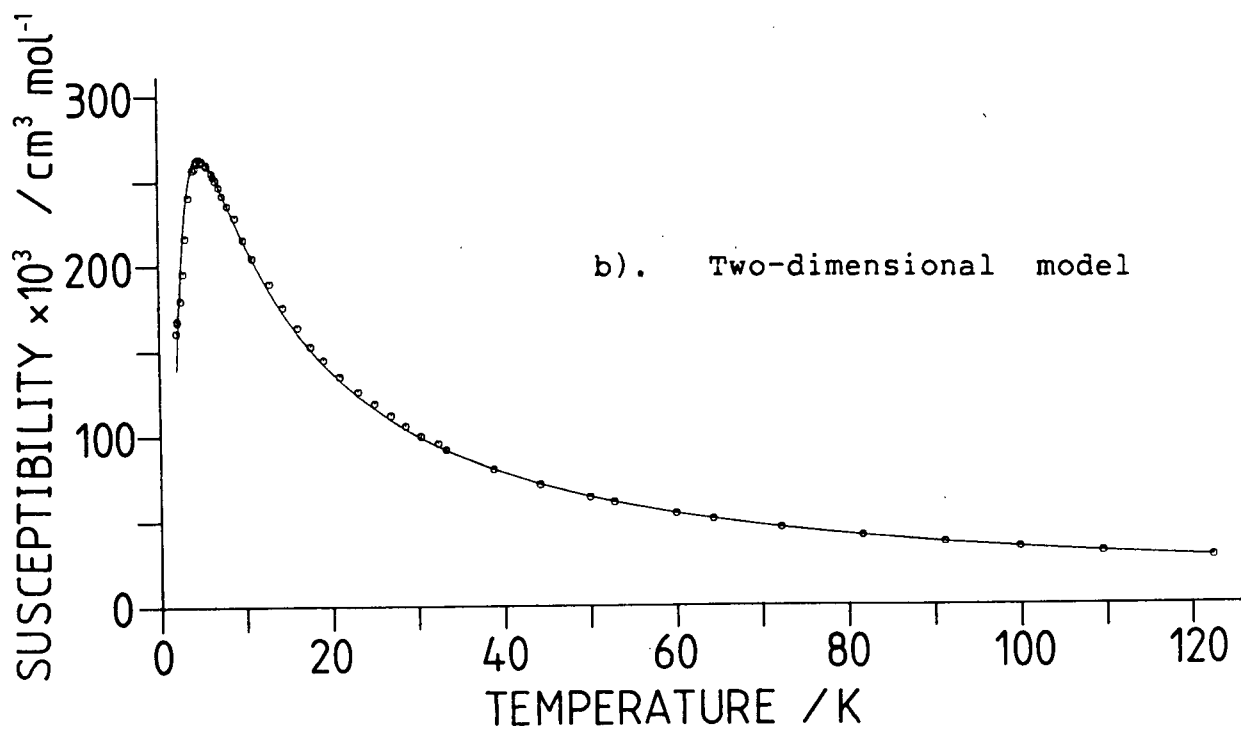
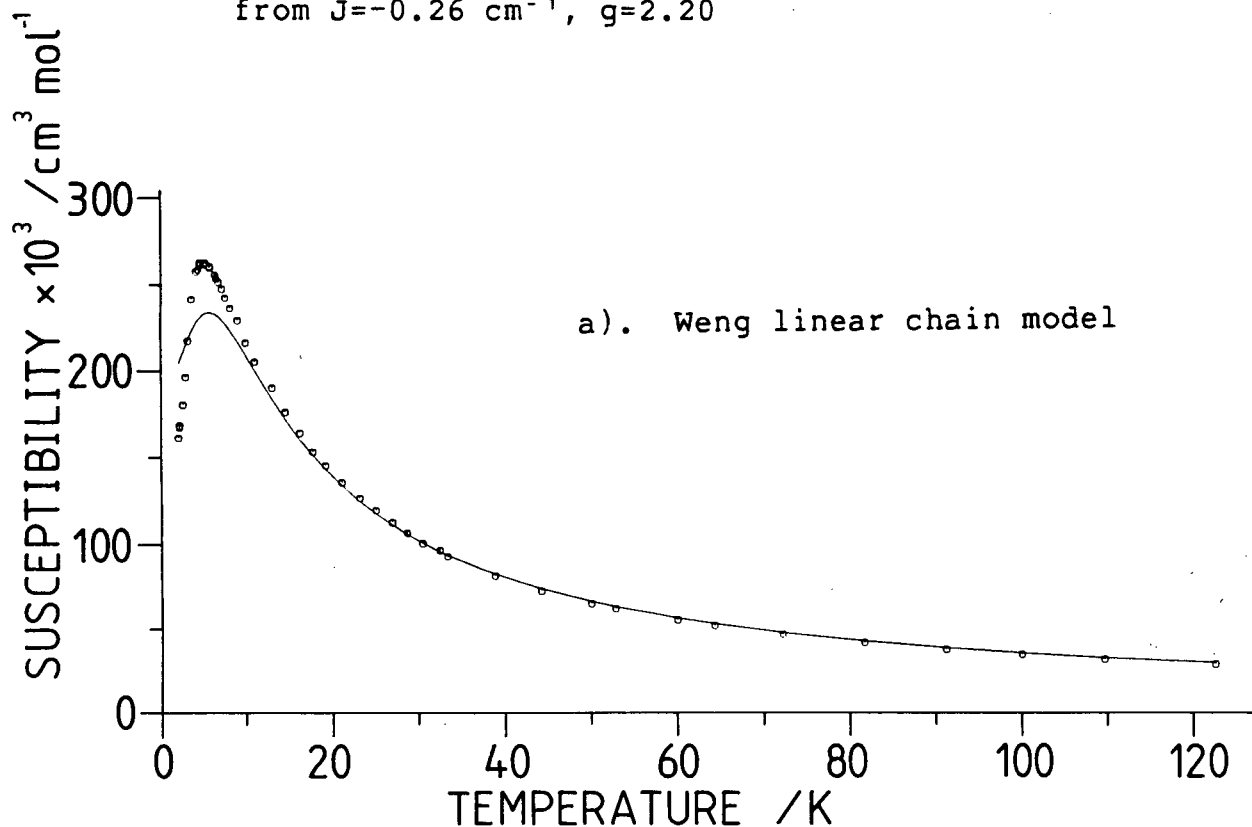


Fig. 4.8 Magnetic Susceptibility vs Temperature for  $\text{Fe}(\text{pyz})(\text{CF}_3\text{SO}_3)_2$

a). Weng linear chain model, solid line generated from  $J = -0.76 \text{ cm}^{-1}$ ,  $g = 2.25$

b). Two-dimensional model, solid line generated from  $J = -0.26 \text{ cm}^{-1}$ ,  $g = 2.20$



The presence of a complex bridging network is likely and this makes the analysis of the susceptibility data rather difficult. The exchange mechanisms are almost certainly different through the pyrazine  $\pi$ -system and through either a sulfonate bridge (O-S-O) or a cyanate bridge (possibly the single nitrogen atom,  $>\text{NCO}$ ). In the extreme case, where one magnetic exchange mechanism is dominant, the magnetic susceptibility may be represented by a one-dimensional linear chain model. In another extreme case, where magnetic exchange proceeds to an equal extent through both bridging ligands then a model which allows for interactions in two dimensions may be more appropriate. From an experimental consideration, Mössbauer spectroscopy (Section 4.3.4.1) demonstrates that both  $\text{Fe}(\text{pyz})(\text{NCO})_2$  and  $\text{Fe}(\text{pyz})(\text{CF}_3\text{SO}_3)_2$  magnetically order and in the presence of long-range three-dimensional interactions any model which allows for interactions between neighbouring centres along a linear chain or throughout a two-dimensional lattice will have limited application.

With these limitations in mind, the magnetic properties of the two compounds were analysed via a linear chain model and a two-dimensional model for  $S=2$  in the isotropic Heisenberg limit. For the anisotropic case, the Ising limit, closed form solutions exist for both parallel and perpendicular susceptibilities for only the  $S=1/2$  linear chains, but these models are of limited application to  $S=2$  systems. Within the Heisenberg limit, two theoretical approximations have been derived for antiferromagnetic linear chain systems which may be applied to

S=2. Wagner and Friedberg<sup>169</sup> have scaled the exact results of Fisher<sup>170</sup> to the series expansion results of Rushbrooke and Wood<sup>171</sup> and obtained the following expression for magnetic susceptibility:

$$\chi_m = \frac{Ng^2\beta^2 S(S+1)}{kT} \cdot \frac{1+U}{1-U} \quad \dots \text{Eqn. 4.1}$$

where  $U = \coth K - 1/K$  and  $K = 2JS(S+1)/kT$ .

The other approximation method is an interpolation scheme developed by Weng.<sup>172</sup> Hiller et al.<sup>173</sup> have generated a series of coefficients to reproduce Weng's numerical results. Accordingly:

$$\chi_m = \frac{Ng^2\beta^2}{kT} \frac{[A+Bx^2]}{[1+Cx+Dx^3]} \quad \dots \text{Eqn. 4.2}$$

where  $x = |J|/kT$ , and for S=2, A=2.000, B=71.938, C=10.482, D=955.56.

The experimental results for both compounds were analysed using these two models. The models produce similarly shaped curves with a rounded maximum. With the J and g values which were tried, the computed curves never gave a satisfactory match to the experimental data over the entire temperature range. Agreement between computed and experimental curves is reasonable above the susceptibility maximum but in the region of the maximum, and at lower temperatures, discrepancies between the two curves become larger. The Weng model was used to generate the solid lines in Figs. 4.7a and 4.8a; the lines were

generated by using the following parameters:

	<u>WENG</u>		
	$-J/\text{cm}^{-1}$	g	F
$\text{Fe}(\text{pyz})(\text{CF}_3\text{SO}_3)_2$	0.76	2.25	0.086
$\text{Fe}(\text{pyz})(\text{NCO})_2$	5.18	2.28	0.158

By using values of J and g which closely resemble those given above, the model based upon the Wagner and Friedberg approach resulted in fits very similar to those shown in Figs. 4.7 and 4.8.

	<u>WAGNER AND FRIEDBERG</u>		
	$-J/\text{cm}^{-1}$	g	F
$\text{Fe}(\text{pyz})(\text{CF}_3\text{SO}_3)_2$	0.84	2.26	0.104
$\text{Fe}(\text{pyz})(\text{NCO})_2$	5.18	2.31	0.158

From the fits it appears that the magnetic properties of these two complexes are not well represented by the linear chain models.

Attempts were made to fit the magnetic susceptibility data for both complexes to the Lines' two-dimensional model which was used to represent the magnetic properties of  $\text{Cu}(\text{pyz})_2(\text{CH}_3\text{SO}_3)_2$  (Section 3.3.4.1) and  $\text{Fe}(\text{pyz})_2(\text{NCS})_2$  (Section 3.3.4.3). The best fit to the cyanate data is shown in Fig. 4.7 where the solid line was generated using the following parameters:  $J=-3.94$

$\text{cm}^{-1}$ ,  $g=2.31$ . This fit is not entirely adequate; the calculated magnetic susceptibility values diverge considerably from the experimental data especially at temperature below 35 K. This may be attributed to either an inadequacy of the model or its inapplicability to iron(II) complexes. The model ignores long-range three-dimensional magnetic ordering which is not negligible in  $\text{Fe}(\text{pyz})(\text{NCO})_2$  as Mössbauer spectroscopy indicates a transition to a magnetically-ordered state at 27 K (Section 4.3.4.1).

For  $\text{Fe}(\text{pyz})(\text{CF}_3\text{SO}_3)_2$ , the agreement between the experimental and calculated magnetic susceptibility data from the Lines' two-dimensional model is excellent. The solid line through the data points (Fig. 4.8) represents the best fit using the following parameter values:  $J=-0.26 \text{ cm}^{-1}$  and  $g=2.20$  ( $F=0.0381$ ). This may reflect the two-dimensional nature of the exchange interaction in  $\text{Fe}(\text{pyz})(\text{CF}_3\text{SO}_3)_2$ .

The success of the two-dimensional model in representing the magnetic susceptibility data for these two complexes may be a result of their proposed structures. For both complexes bridging anions may give rise to a one-dimensional linear chain; these chains are then cross-linked through pyrazine (Fig. 4.1d(i)). Exchange interactions have been observed previously in  $\text{Fe}(\text{py})_2(\text{NCO})_2$ .<sup>67</sup> The bis(pyridine) complex and  $\text{Fe}(\text{pyz})(\text{NCO})_2$  are proposed to contain cyanate ligands which link metal centres by using a one atom bridge, i.e., the single nitrogen. For  $\text{Fe}(\text{py})_2(\text{NCO})_2$  this results in a linear chain structure (Fig. 4.1c(i)) and the coordination sphere around the metal is



completed by nitrogen donors from pyridine groups. In spite of the structural similarities between these two complexes caused by the presence of bridging anionic ligands, their magnetic properties are strikingly different. The present study indicates that  $\text{Fe}(\text{pyz})(\text{NCO})_2$  is antiferromagnetic; whereas, the earlier magnetic susceptibility study<sup>6,7</sup> showed that  $\text{Fe}(\text{py})_2(\text{NCO})_2$  is ferromagnetic. The lack of X-ray structural data for both complexes makes it difficult to explain the pronounced difference between their magnetic properties, however, the following rationale is put forward. Since  $\text{Fe}(\text{py})_2(\text{NCO})_2$  is ferromagnetic, the orbital overlap through the nitrogen atom of the bridging cyanate group must be of an orthogonal nature. A similar ferromagnetic interaction along the chains in  $\text{Fe}(\text{pyz})(\text{NCO})_2$  might be expected. The chains in the pyridine complex are effectively isolated; for the pyrazine complex, however, adjacent chains are linked through bridging pyrazine. The  $\pi$ -system of pyrazine is likely to present an antiferromagnetic exchange pathway, and hence, the neighbouring chains are coupled in an antiferromagnetic sense, resulting in a net antiferromagnetic interaction.

The results of the magnetic measurements for  $\text{Fe}(\text{py})_2(\text{CF}_3\text{SO}_3)_2$ ,  $\text{Fe}(\text{pyz})(\text{p-CH}_3\text{C}_6\text{H}_4\text{SO}_3)_2$ , and its bis(methanol) solvate, and  $\text{Fe}(\text{pyz})\text{Cl}_2$  are tabulated in Appendix IX, Part B. The magnetic moment data for these complexes all decrease with decreasing temperature. None of these complexes, however, exhibits a maximum in the magnetic susceptibility data and hence conclusive evidence for magnetic interactions is lacking. The

absence of, or much weaker degree of, magnetic exchange in these compounds, makes for an interesting comparison with complexes such as  $\text{Fe}(\text{pyz})(\text{NCO})_2$  and  $\text{Fe}(\text{pyz})(\text{CF}_3\text{SO}_3)_2$  which exhibit significant exchange effects. For example, it may be expected that the structures of the mono(pyrazine)iron(II) cyanate and chloride derivatives would be similar. Spectroscopic evidence suggests both complexes possess an  $\text{FeN}_2\text{X}_4$  chromophore and that bridging anionic ligands as well as bridging pyrazine groups are present. Indeed, there are numerous examples of complexes in which bridging halide anions act as efficient agents for the propagation of magnetic exchange interactions<sup>161</sup> and it is surprising that such interactions are undetected in  $\text{Fe}(\text{pyz})\text{Cl}_2$  even at temperatures as low as 2 K.

Spectroscopic evidence also indicates a close structural relationship between  $\text{Fe}(\text{pyz})(\text{p-CH}_3\text{C}_6\text{H}_4\text{SO}_3)_2$  and  $\text{Fe}(\text{pyz})(\text{CF}_3\text{SO}_3)_2$ , i.e., bridging pyrazine and bidentate bridging anionic ligands. The magnetic properties of the two materials, however, are quite distinct. The p-tosylate derivative exhibits a weakly temperature-dependent magnetic moment in comparison to the relatively greater temperature-dependent moment exhibited by the triflate derivative. Due to lack of X-ray structural evidence for these complexes it is difficult to rationalise these differences but a possible explanation may lie in the more weakly basic nature of the triflate relative to the p-tosylate anion. This could result in a stronger iron-pyrazine interaction in the triflate derivative and therefore a more significant exchange effect via pyrazine.

The four iron(II) triflate derivatives prepared in this study provide for an interesting comparison (Table 4.1).

Table 4.1 Selected Magnetic Moment Data for Iron(II) Triflate Complexes

COMPOUND	TEMP/K	MAGNETIC MOMENT/B.M.
$\text{Fe}(\text{py})_4(\text{CF}_3\text{SO}_3)_2$	300	5.38
	4.2	4.54
$\text{Fe}(\text{py})_2(\text{CF}_3\text{SO}_3)_2$	300	5.54
	4.2	3.61
$\text{Fe}(\text{pyz})_2(\text{CF}_3\text{SO}_3)_2 \cdot \text{CH}_3\text{OH}$	300	5.31
	4.2	3.34
$\text{Fe}(\text{pyz})(\text{CF}_3\text{SO}_3)_2$	300	5.42
	4.2	3.04

For each compound the magnitude of the magnetic moment at 300 K lies in the narrow range 5.3-5.5 B.M.; whereas, at 4.2 K a significant spread in magnetic moment values occurs. At 4.2 K the magnetic moment values are in the order:  $\text{Fe}(\text{py})_4(\text{CF}_3\text{SO}_3)_2 > \text{Fe}(\text{py})_2(\text{CF}_3\text{SO}_3)_2 > \text{Fe}(\text{pyz})_2(\text{CF}_3\text{SO}_3)_2 \cdot \text{CH}_3\text{OH} > \text{Fe}(\text{pyz})(\text{CF}_3\text{SO}_3)_2$ . This order indicates an increase in antiferromagnetic interactions from the tetrakis(pyridine) complex to the mono(pyrazine) complex which appears to be in agreement with the proposed nature of the bridging system in each complex, i.e., the lack of a bridging network in  $\text{Fe}(\text{py})_4(\text{CF}_3\text{SO}_3)_2$ , bridging triflate only in  $\text{Fe}(\text{py})_2(\text{CF}_3\text{SO}_3)_2$ , bridging pyrazine in  $\text{Fe}(\text{pyz})_2(\text{CF}_3\text{SO}_3)_2 \cdot \text{CH}_3\text{OH}$  and both bridging pyrazine and bridging triflate anions in  $\text{Fe}(\text{pyz})(\text{CF}_3\text{SO}_3)_2$ . No magnetic interactions

are observed in the complex which lacks bridging ligands and the magnetic interaction increases with the increasing number of bridging ligands; the combination of bridging triflate and bridging pyrazine groups providing the most facile magnetic exchange pathway in this series of complexes.

#### 4.3.4 Mössbauer Spectroscopy

In all cases Mössbauer spectra were recorded at liquid nitrogen and room temperatures and the results are given in Appendix X, Parts A and B. Because of the presence of antiferromagnetic interactions in  $\text{Fe}(\text{pyz})(\text{NCO})_2$  and  $\text{Fe}(\text{pyz})(\text{CF}_3\text{SO}_3)_2$  additional spectra were measured from temperatures slightly above the temperature of the susceptibility maximum down to 4.2 and 1.6 K respectively. For the cyanate derivative, the analysis of the spectra provided substantial evidence for structure; however, such a treatment for the triflate derivative has still to be performed.

At liquid nitrogen temperature, the bis(pyridine) and mono(pyrazine) complexes exhibit isomer shift values in the range of 1.0-1.3 mm s<sup>-1</sup> as expected for octahedral high-spin iron(II) complexes. Small differences in isomer shift values are observed for these complexes which may be correlated with the nature of the metal chromophore. For example, the triflate derivatives,  $\text{Fe}(\text{py})_2(\text{CF}_3\text{SO}_3)_2$  and  $\text{Fe}(\text{pyz})(\text{CF}_3\text{SO}_3)_2$  have isomer shifts which are slightly higher than that of  $\text{Fe}(\text{py})_4(\text{CF}_3\text{SO}_3)_2$ . This increase probably arises from the more ionic bonding in the first two complexes which contain an  $\text{FeN}_2\text{O}_4$  chromophore compared to an  $\text{FeN}_4\text{O}_2$  chromophore in  $\text{Fe}(\text{py})_4(\text{CF}_3\text{SO}_3)_2$ . A similar increase in isomer shift is observed for the p-tosylate derivatives.

#### 4.3.4.1 Low-temperature Mössbauer studies on $\text{Fe}(\text{pyz})(\text{NCO})_2$ and $\text{Fe}(\text{pyz})(\text{CF}_3\text{SO}_3)_2$

The magnetic susceptibility results for both compounds (Section 4.3.3) are characteristic of antiferromagnetic materials. Low-temperature Mössbauer spectra were recorded to determine the extent of any three-dimensional interactions. For  $\text{Fe}(\text{pyz})(\text{NCO})_2$ , the low-temperature (4.2–31.4 K) Mössbauer spectra are shown in Fig. 4.9. The spectrum at 31.4 K is essentially the same as that measured at 78 K. There is some slight temperature-independent asymmetry in the intensity of the two lines of the quadrupole doublet at 78 K which persists down to 31.4 K; this is attributed to a texture effect arising from a preferred orientation of the crystallites in the absorber. Between 31.4 and 27.0 K the lines of the quadrupole doublet broaden asymmetrically; this can be seen from the linewidths and the intensity ratios given in Table 4.2. This line broadening is evidence for slow paramagnetic relaxation, probably as a result of residual short-range correlations between metal centres. Between 27.0 and 26.8 K resolved magnetic hyperfine splitting becomes apparent as a result of long-range three-dimensional ordering. From this observation it is concluded that the Neel temperature is within this temperature range. At temperatures lower than  $T_N$  the quadrupole doublet persists and the spectra consist of two components, a paramagnetic phase and a magnetically-ordered phase.

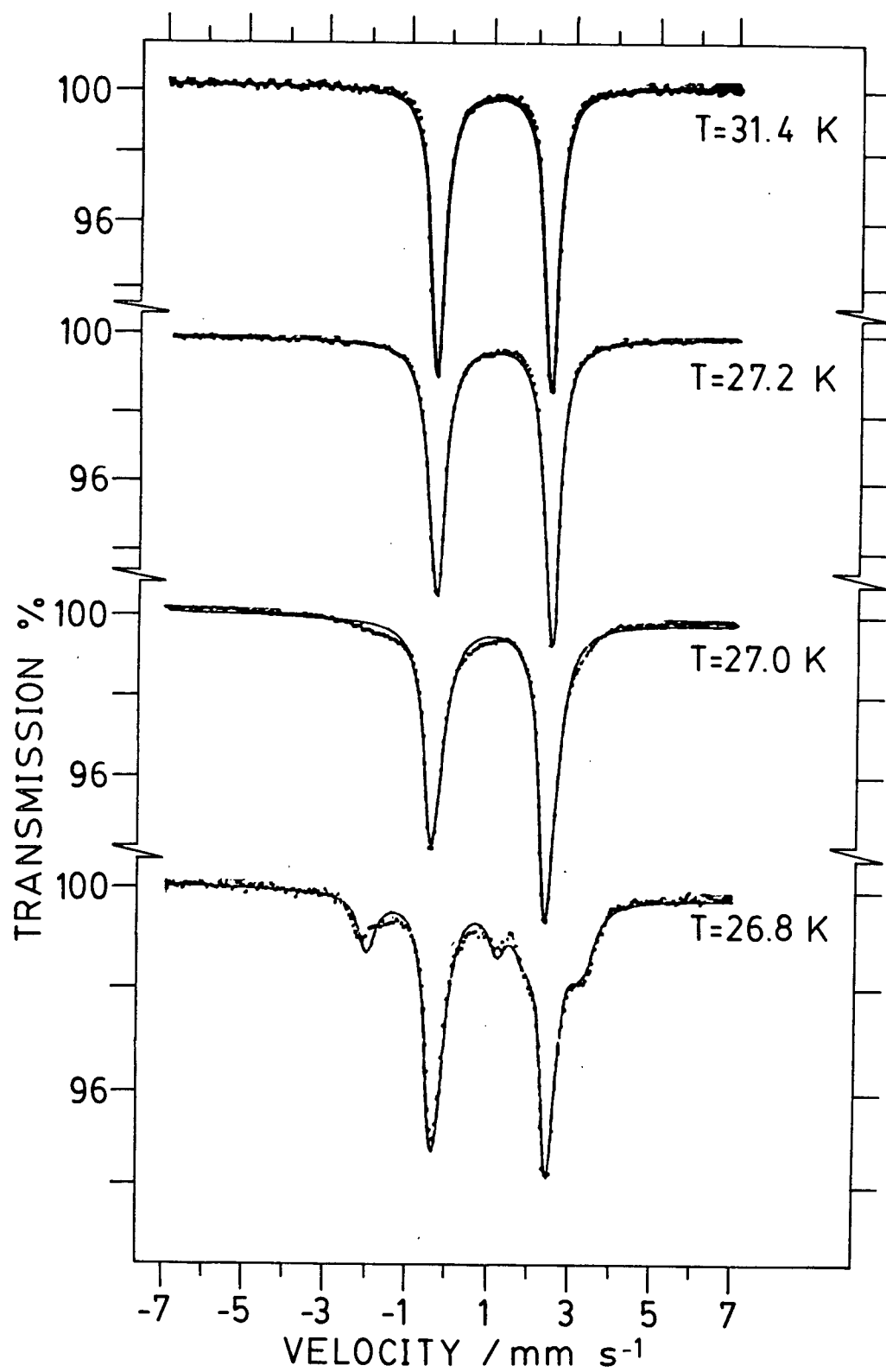
Fig. 4.9 Low-Temperature Mössbauer Spectra of  $\text{Fe}(\text{pyz})(\text{NCO})_2$ 

Fig. 4.9 Continued

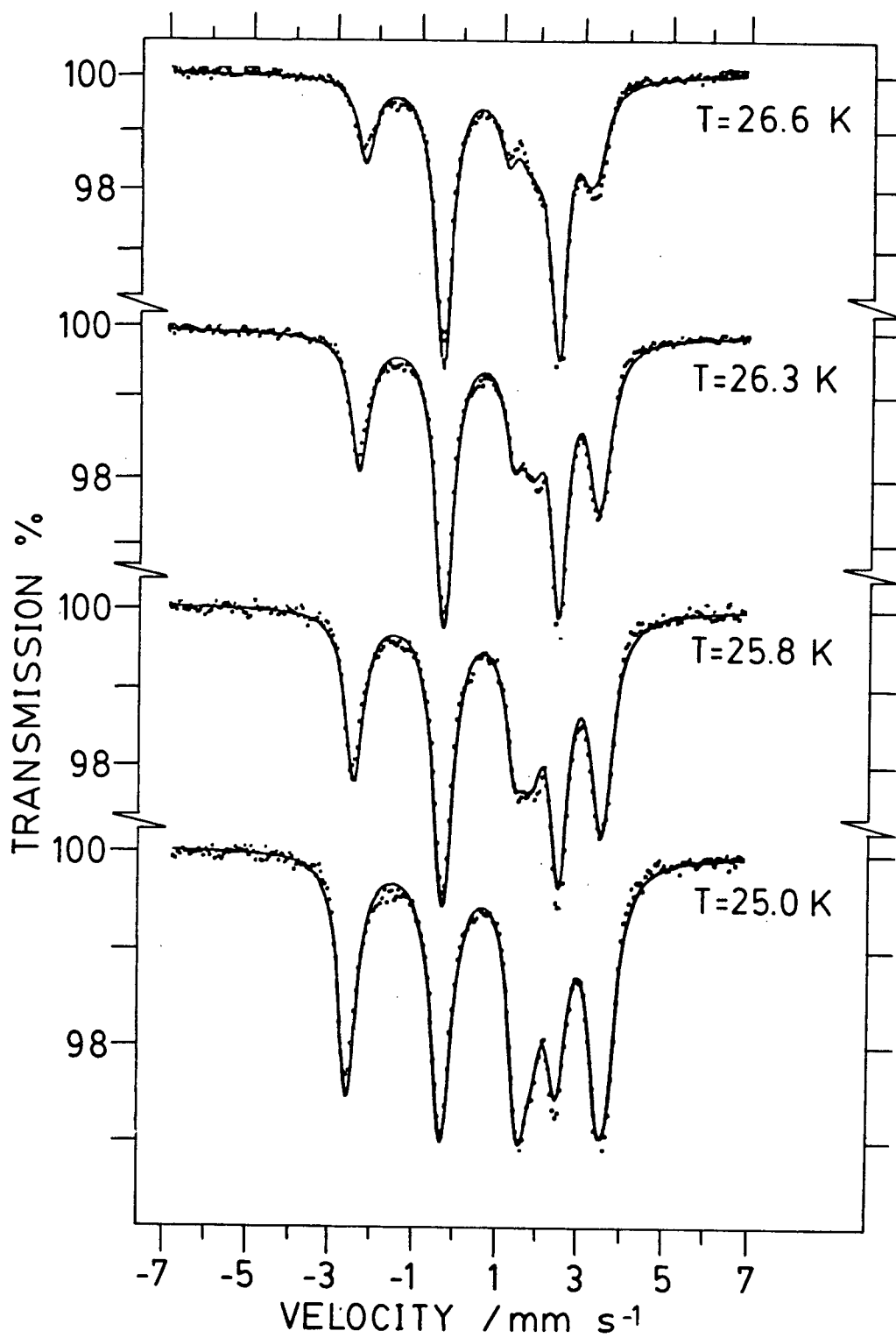




Fig. 4.9 Continued

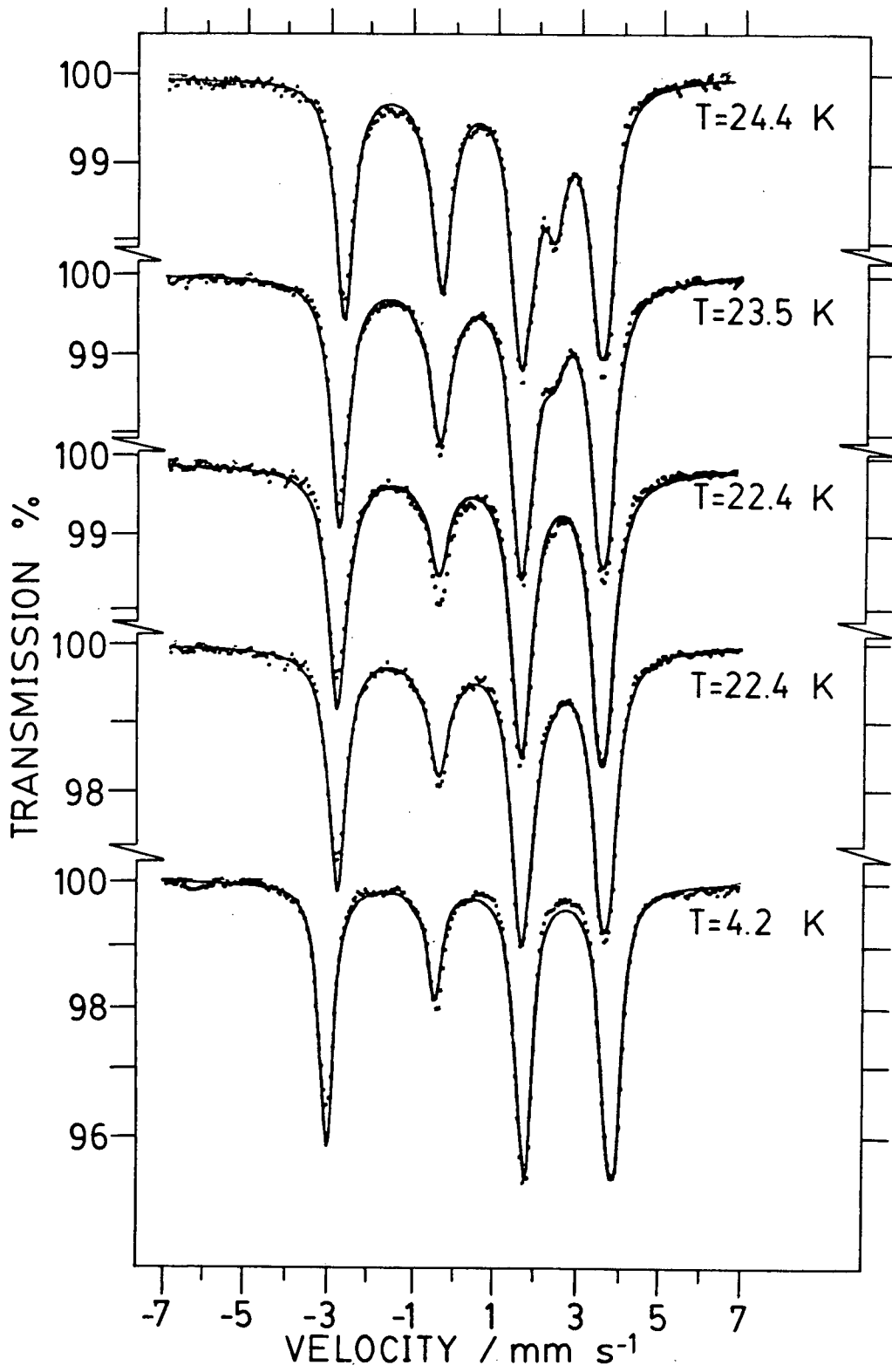


Table 4.2 Linewidths and Intensities (27.0-31.4 K) for  $\text{Fe}(\text{pyz})(\text{NCO})_2$

TEMP/K	$\Gamma_1$ <sup>1</sup>	$\Gamma_2$	$I_1/I_2$
27.0	0.28	0.25	0.750
27.2	0.24	0.21	0.802
27.4	0.26	0.23	0.845
31.4	0.20	0.20	0.917

1). Linewidths are in units of  $\text{mm s}^{-1}$  and subscripts 1 and 2 refer to the low and high velocity lines respectively

As the temperature is decreased, the disappearance of the paramagnetic component can be seen by the decrease in the intensity of the line at approximately  $2.5 \text{ mm s}^{-1}$ . At a temperature of 22.4 K ( $T/T_N=0.83$ ) the intensity of this line has decreased to such an extent that only a shoulder is seen to the high-velocity side of the peak centred at approximately  $1.7 \text{ mm s}^{-1}$ . Below 22.4 K, the paramagnetic phase appears to have been converted entirely to the antiferromagnetically-ordered state and the spectra are as a result of just this one component. This superparamagnetic behaviour could arise from the presence of small domain clusters which may arise during the rapid precipitation of the complex.

The model used to describe the Mössbauer spectra of  $\text{Fe}(\text{pyz})_2(\text{NCS})_2$  (Section 3.3.5.3) was also employed to analyse the Mössbauer spectra of the cyanate compound. For  $\text{Fe}(\text{pyz})(\text{NCO})_2$  the Mössbauer spectra in the temperature range of

22-27 K were computed assuming one antiferromagnetic component and one paramagnetic component, the relative amounts of the two components used to fit the spectra are related by the ratio  $I_{\text{afm}}/I_{\text{tot}}$  (Table 4.3). Below 22.4 K, this ratio is unity, indicating the presence of only the ordered phase; on the other hand, the susceptibility data (Section 4.3.2.2) suggest that a small amount of paramagnetic phase persists to below 11 K. It appears that magnetic susceptibility measurements are a more sensitive means of detecting such "impurities". At 22.4 K, the effect of ignoring any paramagnetic component may be seen. At this temperature the spectrum was fitted in two different ways. The first method assumes the presence of only the antiferromagnetic phase; whereas, the second fit takes into account both components. It can be seen that the second fit is the better of the two.

All spectra at  $T \leq 27.0$  K gave good fits with the following parameters:

$$\begin{array}{ll}
 \delta = 1.17 \pm 0.01 \text{ mm s}^{-1} & \Delta E_{\text{q}} = +2.78 \pm 0.02 \text{ mm s}^{-1} \\
 \Gamma = 0.23 \pm 0.02 \text{ mm s}^{-1} & \eta = 0.44 \pm 0.03 \\
 \theta = 90 \pm 2^\circ & \phi = 90 \pm 5^\circ
 \end{array}$$

Table 4.3 Internal Hyperfine Field and Intensity Ratios<sup>1</sup> for  
 $\text{Fe}(\text{pyz})(\text{NCO})_2$

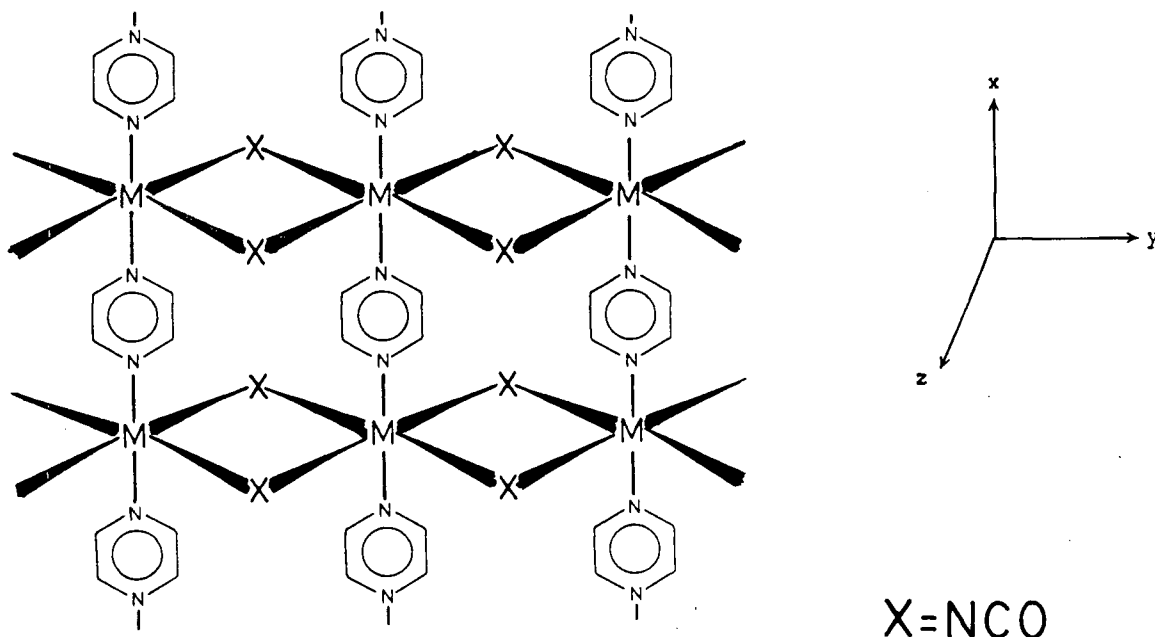
Temp/K	$H_{\text{int}}/\text{T}$	$I_{\text{afm}}/I_{\text{tot}}$
4.2	17.9	1.000
18.2	17.5	1.000
22.4	16.7	0.952
23.5	16.2	0.893
24.4	15.7	0.813
25.0	15.1	0.722
25.4	14.7	0.657
25.8	14.3	0.595
26.3	13.8	0.522
26.6	12.7	0.399
26.8	11.6	0.306
27.1	6.8	0.163

1)  $I_{\text{afm}}$  represents the fraction of the sample which is in the antiferromagnetic phase

The internal hyperfine field,  $H_{\text{int}}$  as a function of temperature is given in Table 4.3. From a consideration of these values several important conclusions were drawn concerning the structure of  $\text{Fe}(\text{pyz})(\text{NCO})_2$ . Spectroscopic evidence suggests that this cyanate complex contains both bridging anions and bridging pyrazine and possible structures are represented by those shown in Fig. 4.1d. If the structure were as in Fig. 4.1(d) (ii), then by analogy with  $\text{Fe}(\text{pyz})_2(\text{NCS})_2$ , an axially symmetric E.F.G. would be expected which is certainly not the case for the cyanate species ( $\eta=0.44$ ), and also the angle  $\phi$  would be expected to be indeterminate; whereas, the simulated spectra require that this angle be close to  $90^\circ$ . On the other hand, for the structure represented by that shown in Fig. 4.1d (i), one can put forward an interpretation of the parameters that is plausible. A not unreasonable choice of E.F.G. axis

system is shown for this structure in Fig. 4.10.

Fig. 4.10 Possible E.F.G. Axis System for  $\text{Fe}(\text{pyz})(\text{NCO})_2$

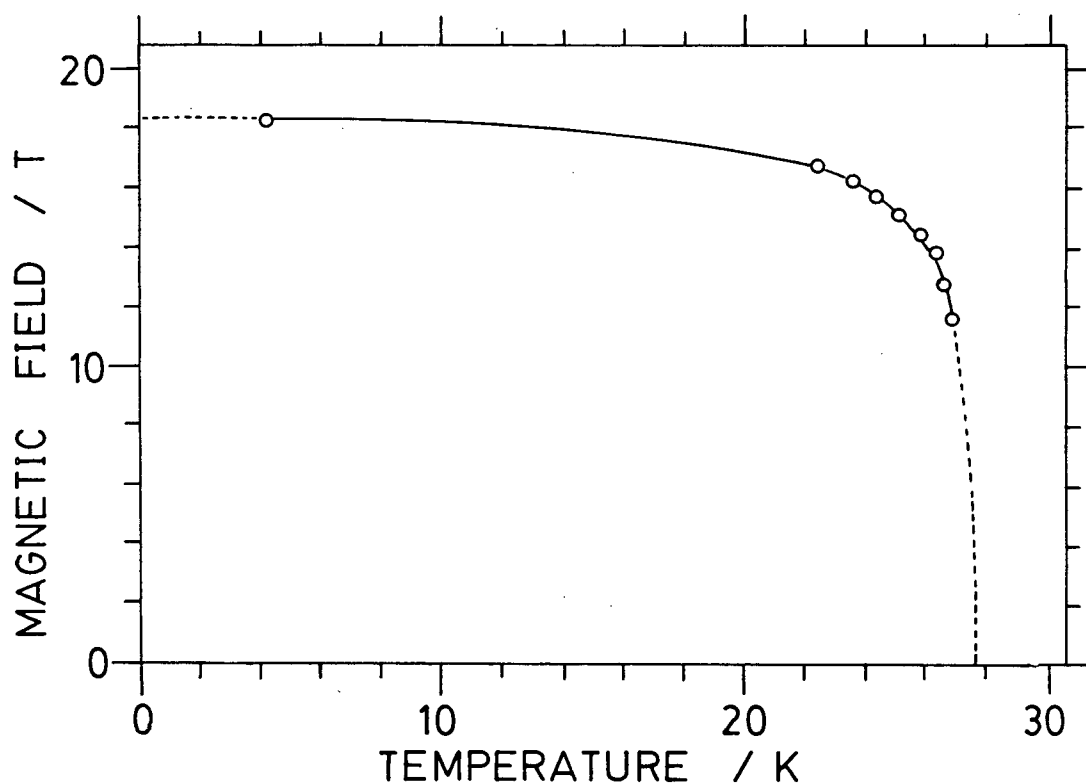


The  $xy$ -plane of the E.F.G. axis system is in the plane of the paper and the  $z$ -axis is normal to this plane. The experimental result gives  $e^2qQ > 0$ ,  $\eta = 0.44$  and  $\theta$  and  $\phi$  approximately  $90^\circ$ , so that  $H_{\text{int}}$  is parallel to  $V_{yy}$ . From the sign and magnitude of  $e^2qQ$  and the magnitude of  $\eta$ , it is clear that an axially compressed structure is required and that the  $x$ - and  $y$ -directions must be inequivalent. The structure (Fig. 4.10) would fulfill these two requirements if the  $\text{Fe-N}(\text{anion})$  bonds were shorter than the  $\text{Fe-N}(\text{pyz})$  bonds. The observation that  $H_{\text{int}}$  is parallel to  $V_{yy}$  indicates that the spins lie close to this axis which indicates that the exchange coupling is stronger through the cyanate ligands than through the pyrazine rings

which is not unreasonable in view of the fact that magnetic exchange interactions through the pyrazine  $\pi$ -system are usually weak; whereas, through the single nitrogen atom of the cyanate anion they are likely to be significantly stronger.

The hyperfine field at the iron nucleus (Table 4.3) is plotted as a function of temperature (Fig 4.11).

Fig. 4.11 Hyperfine Field vs Temperature for  $\text{Fe}(\text{pyz})(\text{NCO})_2$



The hyperfine field saturates rapidly below 27.0 K and  $H_{\text{int}}$  at 0 K is found, by extrapolation, to be approximately 18.3 T. The temperature dependence of the internal hyperfine field provides support for the two-dimensional nature of the exchange interaction. In the critical region, the sublattice magnetisation,  $M(T)$ , varies in the following way:<sup>174</sup>

$$M(T) = M(0)D(1-T/T_N)^\beta \quad \dots \text{Eqn. 4.3}$$

where  $\beta$  is the critical exponent,  $D$  is a reduction factor and  $M(0)$  is the magnetisation at 0 K. If one assumes that  $M(T)$  is proportional to the internal field one can replace  $M$  by  $H_{\text{int}}$ . A plot of  $\ln(H_{\text{int}}/H(0))$  versus  $\ln(1-T/T_N)$  should result in a straight line whose slope is  $\beta$ . In the present study, such a log-log plot in the temperature range of 22-27 K gives a straight line with a slope of 0.13. Theoretical estimates<sup>175</sup> have been made for the value of  $\beta$ ; for example, for a three dimensional Heisenberg model a  $\beta$  value of 0.333 has been calculated and for a two-dimensional Ising model  $\beta=0.125$ . There have been no theoretical estimates of  $\beta$  for either the two-dimensional Heisenberg or the three-dimensional Ising model. The value of  $\beta$  of 0.13 found in the present study, is close to that predicted by the two-dimensional model and indicates that  $\text{Fe}(\text{pyz})(\text{NCO})_2$  may be regarded as a two-dimensional antiferromagnet even in the ordered phase.

The magnitude of the internal magnetic hyperfine field is not unreasonable when one considers the factors which constitute

$H_{\text{int}}$  (Eqn. 3.15). For high-spin iron(II)  $\langle S \rangle = 2$  and thus the expected contribution from the Fermi contact term,  $H_F$ , is approximately 44.0 T. The orbital contribution,  $H_1$ , is expected to oppose  $H_F$  and to be relatively small in view of the near spin-only magnetic moment and the orbital singlet ground term of the complex. The dipolar contribution,  $H_{\text{dip}}$ , has been assumed to be appreciable for complexes with a large electric field gradient and as for  $H_1$  usually has the opposite sign to  $H_F$ . Thus the value of  $H_{\text{int}}$  is expected to be somewhat reduced from the Fermi contact value primarily by the dipolar contribution and to a lesser extent by the orbital contribution. This is as observed and the  $H_{\text{int}}$  value at 4.2 K is 18.3 T.

Low-temperature (4.2-1.6 K) Mössbauer spectra for  $\text{Fe}(\text{pyz})(\text{CF}_3\text{SO}_3)_2$  are shown in Fig. 4.12. The spectrum at 4.2 K shows considerable line broadening and asymmetry which may be attributed to either texture effects and/or the effects of spin relaxation. Between 3.80 and 3.70 K the lines show further broadening and there is evidence for the development of a magnetic hyperfine pattern as magnetic ordering sets in. The Neel temperature is taken to be in this temperature range. Below 3.70 K, the spectra clearly show the combined effects of magnetic and quadrupole interactions. At the present time only a limited attempt has been made to fit the spectra. A preliminary fit of the spectrum at 1.60 K is shown in Fig. 4.13. The fit, represented by the solid line, is not totally satisfactory, especially with regard to line intensities, but this may also be due to intermediate spin-lattice relaxation



rates. The values which were used to generate the fit are as follows:

$$\begin{array}{ll}
 \delta = 1.31 \text{ mm s}^{-1} & \Delta E_q = +3.33 \text{ mm s}^{-1} \\
 \Gamma = 0.25 \text{ mm s}^{-1} & \\
 \theta = 77^\circ & \phi \text{ indeterminate} \\
 H_{\text{int}} = 25 \text{ T} & \eta = 0
 \end{array}$$

The values of  $\theta$ ,  $\phi$  and  $\eta$  are significantly different from those for  $\text{Fe}(\text{pyz})(\text{NCO})_2$ . The values of  $\eta$  and  $\phi$  indicate an effective axial E.F.G. and the equivalence of the x- and y-axes; presumably  $V_{zz}$  lies along the N-Fe-N axis. The spins are then canted away from this axis by  $77^\circ$  towards the xy-plane. This indicates that the strength of the magnetic interaction, whether it is through pyrazine or O-S-O bridges, is not sufficiently strong to align the spins in the xy-plane or along the N-Fe-N axis.

Fig. 4.12 Low-Temperature Mössbauer Spectra of  $\text{Fe}(\text{pyz})(\text{CF}_3\text{SO}_3)_2$

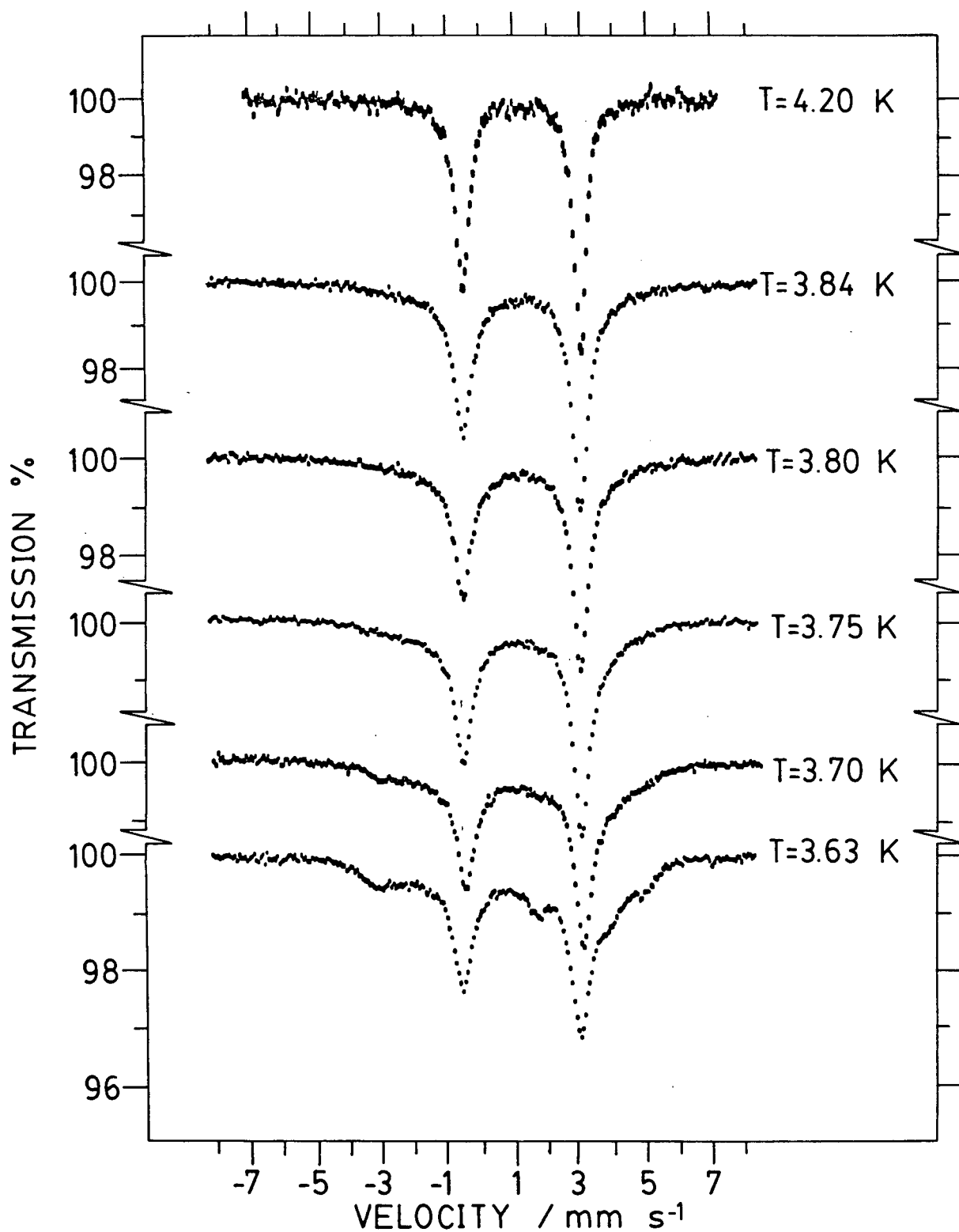


Fig. 4.12 Continued

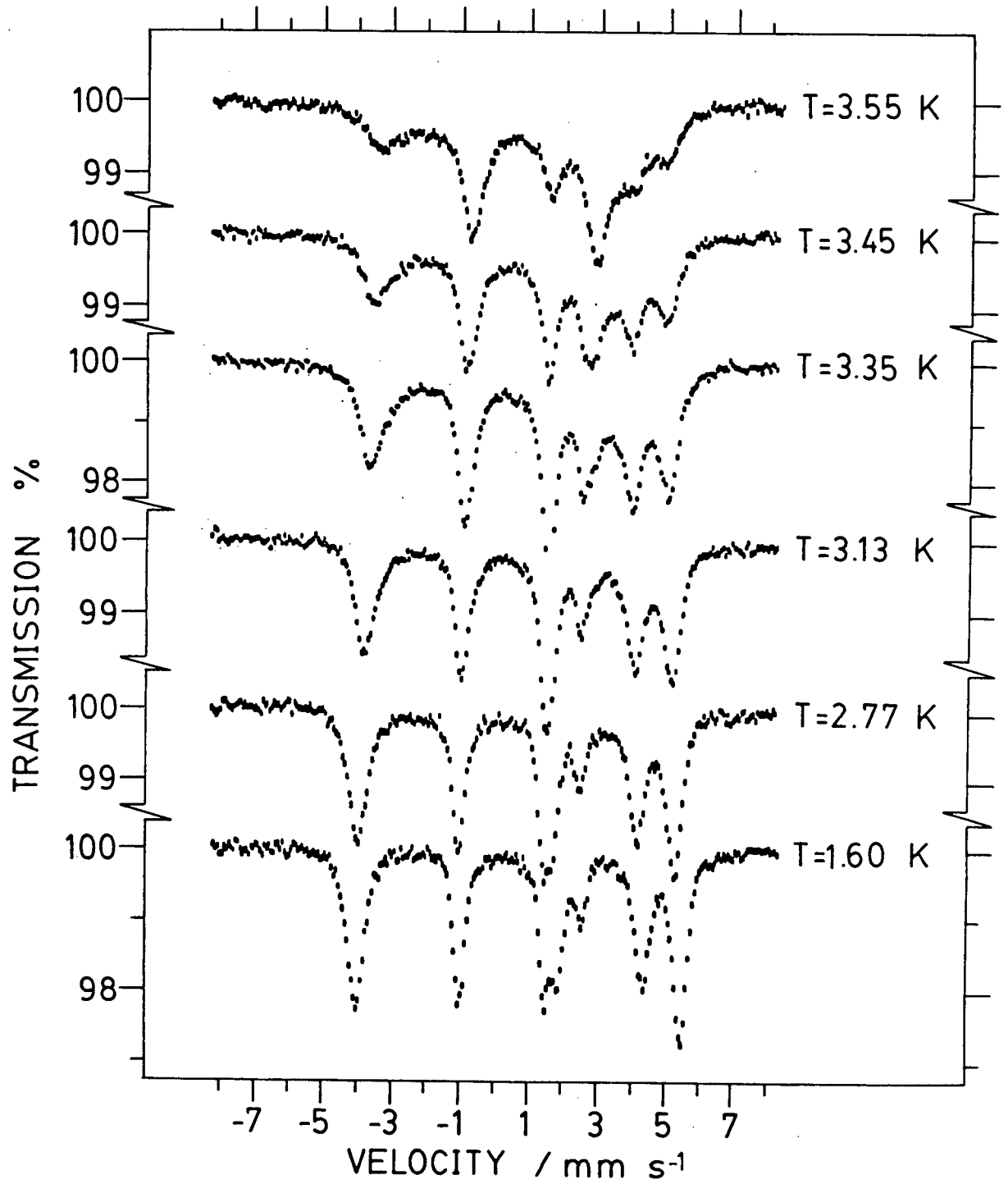
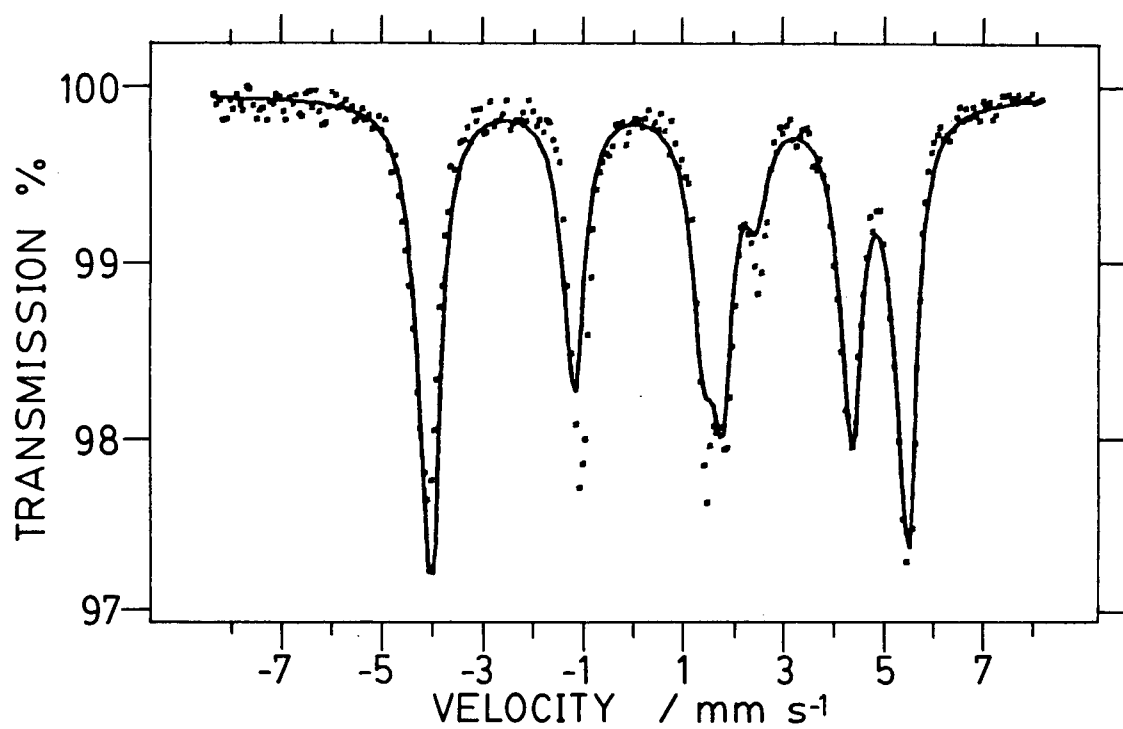


Fig. 4.13 Mössbauer Spectrum of  $\text{Fe}(\text{pyz})(\text{CF}_3\text{SO}_3)_2$  at 1.60 K



#### 4.3.5 Thermal Studies

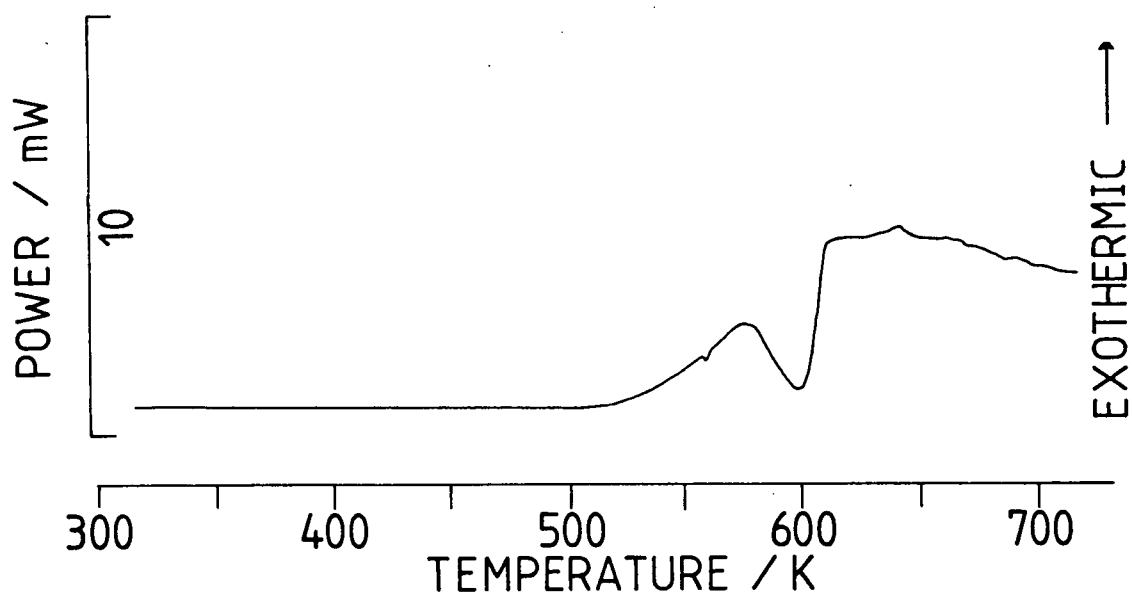
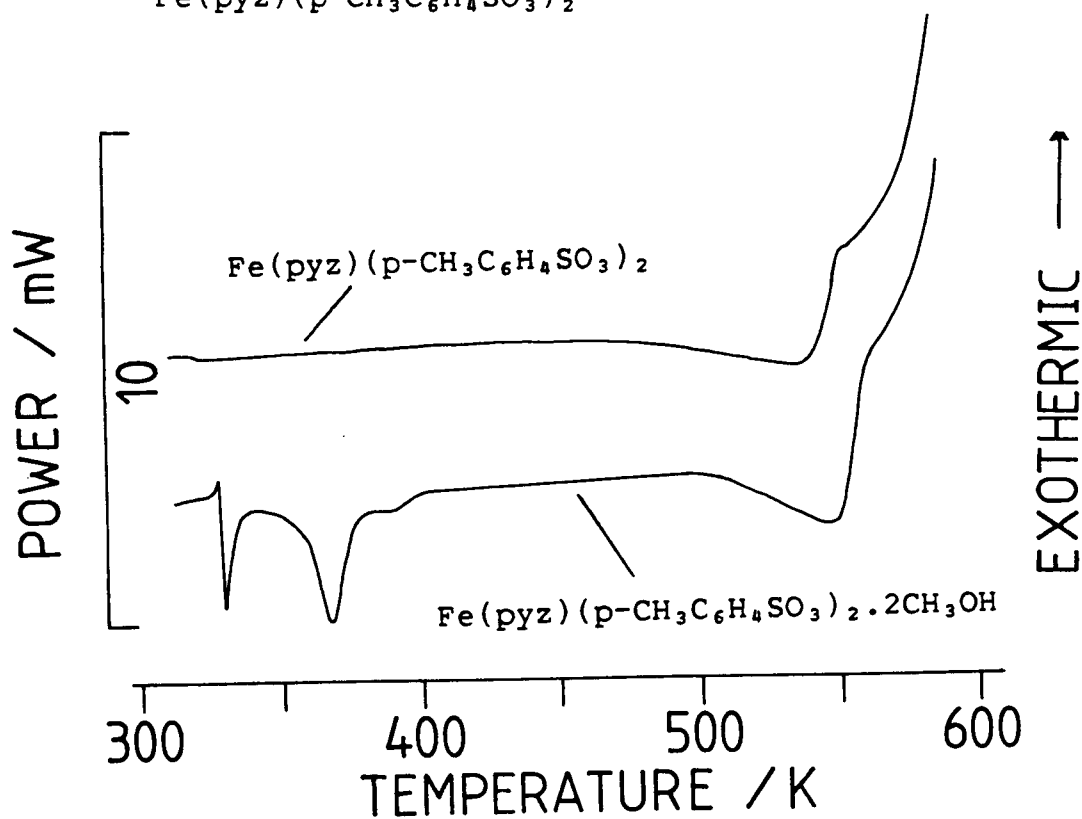
The thermal parameters for the mono(pyrazine) and bis(pyridine) complexes prepared in this study are given in Table 4.4. From these data it can be seen that in general the D.S.C. curves for these complexes are very similar to those of the corresponding tetrakis(pyridine) or bis(pyrazine) complexes, once the first two pyridine groups or a single pyrazine ligand has been removed. For example, the last two pyridine groups in  $\text{Fe}(\text{py})_4(\text{CF}_3\text{SO}_3)_2$  are removed at 513 K ( $\Delta H = 60 \text{ kJ mol}^{-1}$ ) which corresponds reasonably closely to the values for the loss of the pyridine groups from  $\text{Fe}(\text{py})_2(\text{CF}_3\text{SO}_3)_2$  (Table 4.4). Similar comparisons exist for the pairs of compounds:  $\text{Fe}(\text{pyz})_2(\text{CF}_3\text{SO}_3)_2 \cdot \text{CH}_3\text{OH}$  and  $\text{Fe}(\text{pyz})(\text{CF}_3\text{SO}_3)_2$ ,  $\text{Cu}(\text{pyz})_4(\text{CF}_3\text{SO}_3)_2 \cdot \text{H}_2\text{O}$  and  $\text{Cu}(\text{pyz})(\text{CF}_3\text{SO}_3)_2$ , and  $\text{Fe}(\text{pyz})_2\text{Cl}_2$  and  $\text{Fe}(\text{pyz})\text{Cl}_2$ . For  $\text{Fe}(\text{pyz})(\text{NCO})_2$  in the temperature range 310–520 K one endothermic event is noted (Fig. 4.14) and is probably associated with the loss of pyrazine.

The D.S.C. curve for  $\text{Fe}(\text{pyz})(p\text{-CH}_3\text{C}_6\text{H}_4\text{SO}_3)_2 \cdot 2\text{CH}_3\text{OH}$  is more complex than the corresponding anhydrous species (Fig. 4.15). Two thermal events are observed at relatively low temperatures for the bis(methanol) solvate. These events are probably associated with the consecutive loss of each methanol molecule. The  $\Delta H$  values for the two events, 13 and 33  $\text{kJ mol}^{-1}$  indicate that one methanol molecule being more strongly bound than the other. After the solvent molecules are removed from  $\text{Fe}(\text{pyz})(p\text{-CH}_3\text{C}_6\text{H}_4\text{SO}_3)_2 \cdot 2\text{CH}_3\text{OH}$  the thermogram is similar to that of the anhydrous species. One broad endothermic peak occurs at

approximately 545 K in both instances which is probably associated with the removal of the pyrazine ligand. There is poor agreement between the  $\Delta H$  values for this event in the two compounds but this discrepancy may be due to the broad nature of this event together with the proximity of the exothermic decomposition of the complexes slightly above this temperature.

Table 4.4 Thermal Parameters for Bis(pyridine) and Mono(pyrazine) Complexes

Compound	Peak Temp. K	$\Delta H$ kJ mol <sup>-1</sup>
$\text{Fe}(\text{py})_2(\text{CF}_3\text{SO}_3)_2$	557	54
$\text{Fe}(\text{pyz})(\text{CF}_3\text{SO}_3)_2$	606	64
$\text{Fe}(\text{pyz})(p\text{-CH}_3\text{C}_6\text{H}_4\text{SO}_3)_2 \cdot 2\text{CH}_3\text{OH}$	329	13
	367	33
	548	100
$\text{Fe}(\text{pyz})(p\text{-CH}_3\text{C}_6\text{H}_4\text{SO}_3)_2$	543	47
$\text{Fe}(\text{pyz})\text{Cl}_2$	730	60
$\text{Fe}(\text{pyz})(\text{NCO})_2$	605	40
$\text{Cu}(\text{pyz})(\text{CF}_3\text{SO}_3)_2$	650	90

Fig. 4.14 D.S.C. Curve for  $\text{Fe}(\text{pyz})(\text{NCO})_2$ Fig. 4.15 D.S.C Curves for  $\text{Fe}(\text{pyz})(\text{p-CH}_3\text{C}_6\text{H}_4\text{SO}_3)_2 \cdot 2\text{CH}_3\text{OH}$  and  $\text{Fe}(\text{pyz})(\text{p-CH}_3\text{C}_6\text{H}_4\text{SO}_3)_2$ 

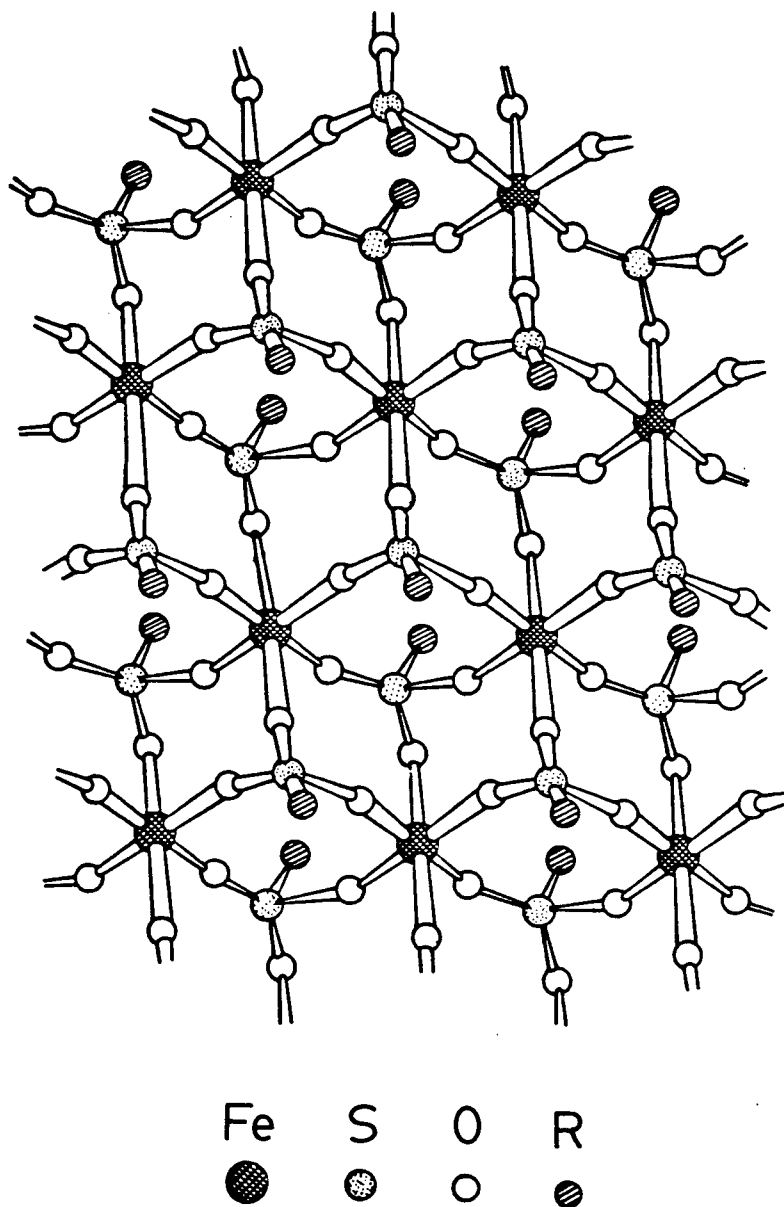
## CHAPTER 5

### MAGNETIC PROPERTIES OF IRON(II) SULFONATE COMPLEXES

#### 5.1 INTRODUCTION

The iron(II) sulfonate complexes,  $\text{Fe}(\text{RSO}_3)_2$  (where R is F,  $\text{CF}_3$ ,  $\text{CH}_3$  or  $p\text{-CH}_3\text{C}_6\text{H}_4$ ) have been prepared and characterised previously in this laboratory.<sup>23-26</sup> From these earlier studies and by analogy to the known structure of  $\text{Ca}(\text{CH}_3\text{SO}_3)_2$ ,<sup>16</sup> it was proposed that these compounds adopt a polymeric two-dimensional layer structure, in which each sulfonate anion acts as a tridentate bridging ligand to three different metal centres (Fig. 5.1). Each metal site is surrounded by an octahedral arrangement of oxygen atoms, with each oxygen atom being from a different sulfonate anion. Previous studies<sup>25 26</sup> have shown  $\text{Fe}(\text{CH}_3\text{SO}_3)_2$  to exist in two forms; both isomers exhibit magnetic moments which show a more significant temperature dependence (80-300 K) than those observed for the other iron(II) sulfonate compounds. Mössbauer spectroscopy has shown  $\beta\text{-Fe}(\text{CH}_3\text{SO}_3)_2$  to undergo a magnetic phase transition to an antiferromagnetically-ordered state at approximately 23 K.<sup>26</sup> To conclude these previous studies, low-temperature magnetic susceptibility measurements (4.2-130 K) were undertaken in the current work in order to further investigate the magnetic properties of  $\beta\text{-Fe}(\text{CH}_3\text{SO}_3)_2$  in the region of the phase transition and to compare these magnetic properties with those of the other anhydrous iron(II) sulfonate complexes.



Fig. 5.1 Proposed Structure of  $\text{Fe}(\text{RSO}_3)_2$  Compounds

## 5.2 SYNTHETIC METHODS

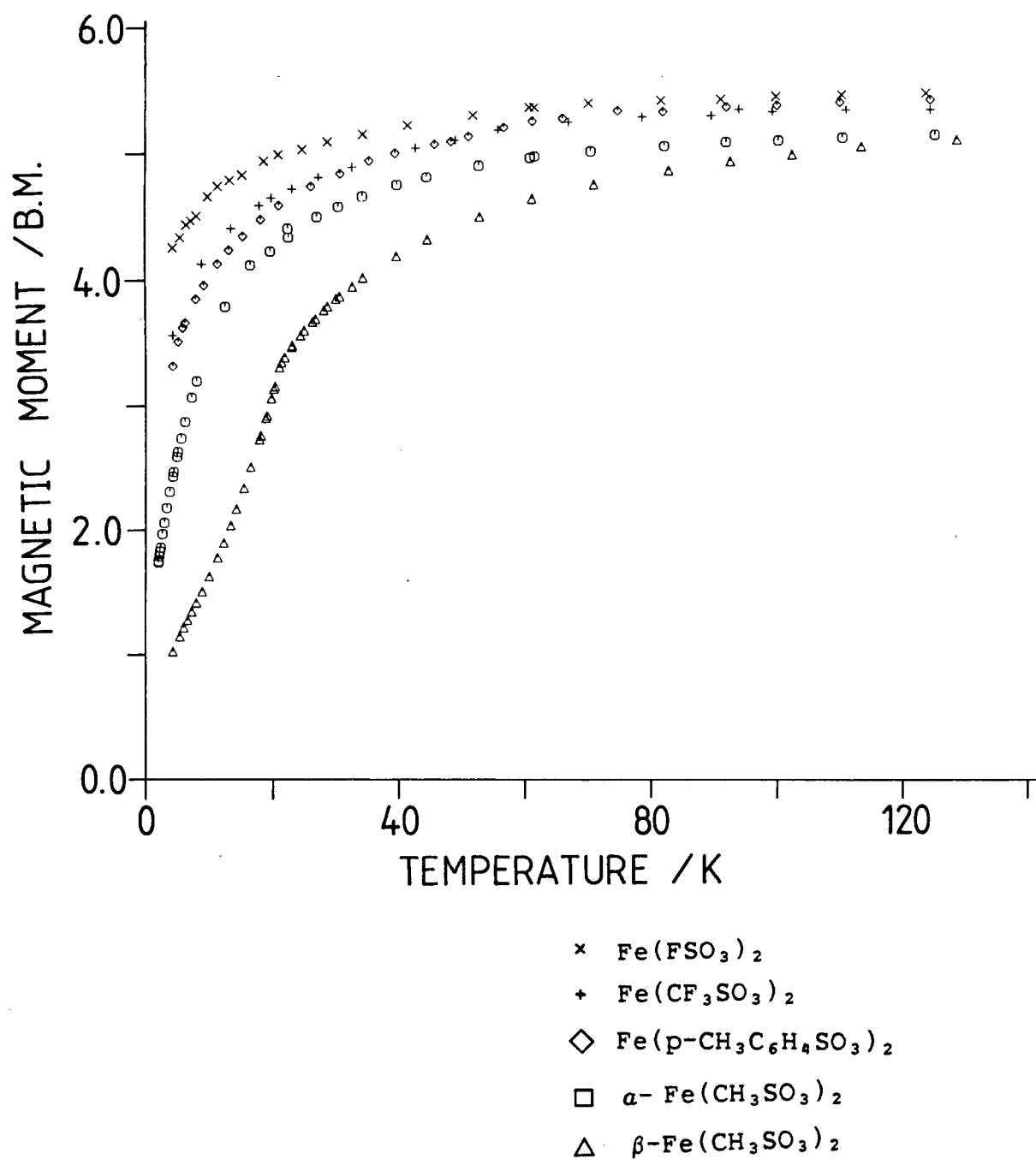
The detailed synthetic procedures for the preparation of the iron(II) sulfonate complexes have been described previously.<sup>23, 25</sup> These methods were followed in the present study and the purity of the products was determined by elemental analysis and infrared spectroscopy.

## 5.3 RESULTS AND DISCUSSION

The magnetic susceptibility data are listed in Appendix IX, Part C. The data obtained from the magnetometer technique and the Gouy method<sup>25</sup> are in excellent agreement in the temperature region (80-130 K) where the two techniques provide overlapping data sets. The temperature dependence (4.2-130 K) of the magnetic moment data for these compounds is illustrated in Fig. 5.2; for  $\alpha\text{-Fe}(\text{CH}_3\text{SO}_3)_2$  additional data were obtained down to a temperature of 1.97 K.

### 5.3.1 $\text{Fe}(\text{FSO}_3)_2$ , $\text{Fe}(\text{CF}_3\text{SO}_3)_2$ and $\text{Fe}(\text{p-CH}_3\text{C}_6\text{H}_4\text{SO}_3)_2$

The magnetic moment data for these compounds show a similar temperature dependence (Fig. 5.2) and the magnetic susceptibility data follow Curie-Weiss behaviour, no maximum being observed. For  $\text{Fe}(\text{FSO}_3)_2$ <sup>24</sup> and  $\text{Fe}(\text{p-CH}_3\text{C}_6\text{H}_4\text{SO}_3)_2$ ,<sup>176</sup> these results are consistent with the Mössbauer spectral studies in which, at 4.2 K, a symmetric quadrupole doublet is observed, indicative of these compounds behaving as paramagnets with no evidence for magnetic hyperfine interactions.<sup>177</sup> In the case of  $\text{Fe}(\text{CF}_3\text{SO}_3)_2$  the Mössbauer spectrum at 4.2 K exhibits a

Fig. 5.2 Magnetic Moments vs Temperature for  $\text{Fe}(\text{RSO}_3)_2$  Compounds

quadrupole doublet which shows a small degree of asymmetric line broadening and some evidence for magnetic hyperfine interactions. These observations were attributed to a decrease in the spin-lattice relaxation rate at low temperatures and not to magnetic exchange interactions.<sup>177</sup> In this study, the low-temperature magnetic susceptibility results are consistent with these earlier conclusions.

For these  $\text{Fe}(\text{RSO}_3)_2$  compounds, the magnetic moment data (80-300 K) were previously analysed in terms of the Figgis model.<sup>64</sup> The method involved obtaining  $\Delta$  and  $\lambda$  values by fitting the temperature dependence of the quadrupole splitting and varying the orbital reduction factor,  $\kappa$ , until agreement was attained between the computed and experimental magnetic moment values. These values obtained from the previous studies are given in Table 5.1.

Table 5.1 Crystal-Field Splitting Parameters for  $\text{Fe}(\text{RSO}_3)_2$  Compounds<sup>1</sup>

R	$\Delta/\text{cm}^{-1}$	$\lambda/\text{cm}^{-1}$	$\kappa$
$\text{F}^1$	-290	-90	0.95
$\text{CF}_3^2$	-180	-90	0.80
$\text{p-CH}_3\text{C}_6\text{H}_4^2$	-270	-90	0.75

1). Values from reference 24

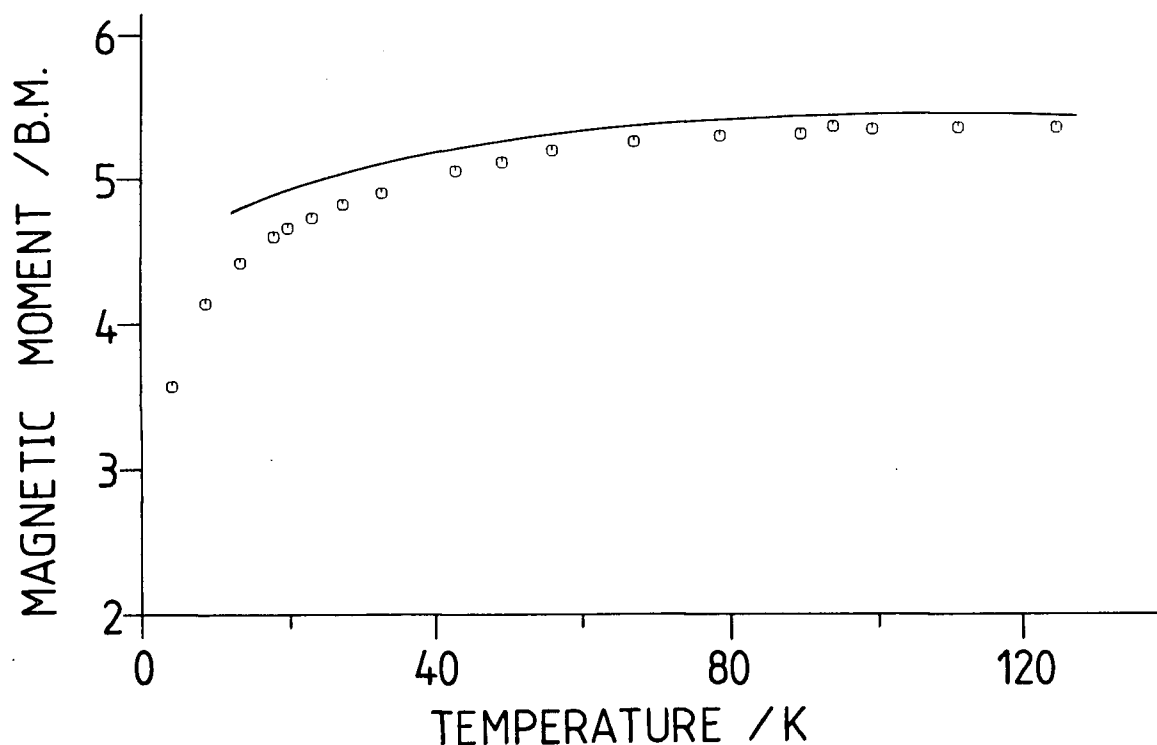
2). Values from reference 25

With the additional magnetic moment data it was of interest to

observe whether these parameters applied to the low-temperature region. In general, it was found that at lower temperatures the agreement between calculated and experimental magnetic moment values is poor. In particular, at temperatures below approximately 50 K the observed magnetic moment data are significantly less than the values predicted by the model (Fig. 5.3). As noted in Section 3.3.4.2, several criticisms have been laid against this model and it appears that for these compounds either the model is not valid over the entire temperature range of 4.2-300 K or weak antiferromagnetic exchange interactions may be present which reduce the magnetic moment values.

Fig. 5.3 Magnetic Moment vs Temperature for  $\text{Fe}(\text{CF}_3\text{SO}_3)_2$

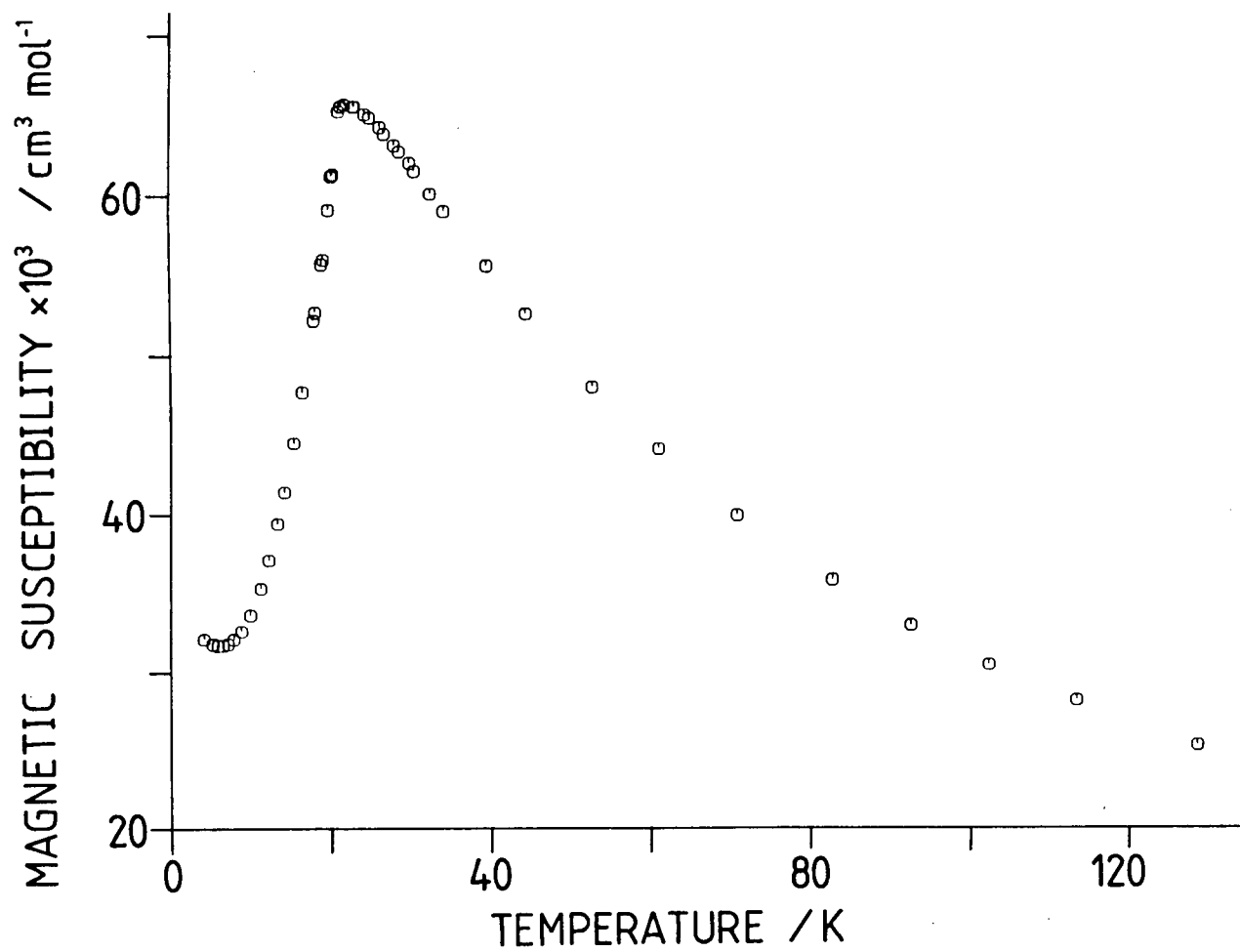
Figgis Model, line generated from  $\Delta=180 \text{ cm}^{-1}$ ,  $\lambda=-90 \text{ cm}^{-1}$ ,  $\kappa=0.80$



### 5.3.2 $\alpha$ - and $\beta$ -Fe(CH<sub>3</sub>SO<sub>3</sub>)<sub>2</sub>

For the  $\alpha$  and  $\beta$  isomers of Fe(CH<sub>3</sub>SO<sub>3</sub>)<sub>2</sub> the temperature dependencies of the magnetic moment data (Fig. 5.2) are much more pronounced than those of the iron(II) sulfonate compounds discussed in the preceding section. The magnetic moment for  $\beta$ -Fe(CH<sub>3</sub>SO<sub>3</sub>)<sub>2</sub> falls monotonically with decreasing temperature to approximately 25 K. A discontinuity in the magnetic moment plot is observed at approximately 23 K and the magnetic moment then decreases to 1.04 B.M. at 4.2 K. This type of magnetic behaviour is ascribed to antiferromagnetic exchange interactions which are clearly observed in the magnetic susceptibility data (Fig. 5.4). The magnetic susceptibility increases as the temperature decreases and exhibits a maximum at approximately 22.5 K. Below this temperature the magnetic susceptibility decreases until a slight increase is noted at temperatures below approximately 5.5 K. This small increase in the susceptibility at low temperatures is sometimes observed in antiferromagnetic species and is often attributed to the presence of a small amount of paramagnetic "impurity". In this case, the impurity is possibly  $\alpha$ -Fe(CH<sub>3</sub>SO<sub>3</sub>)<sub>2</sub>, as the  $\beta$  isomer is prepared by conversion of the paramagnetic  $\alpha$  modification,<sup>25</sup> and it is difficult to detect the presence of a small amount of unconverted  $\alpha$  form in the  $\beta$  product.

Fig. 5.4 Magnetic Susceptibility vs Temperature for  $\beta\text{-Fe}(\text{CH}_3\text{SO}_3)_2$



In the case of  $\beta\text{-Fe}(\text{CH}_3\text{SO}_3)_2$ , at a temperature slightly below that of the maximum in the magnetic susceptibility curve, a sharp decrease in the magnetic susceptibility is observed. This is indicative of a transition from short-range magnetic interactions, possibly of a two-dimensional type, to long-range three-dimensional magnetic ordering. The onset of three-dimensional ordering occurs at approximately 22.5 K which is in good agreement the temperature of 23 K at which the Mössbauer quadrupole doublet splits into a complex magnetic hyperfine pattern.

$\alpha\text{-Fe}(\text{CH}_3\text{SO}_3)_2$  also shows a significantly temperature-dependent magnetic moment; however, in contrast to the  $\beta$  isomer, no maximum is observed in the magnetic susceptibility curve, even down to a temperature of 1.97 K. This indicates that short-range exchange interactions in the  $\alpha$  isomer are much weaker than those present in  $\beta\text{-Fe}(\text{CH}_2\text{SO}_3)_2$ . At 4.2 K, Mössbauer spectroscopy<sup>26</sup> shows a single quadrupole doublet and these observations are consistent with the  $\alpha$  isomer being antiferromagnetic, i.e., exhibits short-range order, but with no indication of long-range magnetic ordering.

Magnetic exchange interactions have been observed in other iron(II) sulfate complexes. Indeed,  $\text{FeSO}_4$  was one of the first compounds to reveal a maximum in the magnetic susceptibility versus temperature plot;<sup>178</sup> bridging sulfate anions result in an extended three-dimensional lattice and superexchange is through O-S-O bridges.<sup>179</sup> Other iron(II) compounds with O-S-O bridging units have been found to exhibit magnetic properties



characteristic of low-dimensional materials and in some cases Mössbauer spectroscopy has demonstrated a transition to a magnetically-ordered state.<sup>180-183</sup> In some instances, the compounds were found to be linear chain compounds and the magnetic properties have been analysed in terms of an exchange Hamiltonian in either the Ising or Heisenberg limit.<sup>182 183</sup> In the case of  $\beta\text{-Fe}(\text{CH}_3\text{SO}_3)_2$ , however, analysing the magnetic data is made difficult by several factors. The choice of either the Heisenberg or Ising case is usually not appropriate for iron(II) complexes. These models do not apply to a system where three-dimensional interactions are also present, as is true in the case of  $\beta\text{-Fe}(\text{CH}_3\text{SO}_3)_2$  below 22.5 K. The two-dimensional model which was used in this study for analysing the magnetic susceptibility data of both  $\text{Cu}(\text{pyz})_2(\text{CH}_3\text{SO}_3)_2$  and  $\text{Fe}(\text{pyz})_2(\text{NCS})_2$  is not applicable in this instance as this model takes into account interactions between one paramagnetic centre and the four nearest neighbours in a square array. For  $\beta\text{-Fe}(\text{CH}_3\text{SO}_3)_2$  the proposed two-dimensional lattice consists of each metal centre being surrounded by six nearest neighbours (Fig. 5.1).

From the results presented here, it is demonstrated that the only iron(II) sulfonate compound to show definite evidence for three-dimensional long-range magnetic ordering is  $\beta\text{-Fe}(\text{CH}_3\text{SO}_3)_2$ . From the temperature at which the maximum is observed in the magnetic susceptibility data, a relatively strong degree of magnetic interaction is inferred, especially as the magnetic pathway is presumably via the three-atom bridge, O-S-O; whereas, in the other iron(II) sulfonate compounds

exchange interactions, if present at all, are much less significant. Mössbauer studies<sup>25</sup> on these complexes indicate that the  $\text{FeO}_6$  chromophore present in the  $\alpha$  modification of  $\text{Fe}(\text{CH}_3\text{SO}_3)_2$  is distorted by a trigonal compression, while that in the  $\beta$  form is trigonally elongated. The presence of a trigonally elongated  $\text{FeO}_6$  octahedron, however, is not a sufficient condition for determining the extent of magnetic exchange interactions in these complexes. Mössbauer spectroscopy also suggests the presence of this type of chromophore in the fluorosulfonate, triflate and p-tosylate compounds, but there is no evidence for significant magnetic exchange interactions in these complexes. The degree of magnetic exchange in these compounds is presumably a function of the O-S-O bridging angle, the Fe-O and S-O bond distances and the steric and electronic properties of the R group. Unfortunately, in the absence of any X-ray crystallographic evidence it is difficult to make detailed magneto-structural correlations for these compounds in order to explain the strong magnetic interaction observed for  $\beta\text{-Fe}(\text{CH}_3\text{SO}_3)_2$ .

## CHAPTER 6

### SUMMARY AND CONCLUSIONS

The present study involved the synthesis and characterisation of divalent iron and copper complexes with the neutral donor ligands pyrazine or pyridine and a range of anions of varying coordinating ability. In the pyrazine complexes, the neutral ligand was found to coordinate in either a uni- or bidentate mode and these two different modes held significant consequences for the magnetic properties of the materials. Pyridine, as expected, was found to coordinate only as a unidentate ligand using its unique nitrogen donor atom. Spectroscopic methods were used not only to identify the coordination modes of the neutral ligands but also the anionic ligands and several of the anions were found to coordinate in either a uni- or a bidentate mode. Based upon magneto-structural correlations it is possible to divide the complexes into three groups and each group can be further subdivided dependent upon the type of bridging ligands present (Table 6.1).

#### GROUP 1

The complexes of Group 1 show only a moderate temperature dependence to their magnetic moments over a wide temperature range (50-300 K), with a slight increase in temperature dependence at temperatures below 20 K. These complexes are considered to be magnetically dilute.

Table 6.1 Classification of Complexes

GROUP 1 MAGNETICALLY DILUTE

A	B
$\text{Fe}(\text{py})_4(\text{CF}_3\text{SO}_3)_2$	$\text{Fe}(\text{pyz})_2\text{Cl}_2$
$\text{Fe}(\text{py})_4(\text{CH}_3\text{SO}_3)_2$	$\text{Fe}(\text{pyz})_2\text{Br}_2$
$\text{Fe}(\text{py})_4(\text{p-CH}_3\text{C}_6\text{H}_4\text{SO}_3)_2$	$\text{Fe}(\text{pyz})_2\text{I}_2$
$\text{Fe}(2\text{-mepyz})_4(\text{CH}_3\text{SO}_3)_2$	$\text{Fe}(\text{pyz})_2(\text{ClO}_4)_2$
$\text{Cu}(\text{py})_4(\text{CF}_3\text{SO}_3)_2$	
$\text{Cu}(\text{py})_4(\text{CH}_3\text{SO}_3)_2$	C
$\text{Cu}(\text{pyz})_4(\text{CF}_3\text{SO}_3)_2 \cdot \text{H}_2\text{O}$	$\text{Fe}(\text{pyz})(\text{p-CH}_3\text{C}_6\text{H}_4\text{SO}_3)_2 \cdot 2\text{CH}_3\text{OH}$
$\text{Fe}(\text{pyz})_4(\text{AsF}_6)_2 \cdot 2\text{H}_2\text{O}$	$\text{Fe}(\text{pyz})(\text{p-CH}_3\text{C}_6\text{H}_4\text{SO}_3)_2$

GROUP 2 MAGNETICALLY CONCENTRATED

A	B
$\text{Fe}(\text{pyz})_2(\text{NCS})_2$	$\text{Fe}(\text{pyz})(\text{NCO})_2$
$\text{Cu}(\text{pyz})_2(\text{CH}_3\text{SO}_3)_2$	$\text{Fe}(\text{pyz})(\text{CF}_3\text{SO}_3)_2$
	$\text{Cu}(\text{pyz})(\text{CF}_3\text{SO}_3)_2$

GROUP 3 MAGNETIC PROPERTIES INTERMEDIATE BETWEEN GROUPS 1 AND 2

A	B
$\text{Fe}(\text{pyz})_2(\text{CF}_3\text{SO}_3)_2 \cdot \text{CH}_3\text{OH}$	$\text{Fe}(\text{pyz})\text{Cl}_2$
$\text{Fe}(\text{pyz})_2(\text{CH}_3\text{SO}_3)_2$	
	C
	$\text{Fe}(\text{py})_2(\text{CF}_3\text{SO}_3)_2$

(1A) The complexes in this sub-group are of stoichiometry  $ML_4(RSO_3)_2$  and for several compounds of this type X-ray crystallography has shown conclusively that the metal centres are well isolated from each other and the magnetic properties are consistent with their formulation as monomeric molecular species.  $Fe(pyz)_4(AsF_6)_2 \cdot 2H_2O$  falls into this category as the spectroscopic properties are also consistent with a monomeric structure.

(1B) Although pyrazine adopts a bridging configuration in the  $Fe(pyz)_2X_2$  complexes (where  $X^-$  is  $Cl^-$ ,  $Br^-$ ,  $I^-$  or  $ClO_4^-$ ), the magnetic properties are similar to those of the complexes of sub-group 1A, showing no evidence for magnetic exchange.

(1C) The structure of the mono(pyrazine) p-tosylate complexes consists of bridging anionic ligands and bridging pyrazine. In spite of this bridging network the magnetic results do not indicate any significant magnetic interactions.

## GROUP 2

The complexes of group 2 exhibit magnetic properties which show definite evidence for magnetic concentration of an antiferromagnetic nature. This evidence comes from the observation of a substantial temperature dependence of the magnetic moment, together with a maximum in the magnetic susceptibility data, and, in the case of the iron(II) compounds, a complex magnetic hyperfine Mössbauer spectrum resulting from magnetic ordering. The complexes in this group may be divided into two sub-categories dependent upon the proposed bridging

network.

(2A) The structures of complexes in this sub-category consist of two-dimensional lattices resulting from bridging pyrazine ligands. X-ray crystallography has demonstrated this type of structure to be present in  $\text{Cu}(\text{pyz})_2(\text{CH}_3\text{SO}_3)_2$  and it is concluded that the two distinct copper-pyrazine interactions result in inequivalent pathways for magnetic exchange. Two-dimensional short-range and long-range interactions are present in the second member of this sub-category,  $\text{Fe}(\text{pyz})_2(\text{NCS})_2$  and, in this instance, spectroscopic data indicate the presence of equivalent magnetic exchange pathways through bridging pyrazine ligands.

(2B) Magnetic exchange interactions are also observed for the members of this sub-category, i.e., the mono(pyrazine) complexes:  $\text{Fe}(\text{pyz})(\text{NCO})_2$ ,  $\text{Fe}(\text{pyz})(\text{CF}_3\text{SO}_3)_2$  and  $\text{Cu}(\text{pyz})(\text{CF}_3\text{SO}_3)_2$ . The compounds in this group, however, differ structurally from those in group 2A in that there is strong spectroscopic evidence to indicate the presence of bridging anions as well as bridging pyrazine ligands. Further research to obtain single-crystal X-ray structural data is required to confirm this structural feature.

### GROUP 3

The magnetic properties of the third class of compound are intermediate between those of the first two groups. For these compounds the magnetic moment shows a significant temperature dependence; the temperature dependence being greater

than that observed for the analogous complexes in group 1. Unlike the compounds of group 2, however, the compounds of group 3 exhibit no maximum in the magnetic susceptibility data and hence, while magnetic exchange interactions are postulated for this group of complexes, they are of a weaker nature than those present in the compounds of group 2.

Spectroscopic evidence enabled compounds in this group to be further classified in accord with the nature of the bridging ligand network.

(3A) The  $\text{Fe}(\text{pyz})_2(\text{RSO}_3)_2$  compounds (where R is  $\text{CF}_3$  or  $\text{CH}_3$ ) contain bridging pyrazine ligands and non-bridging anions resulting in two-dimensional lattices.

(3B)  $\text{Fe}(\text{pyz})\text{Cl}_2$  contains bridging anions and bridging pyrazine ligands

(3C) Bridging anions are present in  $\text{Fe}(\text{py})_2(\text{CF}_3\text{SO}_3)_2$

From this classification of magnetic properties and structures it is possible to draw some important conclusions regarding, in particular, the ability of pyrazine to transmit magnetic exchange effects. The complexes which contain only terminal pyrazine ligands all appear in Group 1 and are effectively magnetically dilute. In terms of this inability to transmit magnetic exchange effects terminal pyrazine ligands behave no differently from pyridine.

Two copper complexes which contain bridging pyrazine ligands were prepared, and both appear in Group 2. In  $\text{Cu}(\text{pyz})_2(\text{CH}_3\text{SO}_3)_2$ , there are two bridging pyrazine ligands per copper resulting in a two-dimensional array, and while both

neutral ligands may contribute to the exchange effect, an X-ray structure determination shows that one is particularly strongly bound, generating what is effectively a one-dimensional type of exchange. In the other copper complex,  $\text{Cu}(\text{pyz})(\text{CF}_3\text{SO}_3)_2$ , the bridging pyrazine is thought to provide the main pathway for exchange. These results, considered in conjunction with previous studies on copper-pyrazine complexes, show that pyrazine is an efficient ligand for propagating magnetic exchange between copper centres.

The situation in regard to bridging pyrazine and magnetic exchange in iron(II) complexes is by no means straightforward. The iron complexes of Groups 1A, 2A and 3A all have stoichiometries  $\text{Fe}(\text{pyz})_2\text{X}_2$  with bridging pyrazine ligands forming a two-dimensional array and terminal anionic ligands. The presence of a similar bridging pathway in these complexes is obviously not a sufficient condition for predicting the extent of magnetic exchange in these complexes. The nature of the terminal ligand is playing a vital role here. Where X is either a halide or perchlorate, the complex is magnetically dilute; where the anionic ligand is sulfonate, there is evidence for weak exchange and where X is thiocyanate, relatively strong exchange effects are observed. At the present time, it does not seem possible to correlate these different effects with either electronic or steric properties of the various anionic ligands. It should be noted, however, as has been observed previously for pyrazine-bridged copper complexes, that small differences in pyrazine ring orientation in these complexes, caused by the



different terminal anions, may significantly affect the efficiency of the exchange through pyrazine. For this reason, it would be useful to obtain single-crystal X-ray structure data on complexes of this type. In the present study, several attempts to obtain single crystals of these species were made, but were unsuccessful.

Finally, it is noted that the iron complexes in groups 1C, 2B and 3B have stoichiometries  $\text{Fe}(\text{pyz})\text{X}_2$ , and all have bridging anions in addition to a one-dimensional bridging pyrazine network. Again, in spite of possible similarities in structure, a range of magnetic properties are observed. While the difference in the two sulfonate derivatives may be accounted for on the basis of the different basicities of the anions, as mentioned earlier, it is difficult to rationalise the magnetic properties of the other complexes in terms of anionic properties. Differences in orientation of bridging pyrazine ligands possibly accounts for the different magnetic properties and single-crystal X-ray diffraction studies would be invaluable in this regard.

The magnetic properties of the complexes were treated from several theoretical standpoints. For the copper complexes,  $\text{Cu}(\text{pyz})_2(\text{CH}_3\text{SO}_3)_2$  and  $\text{Cu}(\text{pyz})(\text{CF}_3\text{SO}_3)_2$ , the magnetic properties were analysed in two different ways by considering magnetic interactions throughout a two-dimensional lattice or along a one-dimensional chain. In spite of the two-dimensional structure of both complexes the fact that pyrazine bridges strongly in one dimension results in one-dimensional magnetic

behaviour.

The magnetic properties of the iron(II) compounds were analysed in several ways; the models are based upon crystal-field effects, zero-field splitting or one or two-dimensional magnetic exchange effects. The first two models were used successfully to analyse the data for the monomeric complexes in which no magnetic interactions were present. The magnetic properties of complexes showing antiferromagnetic superexchange interactions were, in general, well analysed via the two-dimensional square-lattice model.

## REFERENCES

1. Reviews of the chemistry and physics of low-dimensional solids may be found in the following texts:  
 a). Miller, J.S.; Epstein, A.J., Eds.; "Synthesis and Properties of Low-Dimensional Materials", Ann. N.Y. Acad. Sci. 1978, 313.  
 b). Keller, H.J., Ed.; "Low-Dimensional Cooperative Phenomena", Plenum Press: New York, 1975.  
 c). Alcacer, L., Ed.; "The Physics and Chemistry of Low-Dimensional Solids", Reidel: Dordrecht, 1980.  
 d). Miller, J.S.; Epstein, A.J. Prog. Inorg. Chem. 1976, 20, 1.
2. a). Heeger, A.J. "Highly Conducting One-Dimensional Solids", Devreese, J.T.; Evrard, R.P.; Van Doren, V.E., Eds. Plenum Press: New York, 1979, p.69.  
 b). Keller, H.J., Ed.; "Chemistry and Physics of One-Dimensional Metals", Plenum Press: New York, 1977.
3. a). Paushkin, Y.M.; Vishnyakova, T.P.; Lunia, A.F.; Nizova, S.A. "Organic Polymeric Semiconductors", Wiley: New York, 1974.  
 b). Baughman, R.H.; Chance, R.R. "Synthesis and Properties of Low-Dimensional Materials", Miller, J.S., Ed., Ann. N.Y. Acad. Sci. 1978, 313, 705.
4. a). Geserich, H.P.; Pintschovious, L. Adv. Solid St. Phys. 1976, 16, 65.  
 b). Greene, R.L.; Street, G.B. "Chemistry and Physics of One-Dimensional Metals", Keller, H.J., Ed., Plenum Press: New York, 1977, p. 177.  
 c). Labes, M. M.; Love, P.; Nichols, L. F. Chem. Rev. 1979, 79, 1.
5. Bernard, C.; Herold, A.; Lelaurain, M.; Robert, G. Compt. Rend. Seanc. Acad. Sci 1976, 283C, 625.
6. a). Ebert, L.B. Ann. Rev. Mater. Sci. 1976, 6, 181.  
 b). Fischer, J.E.; Thompson, T.E. Phys. Today 1978, 31, 36.
7. Halbert, T.R.; Scanlon, J. Mater. Res. Bull. 1979, 14, 415.
8. Whittingham, M.S. Science (Washington, D.C.) 1976, 192, 1126.
9. Dines, M.B. Inorg. Chem. 1978, 17, 763.
10. a). Whittingham, M.S. J. Chem. Soc., Chem. Commun. 1974, 328.  
 b). Whittingham, M.S. J. Electrochem. Soc. 1976, 123, 315.  
 c). Whittingham, M.S.; Chianelli, R.R. "Reactivity in

Solids", Plenum Press: New York, 1977.

11. Knop, W. Justus Liebigs Ann. Chem. 1842, 43, 111.
12. Krogman, K.; Hausen, H.D. Z. Anorg. Allg. Chem. 1968, 358, 67.
13. a). Hoffman, B.M.; Martinsen, J.; Pace, L.J. Ibers, J.A. "Extended Linear Chain Compounds", Vol. 3, Miller, J.S., Ed., Plenum Press: New York, 1983.  
b). Hoffman, B.M.; Ibers, J.A. Acc. Chem. Res. 1983, 16, 15.
14. Oliver, K.W.; Rettig, S.J.; Thompson, R.C.; Trotter, J. Can. J. Chem. 1982, 60, 2017.
15. Dines, M.B.; Marroco, M. "Extended Linear Chain Compounds", Vol. 2, Miller, J.S., Ed., Plenum Press: New York, 1982, p. 31.
16. Charbonnier, F.; Faure, R.; Loiseleur, H.; Acta Crystallogr., Sect. B, 1977, B33, 1478.
17. Bleaney, B.; Bowers, K.O. Roy. Soc. London, Proc. 1952, 214A, 451.
18. Kato, M.; Jonasson, H.B.; Fanning, J.C. Chem. Rev. 1964, 39, 1030.
19. Crawford, V.H.; Richardson, H.W.; Wasson, J.R.; Hodgson, D.J.; Hatfield, W.E. Inorg. Chem. 1976, 15, 2107.
20. Haynes, J.S.; Oliver, K.W.; Rettig, S.J.; Thompson, R.C. Trotter, J. Can. J. Chem. 1984, 62, 891.
21. Haynes, J.S.; Oliver, K.W.; Thompson, R.C. Can. J. Chem. 1985, 63, 1111.
22. Cicha, W.V.; Haynes, J.S.; Oliver, K.W.; Rettig, S.J.; Thompson, R.C.; Trotter, J. Can. J. Chem. 1985, 63, 1055.
23. Alleyne, C.S.; Mailer, K.; Thompson, R.C. Can. J. Chem. 1974, 52, 336.
24. Sams, J.R.; Thompson, R.C.; Tsin, T.B. Can. J. Chem. 1977, 55, 115.
25. Haynes, J.S.; Sams, J.R.; Thompson, R.C. Can. J. Chem. 1981, 59, 669.
26. Haynes, J.S.; Sams, J.R.; Thompson, R.C. Chem. Phys. Lett. 1980, 75, 596.
27. Kamei, H. J. Phys. Chem. 1965, 69, 2791.

28. a). Chia, A.S.; Trimble, R.F. J. Phys. Chem. 1961, 65, 863.  
 b). Brignell, P.J.; Johnson, C.D.; Katritzky, A.R.; Shakir, N.; Tarhan, H.O.; Walker, G. J. Chem. Soc. B, 1967, 2396.
29. Perrin, D.D. "Dissociation Constants of Organic Bases in Aqueous Solution", Butterworths: London, 1965.
30. a). Stoehr, C. J. Prakt. Chem. 1893, 47, 439.  
 b). Brandes, P.; Stoehr, C. J. Prakt. Chem. 1896, 55, 501.
31. Lever, A.B.P.; Lewis, J.; Nyholm, R.S. J. Chem. Soc. 1963, 3156.
32. Lever, A.B.P.; Lewis, J.; Nyholm, R.S. J. Chem. Soc. 1962, 1235.
33. Lever, A.B.P.; Lewis, J.; Nyholm, R.S. J. Chem. Soc. 1963, 5042.
34. Lever, A.B.P.; Lewis, J.; Nyholm, R.S. J. Chem. Soc. 1964, 4761.
35. Sidgewick, N.V. "The Chemical Elements and their Compounds", Oxford University Press: 1950.
36. Bailar, J.C. "The Chemistry of the Coordination Compounds", Reinhold Pub. Co.: New York, 1956.
37. Goldstein, M.; Taylor, F.B.; Unsworth, W.D. J. Chem. Soc., Dalton Trans. 1972, 418.
38. Dorrity, I.A.; Orrell, K.G. J. Inorg. Nucl. Chem. 1974, 36, 230.
39. Goldstein, M. J. Inorg. Nucl. Chem. 1975, 37, 567.
40. Carreck, P.W.; Goldstein, M.; McPartlin, E.M.; Unsworth, W.D. J. Chem. Soc., Chem. Commun. 1971, 1634.
41. Vranka, R.G.; Amma, E.L. Inorg. Chem. 1966, 5, 1020.
42. Santoro, A; Mighell, A.D.; Reimann, C.W. Acta Crystallogr. Sect. B 1970, B26, 979.
43. Darriet, J.; Haddad, M.S.; Duesler, E.N.; Hendrickson, D.N. Inorg. Chem. 1979, 18, 2679.
44. Goldstein, M.; Unsworth, W.D. Spectrochim. Acta 1971, 27A, 1055.
45. Creutz, C.; Taube, H.J. J. Am. Chem. Soc. 1969, 91, 3988.

46. Beattie, J.K.; Hush, N.S.; Taylor, P.R.; Raston, C.L.; White, A.H. J. Chem. Soc., Dalton Trans. 1977, 1121.
47. For reviews see:  
 a). Day, P.; Hush, N.S.; Schatz, P.J. "Mixed Valence Compounds: Theory and Applications in Chemistry, Physics, Geology and Biology", Proceedings of the NATO Advanced Study Group, Brown, D.B., Ed.; Reidel: Dordrecht, 1980.  
 b). Creutz, C. Prog. Inorg. Chem. 1983, 30, 1.
48. Inman, G.W.; Hatfield, W.E. Inorg. Chem. 1972, 11, 3085.
49. Villa, J.F.; Hatfield, W.E. J. Am. Chem. Soc. 1971, 93, 4081.
50. Boyd, P.D.W.; Mitra, S. Inorg. Chem. 1980, 19, 3547.
51. Richardson, H.W.; Hatfield, W.E. J. Am. Chem. Soc. 1976, 98, 835.
52. Haddad, M.S.; Hendrickson, D.N.; Canady, J.P.; Drago, R.S.; Biekzsa, D.S. J. Am. Chem. Soc. 1979, 101, 898.
53. Belford, R.C.E.; Fenton, D.E.; Truter, M.R. J. Chem. Soc., Dalton Trans. 1974, 17.
54. Richardson, H.W.; Wasson, J.R.; Hatfield, W.E. Inorg. Chem. 1977, 16, 484.
55. Morosin, B.; Hughes, R.C.; Soos, Z.G. Acta Crystallogr., Sect. B 1975, B31, 762.
56. Valentine, J.S.; Silverstein, A.J.; Soos, Z.G. J. Am. Chem. Soc. 1974, 96, 97.
57. Baker, E.C.; Raymond, K.N. Inorg. Chem. 1977, 16, 2710.
58. Inoue, M.; Kubo, M. Coord. Chem. Rev. 1976, 21, 1.
59. Matthews, R.W.; Walton, R.A. Inorg. Chem. 1971, 10, 1433.
60. Child, M.D.; Foulds, G.A.; Percy, G.C.; Thornton, D.A. J. Mol. Struct. 1981, 75, 191.
61. Beech, G.; Mortimer, C.T. J. Chem. Soc. A 1967, 1115.
62. Ferraro, J.R.; Zipper, J.; Wozniak, W. App. Spectrosc. 1969, 23, 160.
63. Bayer, R.; Ferraro, J.R. Inorg. Chem. 1969, 8, 1654.
64. Figgis, B.N.; Lewis, J.; Mabbs, F.E.; Webb, G.A. J. Chem. Soc. A 1967, 442.

65. Cotton, F.A.; Troup, J.M. J. Am. Chem. Soc. 1974, 96, 3438.
66. Kubel, F.; Strahle, J. Z. Naturforsch. 1981, 36B, 441.
67. Little, B.F.; Long, G.J. Inorg. Chem. 1978, 17, 3401 and references cited therein.
68. Long, G.J.; Clarke, P.J. Inorg. Chem. 1978, 17, 1394.
69. Sotofte, I.; Rasmussen, S.E. Acta Chem. Scand. 1967, 21, 2028.
70. Long, G.J.; Whitney, D.L. Kennedy, J.E. Inorg. Chem. 1971, 10, 1406.
71. Reiff, W.M.; Frankel, R.B.; Little, B.F.; Long, G.J. Inorg. Chem. 1974, 13, 2153.
72. Foner, S.; Frankel, R.B.; Reiff, W.M.; Little, B.F.; Long, G.J. Solid State Commun. 1975, 16, 159.
73. Foner, S.; Frankel, R.B.; Reiff, W.M.; McNiff, E.J.; Little, B.F.; Long, G.J. AIP Conf. Proc. 1975, No. 24, 363.
74. a). Gerloch, M. "Magnetism and Ligand Field Analysis", Cambridge University Press, 1983.  
 b). Boudreaux, E.A.; Mulay, L.N. "The Theory and Applications of Molecular Paramagnetism", Wiley: New York, 1976.  
 c). Carlin, R.L; Van Duyneveldt, A.J. "Magnetic Properties of Transition-Metal Compounds", Springer-Verlag: New York, 1977.
75. The reader is referred to the following articles:  
 a). Hatfield, W.E.; Estes, W.E.; Marsh, W.E.; Pickens, M.W.; ter Haar, L.W.; Weller, R.R. "Extended Linear Chain Compounds", Miller, J.S., Ed., Plenum Press: New York, 1983, Chapter 2.  
 b). Willett, R.D.; Gaura, R.M.; Landee, C.P. Ibid. Chapter 3.  
 c). Ginsberg, A.P. Inorg. Chim. Acta. Rev. 1971, 5, 45.  
 d). de Jongh, C.J.; Miedema, A.R. Adv. Phys. 1974, 23, 1.
76. Alleyne, C. S.; Thompson, R. C. Can. J. Chem. 1974, 52, 3218.
77. Gill, N.S.; Nuttall, R.H.; Scarfe, D.E.; Sharp, D.W.A. J. Inorg. Nucl. Chem. 1961, 18, 79.
78. Shriver, D.F. "The Manipulation of Air-Sensitive Compounds", McGraw-Hill: New York, 1969.

79. Sparks, L.L.; Powell, R.L. J. Res. Natl. Bur. Standards 1972, 76A, 263.
80. Brown, D.B.; Crawford, V.H.; Hall, J.W.; Hatfield, W.E. J. Phys. Chem. 1977, 81, 1303.
81. Clark, H.C.; O'Brien, R.J. Can. J. Chem. 1961, 39, 1030.
82. Herring, F.G.; Landa, B.; Thompson, R.C.; Schwerdtfeger, C.F. J. Chem. Soc. A 1971, 528.
83. a). Mabbs, F.E.; Machin, D.J. "Magnetism and Transition-Metal Complexes", Chapman and Hall: London, 1973.  
 b). Earnshaw, A. "Introduction to Magnetochemistry", Academic Press: New York, 1968.  
 c). König, E. "Landolt-Börnstein Numerical Data and Fundamental Relationships in Science and Technology. New Series II/2. Hellwege, K.H.; Hellwege, A.M., Eds., Springer-Verlag: Berlin, 1966.
84. Sams, J.R.; Tsin, T.B. Inorg. Chem. 1975, 14, 1573.
85. Paul, R.C.; Kumar, R.C.; Verma, R.D. J. Ind. Chem. Soc. 1979, 56, 251.
86. Alleyne, C.S. M.Sc. Thesis, University of British Columbia, 1973.
87. Arduini, A.L.; Garnett, M.; Thompson, R.C.; Wong, T.C.T. Can. J. Chem. 1975, 53, 3812.
88. Hendrickson, J.B.; Sternback, D.D.; Bair, K.W. Acc. Chem. Res. 1977, 10, 306.
89. Hansen, R.L. J. Org. Chem. 1965, 30, 4322.
90. Dueber, T.E.; Stang, P.J.; Pfeifer, W.D.; Summerville, R.H.; Imhoff, M.A.; Scheyer, P.R.; Hummel, K.; Bocker, S.; Harding, C.E.; Hanack, M. Angew. Chem. Int. Ed. Engl. 1970, 32, 3195.
91. Howells, R.D.; McCown, J.D. Chem. Rev. 1977, 77, 69.
92. Deacon, G.B.; Raston, C.L.; Tunaley, D.; White, A.H. Aust. J. Chem. 1979, 32, 3195.
93. Cragel, J.; Pett, V.B.; Glick, M.D.; DeSimone, R.E. Inorg. Chem. 1978, 17, 2895.
94. Peng, S.-M.; Ibers, J.A.; Millar, M.; Holm, R.H. J. Am. Chem. Soc. 1976, 98, 8037.
95. DeSimone, R.E.; Glick, M.D. Inorg. Chem. 1978, 17, 3574.



96. Charbonnier, F.; Faure, R.; Loiseleur, H. Acta Crystallogr., Sect. B 1977, B33, 1845.
97. Anderson, O.P.; Packard, A.B. Inorg. Chem. 1979, 18, 1129.
98. Komiya, S.; Huffman, J.C.; Kochi, J.K. Inorg. Chem. 1977, 16, 2138.
99. Nieuwpoort, G.; Verschoor, G.C.; Reedijk, J. J. Chem. Soc., Dalton Trans. 1983, 531.
100. Humphrey, M.B.; Lamanna, W.M.; Brookhart, M.; Husk, G.R. Inorg. Chem. 1983, 22, 3355.
101. Dedert, P.L.; Sorrell, T.; Marks, T.J.; Ibers, J.A. Inorg. Chem. 1982, 21, 3506.
102. Charbonnier, F.; Faure, R.; Loiseleur, H. Acta Crystallogr., Sect. B 1978, B34, 1504.
103. Clegg, W.; Akhter, L.; Garner, C.D. J. Chem. Soc., Chem. Commun. 1984, 101.
104. Cocolios, P.; Fournari, P.; Guillard, R.; Lecomte, C.; Protas, J.; Boubel, J. J. Chem. Soc., Dalton Trans. 1980, 2081.
105. Doyle, G.; Eriksen, K.A.; Van Engen, D. Inorg. Chem. 1983, 22, 2892.
106. Dines, M.B.; Bird, P.H. J. Chem. Soc., Chem. Commun. 1973, 12.
107. Bino, A.; Cotton, F.A.; Fanwick, P.E. Inorg. Chem. 1980, 19, 1215.
108. Almenningen, A.; Bastiansen, O.; Hansen, L. Acta Chem. Scand. 1955, 9, 1306.
109. Bak, B.; Hansen-Nygard, L.; Rastrup-Andersen, J. J. Mol. Spectrosc. 1958, 2, 361.
110. Doedens, R.J.; Dahl, L.F. J. Am. Chem. Soc. 1966, 88, 4847.
111. Cox, E.G.; Cruickshank, D.W.J.; Smith, S.A.S. Roy. Soc. London, Proc. 1958, 247A, 1.
112. Johnson, P.L.; Cheer, C.J.; Schaefer, J.P.; James, V.J.; Moore, F.H. Tetrahedron 1972, 28, 2893.
113. Johnson, P.L.; Schaefer, J.P.; James, V.J.; McConnell, J.F. Tetrahedron 1972, 28, 2901.

114. James, V.J.; McConnell, J.F. Tetrahedron 1971, 27, 5475.
115. Arora, S.K.; Sundaralingam, M. Acta Crystallogr., Sect. B, 1971, B27, 1293.
116. Jahn, H.A.; Teller, E. Roy. Soc. London, Proc. 1937, 161A, 220.
117. Mazzi, F. Acta Crystallogr. 1958, 8, 137.
118. Wheatley, P.J. Acta Crystallogr. 1957, 10, 182.
119. Kline, C.H.; Turkevich, J. J. Chem. Phys. 1944, 12, 300.
120. Corrsin, L.; Fox, B.J.; Lord, R.C. J. Chem. Phys. 1953, 21, 1170.
121. Clark, R.J.H.; Williams, C.S. Inorg. Chem. 1965, 4, 350.
122. Burger, H.; Burczyk, K.; Blaschette, A. Monat. fur Chem. 1970, 101, 102.
123. Schomaker, V.; Pauling, L. J. Am. Chem. Soc. 1939, 61, 1769.
124. Lord, R.C.; Marston, A.L.; Miller, F.A. Spectrochim. Acta 1957, 9, 113.
125. Lewis, J.; Nyholm, R.S.; Smith, P.W. J. Chem. Soc. 1961, 4591.
126. Sabatini, A.; Bertini, I. Inorg. Chem. 1965, 4, 959.
127. Bailey, R.A.; Kozak, S.L.; Michelsen, T.W.; Mills, W.N. Coord. Chem. Rev. 1971, 6, 407.
128. Clark, R.J.H.; Williams, C.S. Spectrochim. Acta 1966, 22, 1081.
129. Kinell, P.O.; Strandberg, B. Acta Chem. Scand. 1959, 13, 1607.
130. Hathaway, B.J.; Underhill, A.E. J. Chem. Soc. 1961, 3091.
131. Begun, G.M.; Rutenberg, A.C. Inorg. Chem. 1967, 6, 2212.
132. Thompson, R.C. Unpublished data.
133. Lever, A.B.P.; Mantovani, E. Inorg. Chem. 1971, 10, 817.
134. Hathaway, B.J.; Billings, D.E.; Nicholls, P.; Procter, I.M. J. Chem. Soc. A, 1969, 319.
135. Lever, A.B.P. J. Chem. Ed. 1974, 51, 612.

136. Lines, M.E. J. Phys. Chem. Solids 1970, 31, 101.
137. Sekizaki, M. Acta Crystallogr. Sect. B 1973, B29, 327.
138. Eckberg, R.P.; Hatfield, W.E. J. Chem. Soc., Dalton Trans. 1975, 616.
139. Hall, J.W. Ph.D. Thesis, University of North Carolina, 1977.
140. Estes, W.E.; Hatfield, W.E.; Van Ooijen, J.A.C.; Reedijk, J. J. Chem. Soc., Dalton Trans. 1980, 2121.
141. Bonner, J.C.; Fisher, M.E. Phys. Rev. 1964, 135, A640.
142. König, E.; Chakravarty, A.S. Theor. Chim. Acta 1967, 9, 151.
143. Figgis, B.N. J. Chem. Soc., Faraday Trans. 1961, 57, 198.
144. König, E.; Chakravarty, A.S. Theor. Chim. Acta 1967, 9, 171.
145. Figgis, B.N.; Lewis, J.; Mabbs, F.E. J. Chem. Soc. 1960, 2480.
146. Figgis, B.N.; Lewis, J.; Mabbs, F.E.; Webb, G.A. J. Chem. Soc. A 1966, 1411.
147. Dunn, T.M. J. Chem. Soc., Faraday Trans. 1961, 57, 1441.
148. Gregson, A.K.; Mitra, S. Chem. Phys. Lett. 1969, 3, 528.
149. Figgis, B.N. Trans. Faraday Soc. 1961, 57, 198.
150. a). Edwards, P.R.; Johnson, C.E.; Williams, R.J.D. J. Chem. Phys. 1967, 47, 2074.  
b). Klein, C.L.; O'Connor, C.J.; Majeste, R.J.; Trefonas, L.M. J. Chem. Soc., Dalton Trans. 1982, 2419.
151. Nakano, N.; Otsuka, J.; Tasaki, A. Biochim. Biophys. Acta 1971, 236, 222.
152. Gerloch, M.; McMeeking, R.F.; White, A.M. J. Chem. Soc. Dalton Trans. 1975, 2452.
153. Dockum, B.W.; Reiff, W.M. Inorg. Chem. 1982, 21, 391.
154. Dockum, B.W.; Reiff, W.M. Inorg. Chem. 1982, 21, 1406.
155. Haasnoot, J.G.; Groeneveld, W.L. Z. Naturforsch. 1977, 326, 553.
156. Engelfriet, D.W.; den Brinken, W.; Verschoor, G.C.;

- Gorter, S. Acta Crystallogr. Sect. B 1979, B35, 2922.
157. Engelfriet, D.W.; Groeneveld, W.L.; Nap, G.M. Z. Naturforsch. 1980, 35A, 852.
  158. The reader is referred to the following texts:  
 a). Bancroft, G.N. "Mössbauer Spectroscopy", McGraw-Hill: London, 1973.  
 b). Greenwood, N.N.; Gibb, T.C., "Mössbauer Spectroscopy", Chapman and Hall: London, 1971.
  159. Kundig, W. Nucl. Instr. Meth. 1967, 48, 219.
  160. Tominaga, T.; Morimoto, T.; Takeda, M.; Saito, N. Inorg. Nucl. Chem. Lett. 1966, 2, 193.
  161. Smith, D.W. Coord. Chem. Rev. 1976, 21, 93
  162. Yeats, P.A.; Sams, J.R.; Aubke, F. J. Chem. Soc. Chem. Commun. 1969 791.
  163. Allen, P.A.; Lerbscher, J.A.; Trotter, J. J. Chem. Soc. A, 1971, 2507.
  164. Nelson, J.; Nelson, S.M. J. Chem. Soc. A 1969, 1597.
  165. Forster, D.; Goodgame, D.M.L. J. Chem. Soc. 1965, 1286.
  166. Maki, A.A.; Decius, J.C. J. Chem. Phys. 1959, 31, 772.
  167. Decius, J.C.; Gordon, J. J. Chem. Phys. 1967, 47, 1286.
  168. Britton, D.; Dunitz, J.D. Acta Crystallogr. 1965, 18, 424.
  169. Wagner, G.R.; Friedberg, S.A. Phys. Lett. 1964, 9, 11.
  170. Fisher, M.E. Am. J. Phys. 1964, 32, 343.
  171. Rushbrooke, G.S.; Wood, P.S. Mol. Phys. 1958, 1, 257.
  172. Weng, C.H. Ph.D. Thesis, Carnegie-Mellon University, 1968.
  173. Hiller, W.; Strahle, J.; Datz, A.; Hanack, M.; Hatfield, W.E.; Gutlich, P. J. Am. Chem. Soc. 1984, 106, 329.
  174. See reference 75d, p. 188.
  175. Fisher, M.E. Rept. Prog. Phys. 1967, 30, 615.
  176. Haynes, J.S.; Hume, A.R.; Sams, J.R.; Thompson, R.C. Chem. Phys. 1983, 78, 127.
  177. Haynes, J.S. M.Sc Thesis, University of British Columbia, 1980.

178. a). Kamerlingh Onnes, H.K.; Perrier, A. Commun. Kamerlingh Onnes Lab. University of Leiden, 1912, 12, 129b.  
b). Kamerlingh Onnes, H.K.; Perrier, A. Commun. Kamerkingh Onnes Lab. University of Leiden, 1913, 2, 132e.  
c). Jackson, L.C. Commun. Kamerlingh Onnes Lab. University of Leiden, 1923, 15, 163.
179. Frazer, B.C.; Brown, P.J. Phys. Rev. 1962, 125 1283.
180. Reiff, W.M.; Dockum, B.W. J. Solid State Chem. 1980, 31, 407.
181. Nicolini, C.; Reiff, W.M. J. Solid State Chem. 1982, 44, 141.
182. Cheng, C.; Wong, H.; Reiff, W.M. Inorg. Chem. 1977, 16, 819.
183. Witteveen, H.T.; Reedijk, J. J. Solid State Chem. 1974, 10, 151.

## APPENDIX I, Complete X-ray Structural Parameters

PART A,  $\text{Fe}(\text{py})_4(\text{RSO}_3)_2$  Complexes

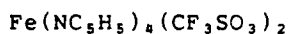
Final positional (fractional  $\times 10^4$ , Fe and S  $\times 10^5$ , H  $\times 10^3$ )  
 and isotropic thermal parameters ( $\bar{U} \times 10^3 \text{ \AA}^2$ )  
 with estimated standard deviations in parentheses\*

Atom	$\bar{x}$	$\bar{y}$	$\bar{z}$	$\bar{U}_{eq}/\bar{U}_{iso}$
$\text{Fe}(\text{NC}_5\text{H}_5)_4(\text{CH}_3\text{SO}_3)_2$				
Fe(1)	40090	68958( 6)	63300	37
Fe(2)	90418( 6)	66988( 6)	62924( 5)	34
S(1)	49188(10)	91714(12)	78340( 8)	43
S(2)	35615(10)	44572(15)	48373( 9)	53
S(3)	86211(10)	94617(13)	49533( 8)	49
S(4)	96112( 9)	35613(13)	73588( 8)	46
O(1)	4294( 2)	8465( 4)	7167( 2)	56
O(2)	3596( 3)	5326( 4)	5495( 2)	59
O(3)	8660( 2)	8477( 4)	5578( 2)	48
O(4)	9304( 2)	5035( 4)	7085( 2)	54
O(5)	5211( 4)	8176( 5)	8462( 2)	85
O(6)	5602( 3)	9844( 4)	7654( 3)	69
O(7)	3246( 4)	5303( 7)	4163( 3)	114
O(8)	4361( 3)	3759( 6)	4933( 4)	108
O(9)	8199( 3)	8814( 5)	4229( 2)	75
O(10)	9486( 3)	10013( 5)	5041( 3)	82
O(11)	10516( 3)	3528( 5)	7723( 4)	98
O(12)	9261( 4)	2481( 4)	6798( 3)	95
N(1)	3310( 3)	5609( 5)	6971( 2)	45
N(2)	2842( 3)	8207( 4)	5735( 2)	43
N(3)	4719( 3)	8146( 4)	5707( 2)	44
N(4)	5179( 3)	5584( 4)	6892( 2)	42
N(5)	7829( 3)	5567( 4)	5617( 2)	41
N(6)	8394( 3)	7831( 4)	7014( 2)	41
N(7)	10235( 2)	7832( 4)	6966( 2)	39
N(8)	9714( 3)	5687( 4)	5575( 2)	40
C(1)	4327( 5)	10595( 8)	8065( 4)	84
C(2)	2814( 6)	3064( 9)	4803( 6)	115
C(3)	8053( 5)	10997( 7)	5078( 4)	76
C(4)	9162( 8)	3212(10)	8066( 6)	121
C(5)	3678( 3)	5335( 6)	7704( 3)	50
C(6)	3329( 4)	4370( 6)	8094( 3)	55
C(7)	2574( 4)	3680( 7)	7715( 4)	64
C(8)	2174( 4)	3992( 7)	6959( 4)	62
C(9)	2561( 3)	4945( 6)	6608( 3)	51
C(10)	2413( 3)	8901( 6)	6123( 3)	52
C(11)	1711( 4)	9793( 7)	5779( 4)	63
C(12)	1440( 3)	9947( 7)	5012( 4)	60
C(13)	1861( 3)	9243( 6)	4596( 3)	54
C(14)	2564( 3)	8396( 6)	4978( 3)	47

continued...

## PART A ,Continued

C(15)	4699( 4)	9600( 6)	5691( 3)	55
C(16)	5092( 4)	10451( 6)	5288( 4)	68
C(17)	5538( 4)	9730( 8)	4887( 4)	76
C(18)	5577( 4)	8237( 8)	4910( 4)	71
C(19)	5165( 4)	7479( 6)	5328( 3)	56
C(20)	5138( 4)	4123( 5)	6946( 3)	55
C(21)	5839( 4)	3282( 6)	7356( 4)	67
C(22)	6595( 4)	3957( 7)	7713( 4)	68
C(23)	6655( 3)	5453( 7)	7651( 3)	61
C(24)	5937( 3)	6221( 5)	7235( 3)	48
C(25)	7508( 3)	5660( 6)	4868( 3)	48
C(26)	6751( 4)	4996( 7)	4429( 3)	61
C(27)	6295( 4)	4203( 7)	4795( 4)	63
C(28)	6614( 4)	4084( 7)	5560( 4)	65
C(29)	7382( 3)	4771( 6)	5960( 3)	54
C(30)	7667( 4)	8587( 6)	6689( 3)	53
C(31)	7299( 4)	9422( 7)	7109( 4)	76
C(32)	7695( 6)	9505( 8)	7873( 5)	88
C(33)	8430( 5)	8732( 9)	8216( 3)	77
C(34)	8747( 4)	7873( 6)	7756( 3)	53
C(35)	10269( 3)	9285( 5)	7072( 3)	44
C(36)	10989( 4)	10003( 6)	7534( 4)	57
C(37)	11716( 4)	9201( 6)	7913( 3)	58
C(38)	11702( 3)	7717( 6)	7804( 3)	56
C(39)	10960( 3)	7057( 5)	7331( 3)	48
C(40)	9624( 4)	4273( 5)	5386( 3)	51
C(41)	9979( 4)	3634( 6)	4892( 3)	57
C(42)	10457( 4)	4469( 7)	4581( 3)	59
C(43)	10567( 4)	5934( 6)	4775( 3)	58
C(44)	10187( 3)	6502( 5)	5270( 3)	48

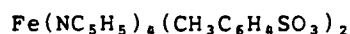


Fe	46180	49617(16)	49420	37
S(1)	68694(23)	25378(29)	43403(18)	50
S(2)	28680(25)	74813(30)	60146(18)	50
F(1)	7322( 7)	239( 8)	3430( 6)	106
F(2)	5526( 7)	224( 6)	4010( 4)	87
F(3)	5718( 7)	1490( 8)	2821( 4)	85
F(4)	1614( 8)	9892( 8)	5878( 6)	107
F(5)	3071( 7)	9703( 7)	4959( 5)	96
F(6)	1321( 7)	8558( 9)	4687( 5)	104
O(1)	5659( 6)	3246( 7)	4450( 5)	57
O(2)	7693( 6)	3349( 9)	3817( 5)	78
O(3)	7431( 8)	1896( 8)	5164( 5)	84
O(4)	3466( 6)	6670( 7)	5333( 4)	49
O(5)	1798( 7)	6761( 9)	6331( 5)	79
O(6)	3778( 7)	8136( 8)	6684( 5)	72
N(1)	4607( 7)	3841( 9)	6284( 5)	41
N(2)	4608( 7)	6101(10)	3611( 5)	46
N(3)	2873( 7)	3798( 9)	4405( 5)	40
N(4)	6357( 6)	6139( 9)	5508( 5)	43
C(1)	6318( 9)	1058(11)	3614( 7)	56
C(2)	2180(11)	8993(13)	5362( 8)	72

continued...

## PART A, Continued

C(3)	4487( 9)	2407(11)	6314( 7)	57
C(4)	4400(11)	1644(11)	7116( 8)	69
C(5)	4387(11)	2401(18)	7927( 7)	77
C(6)	4534(10)	3857(12)	7914( 7)	65
C(7)	4624(10)	4525( 9)	7084( 7)	57
C(8)	3551( 9)	6801(10)	3244( 6)	57
C(9)	3495( 9)	7604(12)	2457( 7)	65
C(10)	4605(11)	7724(13)	2027( 7)	62
C(11)	5675(10)	7023(12)	2376( 7)	68
C(12)	5655( 8)	6206(10)	3167( 6)	51
C(13)	2805( 8)	3078(10)	3607( 6)	52
C(14)	1714( 9)	2362(11)	3240( 6)	60
C(15)	682(10)	2319(14)	3710( 7)	63
C(16)	710( 8)	3058(11)	4531( 7)	56
C(17)	1832( 8)	3778( 9)	4861( 6)	46
C(18)	6437( 9)	7551(10)	5398( 6)	58
C(19)	7541(11)	8315(11)	5662( 7)	63
C(20)	8638( 9)	7590(16)	6058( 7)	61
C(21)	8552( 8)	6156(12)	6167( 7)	60
C(22)	7408( 9)	5466( 9)	5899( 6)	54



Fe	25000	25000	25000	31
S	18614( 2)	3502( 8)	21696( 5)	43
O(1)	2140(<1)	1019( 2)	2555( 1)	44
O(2)	1628( 1)	1335( 3)	1905( 2)	78
O(3)	1968( 1)	-607( 3)	1611( 2)	71
N(1)	2253( 1)	3772( 3)	1619( 2)	39
N(2)	2224( 1)	3554( 3)	3445( 2)	39
C(1)	1669( 1)	-573( 3)	2916( 2)	40
C(2)	1764( 1)	-1870( 4)	3082( 2)	57
C(3)	1608( 1)	-2583( 4)	3651( 3)	67
C(4)	1360( 1)	-2029( 4)	4083( 2)	58
C(5)	1269( 1)	-705( 5)	3913( 3)	65
C(6)	1419( 1)	14( 4)	3341( 3)	55
C(7)	1188( 2)	-2812( 7)	4703( 4)	88
C(8)	2241( 1)	5125( 3)	1714( 2)	49
C(9)	2094( 1)	5967( 5)	1186( 3)	63
C(10)	1952( 1)	5438( 5)	540( 3)	72
C(11)	1969( 1)	4054( 6)	436( 3)	69
C(12)	2118( 1)	3266( 4)	983( 2)	50
C(13)	2373( 1)	4113( 4)	4051( 2)	56
C(14)	2211( 1)	4450( 5)	4720( 2)	68
C(15)	1884( 1)	4246( 5)	4773( 2)	58
C(16)	1723( 1)	3710( 4)	4158( 2)	50
C(17)	1899( 1)	3371( 3)	3504( 2)	42
H(2)	189( 1)	-221( 5)	282( 3)	64(14)
H(3)	166( 2)	-357( 8)	386( 5)	137(23)
H(5)	110( 2)	-35( 8)	429( 6)	164(31)
H(6)	136( 1)	97( 5)	325( 3)	62(11)
H(7a)	115( 1)	-380( 7)	449( 4)	111(20)
H(7b)	135( 1)	-312( 6)	491( 4)	85(19)
H(7c)	98( 3)	-254( 9)	484( 8)	187(39)
H(8)	233( 1)	550( 3)	211( 3)	37( 8)
H(9)	206( 1)	685( 6)	123( 3)	75(14)
H(10)	188( 2)	616( 7)	11( 5)	125(22)
H(11)	187( 1)	371( 5)	4( 3)	74(14)
H(12)	214( 1)	235( 4)	95( 2)	42( 9)
H(13)	259( 1)	421( 3)	399( 2)	44( 9)
H(14)	233( 1)	477( 4)	511( 3)	71(13)
H(15)	176( 1)	446( 6)	522( 4)	99(18)
H(16)	148( 1)	357( 5)	417( 3)	78(14)
H(17)	178( 1)	296( 3)	306( 2)	35( 8)

\*  $\underline{U}_{\text{eq}} = 1/3 \text{ trace}(\text{diagonalized } \underline{U})$



## PART A, Continued

Bond lengths (Å) with estimated  
standard deviations in parentheses

Bond	uncorr.	corr.	Bond	uncorr.	corr.
$\text{Fe}(\text{NC}_5\text{H}_5)_4(\text{CH}_3\text{SO}_3)_2$					
Fe(1)-O(1)	2.052(3)	2.057	N(6)-C(30)	1.338(6)	1.339
Fe(1)-O(2)	2.054(3)	2.059	N(6)-C(34)	1.309(6)	1.310
Fe(1)-N(1)	2.254(4)	2.258	N(7)-C(35)	1.337(6)	1.339
Fe(1)-N(2)	2.219(4)	2.223	N(7)-C(39)	1.358(6)	1.360
Fe(1)-N(3)	2.227(4)	2.231	N(8)-C(40)	1.331(6)	1.332
Fe(1)-N(4)	2.211(4)	2.214	N(8)-C(44)	1.338(6)	1.339
Fe(2)-O(3)	2.057(3)	2.062	C(5)-C(6)	1.389(7)	1.390
Fe(2)-O(4)	2.059(3)	2.064	C(6)-C(7)	1.360(8)	1.362
Fe(2)-N(5)	2.224(4)	2.228	C(7)-C(8)	1.370(9)	1.372
Fe(2)-N(6)	2.239(4)	2.243	C(8)-C(9)	1.371(8)	1.373
Fe(2)-N(7)	2.201(4)	2.205	C(10)-C(11)	1.382(8)	1.383
Fe(2)-N(8)	2.213(4)	2.217	C(11)-C(12)	1.356(8)	1.358
S(1)-O(1)	1.469(4)	1.491	C(12)-C(13)	1.367(8)	1.368
S(1)-O(5)	1.431(4)	1.455	C(13)-C(14)	1.374(7)	1.374
S(1)-O(6)	1.422(4)	1.445	C(15)-C(16)	1.386(8)	1.387
S(1)-C(1)	1.764(6)	1.788	C(16)-C(17)	1.384(10)	1.386
S(2)-O(2)	1.446(4)	1.478	C(17)-C(18)	1.363(9)	1.364
S(2)-O(7)	1.416(5)	1.448	C(18)-C(19)	1.383(8)	1.384
S(2)-O(8)	1.421(5)	1.453	C(20)-C(21)	1.383(8)	1.383
S(2)-C(2)	1.758(7)	1.788	C(21)-C(22)	1.349(9)	1.350
S(3)-O(3)	1.456(3)	1.475	C(22)-C(23)	1.374(9)	1.376
S(3)-O(9)	1.422(4)	1.440	C(23)-C(24)	1.369(7)	1.370
S(3)-O(10)	1.470(4)	1.490	C(25)-C(26)	1.380(8)	1.382
S(3)-C(3)	1.745(6)	1.763	C(26)-C(27)	1.381(9)	1.383
S(4)-O(4)	1.466(3)	1.484	C(27)-C(28)	1.349(9)	1.352
S(4)-O(11)	1.417(5)	1.445	C(28)-C(29)	1.384(8)	1.386
S(4)-O(12)	1.411(4)	1.439	C(30)-C(31)	1.375(8)	1.375
S(4)-C(4)	1.750(9)	1.787	C(31)-C(32)	1.355(10)	1.357
N(1)-C(5)	1.319(6)	1.321	C(32)-C(33)	1.361(11)	1.362
N(1)-C(9)	1.336(6)	1.339	C(33)-C(34)	1.390(8)	1.390
N(2)-C(10)	1.332(7)	1.333	C(35)-C(36)	1.376(7)	1.376
N(2)-C(14)	1.341(6)	1.343	C(36)-C(37)	1.378(8)	1.379
N(3)-C(15)	1.326(6)	1.327	C(37)-C(38)	1.367(8)	1.369
N(3)-C(19)	1.330(7)	1.332	C(38)-C(39)	1.381(7)	1.381
N(4)-C(20)	1.339(6)	1.341	C(40)-C(41)	1.379(7)	1.380
N(4)-C(24)	1.330(6)	1.331	C(41)-C(42)	1.361(8)	1.362
N(5)-C(25)	1.319(6)	1.322	C(42)-C(43)	1.379(8)	1.380
N(5)-C(29)	1.344(6)	1.347	C(43)-C(44)	1.383(8)	1.384

continued...

## PART A, Continued

 $\text{Fe}(\text{NC}_5\text{H}_5)_4(\text{CF}_3\text{SO}_3)_2$ 

Fe -O(1)	2.102(6)	2.107	N(2)-C(8)	1.343(11)	1.345
Fe -O(4)	2.110(6)	2.115	N(2)-C(12)	1.337(11)	1.338
Fe -N(1)	2.223(8)	2.227	N(3)-C(13)	1.340(11)	1.342
Fe -N(2)	2.215(8)	2.219	N(3)-C(17)	1.338(10)	1.339
Fe -N(3)	2.190(7)	2.193	N(4)-C(18)	1.326(12)	1.328
Fe -N(4)	2.203(7)	2.206	N(4)-C(22)	1.337(11)	1.338
S(1)-O(1)	1.452(7)	1.471	C(3)-C(4)	1.383(13)	1.384
S(1)-O(2)	1.429(7)	1.449	C(4)-C(5)	1.38(2)	1.38
S(1)-O(3)	1.412(7)	1.427	C(5)-C(6)	1.36(2)	1.37
S(1)-C(1)	1.793(10)	1.813	C(6)-C(7)	1.375(13)	1.377
S(2)-O(4)	1.446(7)	1.461	C(8)-C(9)	1.368(13)	1.368
S(2)-O(5)	1.425(7)	1.441	C(9)-C(10)	1.383(13)	1.385
S(2)-O(6)	1.423(7)	1.439	C(10)-C(11)	1.346(14)	1.348
S(2)-C(2)	1.803(11)	1.822	C(11)-C(12)	1.385(13)	1.386
F(1)-C(1)	1.348(10)	1.372	C(13)-C(14)	1.377(12)	1.378
F(2)-C(1)	1.315(11)	1.339	C(14)-C(15)	1.343(14)	1.345
F(3)-C(1)	1.319(10)	1.343	C(15)-C(16)	1.381(14)	1.382
F(4)-C(2)	1.310(12)	1.330	C(16)-C(17)	1.391(11)	1.391
F(5)-C(2)	1.331(12)	1.354	C(18)-C(19)	1.374(13)	1.375
F(6)-C(2)	1.323(12)	1.348	C(19)-C(20)	1.400(14)	1.401
N(1)-C(3)	1.340(12)	1.342	C(20)-C(21)	1.35(2)	1.35
N(1)-C(7)	1.331(12)	1.332	C(21)-C(22)	1.376(12)	1.376

 $\text{Fe}(\text{NC}_5\text{H}_5)_4(\text{CH}_3\text{C}_6\text{H}_4\text{SO}_3)_2$ 

Fe -O(1)	2.076(2)	2.080	C(2)-C(3)	1.371(6)	1.378
Fe -N(1)	2.221(3)	2.226	C(3)-C(4)	1.373(6)	1.387
Fe -N(2)	2.245(3)	2.248	C(4)-C(5)	1.391(6)	1.407
S -O(1)	1.474(2)	1.489	C(4)-C(7)	1.499(6)	1.504
S -O(2)	1.437(3)	1.452	C(5)-C(6)	1.364(6)	1.370
S -O(3)	1.421(3)	1.436	C(8)-C(9)	1.375(6)	1.377
S -C(1)	1.768(3)	1.777	C(9)-C(10)	1.365(7)	1.368
N(1)-C(8)	1.347(4)	1.349	C(10)-C(11)	1.380(8)	1.382
N(1)-C(12)	1.330(4)	1.333	C(11)-C(12)	1.372(6)	1.375
N(2)-C(13)	1.335(4)	1.335	C(13)-C(14)	1.376(6)	1.376
N(2)-C(17)	1.341(4)	1.343	C(14)-C(15)	1.355(6)	1.356
C(1)-C(2)	1.369(5)	1.384	C(15)-C(16)	1.360(6)	1.362
C(1)-C(6)	1.386(5)	1.401	C(16)-C(17)	1.384(5)	1.385

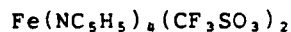
## PART A, Continued

Bond angles (deg) with estimated  
standard deviations in parentheses

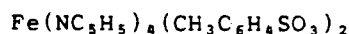
Bonds	Angle(deg)	Bonds	Angle(deg)
$\text{Fe}(\text{NC}_5\text{H}_5)_4(\text{CH}_3\text{SO}_3)_2$			
O(1)-Fe(1)-O(2)	174.1(2)	Fe(1)-N(2)-C(10)	121.0(3)
O(1)-Fe(1)-N(1)	89.1(2)	Fe(1)-N(2)-C(14)	121.6(3)
O(1)-Fe(1)-N(2)	86.63(15)	C(10)-N(2)-C(14)	117.3(4)
O(1)-Fe(1)-N(3)	90.95(15)	Fe(1)-N(3)-C(15)	120.7(4)
O(1)-Fe(1)-N(4)	94.49(15)	Fe(1)-N(3)-C(19)	122.0(3)
O(2)-Fe(1)-N(1)	86.8(2)	C(15)-N(3)-C(19)	117.3(5)
O(2)-Fe(1)-N(2)	89.28(15)	Fe(1)-N(4)-C(20)	121.0(3)
O(2)-Fe(1)-N(3)	93.28(15)	Fe(1)-N(4)-C(24)	121.4(3)
O(2)-Fe(1)-N(4)	89.69(15)	C(20)-N(4)-C(24)	117.5(4)
N(1)-Fe(1)-N(2)	91.78(15)	Fe(2)-N(5)-C(25)	122.1(3)
N(1)-Fe(1)-N(3)	179.06(15)	Fe(2)-N(5)-C(29)	121.0(3)
N(1)-Fe(1)-N(4)	89.44(15)	C(25)-N(5)-C(29)	116.9(4)
N(2)-Fe(1)-N(3)	89.16(15)	Fe(2)-N(6)-C(30)	120.2(3)
N(2)-Fe(1)-N(4)	178.4(2)	Fe(2)-N(6)-C(34)	121.3(3)
N(3)-Fe(1)-N(4)	89.62(15)	C(30)-N(6)-C(34)	118.2(4)
O(3)-Fe(2)-O(4)	171.62(15)	Fe(2)-N(7)-C(35)	122.3(3)
O(3)-Fe(2)-N(5)	88.81(14)	Fe(2)-N(7)-C(39)	120.6(3)
O(3)-Fe(2)-N(6)	85.66(14)	C(35)-N(7)-C(39)	117.1(4)
O(3)-Fe(2)-N(7)	91.07(14)	Fe(2)-N(8)-C(40)	122.0(3)
O(3)-Fe(2)-N(8)	92.36(14)	Fe(2)-N(8)-C(44)	120.8(3)
O(4)-Fe(2)-N(5)	89.71(15)	C(40)-N(8)-C(44)	117.0(4)
O(4)-Fe(2)-N(6)	86.15(15)	N(1)-C(5)-C(6)	122.6(5)
O(4)-Fe(2)-N(7)	90.33(14)	C(5)-C(6)-C(7)	119.3(5)
O(4)-Fe(2)-N(8)	95.89(15)	C(6)-C(7)-C(8)	118.5(5)
N(5)-Fe(2)-N(6)	91.86(15)	C(7)-C(8)-C(9)	118.9(5)
N(5)-Fe(2)-N(7)	179.44(15)	N(1)-C(9)-C(8)	123.2(5)
N(5)-Fe(2)-N(8)	90.23(15)	N(2)-C(10)-C(11)	122.9(5)
N(6)-Fe(2)-N(7)	87.59(15)	C(10)-C(11)-C(12)	118.4(5)
N(6)-Fe(2)-N(8)	177.09(15)	C(11)-C(12)-C(13)	120.2(5)
N(7)-Fe(2)-N(8)	90.32(15)	C(12)-C(13)-C(14)	118.2(5)
O(1)-S(1)-O(5)	111.2(2)	N(2)-C(14)-C(13)	123.0(5)
O(1)-S(1)-O(6)	111.9(3)	N(3)-C(15)-C(16)	124.0(6)
O(1)-S(1)-C(1)	104.0(3)	C(15)-C(16)-C(17)	117.6(5)
O(5)-S(1)-O(6)	113.2(3)	C(16)-C(17)-C(18)	119.0(6)
O(5)-S(1)-C(1)	109.0(4)	C(17)-C(18)-C(19)	119.3(6)
O(6)-S(1)-C(1)	107.0(3)	N(3)-C(19)-C(18)	122.8(5)
O(2)-S(2)-O(7)	110.7(3)	N(4)-C(20)-C(21)	122.6(5)
O(2)-S(2)-O(8)	111.8(3)	C(20)-C(21)-C(22)	118.8(5)
O(2)-S(2)-C(2)	104.5(3)	C(21)-C(22)-C(23)	119.5(5)
O(7)-S(2)-O(8)	113.6(4)	C(22)-C(23)-C(24)	118.8(5)
O(7)-S(2)-C(2)	108.6(4)	N(4)-C(24)-C(23)	122.8(5)
O(8)-S(2)-C(2)	107.0(4)	N(5)-C(25)-C(26)	123.9(5)
O(3)-S(3)-O(9)	112.4(2)	C(25)-C(26)-C(27)	118.2(5)
O(3)-S(3)-O(10)	110.2(3)	C(26)-C(27)-C(28)	119.0(5)
O(3)-S(3)-C(3)	105.4(3)	C(27)-C(28)-C(29)	119.5(5)
O(9)-S(3)-O(10)	113.0(3)	N(5)-C(29)-C(28)	122.6(5)
O(9)-S(3)-C(3)	110.4(3)	N(6)-C(30)-C(31)	121.9(5)
O(10)-S(3)-C(3)	105.0(3)	C(30)-C(31)-C(32)	119.0(6)
O(4)-S(4)-O(11)	111.8(3)	C(31)-C(32)-C(33)	120.0(6)
O(4)-S(4)-O(12)	112.0(2)	C(32)-C(33)-C(34)	117.6(6)
O(4)-S(4)-C(4)	104.2(3)	N(6)-C(34)-C(33)	123.1(6)
O(11)-S(4)-O(12)	116.2(4)	N(7)-C(35)-C(36)	123.3(5)
O(11)-S(4)-C(4)	106.4(5)	C(35)-C(36)-C(37)	119.1(5)
O(12)-S(4)-C(4)	105.2(4)	C(36)-C(37)-C(38)	118.7(5)
Fe(1)-O(1)-S(1)	149.8(2)	C(37)-C(38)-C(39)	119.5(5)
Fe(1)-O(2)-S(2)	158.9(3)	N(7)-C(39)-C(38)	122.3(4)
Fe(2)-O(3)-S(3)	157.8(2)	N(8)-C(40)-C(41)	123.5(5)
Fe(2)-O(4)-S(4)	152.8(3)	C(40)-C(41)-C(42)	119.3(5)
Fe(1)-N(1)-C(5)	120.7(3)	C(41)-C(42)-C(43)	118.3(5)
Fe(1)-N(1)-C(9)	121.3(3)	C(42)-C(43)-C(44)	119.2(5)
C(5)-N(1)-C(9)	117.5(4)	N(8)-C(44)-C(43)	122.7(4)

continued...

## PART A, Continued



O(1)-Fe -O(4)	175.2(3)	C(13)-N(3)-C(17)	117.3(7)
O(1)-Fe -N(1)	90.0(3)	Fe -N(4)-C(18)	120.4(6)
O(1)-Fe -N(2)	90.8(3)	Fe -N(4)-C(22)	122.2(6)
O(1)-Fe -N(3)	86.8(3)	C(18)-N(4)-C(22)	117.1(7)
O(1)-Fe -N(4)	93.9(3)	S(1)-C(1)-F(1)	110.2(7)
O(4)-Fe -N(1)	93.1(3)	S(1)-C(1)-F(2)	111.6(7)
O(4)-Fe -N(2)	86.1(3)	S(1)-C(1)-F(3)	112.2(7)
O(4)-Fe -N(3)	89.5(3)	F(1)-C(1)-F(2)	107.3(9)
O(4)-Fe -N(4)	89.8(3)	F(1)-C(1)-F(3)	107.5(8)
N(1)-Fe -N(2)	179.2(4)	F(2)-C(1)-F(3)	107.8(8)
N(1)-Fe -N(3)	90.0(3)	S(2)-C(2)-F(4)	111.9(8)
N(1)-Fe -N(4)	89.2(3)	S(2)-C(2)-F(5)	111.3(7)
N(2)-Fe -N(3)	89.9(3)	S(2)-C(2)-F(6)	110.8(8)
N(2)-Fe -N(4)	90.9(3)	F(4)-C(2)-F(5)	108.8(10)
N(3)-Fe -N(4)	178.9(3)	F(4)-C(2)-F(6)	108.2(9)
O(1)-S(1)-O(2)	113.8(5)	F(5)-C(2)-F(6)	105.7(10)
O(1)-S(1)-O(3)	112.5(5)	N(1)-C(3)-C(4)	123.6(9)
O(1)-S(1)-C(1)	100.8(4)	C(3)-C(4)-C(5)	118.3(10)
O(2)-S(1)-O(3)	117.5(5)	C(4)-C(5)-C(6)	118.9(10)
O(2)-S(1)-C(1)	105.1(5)	C(5)-C(6)-C(7)	118.7(9)
O(3)-S(1)-C(1)	104.9(5)	N(1)-C(7)-C(6)	124.4(8)
O(4)-S(2)-O(5)	113.2(5)	N(2)-C(8)-C(9)	123.9(9)
O(4)-S(2)-O(6)	112.9(4)	C(8)-C(9)-C(10)	117.8(9)
O(4)-S(2)-C(2)	102.7(5)	C(9)-C(10)-C(11)	119.5(10)
O(5)-S(2)-O(6)	117.8(5)	C(10)-C(11)-C(12)	119.5(9)
O(5)-S(2)-C(2)	104.9(5)	N(2)-C(12)-C(11)	122.3(8)
O(6)-S(2)-C(2)	103.1(5)	N(3)-C(13)-C(14)	122.9(8)
Fe -O(1)-S(1)	150.8(4)	C(13)-C(14)-C(15)	119.5(9)
Fe -O(4)-S(2)	152.0(4)	C(14)-C(15)-C(16)	119.3(9)
Fe -N(1)-C(3)	120.3(6)	C(15)-C(16)-C(17)	118.5(8)
Fe -N(1)-C(7)	123.5(6)	N(3)-C(17)-C(16)	122.4(8)
C(3)-N(1)-C(7)	116.0(8)	N(4)-C(18)-C(19)	122.7(9)
Fe -N(2)-C(8)	120.4(6)	C(18)-C(19)-C(20)	119.4(10)
Fe -N(2)-C(12)	122.5(6)	C(19)-C(20)-C(21)	117.6(9)
C(8)-N(2)-C(12)	116.9(8)	C(20)-C(21)-C(22)	119.7(8)
Fe -N(3)-C(13)	121.4(6)	N(4)-C(22)-C(21)	123.4(8)
Fe -N(3)-C(17)	121.3(6)		



O(1)-Fe -N(1)	96.22(9)	C(13)-N(2)-C(17)	116.4(3)
O(1)-Fe -N(2)	86.38(9)	S -C(1)-C(2)	120.6(3)
O(1)-Fe -O(1)'	174.69(14)	S -C(1)-C(6)	120.1(3)
O(1)-Fe -N(1)'	87.44(9)	C(2)-C(1)-C(6)	119.3(3)
O(1)-Fe -N(2)'	89.75(9)	C(1)-C(2)-C(3)	119.9(4)
N(1)-Fe -N(2)	90.73(9)	C(2)-C(3)-C(4)	122.2(4)
N(1)-Fe -N(1)'	92.99(14)	C(3)-C(4)-C(5)	117.0(4)
N(1)-Fe -N(2)'	173.10(10)	C(3)-C(4)-C(7)	122.2(5)
N(2)-Fe -N(2)'	86.18(14)	C(5)-C(4)-C(7)	120.8(5)
O(1)-S -O(2)	110.6(2)	C(4)-C(5)-C(6)	121.6(4)
O(1)-S -O(3)	111.8(2)	C(1)-C(6)-C(5)	120.0(4)
O(1)-S -C(1)	103.92(14)	N(1)-C(8)-C(9)	122.3(4)
O(2)-S -O(3)	115.8(2)	C(8)-C(9)-C(10)	120.1(4)
O(2)-S -C(1)	106.7(2)	C(9)-C(10)-C(11)	117.8(4)
O(3)-S -C(1)	107.0(2)	C(10)-C(11)-C(12)	119.5(4)
Fe -O(1)-S	147.1(2)	N(1)-C(12)-C(11)	123.0(4)
Fe -N(1)-C(8)	119.6(2)	N(2)-C(13)-C(14)	123.2(3)
Fe -N(1)-C(12)	123.1(2)	C(13)-C(14)-C(15)	119.6(4)
C(8)-N(1)-C(12)	117.3(3)	C(14)-C(15)-C(16)	118.7(3)
Fe -N(2)-C(13)	122.6(2)	C(15)-C(16)-C(17)	119.2(3)
Fe -N(2)-C(17)	119.3(2)	N(2)-C(17)-C(16)	122.9(3)

Here and elsewhere primed atoms have coordinates related by the symmetry operation:  $1/2-x, 1/2-y, z$ .

PART B,  $\text{Cu}(\text{py})_4(\text{CF}_3\text{SO}_3)_2$ 

Final positional (fractional  $\times 10^4$ , Cu and S  $\times 10^5$ )  
 and isotropic thermal parameters ( $\bar{U} \times 10^3 \text{ \AA}^2$ )  
 with estimated standard deviations in parentheses

Atom	$\bar{x}$	$\bar{y}$	$\bar{z}$	$\bar{U}_{eq} / \bar{U}_{iso}$
Cu	50000	38590( 6)	25000	58
S	22562(16)	38966(11)	10286(11)	61
F(1)	1735( 7)	4037( 5)	-477( 3)	150
F(2)	3449( 6)	3370( 3)	-200( 3)	145
F(3)	3422( 5)	4670( 3)	-100( 3)	136
O(1)	3452( 4)	3856( 3)	1436( 3)	74
O(2)	1572( 5)	4636( 3)	1183( 4)	104
O(3)	1537( 4)	3159( 3)	1041( 3)	81
N(1)	5000	5114( 4)	2500	50
N(2)	5000	2598( 4)	2500	68
N(3)	3633( 5)	3824( 3)	3338( 4)	57
C(1)	2679(11)	4027( 5)	-20( 6)	106
C(2)	4801( 7)	5536( 4)	1838( 4)	67
C(3)	4781( 9)	6387( 4)	1824( 5)	81
C(4)	5000	6807( 5)	2500	90
C(5)	3977( 6)	2186( 4)	2268( 4)	77
C(6)	3954( 7)	1342( 4)	2248( 5)	92
C(7)	5000	918( 5)	2500	99
C(8)	3774( 6)	3416( 4)	4018( 5)	70
C(9)	2873( 9)	3322( 5)	4559( 5)	92
C(10)	1699( 9)	3684( 6)	4423( 6)	105
C(11)	1528( 7)	4102( 5)	3743( 5)	91
C(12)	2506( 7)	4177( 4)	3220( 4)	66

Calculated hydrogen coordinates (fractional  $\times 10^4$ )  
 and isotropic thermal parameters ( $\bar{U} \times 10^3 \text{ \AA}^2$ )

Atom	$\bar{x}$	$\bar{y}$	$\bar{z}$	$\bar{U}_{eq}$
H(2)	4664	5239	1346	80
H(3)	4613	6677	1332	93
H(4)	5000	7403	2500	103
H(5)	3227	2488	2110	90
H(6)	3211	1052	2059	105
H(7)	5000	322	2500	112
H(8)	4593	3170	4124	83
H(9)	3030	3008	5039	104
H(10)	1021	3635	4809	117
H(11)	714	4350	3626	104
H(12)	2379	4500	2742	79

## PART B, Continued

Final anisotropic thermal parameters ( $\underline{U}_{ij} \times 10^3$ , Cu and S  $\times 10^4 \text{ \AA}^2$ )\*

and their estimated standard deviations

Atom	$\underline{U}_{11}$	$\underline{U}_{22}$	$\underline{U}_{33}$	$\underline{U}_{12}$	$\underline{U}_{13}$	$\underline{U}_{23}$
Cu	466( 6)	369( 5)	899( 8)	0	67( 7)	0
S	541( 9)	552( 9)	749(12)	28(12)	-33(10)	-27(11)
F(1)	175( 7)	200( 8)	74( 4)	-59( 6)	-73( 4)	45( 4)
F(2)	184( 6)	140( 5)	113( 4)	-29( 4)	61( 4)	-34( 4)
F(3)	165( 5)	118( 4)	124( 4)	-52( 4)	13( 4)	37( 4)
O(1)	52( 3)	77( 3)	94( 3)	9( 3)	-10( 2)	1( 3)
O(2)	74( 3)	76( 3)	163( 5)	25( 3)	-7( 4)	-27( 4)
O(3)	68( 3)	66( 3)	107( 4)	-23( 3)	11( 3)	-2( 3)
N(1)	55( 4)	36( 4)	58( 5)	0	14( 6)	0
N(2)	52( 4)	37( 4)	114( 7)	0	-7( 6)	0
N(3)	48( 3)	40( 3)	83( 4)	-1( 3)	5( 3)	6( 4)
C(1)	130( 8)	73( 6)	116( 9)	-10( 6)	32( 8)	12( 6)
C(2)	79( 5)	52( 4)	70( 5)	0( 4)	8( 5)	6( 4)
C(3)	100( 7)	50( 4)	93( 6)	9( 5)	18( 6)	17( 4)
C(4)	104( 8)	38( 6)	128(12)	0	44(11)	0
C(5)	62( 4)	46( 4)	123( 8)	-5( 3)	-20( 5)	6( 4)
C(6)	77( 5)	49( 4)	150( 9)	-21( 3)	-14( 6)	-1( 4)
C(7)	101( 9)	37( 5)	160(11)	0	-6(10)	0
C(8)	50( 4)	62( 4)	98( 6)	-15( 4)	2( 5)	31( 5)
C(9)	75( 6)	99( 6)	100( 7)	-20( 5)	-7( 6)	45( 5)
C(10)	81( 6)	135( 8)	98( 7)	-21( 6)	33( 6)	37( 7)
C(11)	58( 5)	124( 8)	92( 7)	14( 5)	12( 5)	26( 6)
C(12)	61( 5)	61( 4)	76( 5)	5( 4)	11( 4)	10( 4)

\*The anisotropic thermal parameters employed in the refinement are  $\underline{U}_{ij}$  in the expression:

$$\underline{f} = \underline{f}^0 \exp(-2\pi^2 \sum_{i,j} \underline{U}_{ij} \underline{h}_i \underline{h}_j \underline{a}_i^* \underline{a}_j^*)$$

## PART B, Continued

Bond lengths (Å) with estimated  
standard deviations in parentheses

Bond	Length(Å)	Bond	Length(Å)
Cu -O(1)	2.425(4)	N(2)-C(5)	1.331(6)
Cu -N(1)	2.045(6)	N(3)-C(8)	1.331(8)
Cu -N(2)	2.053(6)	N(3)-C(12)	1.336(7)
Cu -N(3)	2.020(5)	C(2)-C(3)	1.386(8)
S -O(1)	1.439(4)	C(3)-C(4)	1.347(8)
S -O(2)	1.428(5)	C(5)-C(6)	1.375(9)
S -O(3)	1.422(4)	C(6)-C(7)	1.370(8)
S -C(1)	1.832(10)	C(8)-C(9)	1.326(10)
F(1)-C(1)	1.259(11)	C(9)-C(10)	1.392(11)
F(2)-C(1)	1.378(9)	C(10)-C(11)	1.343(10)
F(3)-C(1)	1.317(9)	C(11)-C(12)	1.363(9)
N(1)-C(2)	1.325(7)		

Bond angles (deg) with estimated  
standard deviations in parentheses

Bonds	Angle(deg)	Bonds	Angle(deg)
O(1)-Cu -N(1)	90.12(11)	Cu -N(3)-C(8)	122.3(5)
O(1)-Cu -N(2)	89.88(11)	Cu -N(3)-C(12)	121.4(5)
O(1)-Cu -N(3)	91.9(2)	C(8)-N(3)-C(12)	116.2(6)
O(1)-Cu -O(1)'	179.8(2)	S -C(1)-F(1)	113.4(7)
O(1)-Cu -N(3)'	88.1(2)	S -C(1)-F(2)	105.4(6)
N(1)-Cu -N(2)	180	S -C(1)-F(3)	109.7(7)
N(1)-Cu -N(3)	91.59(15)	F(1)-C(1)-F(2)	110.1(10)
N(2)-Cu -N(3)	88.41(15)	F(1)-C(1)-F(3)	113.5(9)
N(3)-Cu -N(3)'	176.8(3)	F(2)-C(1)-F(3)	104.1(8)
O(1)-S -O(2)	113.3(3)	N(1)-C(2)-C(3)	122.3(7)
O(1)-S -O(3)	115.0(3)	C(2)-C(3)-C(4)	119.4(7)
O(1)-S -C(1)	104.5(4)	C(3)-C(4)-C(3)'	118.9(8)
O(2)-S -O(3)	116.1(3)	N(2)-C(5)-C(6)	121.7(6)
O(2)-S -C(1)	101.6(4)	C(5)-C(6)-C(7)	118.9(6)
O(3)-S -C(1)	104.0(4)	C(6)-C(7)-C(6)'	119.4(8)
Cu -O(1)-S	160.7(3)	N(3)-C(8)-C(9)	124.6(6)
Cu -N(1)-C(2)	121.2(4)	C(8)-C(9)-C(10)	118.5(7)
C(2)-N(1)-C(2)'	117.6(7)	C(9)-C(10)-C(11)	118.3(8)
Cu -N(2)-C(5)	120.3(3)	C(10)-C(11)-C(12)	119.6(7)
C(5)-N(2)-C(5)'	119.3(7)	N(3)-C(12)-C(11)	122.7(6)

## PART B, Continued

Torsion angles (deg) with estimated  
standard deviations in parentheses

Atoms		Value(deg)		
N(1)-Cu	-O(1)-S	-81.6(9)	O(3)-S	-C(1)-F(1) 55.9(8)
N(2)-Cu	-O(1)-S	98.4(9)	O(3)-S	-C(1)-F(2) -64.6(7)
N(3)-Cu	-O(1)-S	10.0(9)	O(3)-S	-C(1)-F(3) -176.1(7)
O(1)'-Cu	-O(1)-S	98.4(9)	Cu	-N(1)-C(2)-C(3) 179.2(6)
N(3)'-Cu	-O(1)-S	-173.2(10)	C(2)'	-N(1)-C(2)-C(3) -0.8(6)
O(1)-Cu	-N(1)-C(2)	-31.7(4)	Cu	-N(2)-C(5)-C(6) 178.8(6)
O(1)-Cu	-N(1)-C(2)'	148.3(4)	C(5)'	-N(2)-C(5)-C(6) -1.2(6)
N(2)-Cu	-N(1)-C(2)	148	Cu	-N(3)-C(8)-C(9) -174.6(6)
N(2)-Cu	-N(1)-C(2)'	148	C(12)	-N(3)-C(8)-C(9) 2.0(10)
N(3)-Cu	-N(1)-C(2)	-123.6(4)	Cu	-N(3)-C(12)-C(11) 174.0(6)
N(3)-Cu	-N(1)-C(2)'	56.4(4)	C(8)	-N(3)-C(12)-C(11) -2.6(10)
O(1)'-Cu	-N(1)-C(2)	148.3(4)	N(1)	-C(2)-C(3)-C(4) 1.6(13)
O(1)'-Cu	-N(1)-C(2)'	-31.7(4)	C(2)	-C(3)-C(4)-C(3)' -0.8(6)
N(3)'-Cu	-N(1)-C(2)	56.4(4)	N(2)	-C(5)-C(6)-C(7) 2.3(11)
N(3)'-Cu	-N(1)-C(2)'	-123.6(4)	C(5)	-C(6)-C(7)-C(6)' -1.1(5)
O(1)-Cu	-N(2)-C(5)	-27.8(4)	N(3)	-C(8)-C(9)-C(10) -1.2(13)
O(1)-Cu	-N(2)-C(5)'	152.2(4)	C(8)	-C(9)-C(10)-C(11) 1.0(14)
N(1)-Cu	-N(2)-C(5)	152	C(9)	-C(10)-C(11)-C(12) -1.6(13)
N(1)-Cu	-N(2)-C(5)'	152	C(10)	-C(11)-C(12)-N(3) 2.5(12)
N(3)-Cu	-N(2)-C(5)	64.2(4)		
N(3)-Cu	-N(2)-C(5)'	-115.8(4)		
O(1)'-Cu	-N(2)-C(5)	152.2(4)		
O(1)'-Cu	-N(2)-C(5)'	-27.8(4)		
N(3)'-Cu	-N(2)-C(5)	-115.8(4)		
N(3)'-Cu	-N(2)-C(5)'	64.2(4)		
O(1)-Cu	-N(3)-C(8)	144.8(5)		
O(1)-Cu	-N(3)-C(12)	-31.6(5)		
N(1)-Cu	-N(3)-C(8)	-125.0(5)		
N(1)-Cu	-N(3)-C(12)	58.6(5)		
N(2)-Cu	-N(3)-C(8)	55.0(5)		
N(2)-Cu	-N(3)-C(12)	-121.4(5)		
O(1)'-Cu	-N(3)-C(8)	-34.9(5)		
O(1)'-Cu	-N(3)-C(12)	148.7(5)		
N(3)'-Cu	-N(3)-C(8)	55.0(5)		
N(3)'-Cu	-N(3)-C(12)	-121.4(5)		
O(2)-S	-O(1)-Cu	56.2(10)		
O(3)-S	-O(1)-Cu	-80.7(10)		
C(1)-S	-O(1)-Cu	165.9(9)		
O(1)-S	-C(1)-F(1)	176.9(7)		
O(1)-S	-C(1)-F(2)	56.4(7)		
O(1)-S	-C(1)-F(3)	-55.1(8)		
O(2)-S	-C(1)-F(1)	-65.0(8)		
O(2)-S	-C(1)-F(2)	174.5(6)		
O(2)-S	-C(1)-F(3)	63.0(8)		

continued /...



PART C,  $\text{Cu}(\text{pyz})_2(\text{CH}_3\text{SO}_3)_2$ 

Final positional (fractional  $\times 10^5$ , H  $\times 10^4$ )  
 and isotropic thermal parameters ( $\text{Å}^2 \times 10^3$ )  
 with estimated standard deviations in parentheses

Atom	$\underline{x}$	$\underline{y}$	$\underline{z}$	$\underline{U}_{\text{eq}}/\underline{U}_{\text{iso}}$
Cu	50000	50000	50000	23
S	54201( 6)	25913( 3)	50000	22
O(1)	44607(17)	35490(10)	50000	23
O(2)	63567(18)	24874( 9)	32452(22)	45
N(1)	50000	50000	20228(23)	21
N(2)	17181(21)	50709(12)	50000	27
C(1)	39006(28)	16391(15)	50000	32
C(2)	40744(16)	43483( 9)	10041(18)	23
C(3)	7585(26)	58949(16)	50000	30
C(4)	9358(25)	41751(15)	50000	28
H(1a)	4467(51)	851(33)	5000	67(11)
H(1b)	3239(25)	1709(15)	3882(28)	42( 5)
H(2)	3471(21)	3887(13)	1702(26)	29( 4)
H(3)	1236(31)	6524(22)	5000	24( 6)
H(4)	1412(32)	3600(24)	5000	34( 7)

## PART C, Continued

Final anisotropic thermal parameters ( $\underline{U}_{ij} \times 10^4 \text{ \AA}^2$ )\*  
and their estimated standard deviations

Atom	$\underline{U}_{11}$	$\underline{U}_{22}$	$\underline{U}_{33}$	$\underline{U}_{12}$	$\underline{U}_{13}$	$\underline{U}_{23}$
Cu	412( 2)	155( 2)	120( 2)	-26( 1)	0	0
S	202( 2)	175( 2)	277( 2)	16( 1)	0	0
O(1)	263( 6)	164( 5)	258( 6)	18( 4)	0	0
O(2)	414( 6)	424( 6)	528( 8)	-21( 4)	246( 6)	-135( 6)
N(1)	267( 7)	213( 7)	138( 6)	-41( 4)	0	0
N(2)	225( 7)	298( 8)	302( 8)	-10( 5)	0	0
C(1)	333(10)	245( 8)	396(11)	-59( 7)	0	0
C(2)	300( 6)	248( 5)	156( 5)	-95( 4)	9( 4)	7( 4)
C(3)	270(10)	258( 8)	372(11)	-38( 7)	0	0
C(4)	245( 9)	251( 8)	347(10)	18( 6)	0	0

\*The anisotropic thermal parameters employed in the refinement are  $\underline{U}_{ij}$  in the expression:

$$\underline{f} = \underline{f}^0 \exp(-2\pi^2 \sum_{i,j} \underline{U}_{ij} \underline{h}_i \underline{h}_j \underline{a}_i^* \underline{a}_j^*)$$

## PART C, Continued

Bond lengths (Å) with estimated  
standard deviations in parentheses

Bond	Length(Å)	Bond	Length(Å)
Cu -O(1)	1.9559(13)	N(1)-C(2)	1.3431(14)
Cu -N(1)	2.058(2)	N(2)-C(3)	1.338(3)
Cu -N(2)	2.692(2)	N(2)-C(4)	1.340(2)
S -O(1)	1.4832(13)	C(2)-C(2) <sup>1</sup>	1.388(2)
S -O(2)	1.4423(13)	C(3)-C(4) <sup>2</sup>	1.392(3)
S -C(1)	1.765(2)		

Table

Bond angles (deg) with estimated  
standard deviations in parentheses

Bonds	Angle(deg)	Bonds	Angle(deg)
O(1)-Cu -N(1)	90	O(2)-S -C(1)	107.99(7)
O(1)-Cu -N(2)	78.92(5)	O(2)-S -O(2) <sup>4</sup>	114.53(14)
O(1)-Cu -O(1) <sup>3</sup>	180	Cu -O(1)-S	134.90(9)
O(1)-Cu -N(2) <sup>3</sup>	101.08(5)	Cu -N(1)-C(2)	121.62(7)
O(1)-Cu -N(1) <sup>4</sup>	90	Cu -N(1)-C(2) <sup>3</sup>	121.62(7)
N(1)-Cu -N(2)	90	C(2)-N(1)-C(2) <sup>3</sup>	116.75(15)
N(1)-Cu -N(2) <sup>3</sup>	90	Cu -N(2)-C(3)	128.01(13)
N(1)-Cu -N(1) <sup>4</sup>	180	Cu -N(2)-C(4)	116.62(12)
N(2)-Cu -N(2) <sup>3</sup>	180	C(3)-N(2)-C(4)	115.4(2)
O(1)-S -O(2)	111.26(6)	N(1)-C(2)-C(2) <sup>1</sup>	121.62(7)
O(1)-S -C(1)	103.07(9)	N(2)-C(3)-C(4) <sup>2</sup>	122.2(2)
O(1)-S -O(2) <sup>4</sup>	111.26(6)	N(2)-C(4)-C(3) <sup>2</sup>	122.4(2)

## PART C, Continued

Bond lengths involving hydrogen atoms (Å) with  
estimated standard deviations in parentheses

Bond	Length(Å)	Bond	Length(Å)
C(1)-H(1a)	1.13(4)	C(3)-H(3)	0.91(3)
C(1)-H(1b)	0.95(2)	C(4)-H(4)	0.85(3)
C(2)-H(2)	0.92(2)		

Table

Bond angles involving hydrogen atoms (deg) with  
estimated standard deviations in parentheses

Bonds	Angle(deg)	Bonds	Angle(deg)
S -C(1)-H(1a)	111(2)	N(1)-C(2)-H(2)	116.7(11)
S -C(1)-H(1b)	109.6(12)	C(2) <sup>1</sup> -C(2)-H(2)	121.7(4)
S -C(1)-H(1b) <sup>a</sup>	109.6(12)	N(2)-C(3)-H(3)	119(2)
H(1a)-C(1)-H(1b)	109(2)	C(4) <sup>2</sup> -C(3)-H(3)	119(2)
H(1a)-C(1)-H(1b) <sup>a</sup>	109(2)	N(2)-C(4)-H(4)	124(2)
H(1b)-C(1)-H(1b) <sup>a</sup>	109(2)	C(3) <sup>2</sup> -C(4)-H(4)	114(2)

APPENDIX II. Vibrational Assignments for Pyridine<sup>1</sup> and some of its Complexes<sup>2</sup>

Pyridine Assignment	3080s 20b	3054s 2	3030s 20a	3004s 8b+19b	1580s 8a	1482s 19a	1437s 19b	1217s 9a	1146s 15	1067s 18a	1029s 12	990s 1	938w 5	883w 10a	746s 10b	702s 11	601s 6a	405s 16b
Fe(py) <sub>4</sub> (CF <sub>3</sub> SO <sub>3</sub> ) <sub>2</sub>	3100sh	3065w	3040w	3010w	1632w 1603s 1577w	1490m	1448s	1225sh	1160sh	1070m	1040sh	1010m 995w	960w	880w	765s	712s 704s	632sh	428m
Fe(py) <sub>4</sub> (CH <sub>3</sub> SO <sub>3</sub> ) <sub>2</sub>	3100sh	3040-3000w.br			1601m 1574w	1486w	1445s	1232sh 1219w	1145sh	1060sh	a	1006m	960w	880w	770s 760sh	705s	626s	427m
Fe(py) <sub>4</sub> (p-CH <sub>3</sub> C <sub>6</sub> H <sub>4</sub> SO <sub>3</sub> ) <sub>2</sub>	3080w	3060w	3050w 3040w	3005w	1600s 1571m	1489m	1446s	1229w 1221m	1150sh	1072m	a	1010s	a	896m 886m	766m 758m	714s 705s	625m	425m
Cu(py) <sub>4</sub> (CF <sub>3</sub> SO <sub>3</sub> ) <sub>2</sub>	3200-3000w.br				1607m	1490w	1450s	1228m	1170sh	1081m 1072m	1022w	991vw	960vw	892vw	770sh 760sh	704s	a	443w
Cu(py) <sub>4</sub> (CH <sub>3</sub> SO <sub>3</sub> ) <sub>2</sub>	3115w 3095w	3070w	3043w	3015w	1606m 1573w	1494m 1484m	1448s	1220m 1211m	1154s 1143s	1081w 1070m	1018m	1001w	960w	895w	767s	705s	641s	440m 429w
Fe(py) <sub>2</sub> (CF <sub>3</sub> SO <sub>3</sub> ) <sub>2</sub>	3080w	3060w			1610m 1574vw	1493m	1448s	a	1158sh 1154m	1073m	a	1015w	951vw	890vw	755m	702s	a	430m 424sh

1). From reference 119

2). All values are in cm<sup>-1</sup>

a). obscured by anion absorption

APPENDIX III. Vibrational Assignments for Sulfonate Anions  
and Unassigned Bands<sup>1, 2</sup>

PART A. Compounds Containing the  $\text{CF}_3\text{SO}_3^-$  Anion

COMPOUND	ANION VIBRATIONS ( $\text{C}_{3v}$ SYMMETRY)					$\nu_6$ AND UNASSIGNED VIBRATIONS					
	$\nu_4$ (E)	$\nu_1$ ( $A_1$ )	$\nu_2$ ( $A_1$ )	$\nu_5$ (E)	$\nu_3$ ( $A_1$ )						
$\text{Fe}(\text{py})_4(\text{CF}_3\text{SO}_3)_2$	1329s 1320s 1240s	1035s	756sh	527m 518m	636s	1305sh	1285w 1219s	1180sh 1170s 1110w	675w 656m	594w 576w	394w 372w 325w
$\text{Cu}(\text{py})_4(\text{CF}_3\text{SO}_3)_2$	1293s 1250s	1035s	765m	525m	642s		1280sh 1245sh 1228m	1161s	658m	582w	
$\text{Cu}(\text{pyz})_4(\text{CF}_3\text{SO}_3)_2 \cdot \text{H}_2\text{O}$	1280s 1225s	1027s	761w	521m	635s	3400m.br 1630w.br	1245s	1172m 1150s	751w 702w 672w	580w	360w
$\text{Fe}(\text{pyz})_2(\text{CF}_3\text{SO}_3)_2 \cdot \text{CH}_3\text{OH}$	1331s 1325s 1236s	1033s	756w	529w 520m	639s	3400-2500m.br	1304sh	1251sh 1206s 1160sh		595w 580w	436w 380w 360sh
$\text{Fe}(\text{py})_2(\text{CF}_3\text{SO}_3)_2$	1316s 1205s	1039s	769w	522m	635s		1304sh	1271w 1232s	1184s	984vw	590w 380vw
$\text{Fe}(\text{pyz})(\text{CF}_3\text{SO}_3)_2$	1320s 1205s	1037s	773w	524m	639s		1226sh	1186s 1154m		587m	391w 356vw 336w
$\text{Cu}(\text{pyz})(\text{CF}_3\text{SO}_3)_2$	1310s 1209s	1030s	771w	528sh 521m	640s		1231m	1195sh 1185sh 1160m 1140sh		598w 584w	

1) All values are in  $\text{cm}^{-1}$

2) Assignments made according to reference 122

## APPENDIX III. Continued

PART B. Compounds Containing the  $\text{CH}_3\text{SO}_3^-$  Anion

COMPOUND	ANION VIBRATIONS ( $\text{C}_{3v}$ SYMMETRY)					$\nu_6$ AND UNASSIGNED VIBRATIONS		
	$\nu_4$ (E)	$\nu_1$ ( $\text{A}_1$ )	$\nu_2$ ( $\text{A}_1$ )	$\nu_5$ (E)	$\nu_3$ ( $\text{A}_1$ )			
$\text{Fe}(\text{py})_4(\text{CH}_3\text{SO}_3)_2$	1252s 1162s	1038s	779sh	543m 523m	556s	1325w 1315sh		364w
$\text{Cu}(\text{py})_4(\text{CH}_3\text{SO}_3)_2$	1232s 1183s	1043s	773s	532s	559s	1419w 1330w 1312w	1105w	
$\text{Fe}(2\text{-mepyz})_4(\text{CH}_3\text{SO}_3)_2$	1247s 1152s	1035s	779s	541s 524s	557s	1340w 1316w		495w 370m
$\text{Fe}(\text{pyz})_2(\text{CH}_3\text{SO}_3)_2$	1264s 1160s	1038s	783s	548m 519s	565s 558sh	1341m 1321m 1240m	447w	392sh 372m 347sh
$\text{Cu}(\text{pyz})_2(\text{CH}_3\text{SO}_3)_2$	1257s 1162s	1035s	778s	542m 529m	572s	1345w 1330vw		360w

## APPENDIX III. Continued

PART C. Compounds Containing the  $\text{p-CH}_3\text{C}_6\text{H}_4\text{SO}_3^-$  Anion

COMPOUND	ANION VIBRATIONS ( $\text{C}_{3v}$ SYMMETRY)					$\nu_6$ AND UNASSIGNED VIBRATIONS							
	$\nu_4$ (E)	$\nu_1$ ( $\text{A}_1$ )	$\nu_2$ ( $\text{A}_1$ )	$\nu_5$ (E)	$\nu_3$ ( $\text{A}_1$ )								
$\text{Fe}(\text{py})_4(\text{p-CH}_3\text{C}_6\text{H}_4\text{SO}_3)_2$	1260s 1170s	1030s	682s	547w	577m	1660w 1630vw 1237w	1290m 1249m	1181sh 1116s	844w 819m 802w	653w	497w	385m 307m	
$\text{Fe}(\text{pyz})(\text{p-CH}_3\text{C}_6\text{H}_4\text{SO}_3)_2 \cdot 2\text{CH}_3\text{OH}$	1248s 1158s	1037s	686s	557m	573s	3270s.br 3130w	1640vw 1600w	1282sh 1207vw	1119s	890w	710w	627m	492vw 392m 448vw 380sh 309m
$\text{Fe}(\text{pyz})(\text{p-CH}_3\text{C}_6\text{H}_4\text{SO}_3)_2$	1257s 1141s	1045s	682s	555s	584m	3120w	1598w	1287w 1211w	1180sh 1125s	894vw 854w	714w 709sh	498w 415sh 405m	374m 302m

APPENDIX IV. Vibrational Assignments for Pyrazine<sup>1</sup> and  
Bis(pyrazine) Complexes<sup>2</sup>

Pyrazine	3066w	1490s	1178m	1067vs	926vw	823vw	789w	597w
	2973w	1418vs	1148vs	1048vw		804vs	752vw	417m
			1125w	1032vw			700vw	
			1110m	1022m				
				1006w				
<hr/>								
Fe(pyz) <sub>2</sub> Cl <sub>2</sub>	3104w	1483m	1163m	1086vw	993w	822s		473s
	3093vw	1415sh	1154s	1052s	990w	819m		470sh
		1411s	1120s			812s		
			1114s					
Fe(pyz) <sub>2</sub> Br <sub>2</sub>	3095vw	1480w	1155m	1087vw	989w	875vw		474s
	3085w	1412s	1119m	1054s		816s		470s
Fe(pyz) <sub>2</sub> I <sub>2</sub>	3096vw	1485w	1152m	1089w	988m	817s		472s
	3075w	1414sh	1118m	1056s				
		1410s						
Fe(pyz) <sub>2</sub> (NCS) <sub>2</sub>	3110m	1489m	1161s	1083w	982w		799s	461s
	3090m	1415s	1125s	1051s	972w		790s	
	3040m		1112m		970sh			
Fe(pyz) <sub>2</sub> (CF <sub>3</sub> SO <sub>3</sub> ) <sub>2</sub> ·CH <sub>3</sub> OH	3127m	1492w	1147w	1090vw		836m		480m
	3108m	1426m	1126w	1083w		827m		472m
	3060w		1121w	1060m		815w		
			1101w	1057sh				
				1007m				
Fe(pyz) <sub>2</sub> (CH <sub>3</sub> SO <sub>3</sub> ) <sub>2</sub>	3105m	1490w	1121w	1056sh	997w	848m		478m
	3095m	1422s	1105w	1007w	987w	826m		468m
	3030w				975vw			
					967w			
Cu(pyz) <sub>2</sub> (CH <sub>3</sub> SO <sub>3</sub> ) <sub>2</sub>	3139w	1422m	1150sh	1099m	976w	846m		494s
	3120w	1418sh	1140s	1082w		813m		440m
	3100w		1131m	1071m				
	3050w		1116m					
	3020w		1101sh					
Fe(pyz) <sub>2</sub> (ClO <sub>4</sub> ) <sub>2</sub>	3120sh	1426m	1175sh	1095w	997w	825sh	770w	475m
	3110w		1120m	1063m		820m		466m
	3020vw							

1). From reference 124

2). All values are in cm<sup>-1</sup>



APPENDIX V. Vibrational Assignments<sup>1</sup> for the Neutral Ligands in  
 $\text{Fe}(\text{2-mepyz})_4(\text{CH}_3\text{SO}_3)_2$ ,  $\text{Cu}(\text{pyz})_4(\text{CF}_3\text{SO}_3)_2 \cdot \text{H}_2\text{O}$  and  
 $\text{Fe}(\text{pyz})_4(\text{AsF}_6)_2 \cdot 2\text{H}_2\text{O}$

COMPOUND	ASSIGNMENTS										
$\text{Fe}(\text{2-mepyz})_4(\text{CH}_3\text{SO}_3)_2$	3120sh	1595w	1410sh	1304w		1076m	990sh	865m	754w	655vw	427s
	3100w	1520w	1400w			1067m	975w	841m	746w		
	3080sh						965sh				
	3020w										
$\text{Cu}(\text{pyz})_4(\text{CF}_3\text{SO}_3)_2 \cdot \text{H}_2\text{O}$	3100w		1421sh		1122m	1083m	974w	805s			460s
			1415m		1115sh	1055m					453s
$\text{Fe}(\text{pyz})_4(\text{AsF}_6)_2 \cdot 2\text{H}_2\text{O}$			1495m	1235w	1169sh	1088w	910w	801m			470m
			1421s		1158m	1055s					451s
			1412m		1146w						439s
					1127m						
					1118w						

1). All values are in  $\text{cm}^{-1}$

APPENDIX VI. Vibrational Assignments for Pyrazine<sup>1</sup> and Mono(pyrazine)  
Complexes<sup>2</sup>

Pyrazine	3066w 2973w	1490s 1483vs	1178m 1148vs 1125w 1110m	1067vs 1048vw 1032vw 1022m 1006w	926vw 823vw 804vs	789w 752vw 700vw	597w 417m
Fe(pyz)Cl <sub>2</sub>	3100m 3040w	1485m 1418s	1168s 1119s	1089w 1054s		794s	475s
Fe(pyz)(NCO) <sub>2</sub>	3100m	1487m 1416s	1171m 1120s	1062s		798s	467s
Fe(pyz)(CF <sub>3</sub> SO <sub>3</sub> ) <sub>2</sub>	3140w 3130vw	1491vw 1428m	1130m	1097w 1064s	806s		477m
Fe(pyz)(p-CH <sub>3</sub> C <sub>6</sub> H <sub>4</sub> SO <sub>3</sub> ) <sub>2</sub> ·2CH <sub>3</sub> OH	3110w 3060w	1495w 1431s		1098m 1058m 1024s 1013s	996m 947w	827m 808s	476m
Fe(pyz)(p-CH <sub>3</sub> C <sub>6</sub> H <sub>4</sub> SO <sub>3</sub> ) <sub>2</sub>	3050w 3020w	1491w 1424m	1156sh	1089m 1054sh 1013m	821m 812s		473m
Cu(pyz)(CF <sub>3</sub> SO <sub>3</sub> ) <sub>2</sub>	3140w 3070w	1432m	1127m 1108m	1081m	813s		504s
Cu(pyz)(CH <sub>3</sub> SO <sub>3</sub> ) <sub>2</sub> ·H <sub>2</sub> O	3135w 3120w	1422m	1115m	1094m 1078m 1001m	965w	838m	506m

1). From reference 124

2). All values are in cm<sup>-1</sup>

## APPENDIX VII. Electronic Spectral Results

## PART A. Iron(II) Compounds Containing Sulfonate Anions

COMPOUND	ABSORPTION MAXIMA (cm <sup>-1</sup> )	
Fe(py) <sub>4</sub> (CF <sub>3</sub> SO <sub>3</sub> ) <sub>2</sub>	11,500	9,000sh
Fe(py) <sub>4</sub> (CH <sub>3</sub> SO <sub>3</sub> ) <sub>2</sub>	11,400	
Fe(py) <sub>4</sub> (p-CH <sub>3</sub> C <sub>6</sub> H <sub>4</sub> SO <sub>3</sub> ) <sub>2</sub>	11,000	
Fe(py) <sub>2</sub> (CF <sub>3</sub> SO <sub>3</sub> ) <sub>2</sub>	10,800	
Fe(2-mepyz) <sub>4</sub> (CH <sub>3</sub> SO <sub>3</sub> ) <sub>2</sub>	9,800	
Fe(pyz) <sub>2</sub> (CF <sub>3</sub> SO <sub>3</sub> ) <sub>2</sub> · CH <sub>3</sub> OH	10,800	
Fe(pyz) <sub>2</sub> (CH <sub>3</sub> SO <sub>3</sub> ) <sub>2</sub>	11,600	9,500sh
Fe(pyz) (CF <sub>3</sub> SO <sub>3</sub> ) <sub>2</sub>	10,900	
Fe(pyz) (p-CH <sub>3</sub> C <sub>6</sub> H <sub>4</sub> SO <sub>3</sub> ) <sub>2</sub> · 2CH <sub>3</sub> OH	10,800	8,900sh
Fe(pyz) (p-CH <sub>3</sub> C <sub>6</sub> H <sub>4</sub> SO <sub>3</sub> ) <sub>2</sub>	10,800	8,900sh

sh : shoulder

## APPENDIX VII. Continued

## PART B. Copper(II) Compounds Containing Sulfonate Anions

COMPOUND	ABSORPTION MAXIMA (cm <sup>-1</sup> )
$\text{Cu}(\text{py})_4(\text{FSO}_3)_2$ <sup>1</sup>	17,200
$\text{Cu}(\text{py})_4(\text{CF}_3\text{SO}_3)_2$	17,400
$\text{Cu}(\text{py})_4(\text{CH}_3\text{SO}_3)_2$	16,800
$\text{Cu}(\text{py})_4(\text{p-CH}_3\text{C}_6\text{H}_4\text{SO}_3)_2$ <sup>1</sup>	16,900
$\text{Cu}(\text{pyz})_4(\text{CF}_3\text{SO}_3)_2 \cdot \text{H}_2\text{O}$	16,100
$\text{Cu}(\text{pyz})_2(\text{CH}_3\text{SO}_3)_2$	14,000
$\text{Cu}(\text{pyz})(\text{CF}_3\text{SO}_3)_2$	13,900
1) From reference 76	

## APPENDIX VII. Continued

## PART C. Iron(II) Pyrazine Complexes Containing Various Anions

COMPOUND	ABSORPTION MAXIMA (cm <sup>-1</sup> )		
$\text{Fe}(\text{pyz})_4(\text{AsF}_6)_2 \cdot 2\text{H}_2\text{O}$		12,500	
$\text{Fe}(\text{pyz})_2\text{Cl}_2$	19,000	11,800	
$\text{Fe}(\text{pyz})_2\text{Br}_2$	19,000	11,200	
$\text{Fe}(\text{pyz})_2\text{I}_2$	16,100	11,000	7,350
$\text{Fe}(\text{pyz})_2(\text{NCS})_2$	19,400	12,900	10,200
$\text{Fe}(\text{pyz})_2(\text{ClO}_4)_2$		11,400	
$\text{Fe}(\text{pyz})\text{Cl}_2$	16,700	11,400	
$\text{Fe}(\text{pyz})(\text{NCO})_2$	16,000	11,200	

APPENDIX VIII. Magnetic Susceptibility Results<sup>1</sup> for Copper(II) Complexes1.  $\text{Cu}(\text{py})_4(\text{CF}_3\text{SO}_3)_2$ 2.  $\text{Cu}(\text{py})_4(\text{CH}_3\text{SO}_3)_2$ 3.  $\text{Cu}(\text{pyz})_4(\text{CF}_3\text{SO}_3)_2 \cdot \text{H}_2\text{O}$ 

T	$\chi_m$	$\mu_{\text{eff.}}$	T	$\chi_m$	$\mu_{\text{eff.}}$	T	$\chi_m$	$\mu_{\text{eff.}}$
9.06	45.9	1.82	4.24	98.3	1.83	4.30	98.6	1.84
10.1	43.3	1.87	6.30	65.9	1.82	4.85	88.5	1.85
11.5	39.4	1.90	7.28	56.2	1.81	5.62	75.6	1.84
12.9	35.0	1.90	8.50	47.9	1.80	6.43	66.2	1.84
14.8	30.5	1.90	9.38	43.5	1.81	6.84	61.8	1.84
17.4	26.0	1.90	10.4	39.3	1.81	7.60	56.4	1.85
21.3	21.3	1.90	11.3	36.2	1.81	8.37	49.7	1.82
25.3	17.8	1.90	13.1	30.8	1.79	9.38	44.0	1.82
29.1	15.5	1.90	15.3	26.4	1.80	9.45	44.1	1.82
32.6	13.7	1.89	21.7	18.7	1.80	11.3	36.7	1.82
37.9	11.8	1.89	27.5	14.7	1.80	13.0	31.6	1.81
42.8	10.2	1.86	34.7	11.4	1.77	14.9	27.4	1.81
47.2	9.09	1.85	44.4	8.56	1.74	17.3	23.7	1.81
51.3	8.32	1.85	52.7	7.16	1.74	21.2	19.4	1.81
55.6	7.71	1.85	55.2	6.94	1.75	22.9	18.0	1.82
61.1	6.95	1.84	60.9	6.19	1.74	25.2	16.3	1.81
Faraday Results			65.9	5.71	1.73	28.8	14.2	1.81
Temperature 295 K			74.7	5.05	1.74	32.4	12.6	1.80
H.dH/dx	$\chi_m$	$\mu_{\text{eff.}}$	81.7	4.61	1.74	37.7	10.7	1.79
0.0526	1.64	1.97	Faraday Results			40.4	9.90	1.79
0.0869	1.57	1.92	Temperature 294 K			42.6	8.50	1.79
			H.dH/dx	$\chi_m$	$\mu_{\text{eff.}}$	51.1	7.85	1.79
			0.0526	1.86	2.09	55.1	7.30	1.79
			0.0869	1.87	2.10	61.2	6.60	1.80
						70.9	5.65	1.79
						82.4	4.80	1.78
						92.5	4.20	1.76
						Faraday Results		
						Temperature 294 K		
						H.dH/dx	$\chi_m$	$\mu_{\text{eff.}}$
						0.0526	1.53	1.90
						0.0869	1.50	1.88

1). Temperatures are in K; molar susceptibilities ( $\chi_m$ ) are in  $10^3 \text{ cm}^3 \text{ mol}^{-1}$ ; magnetic moments ( $\mu$ ) are in B.M.; and magnetic field gradients (H.dH/dx) are in  $\text{T}^2 \text{ cm}^{-1}$ .

## APPENDIX VIII. Continued

4.  $\text{Cu}(\text{pyz})_2(\text{CH}_3\text{SO}_3)_2$       5.  $\text{Cu}(\text{pyz})(\text{CF}_3\text{SO}_3)_2$ 

T	$x_m$	$\mu_{\text{eff.}}$	T	$x_m$	$\mu_{\text{eff.}}$
4.22	21.5	0.851	4.32	20.9	0.849
4.47	21.7	0.880	4.70	21.1	0.890
4.93	22.0	0.930	5.00	21.4	0.924
5.19	22.2	0.959	5.48	21.6	0.972
5.62	22.5	1.00	5.84	21.8	1.01
5.91	22.7	1.03	6.30	22.0	1.05
6.23	22.8	1.06	6.84	22.1	1.10
6.84	22.7	1.11	7.16	22.1	1.12
7.28	22.7	1.15	7.60	22.0	1.16
7.54	22.7	1.17	8.00	21.9	1.18
8.01	22.7	1.20	8.24	21.8	1.20
8.44	22.4	1.23	8.76	21.6	1.23
8.63	22.4	1.24	8.95	21.5	1.24
9.56	21.8	1.29	9.70	21.1	1.28
10.2	21.4	1.32	10.4	20.8	1.31
11.9	20.5	1.40	11.7	19.9	1.36
13.3	19.5	1.44	13.1	19.0	1.41
15.3	18.1	1.49	15.1	17.7	1.46
15.4	18.1	1.49	15.5	17.5	1.47
17.2	16.9	1.52	16.8	16.6	1.49
21.8	14.6	1.59	21.3	14.4	1.56
25.7	13.0	1.63	25.3	12.8	1.61
29.1	11.7	1.65	29.1	11.5	1.63
30.8	11.2	1.66	32.7	10.5	1.65
32.8	10.5	1.66	34.3	10.0	1.65
38.0	9.28	1.68	38.0	9.12	1.66
42.8	8.38	1.69	42.5	8.20	1.67
47.3	7.64	1.70	46.8	7.56	1.68
51.4	7.18	1.72	51.0	7.02	1.69
55.8	6.78	1.74	54.9	6.56	1.70
61.4	6.27	1.75	56.7	6.46	1.71
65.8	5.93	1.77	61.6	5.99	1.71
70.5	5.60	1.78	66.3	5.64	1.73
81.8	4.86	1.78	75.1	4.96	1.73
			82.6	4.47	1.72
			92.5	3.97	1.71
			100.2	3.58	1.69

Faraday Results

Temperature 294 K

H.dH/dx	$x_m$	$\mu$
0.0526	1.48	1.87
0.0869	1.47	1.86

Faraday Results

Temperature 296 K

H.dH/dx	$x_m$	$\mu_{\text{eff.}}$
0.0526	1.56	1.92
0.0869	1.52	1.90

APPENDIX IX. Magnetic Susceptibility Results<sup>1</sup> for Iron(II) ComplexesPART A. Complexes Containing an  $\text{FeN}_4\text{X}_2$  Chromophore1.  $\text{Fe}(\text{py})_4(\text{CF}_3\text{SO}_3)_2$       2.  $\text{Fe}(\text{py})_4(\text{CH}_3\text{SO}_3)_2$       3.  $\text{Fe}(\text{py})_4(\text{p-CH}_3\text{C}_6\text{H}_4\text{SO}_3)_2$ 

T	$\chi_m$	$\mu_{\text{eff.}}$	T	$\chi_m$	$\mu_{\text{eff.}}$	T	$\chi_m$	$\mu_{\text{eff.}}$
4.22	610	4.54	4.22	684	4.80	4.22	646	4.67
4.48	579	4.55	4.48	616	4.70	4.54	605	4.69
5.03	536	4.64	5.11	564	4.80	5.11	567	4.81
5.70	488	4.71	5.76	505	4.82	5.55	524	4.82
6.72	432	4.82	6.38	462	4.86	6.83	434	4.87
7.76	388	4.91	7.81	392	4.95	7.76	388	4.91
9.38	333	4.99	9.32	336	5.00	9.20	336	4.97
10.6	300	5.04	10.7	297	5.04	10.6	296	5.00
11.7	272	5.05	11.8	267	5.01	11.9	261	4.98
13.9	231	5.06	14.1	226	5.04	13.8	227	5.01
15.8	206	5.11	16.3	196	5.05	16.2	195	5.02
19.3	172	5.15	19.4	164	5.04	19.5	162	5.03
22.6	148	5.17	22.6	141	5.04	22.9	139	5.04
26.8	126	5.20	26.8	119	5.05	26.8	119	5.05
30.7	111	5.21	30.7	104	5.06	30.6	105	5.06
34.4	99.2	5.23	34.4	92.7	5.05	34.2	93.3	5.05
39.8	85.9	5.23	39.7	80.8	5.07	39.6	81.1	5.07
44.5	77.2	5.24	44.4	72.3	5.07	44.5	72.8	5.09
52.9	65.2	5.25	52.6	61.6	5.09	52.7	61.7	5.10
60.8	57.3	5.28	60.5	53.8	5.10	61.0	53.9	5.13
61.3	56.7	5.27	61.3	53.3	5.11	61.2	53.7	5.13
70.3	49.6	5.28	70.4	46.5	5.12	70.5	46.6	5.13
81.6	42.8	5.29	80.0	41.0	5.12	80.0	41.4	5.15
83.0	41.8	5.26	81.9	40.1	5.13	82.1	40.2	5.14
91.7	38.1	5.28	92.0	35.8	5.13	91.8	35.9	5.14
100.5	34.8	5.29	100.5	32.7	5.13	100.5	32.9	5.14
106.0	32.8	5.28	105.0	31.6	5.15	105.0	31.9	5.17
110.2	31.6	5.28	110.5	29.7	5.13	111.4	29.7	5.14
125.0	27.9	5.28	125.8	26.2	5.14	124.4	26.6	5.14
131.0	26.7	5.29	130.0	25.6	5.16	131.0	25.6	5.18
156.0	23.0	5.35	153.0	21.8	5.16	154.0	21.8	5.19
181.0	19.8	5.36	178.0	18.8	5.17	180.0	18.8	5.20
206.0	17.4	5.36	201.0	16.5	5.16	204.0	16.7	5.21
232.0	15.8	5.41	226.0	14.8	5.18	229.0	14.9	5.23
256.0	14.3	5.41	250.0	13.4	5.18	253.0	13.4	5.20
282.0	13.1	5.43	276.0	12.2	5.19	278.0	12.4	5.24
307.0	11.8	5.38	297.0	11.4	5.20	304.0	11.4	5.27

## Faraday Results

Temperature 294 K

H.dH/dx	$\chi_m$	$\mu_{\text{eff.}}$
0.0253	12.30	5.38
0.0526	12.33	5.38
0.0869	12.27	5.37

## Faraday Results

Temperature 293 K

H.dH/dx	$\chi_m$	$\mu_{\text{eff.}}$
0.0253	11.49	5.19
0.0526	11.50	5.20
0.0869	11.47	5.18

## Faraday Results

Temperature 294 K

H.dH/dx	$\chi_m$	$\mu_{\text{eff.}}$
0.0253	11.68	5.24
0.0526	11.73	5.25
0.0869	11.68	5.24

1) Temperatures (T) are in K; molar susceptibilities ( $\chi_m$ ) are in  $10^3 \text{ cm}^3 \text{ mol}^{-1}$ ; magnetic moments ( $\mu$ ) are in B.M.; and magnetic field gradients (H.dH/dx) are in  $\text{T}^2 \text{ cm}^{-1}$ .

## APPENDIX IX PART A. Continued

4.  $\text{Fe}(\text{pyz})_2(\text{CF}_3\text{SO}_3)_2 \cdot \text{CH}_3\text{OH}$ 5.  $\text{Fe}(\text{pyz})_2(\text{CH}_3\text{SO}_3)_2$ 6.  $\text{Fe}(\text{2-mepyz})_4(\text{CH}_3\text{SO}_3)_2$ 

T	$x_m$	$\mu_{\text{eff.}}$
4.22	333	3.34
4.65	326	3.48
5.20	314	3.61
5.80	304	3.75
6.60	290	3.91
8.40	256	4.14
10.1	228	4.29
12.1	204	4.43
14.2	183	4.56
16.4	165	4.64
18.4	150	4.70
20.3	138	4.74
22.2	128	4.77
24.6	119	4.83
27.5	108	4.87
30.4	99.2	4.91
33.1	92.1	4.94
35.8	86.1	4.97
41.9	74.3	4.99
47.6	66.2	5.02
59.3	54.0	5.06
68.8	47.1	5.09
80.0	41.9	5.18
80.2	40.6	5.11
90.2	36.4	5.12
98.8	33.2	5.13
110.8	30.1	5.16
120.2	27.3	5.13
130.5	26.0	5.21
155.0	22.1	5.23
180.0	19.2	5.26
205.5	16.9	5.28
230.0	15.2	5.28
255.0	13.8	5.30
280.0	12.6	5.30
305.0	11.6	5.31

## Faraday Results

Temperature 293 K

H.dH/dx	$x_m$	$\mu_{\text{eff.}}$
0.0253	12.09	5.32
0.0526	11.96	5.29
0.0869	11.92	5.29

T	$x_m$	$\mu_{\text{eff.}}$
4.22	338	3.38
4.61	320	3.43
5.11	313	3.58
5.88	291	3.70
7.02	271	3.90
8.06	251	4.03
9.32	232	4.15
10.7	213	4.26
12.2	194	4.36
14.3	173	4.45
16.4	155	4.52
19.7	134	4.60
22.9	117	4.64
26.8	103	4.69
30.7	90.8	4.72
34.2	82.0	4.74
39.7	72.1	4.78
44.6	65.1	4.82
52.8	55.7	4.85
61.1	49.0	4.89
61.3	48.8	4.89
70.5	42.8	4.91
81.9	37.2	4.93
82.0	36.8	4.92
91.8	33.3	4.95
100.5	30.6	4.96
105.0	29.8	5.00
110.6	27.8	4.96
124.4	24.9	4.97
130.0	24.4	5.04
154.0	20.8	5.06
179.0	18.1	5.09
204.0	15.9	5.09
231.0	14.0	5.09
253.0	12.9	5.11
277.0	11.7	5.10
300.0	10.8	5.08

## Faraday Results

Temperature 295 K

H.dH/dx	$x_m$	$\mu_{\text{eff.}}$
0.0252	11.02	5.10
0.0526	11.06	5.11
0.0869	11.04	5.11

T	$x_m$	$\mu_{\text{eff.}}$
4.62	567	4.58
5.14	568	4.83
5.99	550	5.13
6.43	525	5.20
7.04	490	5.25
7.70	449	5.26
8.12	428	5.27
9.32	380	5.32
10.3	347	5.34
11.1	324	5.35
13.2	277	5.41
15.4	241	5.44
17.5	212	5.45
19.3	193	5.46
23.3	161	5.48
27.1	139	5.50
30.8	124	5.52
34.5	110	5.50
39.5	95.9	5.50
44.4	86.0	5.53
48.7	78.3	5.52
53.9	70.7	5.52
59.4	61.6	5.41
64.7	55.1	5.34
70.7	49.5	5.29
75.8	46.0	5.28
80.4	43.5	5.29
84.3	41.4	5.28
93.1	37.3	5.27
103.0	33.8	5.27
113.6	30.6	5.27
125.6	27.8	5.28
137.8	25.2	5.26

## Faraday Results

Temperature 295 K

H.dH/dx	$x_m$	$\mu_{\text{eff.}}$
0.0253	11.70	5.25
0.0526	11.62	5.24
0.0869	11.58	5.23



## APPENDIX IX. PART A. Continued

7. Fe(pyz)<sub>2</sub>Cl<sub>2</sub>

T	$\chi_m$	$\mu_{eff.}$
4.22	661	4.72
4.70	607	4.78
4.93	569	4.74
5.42	528	4.79
5.84	489	4.78
6.58	449	4.86
7.04	421	4.87
7.60	392	4.88
8.04	369	4.86
8.88	340	4.87
9.94	306	4.93
10.5	290	4.94
11.1	274	4.94
12.6	244	4.96
14.6	214	5.00
15.5	199	4.98
16.0	193	4.98
17.7	177	5.01
19.2	163	5.01
20.4	154	5.01
21.2	150	5.03
23.1	137	5.03
25.0	127	5.04
27.0	118	5.05
28.9	110	5.06
30.8	104	5.06
32.4	98.3	5.05
34.2	93.2	5.05
36.9	86.9	5.06
39.5	80.9	5.06
42.6	75.2	5.06
45.6	70.5	5.07
48.4	66.5	5.08
52.5	61.6	5.09
56.5	57.8	5.11
59.9	54.6	5.11
63.9	51.2	5.12
67.9	48.4	5.13
72.0	45.7	5.13
76.2	42.9	5.12
82.1	40.0	5.13
91.2	35.0	5.05
109.5	30.2	5.14
130.0	25.4	5.14
155.7	21.4	5.17
180.5	18.6	5.18
205.6	16.3	5.18
232.0	14.6	5.20
256.6	13.2	5.19
282.6	11.8	5.17
307.3	11.1	5.21

## Faraday Results

## Temperature 295 K

H.dH/dx	$\chi_m$	$\mu_{eff.}$
0.0253	11.49	5.21
0.0526	11.45	5.20
0.0869	11.41	5.19

8. Fe(pyz)<sub>2</sub>Br<sub>2</sub>

T	$\chi_m$	$\mu_{eff.}$
4.22	716	4.92
4.78	656	5.01
5.62	572	5.07
6.91	480	5.15
7.48	442	5.14
8.17	404	5.14
9.19	363	5.17
9.95	339	5.20
10.9	309	5.19
12.7	268	5.20
15.1	226	5.21
17.0	201	5.22
18.4	185	5.22
21.2	162	5.24
25.1	137	5.24
28.8	119	5.24
32.5	106	5.24
37.6	90.8	5.23
40.2	85.5	5.24
42.7	80.5	5.24
46.9	72.5	5.22
51.3	66.4	5.22
55.6	61.9	5.25
61.3	56.5	5.26
70.3	49.7	5.29
82.1	42.4	5.28
92.1	37.7	5.27
100.3	34.8	5.28
107.3	32.4	5.28
130.5	26.7	5.28
155.7	22.6	5.31
180.6	19.6	5.32
206.0	17.2	5.33
230.5	15.3	5.31
255.9	13.7	5.30
281.2	12.5	5.31
305.5	11.6	5.33

## Faraday Results

## Temperature 295 K

H.dH/dx	$\chi_m$	$\mu_{eff.}$
0.0253	12.03	5.33
0.0526	12.00	5.32
0.0869	11.94	5.31

9. Fe(pyz)<sub>2</sub>I<sub>2</sub>

T	$\chi_m$	$\mu_{eff.}$
4.22	528	4.22
4.62	507	4.33
5.16	496	4.52
5.70	473	4.64
6.12	453	4.71
6.78	428	4.82
7.35	408	4.90
8.00	382	4.95
8.83	358	5.03
9.88	324	5.06
10.3	312	5.07
11.1	294	5.11
12.8	262	5.18
14.3	235	5.19
15.1	223	5.19
16.3	210	5.23
17.8	192	5.23
19.3	178	5.25
20.1	171	5.24
23.5	150	5.31
25.3	139	5.31
26.8	131	5.31
27.3	130	5.33
29.0	123	5.34
31.1	116	5.37
32.8	110	5.37
34.1	105	5.36
36.7	98.2	5.37
39.5	91.9	5.39
42.6	85.8	5.41
45.7	86.6	5.43
48.5	76.3	5.44
52.5	71.1	5.46
56.5	66.7	5.49
59.9	63.3	5.51
63.9	59.8	5.53
67.7	56.7	5.54
71.9	53.6	5.55
76.1	50.5	5.55
81.6	47.4	5.56
90.2	42.8	5.55
99.4	39.3	5.59
105.0	37.9	5.64
109.9	35.5	5.59
123.2	31.8	5.60
128.6	31.3	5.67
155.7	26.2	5.72
180.4	22.6	5.71
205.3	19.9	5.71
231.4	17.6	5.70
256.3	15.8	5.68
281.5	14.2	5.65
305.4	12.9	5.62

## Faraday Results

## Temperature 295 K

H.dH/dx	$\chi_m$	$\mu_{eff.}$
0.0253	13.65	5.67
0.0526	13.55	5.65
0.0869	13.46	5.64

## APPENDIX IX, PART A. Continued

10.  $\text{Fe}(\text{pyz})_2(\text{NCS})_2$ 

T	$x_m$	$\mu_{\text{eff.}}$
4.22	104	1.87
4.61	110	2.02
5.76	132	2.46
6.09	142	2.63
6.16	145	2.67
6.83	162	2.97
6.90	162	2.99
7.10	165	3.06
7.50	168	3.17
7.69	168	3.22
7.93	169	3.27
8.00	169	3.29
8.39	169	3.36
8.88	168	3.46
8.94	168	3.46
9.25	167	3.51
9.32	167	3.53
10.0	164	3.62
10.3	162	3.66
10.8	161	3.73
11.3	158	3.78
12.2	153	3.87
13.4	148	3.98
15.6	136	4.13
17.9	126	4.25
21.3	111	4.35
24.9	100	4.46
28.9	89.3	4.54
32.6	81.2	4.60
37.2	73.3	4.67
42.2	66.1	4.72
48.9	58.6	4.79
55.8	52.4	4.83
60.8	48.7	4.87
61.2	48.4	4.87
70.0	42.7	4.89
104.0	29.5	4.96
128.0	24.5	5.00
153.5	20.9	5.06
179.3	18.3	5.12
204.7	16.1	5.14
229.1	14.5	5.15
254.9	13.1	5.17
281.0	12.0	5.19
306.8	11.2	5.25

## Faraday Results

Temperature 295 K

H.dH/dx	$x_m$	$\mu_{\text{eff.}}$
0.0253	11.55	5.22
0.0526	11.54	5.22
0.0869	11.51	5.21

11.  $\text{Fe}(\text{pyz})_2(\text{ClO}_4)_2$ 

T	$x_m$	$\mu_{\text{eff.}}$
4.22	552	4.31
4.65	493	4.28
5.18	460	4.37
6.02	407	4.43
6.83	367	4.47
8.14	319	4.56
9.58	280	4.63
10.8	253	4.67
12.3	224	4.69
14.3	196	4.73
16.6	174	4.80
19.3	151	4.82
22.8	128	4.84
27.1	111	4.90
27.8	108	4.90
30.8	97.9	4.91
34.3	88.4	4.92
36.3	83.8	4.93
44.5	69.5	4.97
52.9	59.2	5.00
61.2	51.8	5.04
71.0	45.0	5.06
82.5	38.9	5.07
93.3	34.6	5.08
102.1	31.5	5.08
114.0	28.5	5.10
129.0	25.2	5.10
155.0	20.7	5.07
181.5	18.0	5.12
206.5	15.9	5.12
232.0	14.2	5.14
255.5	12.9	5.13
281.0	11.8	5.15
304.0	10.8	5.12

## Faraday Results

Temperature 294 K

H.dH/dx	$x_m$	$\mu_{\text{eff.}}$
0.0253	11.27	5.15
0.0526	11.23	5.14
0.0869	11.22	5.14

12.  $\text{Fe}(\text{pyz})_4(\text{AsF}_6)_2 \cdot 2\text{H}_2\text{O}$ 

T	$x_m$	$\mu_{\text{eff.}}$
9.06	247	4.23
11.1	219	4.40
12.8	197	4.49
14.7	177	4.55
16.7	160	4.63
21.8	130	4.76
25.6	113	4.81
29.2	101	4.85
32.7	90.8	4.87
37.9	79.9	4.92
42.8	71.5	4.95
47.2	65.6	4.98
51.3	60.9	5.00
55.5	57.1	5.04
61.0	52.0	5.04
106.0	31.0	5.12
130.0	25.2	5.12
153.2	21.5	5.13
179.3	18.7	5.17
204.0	16.6	5.20
228.5	14.7	5.18
253.4	13.3	5.20
278.5	12.3	5.23
303.5	11.1	5.19

## Faraday Results

Temperature 293 K

H.dH/dx	$x_m$	$\mu_{\text{eff.}}$
0.0253	11.39	5.17
0.0526	11.32	5.15
0.0869	11.42	5.17

APPENDIX IX, PART B. Complexes Containing an  $\text{FeN}_2\text{X}_4$  Chromophore1.  $\text{Fe}(\text{py})_2(\text{CF}_3\text{SO}_3)_2$     2.  $\text{Fe}(\text{pyz})(\text{CF}_3\text{SO}_3)_2$     3.  $\text{Fe}(\text{pyz})(\text{p-CH}_3\text{C}_6\text{H}_4\text{SO}_3)_2$ 

T	$\chi_m$	$\mu_{\text{eff.}}$	T	$\chi_m$	$\mu_{\text{eff.}}$	T	$\chi_m$	$\mu_{\text{eff.}}$
4.22	385	3.61	1.97	161	1.59	4.22	558	4.34
5.28	355	3.87	2.08	167	1.67	5.47	465	4.51
5.64	346	3.95	2.11	168	1.69	6.31	416	4.58
6.15	338	4.08	2.50	180	1.90	7.09	377	4.62
6.95	321	4.22	2.79	196	2.09	8.00	345	4.70
7.68	300	4.48	3.08	217	2.31	9.32	308	4.79
8.72	287	4.61	3.46	241	2.58	11.0	265	4.83
9.57	277	4.72	3.98	257	2.86	15.5	200	4.98
10.6	263	4.75	4.22	258	2.94	20.8	154	5.05
11.4	247	4.75	4.42	262	3.04	25.9	126	5.10
12.6	232	4.84	4.47	261	3.06	30.7	107	5.12
14.6	209	4.94	4.86	261	3.19	39.3	83.6	5.13
16.6	188	5.00	4.98	262	3.23	51.0	65.2	5.16
18.4	174	5.06	5.54	260	3.39	61.0	56.2	5.24
20.5	160	5.12	5.56	259	3.40	61.2	55.3	5.20
21.8	152	5.15	6.16	255	3.55	70.5	48.5	5.23
25.1	138	5.26	6.30	253	3.57	78.0	45.0	5.30
28.2	126	5.33	6.58	251	3.64	81.9	41.9	5.24
31.2	115	5.37	6.98	247	3.71	91.5	37.5	5.24
33.7	108	5.39	7.35	242	3.78	100.7	33.8	5.22
36.2	102	5.43	7.93	236	3.87	108.0	32.7	5.31
39.6	94.0	5.46	8.83	229	4.02	110.3	30.9	5.22
42.6	88.4	5.49	9.75	216	4.10	124.0	28.5	5.31
48.2	79.1	5.52	10.8	205	4.21	124.2	27.5	5.22
55.3	70.9	5.60	12.8	190	4.41	146.5	24.1	5.31
60.8	64.7	5.61	14.3	176	4.48	172.0	20.5	5.30
70.3	56.7	5.65	16.0	164	4.57	180.0	19.5	5.30
81.8	48.8	5.65	17.5	153	4.63	205.9	17.2	5.32
92.3	41.7	5.55	19.0	145	4.69	231.2	15.2	5.29
109.0	35.9	5.59	20.9	135	4.75	254.0	14.0	5.33
130.0	29.7	5.56	23.0	126	4.82	279.1	12.6	5.30
156.0	25.2	5.61	24.9	119	4.86	302.8	11.7	5.32
180.5	21.9	5.62	26.8	112	4.89			
205.5	19.2	5.61	28.5	106	4.91			
230.5	17.1	5.61	30.3	100	4.93			
255.0	15.3	5.59	32.3	95.9	4.98			
281.0	14.0	5.61	33.2	92.4	4.95			
305.0	12.6	5.54	38.7	80.9	5.00			
			44.1	72.0	5.04			
			49.9	64.6	5.08			
			52.7	61.7	5.10			
			59.9	54.9	5.13			
			64.2	48.9	5.16			
			72.1	46.5	5.18			
			81.6	41.5	5.20			
			91.1	37.4	5.22			
			99.9	34.3	5.24			
			109.0	33.0	5.37			
			109.5	31.3	5.24			
			122.4	28.1	5.24			
			130.0	27.6	5.36			
			153.7	23.5	5.38			
			180.6	20.3	5.41			
			205.2	18.0	5.44			
			230.2	16.0	5.44			
			256.0	14.5	5.44			
			281.0	13.1	5.43			
			305.0	12.0	5.42			

## Faraday Results

Temperature 293 K

H.dH/dx	$\chi_m$	$\mu_{\text{eff.}}$
0.0253	12.08	5.32
0.0526	12.06	5.32
0.0869	12.01	5.30

## Faraday Results

Temperature

H.dH/dx	$\chi_m$	$\mu_{\text{eff.}}$
0.0253	13.44	5.59
0.0526	13.31	5.59
0.0869	13.34	5.59

## Faraday Results

Temperature 294 K

H.dH/dx	$\chi_m$	$\mu_{\text{eff.}}$
0.0253	12.66	5.46
0.0526	12.51	5.42
0.0869	12.51	5.42

## APPENDIX IX, PART B. Continued

4.  $\text{Fe}(\text{pyz})(\text{p-CH}_3\text{C}_6\text{H}_4\text{SO}_3)_2 \cdot 2\text{CH}_3\text{OH}$ 

T	$x_m$	$\mu_{\text{eff.}}$
4.22	710	4.88
4.96	583	4.81
6.02	489	4.85
6.83	437	4.89
7.55	397	4.90
8.39	359	4.91
9.64	315	4.93
11.1	280	4.97
12.3	254	4.99
14.9	217	5.09
17.2	191	5.12
19.9	165	5.13
22.9	143	5.13
27.2	122	5.15
31.1	107	5.17
34.8	96.7	5.19
39.9	84.7	5.20
44.7	76.1	5.22
53.0	64.3	5.22
61.4	56.0	5.24
71.0	48.4	5.24
82.8	41.5	5.24
93.7	36.7	5.25
102.4	33.6	5.24
109.0	32.4	5.32
113.5	30.2	5.24
129.1	26.7	5.24
130.0	27.0	5.30
154.7	22.7	5.30
180.1	19.6	5.31
206.0	17.2	5.33
231.3	15.4	5.33
256.2	13.8	5.32
280.7	12.6	5.31
305.1	11.6	5.32

## Faraday Results

Temperature 295 K

H.dH/dx	$x_m$	$\mu_{\text{eff.}}$
0.0253	12.00	5.32
0.0526	12.00	5.32
0.0869	12.01	5.32

5.  $\text{Fe}(\text{pyz})(\text{NCO})_2$ 

T	$x_m$	$\mu_{\text{eff.}}$
4.22	22.8	0.876
4.77	22.9	0.934
5.18	22.9	0.975
5.88	22.9	1.04
6.30	23.0	1.08
7.10	23.0	1.14
8.06	23.1	1.22
9.76	23.2	1.35
10.9	23.3	1.43
13.3	23.8	1.59
15.4	24.5	1.74
18.7	26.3	1.98
21.2	28.8	2.21
22.6	30.9	2.36
24.9	32.7	2.55
26.8	33.8	2.69
29.1	34.4	2.83
30.9	35.0	2.94
32.5	35.1	3.02
34.7	35.4	3.11
36.3	35.3	3.20
38.0	35.6	3.29
39.7	35.3	3.35
42.3	35.3	3.46
44.6	34.9	3.53
48.8	34.6	3.68
52.9	33.8	3.78
57.3	33.2	3.90
61.3	32.4	3.99
66.2	31.6	4.09
74.5	30.0	4.23
81.9	28.5	4.32
91.9	26.8	4.44
100.7	25.4	4.52
109.0	24.5	4.62
110.4	24.0	4.60
123.7	22.3	4.69
129.8	21.8	4.76
155.3	19.3	4.89
180.0	17.2	4.97
206.2	15.5	5.06
231.4	14.1	5.10
255.8	12.8	5.11
281.1	11.9	5.17
305.8	10.9	5.17

## Faraday Results

Temperature 295 K

H.dH/dx	$x_m$	$\mu_{\text{eff.}}$
0.0253	11.45	5.20
0.0526	11.35	5.18
0.0869	11.33	5.17

6.  $\text{Fe}(\text{pyz})\text{Cl}_2$ 

T	$x_m$	$\mu_{\text{eff.}}$
1.86	264	1.98
2.00	262	2.05
2.10	262	2.10
2.20	261	2.14
2.40	258	2.23
2.69	256	2.35
3.04	253	2.48
3.51	249	2.64
4.07	244	2.82
4.20	244	2.86
4.75	238	3.01
5.11	233	3.09
5.47	229	3.17
5.63	230	3.22
6.12	223	3.30
7.16	213	3.49
8.06	205	3.64
9.76	190	3.85
10.9	180	3.97
12.5	169	4.11
14.6	154	4.24
16.6	142	4.35
19.6	128	4.48
23.1	113	4.50
27.1	102	4.69
30.8	92.4	4.77
34.4	84.8	4.83
39.7	76.0	4.91
44.6	69.4	4.97
52.9	60.5	5.06
61.5	53.8	5.14
70.9	47.5	5.19
82.8	41.6	5.25
91.3	38.2	5.28
93.4	37.4	5.28
102.6	34.3	5.31
109.5	33.1	5.39
114.3	31.2	5.34
129.8	27.7	5.36
131.0	28.0	5.42
155.3	23.8	5.44
180.1	21.0	5.50
189.6	19.9	5.49
205.6	18.3	5.48
207.7	18.3	5.52
233.0	16.3	5.51
257.2	14.5	5.47
257.4	14.6	5.48
281.7	13.2	5.45
306.5	12.2	5.47
319.5	11.9	5.51

## Faraday Results

Temperature 294 K

H.dH/dx	$x_m$	$\mu_{\text{eff.}}$
0.0253	12.96	5.52
0.0526	12.80	5.49
0.0869	12.77	5.48

## APPENDIX IX, PART C. Anhydrous Iron(II) Sulfonate Complexes

1.  $\text{Fe}(\text{FSO}_3)_2$ 

T	$\chi_m$	$\mu_{\text{eff.}}$
4.22	540	4.27
5.40	438	4.35
6.38	388	4.45
7.12	352	4.48
8.04	318	4.52
9.81	278	4.67
11.4	247	4.75
13.3	217	4.80
15.3	191	4.84
18.7	164	4.95
21.0	149	5.00
24.8	128	5.04
28.8	113	5.10
34.4	96.7	5.16
41.5	82.5	5.23
51.9	68.0	5.31
60.8	59.3	5.37
61.6	58.4	5.37
70.2	52.0	5.40
81.7	44.9	5.42
91.2	40.4	5.43
100.0	37.2	5.45
110.4	33.8	5.46
123.8	30.2	5.47

2.  $\text{Fe}(\text{CF}_3\text{SO}_3)_2$ 

T	$\chi_m$	$\mu_{\text{eff.}}$
4.22	377	3.57
8.82	243	4.14
13.5	181	4.42
18.0	147	4.60
19.9	136	4.66
23.2	120	4.73
27.4	106	4.82
32.7	92.0	4.90
42.8	74.6	5.05
49.1	66.5	5.11
55.9	60.1	5.19
67.0	51.5	5.25
78.7	44.5	5.29
89.7	39.1	5.30
94.1	38.0	5.35
99.4	35.7	5.33
111.1	32.1	5.34
124.5	28.7	5.34

3.  $\text{Fe}(\text{p-CH}_3\text{C}_6\text{H}_4\text{SO}_3)_2$ 

T	$\chi_m$	$\mu_{\text{eff.}}$
4.22	330	3.33
5.08	305	3.52
5.78	285	3.63
6.17	273	3.67
7.83	237	3.86
9.13	216	3.97
11.3	189	4.14
13.1	172	4.25
15.4	155	4.36
18.2	138	4.49
21.1	125	4.60
26.2	108	4.75
30.8	95.7	4.85
35.4	86.4	4.95
39.5	79.3	5.01
45.8	70.6	5.08
48.4	67.3	5.10
51.2	64.6	5.14
56.8	59.7	5.21
61.3	56.4	5.26
66.1	52.7	5.28
74.8	47.6	5.34
82.0	43.3	5.33
92.1	39.2	5.37
100.1	36.2	5.38
110.1	33.1	5.40
124.5	29.5	5.42

## APPENDIX IX, PART C. Continued

4.  $\alpha$ -Fe(CH<sub>3</sub>SO<sub>3</sub>)<sub>2</sub>5.  $\beta$ -Fe(CH<sub>3</sub>SO<sub>3</sub>)<sub>2</sub>

T	$x_m$	$\mu_{eff.}$	T	$x_m$	$\mu_{eff.}$
1.97	194	1.75	4.22	32.1	1.04
2.00	193	1.76	5.32	31.8	1.16
2.10	192	1.80	5.94	31.7	1.23
2.20	192	1.84	6.58	31.7	1.29
2.30	191	1.87	7.23	31.8	1.36
2.59	189	1.98	7.94	32.1	1.43
2.89	186	2.07	8.88	32.6	1.52
3.29	183	2.19	10.0	33.6	1.64
3.73	180	2.32	11.3	35.3	1.79
4.20	178	2.44	12.3	37.1	1.91
4.35	177	2.48	13.4	39.4	2.05
4.88	173	2.60	14.3	41.4	2.18
4.99	175	2.64	15.5	44.5	2.35
5.55	171	2.75	16.6	47.7	2.52
6.16	168	2.88	18.0	52.2	2.74
7.23	164	3.08	18.2	52.7	2.77
8.00	161	3.21	19.0	55.7	2.91
12.5	145	3.80	19.2	56.0	2.93
16.5	129	4.13	19.9	59.1	3.07
19.7	114	4.24	20.3	61.2	3.15
22.5	109	4.42	20.5	61.3	3.17
22.6	105	4.35	21.2	65.2	3.32
27.1	94.0	4.51	21.5	65.5	3.36
30.5	86.3	4.59	22.0	65.6	3.40
34.3	79.4	4.67	23.1	65.5	3.48
39.8	71.2	4.76	23.2	65.5	3.49
44.5	65.4	4.82	24.5	65.0	3.57
52.8	57.0	4.91	25.1	64.8	3.61
60.9	50.8	4.97	26.4	64.2	3.68
61.6	50.3	4.98	26.9	63.8	3.70
70.5	44.7	5.02	28.2	63.1	3.77
82.2	39.0	5.06	28.8	62.7	3.80
92.0	35.2	5.09	30.1	62.0	3.86
100.3	32.4	5.10	30.7	61.5	3.88
110.5	29.7	5.12	32.7	60.1	3.96
125.2	26.4	5.14	34.4	59.0	4.03
			39.7	55.6	4.20
			44.6	52.6	4.33
			52.9	48.0	4.51
			61.2	44.1	4.65
			71.0	39.9	4.76
			82.9	35.8	4.87
			92.7	32.9	4.94
			102.5	30.4	4.99
			113.5	28.1	5.05
			128.7	25.2	5.10

## APPENDIX X. Mössbauer Spectral Results

PART A. Mössbauer Spectral Parameters<sup>1</sup> for  
Pyridine and Pyrazine Iron(II) Sulfonate Complexes

COMPOUND	TEMP	$\Delta E_q$	$\delta$	$\Gamma_1^2$	$\Gamma_2$
$\text{Fe}(\text{py})_4(\text{CF}_3\text{SO}_3)_2$	293	3.09	1.07	0.26	0.25
	78	3.68	1.14	0.26	0.25
$\text{Fe}(\text{py})_4(\text{CH}_3\text{SO}_3)_2$	293	3.53	1.07	0.28	0.26
	120	3.81	1.07	0.27	0.27
	78	3.83	1.07	0.27	0.26
	30	3.83	1.07	0.25	0.29
	8.4	3.83	1.08	0.30	0.31
$\text{Fe}(\text{py})_4(\text{p-CH}_3\text{C}_6\text{H}_4\text{SO}_3)_2$	293	3.47	1.08	0.26	0.28
	78	3.63	1.16	0.26	0.28
$\text{Fe}(\text{pyz})_2(\text{CF}_3\text{SO}_3)_2 \cdot \text{CH}_3\text{OH}$	293	3.45	1.16	0.32	0.32
	78	3.71	1.25	0.40	0.38
$\text{Fe}(\text{pyz})_2(\text{CH}_3\text{SO}_3)_2$	293	3.08	1.14	0.46	0.46
	78	3.20	1.23	0.43	0.43
$\text{Fe}(2\text{-mepyz})_4(\text{CH}_3\text{SO}_3)_2$	293	3.01	1.19	0.42	0.36
	78	3.40	1.28	0.35	0.32
$\text{Fe}(\text{py})_2(\text{CF}_3\text{SO}_3)_2$	293	1.65	1.19	0.31	0.28
	78	2.45	1.22	0.35	0.34
$\text{Fe}(\text{pyz})(\text{CF}_3\text{SO}_3)_2$	293	2.79	1.19	0.52	0.44
	78	3.59	1.27	0.36	0.35
$\text{Fe}(\text{pyz})(\text{p-CH}_3\text{C}_6\text{H}_4\text{SO}_3)_2 \cdot 2\text{CH}_3\text{OH}$	293	3.21	1.18	0.47	0.39
	78	3.49	1.29	0.44	0.39
$\text{Fe}(\text{pyz})(\text{p-CH}_3\text{C}_6\text{H}_4\text{SO}_3)_2$	293	2.54	1.22	0.43	0.40
	78	2.80	1.24	0.56	0.50

1). Temperatures are in K; quadrupole splittings,  $\Delta E_q$  isomer shifts,  $\delta$  and linewidths,  $\Gamma$ , are in units of  $\text{mm s}^{-1}$

2).  $\Gamma$  values are linewidths at half height.

APPENDIX X, PART B. Mössbauer Spectral Parameters for  
Iron(II) Pyrazine Complexes

COMPOUND	TEMP	$\Delta E_q$	$\delta$	$\Gamma_1$	$\Gamma_2$
$\text{Fe}(\text{pyz})_2\text{Cl}_2$	293	3.19	0.98	0.31	0.30
	78	3.33	1.08	0.33	0.34
$\text{Fe}(\text{pyz})_2\text{Br}_2$	293	3.17	0.98	0.39	0.40
	78	3.47	1.09	0.39	0.33
$\text{Fe}(\text{pyz})_2\text{I}_2$	293	2.01	0.97	0.41	0.35
	78	2.50	1.08	0.39	0.33
$\text{Fe}(\text{pyz})_2(\text{NCS})_2$	293	2.45	1.01	0.33	0.30
	78	2.63	1.11	0.35	0.33
$\text{Fe}(\text{pyz})_2(\text{ClO}_4)_2$	293	3.24	1.07	0.36	0.32
	78	3.74	1.16	0.35	0.33
$\text{Fe}(\text{pyz})\text{Cl}_2$	293	1.72	1.04	0.46	0.39
	78	2.52	1.15	0.48	0.45
$\text{Fe}(\text{pyz})(\text{NCO})_2$	293	2.04	1.05	0.38	0.32
	78	2.75	1.17	0.44	0.42
$\text{Fe}(\text{pyz})_4(\text{AsF}_6)_2 \cdot 2\text{H}_2\text{O}$	293	2.99	1.11	0.36	0.32
	78	3.09	1.19	0.35	0.35



#### PUBLICATIONS

Thompson, R.C.; Haynes, J.S.; Sams, J.R., Chem. Phys. Lett. 1980, 75, 596.

Thompson, R.C.; Haynes, J.S.; Sams, J.R., Can. J. Chem. 1981, 59, 669.

Sams, J.R.; Haynes, J.S.; Hume, A.R.; Thompson, R.C., Chem. Phys. 1983, 78, 127.

Thompson, R.C.; Haynes, J.S.; Oliver, K.W.; Rettig, S.J.; Trotter, J., Can. J. Chem. 1984, 62, 891.

Thompson, R.C.; Haynes, J.S.; Cicha, W.V.; Oliver, K.W.; Rettig, S.J.; Trotter, J., Can. J. Chem. 1985, 63, 1055.

Thompson, R.C.; Haynes, J.S.; Oliver, K.W.; Rettig, S.J.; Trotter, J., Can. J. Chem. 1985, 63, 1111.

Haynes, J.S.; Sams, J.R.; Thompson, R.C., Can. J. Chem. 1985, submitted for publication.

Haynes, J.S.; Rettig, S.J.; Sams, J.R.; Thompson, R.C.; Trotter, J., Can. J. Chem. 1985, submitted for publication.